Kinetics and Regulation of Protein Kinases

APPROVED BY SUPERVISORY COMMITTEE

Elizabeth J. Goldsmith, Supervisor

Daniel Rosenbaum

Jef De Brabander

Margaret Phillips

Kinetics and Regulation of Protein Kinases

by

Alexander Townshend Piala

DISSERTATION

Presented to the Faculty of the Graduate School of Biomedical Sciences

The University of Texas Southwestern Medical Center at Dallas

In Partial Fulfillment of the Requirements

For the Degree of

DOCTOR OF PHILOSOPHY

The University of Texas Southwestern Medical Center at Dallas

August 2015

Kinetics and Regulation of Protein Kinases

Alexander Townshend Piala, Ph.D.
The University of Texas Southwestern Medical Center at Dallas, 2015

Elizabeth J. Goldsmith, Ph.D.

One of the major functions of kinases in biological systems is the relay of signal from an effector to a downstream target. Kinases are regulated by a diversity of mechanisms, both internal and external to the kinase. When the regulation of these kinases is somehow abrogated, disease can result. As such, understanding of these regulatory mechanisms could serve as useful in not only understanding cellular signal propagation, but also the disease states that can arise from their malfunction.

Taking advantage well-developed projects in the Goldsmith lab, three systems were studied: two kinases and one kinase cascade. The MAP3K Thousand and One Kinase 2 was the subject of an inhibitor discovery program using high-throughput screening of a large small-molecule library. Secondly, the mechanism by which the kinase With No Lysine(K) 1 responds to chloride concentration in order to modulate downstream signaling was studied. Finally, a cascade comprising the MAP3K Apoptosis Signaling Kinase 1, MAP/ERK

Kinase 6, and p38α was studied through modeling approaches using data derived from mass spectrometry.

In each case, mechanisms for regulation were discovered. Tight-binding inhibitors of TAO2 were found that may prove useful in both in*in vitro* signaling studies as well as future *in vivo* work. WNK1 was shown to be regulated by direct chloride binding, which inhibits its auto-phosphorylation and thusly its auto-activation. Finally, important kinetic parameters for MAPK cascade signaling were determined, and it was demonstrated that additional species outside the cascade do not appear necessary for switch-like behavior under physiological-like *in vitro* conditions. These diverse regulatory mechanisms showcase how protein kinases manage to synthesize diverse inputs into physiologically meaningful downstream signals.

Table of Contents

List of Tables

List of Figures

List of Abbreviations

Å	Angstrom
μ	Mean
σ	Standard deviation
6-MEQ	6-Methoxy-N-Ethyl-Quinoline
ACE	Angiotensin-Converting Enzyme
AD	Alzheimer Disease
ADP	Adenosine 5'-diphosphate
AIC	Akaike Information Criterion
ANP	Atrial Natriuretic Peptide
APS	Advanced Photon Source
ASK	Apoptosis Signaling Kinase
ATP	Adenosine 5'-triphosphate
CAMK	CAlModulin-dependent protein Kinase
cAMP	Adenosine 3',5'-monophosphate
CCC	Cation-Chloride Cotransporter
Cdc42	Cell Division Control protein 42
cDNA	Circular DNA
CFTR	Cystic Fibrosis Transmembrane conductance Receptor
COS-1	CV-1 Origin, SV40
DMSO	Di-Methyl SulphOxide
DSF	Differential Scanning Fluorimetry
E. coli	*Escherichia coli*
EB (buffer)	Elution Buffer
ENaC	Epithelial Sodium Channel
ESF 921	Expression Systems Formula
GABAA	γ-AminoButyric Acid-gated chloride channel
HEK	Human Embryonic Kidney
IC_{50}	Inhibitory Concentration 50%
IPTG	Isopropyl β-D-1-ThioGalactopyranoside
JNK	c-Jun N-terminal Kinase
KCC	Potasium-Chloride Cotransporter
KCNB1	Potassium Channel, voltage gated Shap related subfamily B
K_m	Michaelis Constant
MAP2K	Mitogen Activated Protein Kinase Kinase
MAP3K	Mitogen Activated Protein Kinase Kinase Kinase
MAPK	Mitogen Activated Protein Kinase
MBP	Myelin Basic Protein

MEK	MAP/ERK Kinase
MEKK	MEK kinase
NCC	Sodium-Chloride Cotransporter
NKCC	Sodum-Potassum-Chloride Cotransporter
Nrp	Neuropilin
NTA	NitriloTriAcetic acid
OSR	Osmotic Stress Regulated
PCR	Polymerase Chain Reaction
PEG	PolyEthylene Glycol
PKA	Protein Kinase A
PP1cγ	Protein Phosphatase 1c gamma
psi	pounds per square inch
PSK	Prostate Specific Kinase
rcf	relative centrifugal force
ROMK	Renal Outer Medullary Potassium channel
rpm	Rotations per minute
RT	Room temperature
RVD	Regulatory Volume Decrease
RVI	Regulatory Volume Increase
S. cerevisiae	*Saccharomyces cerevisiae*
SAR	Structure-Activity Relationship
Ser	Serine
SERT	SERotonin Transporter
SF9	*Spodoptera frugiperda*
SGK1	aldosterone-regulated Serum and Glucocorticoid-induced Kinase
SPAK	Ste20-related Protein Alanine rich Kinase
Ste20	Sterile 20 kinase family
T_m	Melting Temperature
T. ni	*Trichoplusia ni*
TAO	Thousand And One Kinase
TFA	Trifluoro-Acetic Acid
Thr	Threonine
Tyr	Tyrosine
WNK	With No lysine(K)
KDm	Kinase Domain

Chapter 1

Introduction

The transduction of signal from a sensor to an effector is vital to biological systems. Post-translational modification is one of the major mechanisms by which such signals can be transmitted, and one of the major forms of such post-translational modification is phosphorylation, or addition of phosphate. For this reason, protein kinases, or enzymes that phosphorylate other proteins, are important components of signal transduction. Protein kinases are centrally important signaling molecules, and have gotten significant attention as drug targets. They both receive and transmit signal, and the study of the mechanism by which this is regulated is an active research field.

In order to investigate different modes of kinase regulation, I focused on two different kinases and one kinase cascade. The two kinases were Mitogen-Activated Protein Kinane Kinane Kinase Thousand-And-One Kinase 2 (MAP3K TAOK2) and With No Lysine(K) 1 (WNK1), while the cascade comprised of the MAP3K Apoptosis Signaling Kinase 1 (ASK1), the MAP2K MAP/ERK Kinane (MEK6), and the MAPK p38α. In TAO2 I studied drug discovery in MAPK kinase pathway components, in WNK1 I studied kinase receptor mechanisms, and analysis of the cascade allowed for study of signal transduction in the p38 MAP kinase pathway. By using this approach, I could study several systems while taking advantage of several well-developed projects in the Goldsmith laboratory.

The first section of this thesis will focus on the discovery of small molecules that inhibit a clinically relevant protein kinase. The second section of this thesis will focus on a newly discovered mechanism of chloride sensing, and how kinase function is regulated by

chloride concentration. Finally, I will discuss work concerning how the kinetics of protein kinase phosphorylation itself allows for regulation of signal propagation.

1.1 Introduction to kinase cascade signal transduction

Throughout this thesis I will be discussing protein kinases, and all kinases that are being investigated operate within some sort of kinase 'cascade.' In this context, a kinase cascade refers to a process by which some kinase phosphorylates and activates some other kinase, and that kinase goes on to phosphorylate some other substrate. The signals that they transmit are incredibly varied and vital for survival, including growth, pro-apoptotic, anti-apoptotic, stress, and differentiation signals [1]. There are several potential reasons why these signals are transduced through a cascade, such as transporting a signal from the cell membrane to the nucleus, amplifying the strength of a signal, or helping generate a switch-like response from a graded input. Unfortunately, it can be difficult to determine exactly which of these roles a given cascade is performing under a given stimulus, and the relative importance of each. While some cascades appear to be linear, with only a single predefined route, many are dendritic, which makes understanding the exact function of each member difficult. This allows for a single input to generate multiple outputs, and for synthesizing multiple inputs into a specific, physiologically important, output. These cascades can be of variable length— in this work, I will be discussing kinases that exist in cascades that consist of either 2 (WNK) or 4+ (the p38 MAPK cascade) members.

This thesis will deal with Ser/Thr and Ser/Thr/Tyr protein kinases, so named for the residues on which they can attach phosphate groups. For many of the kinases discussed here, two separate phosphorylation events are required in order to render them 'fully active.' The requirement that two sites be phosphorylated on the kinase was recognized by Ferrell *et al.* as a possible mechanism by which these cascades could generate a steady-state sigmoid output in response to a graded input signal [2]. While this output had been observed previously,

this was one of the first major efforts to understand a mechanism that could drive the phenomenon [3, 4]. Later, it was shown that the two phosphorylation events appeared to have an order in some systems [5–7]. This order has since been shown mathematically to increase the sigmoidicity of downstream signaling in response to stimulus, but just because it *could* be used to modify downstream signal does not mean that it *is* widely observed [8]. Whether or not order is observed in other kinases is a question that is addressed in this thesis.

1.2 Mechanisms of cascade regulation

As a mechanism for responding to different signals, kinase cascades must be subject to rigorous regulatory mechanism in order to prevent activation in the absence of stimulus or inactivity when a response is required. These dual requirements, as well as the diversity of signal inputs and physiological regimes under which these cascades function, have resulted in a number of different regulatory mechanisms that operate directly on the cascade components. While my thesis focuses on only three of these mechanisms (upstream activation, small molecule binding, and cascade architecture), there are potentially many. Combinations of different regulatory mechanism allow for the synthesis of diverse inputs into useful physiological outputs.

Phosphorylation

The most basic and essential method of regulation in these cascades is phosphorylation. Without phosphorylation on the activation loop, kinases that function within kinase cascades are not active. Therefore, the balance of phosphorylation and dephosphorylation serves as the fundamental handle for turning on and off the pathway. While this method of regulation is the most obvious, given the nature of kinase cascades, it can be difficult to characterize on a case-by-case basis, as many other modes of regulation operate on the

kinases at this level. That this mode of regulation is required for cascade functionality is also what gives every kinase cascade the possibility of functioning as a switch. This is discussed in more detail below, and explains why WNK1 activity is primarily regulated by *phosphorylation* and not *chloride*.

Small molecule binding

Unsurprisingly, it can also be useful for small molecules to directly influence the activity of kinases. There are several examples of this in the literature, though the two most famous of these are probably the Calmodulin-dependent protein kinases (CAMK) and protein kinase A (PKA). In the case of CAMK, there is an additional extra-kinase domain that is capable of binding both calcium ion and the kinase to be regulated [9]. When this calmodulin domain binds calcium, is is no-longer able to bind the kinase domain, thus freeing the domain for downstream activation of targets [10]. PKA operates similarly, with a cAMP (adenosine 3',5'-monophosphate)- binding subunit external to the kinase domain. When this domain is bound by cAMP, it is incapable of binding and inhibiting the kinase domain. These mechanisms allow the kinases in question to 'sense' the concentration of small molecules in the environment around them, allowing for the cell to swiftly react to a changing environment.

Cascade architecture

The last mechanism of kinase regulation that will be discussed is cascade architecture. The number of kinases involved in a given cascade, the number of phosphorylation events required to activate each species, and the different kinetic aspects of this phosphorylation event all change how the cascade relays signal from upstream sources. Amongst other properties, this can change the sigmodicity of the cascade output, the required input threshold before signal is transmitted through the cascade, or the sensitivity of the cascade to stimulus,

depending on the environment. This is dealt with greater mathematical detail below.

Phosphatase action

One of the critical components of MAPK cascades that has gotten relatively little attention is dephosphorylation. However, the action of phosphatases on the reaction has a number of critical effects on signal propagation. Steady-state phenomena like ultrasensitivity and bistability require the action of phosphatases to prevent the reaction from equilibrating at complete phosphorylation. Furthermore, they allow the system to 'switch off' once upstream signaling has competed. The mathematical relationship between such equilibria and multiple phosphorylation states has been described [11, 12], as has its relationship with order [8].

1.3 Dissertation research topic and goals

While the characterization of kinase activity is vital for understanding how kinases function at a physiological level, how they are *regulated* is just as important. My work is an attempt to characterize some of these mechanisms of regulation, and help understand how they influence signal propagation. In the case of TAO2, I made strides toward the development of small-molecule inhibitors of the kinase domain, which would provide a means by which we could extrinsically regulate TAO2 kinase activity. This would provide not just a useful laboratory tool to disambiguate kinase-dependent and -independent functions, but as an initial step toward a potential anticancer therapeutic. My work in WNK1 helped characterize the mechanism by which the kinase domain is regulated by both chloride and autophosphorylation, revealing one more way cells are able to sense and respond to their environments. Finally, my computational modeling of individual MAPK cascade tiers helped reveal how the kinetic parameters guiding their regulation by phosphorylation could result in the switch-like *in vivo* signal outputs observed by other groups, independent of outside

factors. In each of these cases, I investigated a specific mode of kinase regulation in order to provide the tools and understanding required for further progress in this field.

Chapter 2

Inhibitor Discovery of TAO2

2.1 Introduction

Thousand and One Kinase 2

TAO2 (also known as TAOK2 or PSK1[Prostate Specific Kinase 1]), or Thousand and One Kinase 2, is a Sterile 20-like kinase and a member of the germinal-center kinase-like kinase family due to its N-terminal kinase domain and lack of a Cdc42/Rac-interacting domain. It primarily consists of two different protein isoforms— one is a 1235 residue protein (also called PSK1-α), and the second is a 1049 residue protein (also called PSK1-β). The differences between these two proteins are restricted entirely to the C-terminus, away from the kinase domain. TAO2 is ubiquitously expressed.

Discovery

TAO2 was discovered by PCR of rat cDNA in an effort to find proteins with high homology to Sterile 20p kinase (Ste20p) from *S. cerevisiae* [13]. Ste20p had been previously identified as a member of yeast MAPK cascades, and human proteins related to Ste20p had been shown to phosphorylate and regulate the MAP/ERK kinase family members [14, 15]. As such, it was expected that additional unknown proteins with homology to Ste20p may be previously unidentified members of MAPK cascades. TAO2 was subsequently cloned, expressed, and characterized biochemically in work by Chen *et al.* [16]. These efforts identified TAO2 as a 993 residue MAP3K, laying the foundation for follow-up work to further characterize the physiological role of TAO2 and its structural features.

Biochemistry

The first biochemical studies conducted by Zhu Chen of the Cobb lab provided our first understanding of *in vitro* TAO2 specificity [16]. The high homology of the TAO2 kinase domain with the kinase domains of Ste20p (39%) and MEKK1 (33%) suggested that TAO2 may be a MEK kinase [13]. The kinase domain of TAO2 was identified, and the construct TAO2 1–320 enclosing the kinase domain was expressed and purified. Assays revealed that TAO2 did, in fact, have activity against both MEK3 and MEK6 [16]. Further analysis demonstrated that TAO2 also contained a MEK3/6 binding domain over residues 314–451. Whether or not this activity was physiological was investigated shortly after [17]. Different TAO2 constructs expressed in HEK293 cells were capable of activating several different stress-response kinases, including JNK, p38, and ERK1/2. Consistent with the original biochemical characterization, MEK3 and MEK6 were specifically activated. This suggested a role for TAO2 in the activation of stress-related pathways, but subsequent assays were not able to identify a positive regulator of TAO2 [18].

Subsequent work revealed a potential role for the C-terminal residues of TAO2. Mitsopoulos *et al.* expressed full length TAO2 with an N-terminal Myc tag for immunofluorescence studies in Swiss 3T3 cells [19]. These studies revealed that TAO2 isoform 1, but not isoform 2, localizes to microtubules, and subsequently renders those microtubules resistant to dissolution by nocodazole. Furthermore, introduction of full-length TAO2 also induces the formation of perinuclear microtubule cables. This suggested that TAO2 is capable of regulating microtubule assembly. By generating different size constructs, this regulatory function was localized to residues 745–1235. TAO2 was also shown to phosphorylate both α- and β-tubulin, suggesting that TAO2 may have additional microtubule regulatory function above that demonstrated by the C-terminus.

Role in Apoptosis

The *in vitro* biochemical assays were complimented by several attempts to determine the role TAO2 played in cells. Its positioning as a kinase within the p38α kinase cascade suggested that it may play a part in stress response, but several additional functionalities have been observed. One of these functionalities relates to the the induction of apoptosis. Work by Zihni *et al.* showed that not only does TAO2 isoform 1 (PSK1-α) phosphorylate and activate JNK in COS-1 cells, but it also induces cell contraction, membrane blebbing, and cleavage of poly ADP ribose polymerase, hallmarks of apoptosis, in a kinase-dependent fashion in non small-cell lung cancer line H1299. Use of a JNK inhibitor (SP600125) revealed that this activity was dependent on JNK activation [20]. Subsequent immunofluorescence studies showed that on TAO2 activation, JNK became phosphorylated and activated, which led to caspase-mediated cleavage of the TAO2 C-terminal microtubule domain, which in turn led to transport of TAO2 to the nucleus. Inhibition of any of these steps led to a reduced incidence of apoptosis (as measured by incidence of membrane blebbing).

Role in Neuronal Development

After work potentially associating TAO2 copy number variations with autism spectrum disorder [21], the role of TAO2 in neuronal development was investigated. Calderon de Anda *et al.* observed that TAO2 isoform 1 was exprssed in the brain, and that knockdown reduced actin concentration in growth cones, the number of growth cones, and the number of neurites in cultured neurons [22]. Furthermore, overexpression of TAO2 produced an opposite phenotype. TAO2 also appeared important for the formation of axon formation. The receptor Neuropilin 1 (Nrp1), which causes similar phenotypes when defective, was also shown to bind directly to TAO2, suggesting TAO2 may be directly regulated by Nrp1. Nrp1 and TAO2 colocalized in mouse cortex, and when Nrp1 was knocked down, the amounts of active TAO2 in the cortex was also significantly decreased.

Consistent with the idea that TAO2 is important to neuronal differentiation, dendritic complexity could be restored in cells expressing Nrp1 incompetent to bind its substrate semaphorin 3A when TAO2 was overexpressed. Similarly, expression of constitutively active JNK1 in neurons with TAO2 knocked down managed to partially restore dendritic branching. Together, these results suggest that TAO2 plays an important role in the differentiation of neurons during brain development.

Role in Alzheimers

The dual role of TAO2 in microtubule assembly regulation and signal propagation through phosphorylation made it a potential candidate for Alzheimer disease (AD). AD is typified by the aggregation of the microtubule-associated protein tau, which is hyperphosphorylated in the disease state. These hyperphosphorylated proteins then aggregate, forming neurofibrillary tangles. The exact cause for the appearance of the disease is not known, which is why kinases capable of potentially causing this hyperphosphorylation have been examined in this context. Tavares *et al.* observed that TAO2 is capable of phosphorylating tau on 41 different sites, 9 of which are on the microtubule binding domain [23]. Furthermore, active TAO2 colocalized with phosphorylated tau in samples taken from diseased brain. Because of the role of TAO2 in stress signaling and apoptosis, however, it is difficult to determine whether or not this is causative.

Applicability as an inhibitor target

When determining whether or not a given protein target is acceptable for an inhibitor discovery program, there are several important criteria that should be addressed. First, one should have an assay capable of measuring the activity of the protein you wish to inhibit. Second, the target must have been identified as physiologically meaningful within the context of some human disease. Third, one must be able to express the protein of

interest, or otherwise be able to purify it for assay. Finally, structural information pertinent to the protein in question is useful for post-discovery followup. Only the first of these is mandatory, as without some sort of assay to determine efficacy of your proposed inhibitors it is impossible to begin the screening process; however, each additional facet makes the project more tractable.

In this context, TAO2 was an ideal target for an inhibitor discovery program. Kinases have well-understood chemistry, and there are many established tools for measuring phosphorylation activity— this allowed for relatively simple assay development. TAO2 also appeared important for cancer survival based on a synthetic lethal small-cell lung cancer screen performed by the White lab [24]. This screen assayed protein knockdown using siRNA in the context of a background of low concentration paclitaxol. Knockdown of TAO2 specifically sensitized the cell line to paclitaxol greater than wild-type, suggesting that inhibition of TAO2 could be used in combination with existing chemotherapeutics to good effect. Further, protocol for the expression and purification of the TAO2 kinase domain had already been established [25]. Crystal structures of both the active TAO2 kinase and TAO2 kinase with a pan-kinase inhibitor bound had also been determined by the Goldsmith lab [25, 26]. In combination, these features suggested that TAO2 would be an excellent inhibitor discovery target.

2.2 Approach toward TAO2 inhibitor discovery

With protein expression and purification already described, and conditions for enzymatic activity determined [25], all that was left was the design/optimization of an assay to measure activity in a high throughput fashion. The University of Texas Southwest Medical Center has an in-house screening facility with a 200,000 compound chemical library. Furthermore, they have robotics that allow for swift screening of the entire library in a 384-well plate format. Due to the requirements of the robotics, each well could have a total of 50 µl

of reaction solution over the course of the experiment. As such, an assay had to found that was amenable to these liquid handling requirements.

The assay that was chosen for this project was the 'Kinase-Glo' (Promega) ATP detection assay. The Kinase-Glo system uses luciferase-based ATP-dependent luminescence to determine the concentration of ATP in a given sample. The higher the ATP concentration, the greater the degree of fluorescence. The fluorescence intensity is linear with respect to ATP concentration up to an ATP concentration of 100 µM. For this reason, the assay had to remain within the range of 0–100 µM ATP. While there are other systems that can measure kinase activity more directly, such as measurement of ADP concentration (one product of the phosphotransfer reaction) and direct measurement of ATP/ADP ratio by mass spectrometry, there are advantages to the Kinase-Glo assay that make it the most attractive option.

The first, and probably most significant, of these is the avoidance of false-positive hits. In an assay where kinase activity, or a product of kinase activity, is measured, any inhibitor that inhibits the assay instead of the kinase will appear as a positive hit. These false positives can make analysis of the experimental results more difficult. Because this assay measures only the remaining reactant, any compound that instead inhibits the assay will make it appear as if the well experienced depletion of ATP, i.e., full activity. This raises the possibility of false *negative* results, but compounds so promiscuous that they also affect the assay are less likely to be desirable compounds.

Availability was also a major concern. While measurement of ATP/ADP ratio by mass spectrometry *can* be performed in a high-throughput fashion, such tools were not available to us at the time the assay was conducted. High throughput mass spectrometry requires specific experimental design to detect the small molecules of interest— in this case ATP and ADP. This generates additional assay development requirements that do not exist for the comparatively simple luminescence readout that Kinase-Glo provides. The combination of unavailability and additional development complexity rendered this option unappealing.

There is also an advantage in the relative simplicity of the reaction. The Kinase-Glo assay only has a single reporter enzyme (luciferase) that converts ATP into fluorescence. The major competing choice for a high-throughput amenable assay is ADP-hunter (DiscoveRx), which directly measures the concentration of ADP in the sample. Because ADP is a lower-energy molecule, however, it can not be directly used to generate fluorescence independent of ATP concentration. To solve this problem, the ADP-hunter assay uses pyruvate kinase to transfer phosphate from phosphoenolpyruvate to the ADP generated from the kinase reaction. This generates a quantity of pyruvate proportional to the amount of ADP generated from the kinase reaction. This pyruvate is then converted to acetyl phosphate and hydrogen peroxide through the use of pyruvate oxidase. A peroxidase is then used to convert the hydrogen peroxide to an amount of fluorescence proportional to the amount of ADP originally in the sample. This additional complexity, as well as the increased cost of the assay, made Kinase-Glo much more attractive.

With the assay determined, reaction conditions were optimized for the discovery of TAO2 inhibitors. The plate reader was able to detect changes of ATP concentration within the range of 0–10 µM ATP using the manufacturer's protocol for Kinase-Glo. Concentrations above 10 microM generated luminescence signals above the plate reader's dynamic range. As such, this regime was used in order to minimize the amount of TAO2 required for the assay. Several conditions were tested by varying the concentration of TAO2 using the protocol above. The concentration of TAO2 that gave a linear temporal response as well as consumed 50% of the starting ATP concentration in 90 minutes was used.

For the 200k compound screen, each compound was screened once. In order to make sure that putative hits were capable of inhibiting TAO2, all compounds that provided a $> 3\sigma$ response were screened in triplicate a second time. Each concentration of compound was different within this triplicate measurement, giving final compound concentrations of 10 µM, 3 µM, and 1 µM. This final list of compounds was used for the next triage steps of the TAO2

inhibitor discovery project.

2.3 Materials and methods for protein purification

Expression and purification of TAO2 in *Trichoplusia ni*

These efforts were largely adapted from those reported in [25]. The TAO2 protein was expressed using the Invitrogen 'pFastBac' system in *T. ni* cells. In the pFastBac system, the gene of interest is cloned into a 'pFastBac' plasmid vector. This plasmid was engineered and provided by H. He of the Goldsmith lab (Figure **??**).This vector can be transfected into a specially modified *E. coli* strain, where it is recombined with another plasmid carried by the modified *E. coli* using the left and right arms of the Tn7 transposon and proteins expressed from an additional 'helper plasmid'. This recombined plasmid is referred to as a 'bacmid,' and can then be transfected into insect cells for the production of recombinant viral particles. These viral particles will replicate in insect cells, and force the expression of the gene of interest. The resultant protein can then be purified from the cell lysate.

Bacmid production

1. *E. coli* strain DH10Bac was transformed with the pFastBac vector encoding TAO2 at the polyhedrin promoter site.

2. Colonies were raised on plates containing 50 µg/ml kanamycin, 7 µg/ml gentamicin, 10 µg/ml tetracycline, 100 µg/ml Bluo-gal, and 40 µgml IPTG.

3. White colonies indicate that the gene was incorporated into the 'bacmid,' interrupting the galactosidase gene.

4. White colonies were picked and grown in 10 ml suspension with the above antibiotics.

5. The cells were centrifuged at 16.1 rcf for 10 minutes, and the media was removed via decantation.

6. Cells were suspended in 300 µl Qiagen buffer P1.
7. 300 µl Qiagen buffer P2 was added, and the sample was mixed via inversion.
8. 300 µl Qiagen buffer N3 was added, and the sample mixed thoroughly via inversion.
9. The sample was centrifuged at 16.1 rcf for 10 minutes.
10. The supernatent was removed, and added to 800 µl isopropanol. After this point, all steps are performed using sterile technique.
11. The sample was centrifuged and the pellet was washed with 70% ethyl alcohol.
12. The sample was spun once more, and opened in the hood to dry. The DNA was then suspended in 40 µl EB buffer.

Virus production

1. A solution of 10 µl bacmid DNA from above was added with 10 µl Cellfectin (Invitrogen) to 200 µll Grace's media and allowed to incubate for 20 minutes.
2. The above solution was added to 1 ml of SF9 culture with $1 \cdot 10^6$ cells.
3. After 5 hours, the culture is centrifuged at 16.1 rcf for 10 minutes, and the media is replaced with 2 ml ESF 921.
4. The cell culture above was allowed to grow for 72 hours.
5. Cell culture was centrifuged at 4000 RPM for 40 minutes at 4 °C in a Beckman J6-MI centrifuge.
6. Supernatent was removed and stored at 4 °C in the dark as the 'p0,' or virus isolated after zero passages.

7. The p0 was added to a 1L suspension of SF9 cells at a density of $1 \cdot 10^6$/ml, and allowed to incubate for 72 hours.

8. The cell culture was centrifuged at 4000 RPM for 40 minutes at 4 °C in a Beckman J6-MI centrifuge.

9. Supernatent was removed and stored at 4 °C in the dark as the 'p1,' or virus isolated after one passage.

10. This process was repeated, with 10 ml of the p1 being added to 1L of cells in order to generate the p2.

Growth and infection of SF9 cells

1. SF9 cells (Expression Systems) were grown in ESF 921 (Expression Systems) to a density of 2×10^6 cells/ml.

2. Isolated p2 virus was added at a ratio of 1:100 virus:insect cell culture.

3. Cells were incubated for 48 hours.

4. Cells were harvested through centrifugation using a Beckman J6-MI centrifuge at 4000 rpm for 40 minutes at 4 °C.

5. Supernatent was decanted and the cells were resuspended in Ni buffer A (50mM Tris pH 8.0, 500mM NaCl, 50mM glycerol phosphate, 10mM imidazole, and 30% glycerol.)

6. Cells were flash-frozen in liquid N_2 and stored at -80 °C.

Growth and infection of *T. ni* cells

1. *T. ni* cells (Expression Systems) were grown in ESF 921 (Expression Systems) to a density of 2×10^6 cells/ml.

2. Isolated p2 virus was added at a ratio of 1:100 virus:insect cell culture.

3. Cells were incubated for 48 hours.

4. Cells were harvested through centrifugation using a Beckman J6-MI centrifuge at 4000 rpm for 40 minutes at 4 °C.

5. Supernatent was decanted and the cells were resuspended in Ni buffer A (50mM Tris pH 8.0, 500mM NaCl, 50mM glycerol phosphate, 10mM imidazole, and 30% glycerol.)

6. Cells were flash-frozen in liquid N_2 and stored at -80 °C

Western Blotting

Western blots were conducted as described in Chen *et al.*, except as noted here [17]. Precast 10% gels were purchased from Bio Rad. antiTAO2 pSer181 was purchased from Invitrogen and diluted 1:1000. Primary antibody was allowed to react for two hours. Pierce Fempto was used to visualize the blots. Blots were exposed to film for 30 seconds.

Production of cell-free extract

1. Frozen cell pellets were thawed at RT in a water bath. During thaw, 160 mg of benzamadine and 2.5 mg leupeptin were added per litre of cells.

2. 100 ml Nickel buffer A was added to the cell pellet solution for every 100 ml of cell pellet.

3. 5 µl Benzonase nuclease (Novagen) was added to the cell pellet solution for every 100 ml cell pellet solution, and allowed to react for 30 minutes.

4. Cells were broken mechanically using a french press at 13,000 - 16,000 psi and 4 °C. Cells were broken over 4 passages.

5. The resultant solution was centrifuged at 40,000 rpm in a Beckman Ti-45 rotor at 4 °C for one hour.

6. The supernatant was decanted and passed through a Nalgene Rapid-Flow 2 µm filter.

Immobilized metal-affinity chromatography

7. The filtered extract was loaded onto a column containing 8 ml of Fast-chelating sepherose (Amersham Pharmacia) charged with 0.1 mM $NiSO_4$ and equilibrated with nickel buffer A.

8. The column was washed with 10 column volumes of Ni buffer A, and then eluted with an increase to 250 mM imidazole over a gradient of 10% to 70%.

9. The fractions corresponding to peaks appearing during the imidazole gradient were pooled and run on SDS-PAGE in order to determine presence of TAO2.

10. The fractions containing TAO2 were pooled and buffer exchanged into 200 mM NaCl, 50 mM Tris pH 8.0, and 10% glycerol using membrane dialysis in a Spectra/Por 12–14,000 membrane. During dialysis, 1 mg tobacco edge virus protease was added to remove His tag.

11. The protein solution was passed through 2 ml Ni-NTA agarose (Qigen), and the flowthrough was collected. The plug was washed with 3 ml 50 mM Tris pH 8.0 and 200 mM NaCl and the flowthrough was collected.

12. The protein solution was assayed with Biorad protein assay to determine protein concentration, and the solution was buffer exchanged into 1M NaCl, 50 mM Tris pH 8.0, and 10% glycerol and concentrated to 1.5 mg/ml in an Amicon Ultra-15 3k.

13. The protein solution was then flash-frozen in liquid N_2 for storage.

Purification of MBP from bovine brain

This protocol is an adaption from one provided by the Cobb lab.

1. 25 g brain acetone powder (Sigma) was dissolved in 450 ml of 0.03 N HCl and 0.7 µg/ml pepstatin A.
2. Solution pH was brought to 3.0 by addition with HCl, and the solution stirred for 1.5 hrs at 4 °C.
3. Solution was centrifuged at 14,000 rpm in a Beckman Ti-45 rotor at 4 °C.
4. Supernatent was decanted and urea was added to the supernatant to 4 M. Supernatent was stored at 4 °C
5. Pellet was re-extracted as above.
6. The collected supernatant from both centrifugations was pooled, and 1 M pH 5 citrate was added to a final concentration of 10 mM.
7. The solution was then adjusted to pH 5 and filtered through glass wool.
8. A column packed with 25 ml SP-Sepharose was equilibrated with 100 ml 100 mM citrate pH 5, then equilibrated with a solution of 100 ml 10 mM citrate pH 5 and 4 M urea.
9. The solution was loaded onto the column, and the column was washed with a solution of 150 ml 20 mM glycine, 4 M urea, 50 mM NaCl at pH 9.5.
10. The column was eluted with 20 mM glycine, 4 M urea, and 250 mM NaCl at a pH of 9.5. 10 µl 6 N HCl was added to each 5 ml fraction after it was eluted.
11. The fractions containing MBP were collected and dialyzed against H_2O to remove urea.

12. Dialyzed protein solution was concentrated to 10 mg/ml and flash-frozen in N_2 for storage.

2.4 Materials and methods for high-throughput screen

Conducting the screen

These conditions are an adaptation of a similar TAO2 activity assay from Chen *et al.* [16]. Only the TAO2 concentration was modified during assay optimization, and the reaction was optimized such that the fluorescence generated from the ATP-luciferase reaction was reduced by 50% over the course of 100 minutes.

1. 20 µl of a solution of 50 mM HEPES pH 7.4, 50 mM MgCl2, 1.27mg/ml MBP and 0.005 mg/ml TAO2 was added to each well of a 384 well Corning plate using a Biotek MultiFlo dispenser.

2. 0.2 µl of compound (columns 3 to 22, 50 µM), DMSO negative control (columns 2, 23, and 24), or staurosporine positive control (column 1, 43.4 µM) were added to each well with a Biomek Liquid handler.

3. 10 µl of 50 µg/ml ATP solution was added to each well with a Labsystems Multidrop 384.

4. The plates were incubated at RT for 100 minutes.

5. 20 µl Kinase Glo (Promega) was added to each well, and allowed to incubate for 10 minutes under agitation.

6. Luminescence was read on an Envision Multilabel plate reader.

Confirmation Screen

The confirmation screen was conducted as the original screen above, though only those compounds that demonstrated inhibition $> 3\sigma$ above negative control were tested. Each compound was tested at three different concentrations, 10 µM, 3 µM, and 1 µM, and each was added to the reaction in 0.2 µl DMSO. The hits generated from this secondary screen were used for follow-up assays and further development.

2.5 Results

TAO2 production from insect cells

SF9 cells were the first system used for the expression and purification of TAO2. Cell were infected for 48 hours and TAO2 expression was observed in the whole-cell lysate via western blot (Figure 2.1). Unfortunately, attempts to purify TAO2 from SF9 did not yield substantial protein, and western blots of the nickel column factions showed significant laddering (Figure 2.2). Believing that the laddering was caused by uncontrolled proteolysis, additional protease inhibitors were added to the system in the form of benzamadine and leupeptin. After addition of these inhibitors, a recovery of approximately 0.1–0.2 mg of TAO2 was recovered per liter of SF9 cells as assessed by Bradford assay.

In order to improve these yields, SF9 cells were replaced with *T. ni* cells, and the expression and purification was reattempted. The change in cell type increased the yield to 1-2 mg per liter of cells (Figure 2.3). Subsequent purifications used *T. ni* cells due to the dramatically improved protein yields.

Screen optimization

Condition optimization was carried out as described in the approach. A concentration of 0.005 mg/ml TAO2 was sufficient to consume 50% of the added ATP solution over the course of 100 minutes in the presence of 1 µl DMSO. The quality of the assay was assed by

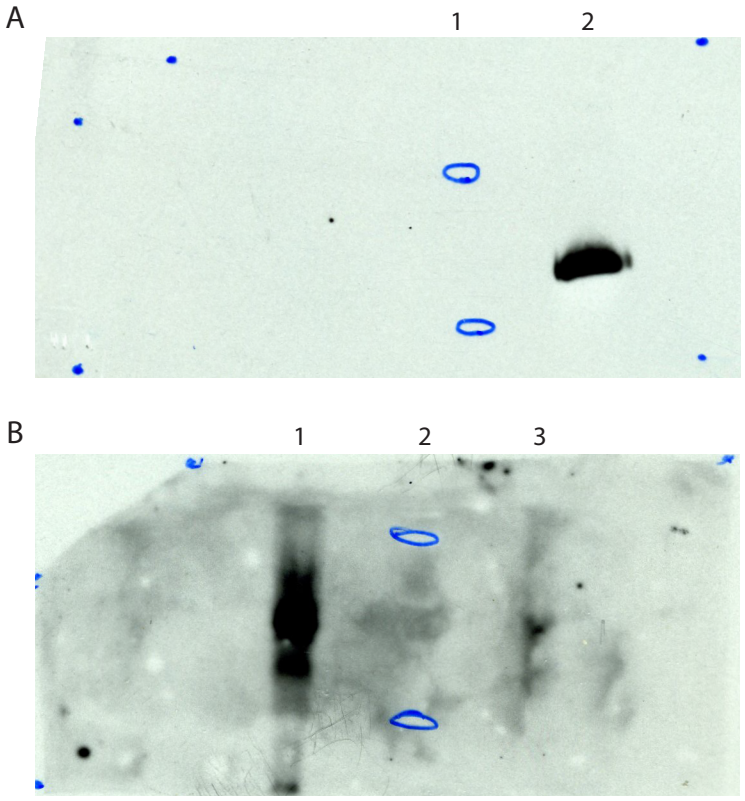

Figure 2.1: **Western blot of TAO2 1–320 expression in SF9 cells.** The presence of TAO2 1–320 is observed in SF9 cell lysate after infection with prepared virus. A blot with a control sample of TAO2 1–320 provided by the Goldsmith lab (A, lane 2) is compared to SF9 cell lysate (B, lane 1). Blue dots indicate the edges of the gel. Blue circles indicate the red bands of Biorad Precision Plus molecular weight marker. A mock culture of SF9 without virus being introduced is shown in panel B, lane 3.

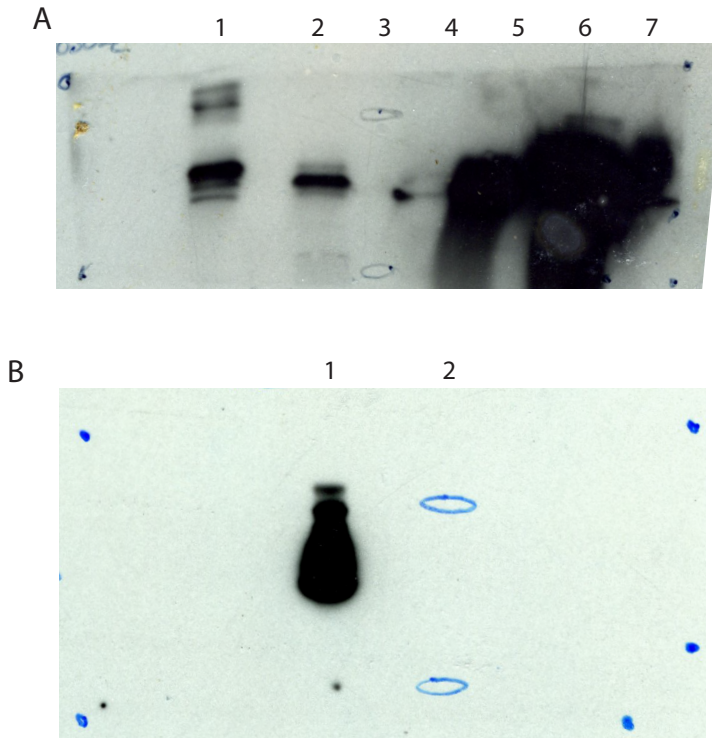

Figure 2.2: **Purification of TAO2 from SF9 cells.** TAO2 1–320 was purified from SF9 cultures through nickel IMAC. A sample was tested every 5 ml of nickel column elution (A, lanes 1-2, 4-7). The molecular weight marker is shown in lane 3. After nickel chromatography, the protein was concentrated and the His-tag was removed with TEV. This protein was then passed through a nickel-sepharose plug. The resulting flowthrough was collected and blotted (B). Lane 1 shows significant laddering post nickel. Lane 2 is the molecular weight marker.

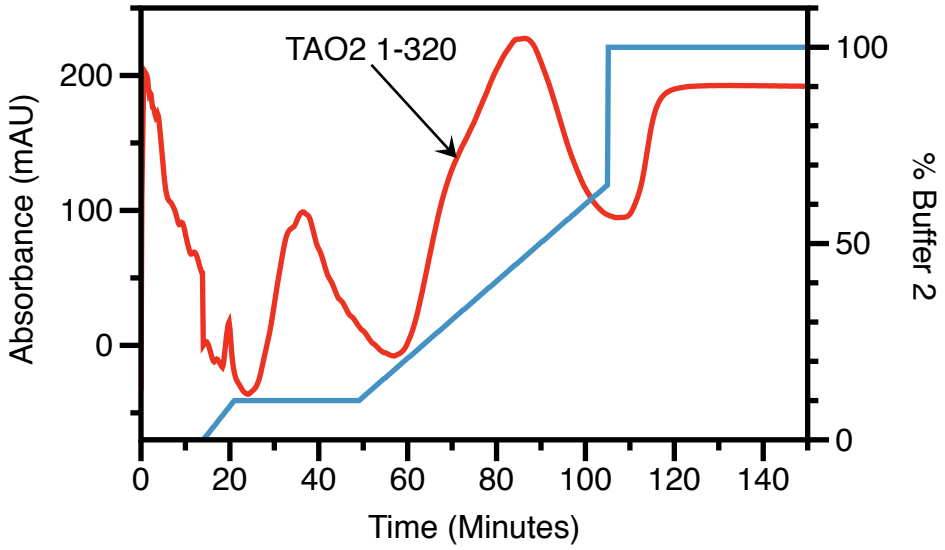

Figure 2.3: **TAO2 1–320 purification from *T. ni* via nickel IMAC** The trace of the elution of TAO2 1–320 is shown. Buffer B contains 250 mM imidazole, as compared to the starting 10 mM imidazole. 10 mg of TAO2 1–320 was isolated from the large labeled peak after concentration as assessed by Bradford assay.

Z' factor, which is $= 1 - \frac{3(\sigma_p + \sigma_n)}{|\mu_p - \mu_n|}$, where σ_p and σ_n are the standard deviations of the positive and negative controls, respectively, and μ_p and μ_n are the mean values of the positive and negative controls. This provides a measure of the significance of the difference between the positive and negative controls. Z' factor of the hand-pipetted plates were in the range of 0.6–0.7, suggesting the assay could identify inhibition of TAO2 with high significance. These conditions were then used for the full screen.

Screen quality

The average Z' factor of the initial screen across all plates was 0.77, indicating a strongly significant difference between the positive and negative controls. In the case of the full screen, all added compounds are taken to be 'negative controls,' as it is expected that the majority of compounds will not have inhibitory activity. The confirmation screen, in contrast, had a specific set of wells that were used as negative controls, with only DMSO added. The average Z' factor across all plates for the confirmation screen was 0.52, which is also excellent and indicative of a strongly significant difference between positive and negative controls.

Identified candidate TAO2 inhibitors

Of the over 200,000 compounds tested in this screen for inhibitory activity against TAO2, 1645 compounds demonstrated inhibition greater than three standard deviations above the mean negative control value in the initial screen. In the subsequent re-screen that tested all 1645 compounds under three different inhibitor concentrations (1 µM, 3.3 µM, and 10 µM), 1181 compounds maintained an inhibition greater than 3 standard deviations above the negative control at the 10 µM concentration. 432 compounds were greater than 10 standard deviations above the negative control mean.

The mean inhibition of compounds in the initial 200k screen was 10 standard devia-

tions above the negative control mean was 58% of the positive control. Because the positive control should almost completely abrogate kinase activity, this suggests that the mean IC_{50} of those compounds was approximately 5 µM under these conditions. Unfortunately, a large number of the top 50 inhibitory compounds were mixtures derived from natural product fractionation, and as such it is difficult to derive the source of the activity in these samples. Many of the identified compounds shared scaffolds with other compounds in the screen. This allows for tentative structure-activity relationships to be determined on the basis of the differential inhibition of each of these compounds. One example of such a scaffold is presented in Figure 2.4. This may provide a useful framework for future approaches to compound optimization in the future.

2.6 Discussion

The 200k screen was able to identify over 100 potential strong inhibitors of TAO2 within the context of the assay. Because of the assay design, false positives are unlikely—if the inhibitor decreased the activity of the reporting luciferase, then the compound would not show up. For this reason, we believe that each of these compounds has some inhibitory activity. Unfortunately, the screen was unable to determine the specificity of binding, if any, whether or not the compounds were ATP competitive, or whether or not the compounds in question would be active either in cells or *in vivo*.

In order to confirm that these compounds bind to TAO2, and to determine their strength of inhibition, secondary assays are required. Furthermore, it is important that these secondary assays use an orthogonal method to measure inhibition of kinase activity. Because the number of compounds has been greatly reduced, the follow-up assays do not have to be as amenable to automation. After the potential series of compounds is further reduced by these secondary assays, efficacy in cells can be tested. The follow-up assays are discussed in the next chapter.

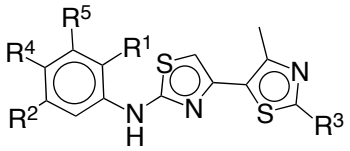

Compound	R^1	R^2	R^3	R^4	logIC_{50} (nM)	Compound	R^1	R^2	R^3	R^4	IC_{50}
4469-0677	H	NO2		H	-1.1 ± 0.26	4469-0678	H	NO2		H	-0.27 ± 0.16
6518569	H	H		NO_2	-0.86 ± 0.28	4469-0658	H	H		NO_2	-0.15 ± 0.13
8010-3863	H			H	-0.71 ± 0.21	4112-3475	OMe	H		H	0.00 ± 0.08
4112-3602	H	Me		H	-0.40 ± 0.15	4469-0723	OMe	Cl	NH_2	H	0.77 ± 0.12
4469-0724	OMe	Cl		H	-0.31 ± 0.14	5760172	OMe	H	NH_2	H	
4112-3604	OMe	H		H	-0.24 ± 0.05	4469-0676	H	NO2	NH_2	H	0.67 ± 0.08
						6554706	H	H	NH_2	NO_2	0.61 ± 0.16
						5758357	H		NH_2	H	0.87 ± 0.10

Figure 2.4: **An inhibitory scaffold identified in the 200k screen.** One series of compounds with similar chemical structure identified from the 200k screen. IC_{50} values are estimated from the three different inhibitor concentrations tested in the re-screen.

Chapter 3

Characterization of inhibitory activity of compounds against TAO2

3.1 Introduction

After the initial set of hits had been identified from the high-throughput screening, each of the compounds had to be acquired and individually characterized. This characterization would allow us to determine which compounds would be most useful for going forward with labor- and cost-intensive cellular assays and specificity assays. Ideally, compounds would be found that have high affinity, are chemically tractable (one can make a series of derivatives for structure-activity-relationship studies), and can be easily acquired. However, the pool of hits generated from the 200k screen is too large to completely characterize, so some method of 'triaging' the compounds before characterization is important. After this triage step, the compounds can be assayed for their ability to inhibit TAO2 1–320 kinase activity *in vitro*. This will give a series of compounds that can be ranked according to efficacy for subsequent cellular assays.

3.2 Approach toward compound characterization

The triage method chosen was Differential Scanning Fluorimetry (DSF). DSF measures the thermal stability of proteins through the use of a lipophilic dye. As the temperature increases, the protein becomes less stable in solution and begins to denature. This denaturation exposes interior hydrophobic pockets, which allow the lipophilic dye to bind. This binding insulates the dye from the surrounding water, preventing quenching and allowing it

to fluoresce. This fluorescence readout, therefore, allows you to detect protein unfolding in the face of thermal challenge, i.e. thermal stability.

Thermal stability increases from protein/small-molecule binding events. Because specific small-molecule binding lowers the energy of the protein/small-molecule complex relative to the energy of the unassociated protein and unassociated small-molecule, additional energy is required to first disassociate the protein, then denature it. This additional energy requirement is the measured 'stabilization.' If you measure the stability of a protein before and after exposure to a small molecule, you are able to determine how much the small molecule stabilizes the protein, which is associated with its affinity.

DSF was chosen over other methods because it detects binding in a manner completely orthogonal to the luciferase-and-ATP dependent Kinase-Glo assay. Furthermore, it is capable of distinguishing between broad inhibition due to nonspecific interactions (e.g. denaturation) and direct binding, as nonspecific interactions tend to broaden DSF peaks and reduce stability, as opposed to increase it. Finally, DSF can be conducted in a 96-well format, allowing many different conditions and compounds to be tested in the same assay.

Once this initial triage was completed, the inhibitory strength of the remaining compounds of interest was tested. There were two methods used to identify inhibitory strength—Kinase Glo and radiometric activity assays. Kinase Glo was attempted first as the technique is much simpler and can be conducted in a high-throughput manner, as described in Chapter 2. Unfortunately, the relative binding affinities as determined by DSF did not track well with several compounds measured by Kinase Glo. Suspecting that the compounds may be acting against the luciferase in the Kinase Glo assay, radiometric activity studies were conducted. Radiometric activity assays measure incorporation of γ-^{32}P-labeled ATP onto a kinase substrate. This assay takes significantly longer to perform than the Kinase Glo assay, but it measures kinase activity directly and is extremely sensitive. Radiometric assays confirmed that the more tightly binding compounds were indeed stronger inhibitors of TAO2 1–320,

and radiometric assays were used for all subsequent activity measurements.

3.3 Methods and Materials

Differential scanning fluorimetry binding assays of selected compounds against TAO2

1. A solution of 5 µM TAO2, 50 mM $MgCl_2$, 50 mM HEPES pH 7.5, and 2.5x Sypro Orange (Life Technologies) was made. Compound or controls were added to the solution if binding was assayed.

2. 25 µl of the reaction solution was added to the wells of a Biorad Multiplate 96 well clear PCR plate. The plate was covered with a Biorad Microseal 'B' seal.

3. Plates were read in a Biorad CFX96 Real-Time PCR system. The temperature was increased from 4 °C to 80 °C, with fluorescence measurements being taken every 0.5 °C in the 6-FAM Fluorescein channel.

4. The fluorescence response to heat curve was fit to binding isotherm in order to determine the inflection point, which was taken as the melt temperature (T_m).

Kinase-Glo assays of selected compounds against TAO2

1. 20 µl of a solution of 50 mM HEPES pH 7.4, 50 mM MgCl2, 1.27mg/ml MBP and 0.005 mg/ml TAO2 was added to a 384 well Corning plate.

2. 0.2 µl of compound (various concentrations, DMSO vector) or DMSO negative control were added to each well.

3. 10 µl of 50 µg/ml ATP solution was added to each well.

4. The plates were incubated at RT for 100 minutes.

5. 20 µl Kinase Glo (Promega) was added to each well, and allowed to incubate for 10 minutes under agitation.

6. Luminescence was read on an Envision Multilabel plate reader.

Radiometric activity assays of selected compounds against TAO2

1. A reaction solution of 0.02 mg/ml TAO2, 50 mM $MgCl_2$, 50 mM HEPES pH 7.5, 1 mg/ml MBP, and increasing compound concentration was made. The compound/DMSO solution was 5% by volume in the final reaction mixture.

2. An ATP solution of 1:20 0.1 µCi/ml ^{32}P γ-labeled ATP:1 mg/ml ATP was made.

3. 10 µl of ATP solution was added to 50 µl of reaction solution, and allowed to react for 30 minutes.

4. Reactions were stopped by blotting onto filter paper, then submerging the paper in 10% trifluoroacetic acid.

5. Paper was washed 4 times in TFA, then put into scintillation vials.

6. 5 ml Complete Counting Cocktail 3a70B (Research Products International Corp.) was added, and the vials were counted on a Beckman scintillation counter for 10 minutes.

3.4 Results

Compounds were tested *via* DSF to observe direct binding

Compounds identified in the 200k screen were ranked according to their apparent potency. Many compounds of high ranking had similarity to other species in the screen—for subsequent assays, preference was given for compounds that did not share scaffolds with other compounds in the screen. These chosen species were assayed *via* DSF (Figure 3.1). Surprisingly, a number of compounds that appeared to have potent inhibitory activity did

not produce a large positive T_m shift. Many of them produced a strong *negavite* shift, suggesting destabilization. It was assumed that these compounds were causing nonspecific precipitation and aggregation, and as such they were not used for followup activity assays.

Compounds were largely selective for TAO2 binding when compared to other kinases

The compounds that produced positive T_m shifts were then examined in the context of other kinases in the MAPK cascade to determine whether or not the compounds identified in the 200k screen were selective. The difference in the T_m shifts between TAO2 and p38α and TAO2 and ASK1 were significant in most cases (Figure 3.2.) While several compounds interacted with p38α and ASK1 as strongly as they interacted with TAO2, most did not. This suggests that the majority of the strongly-inhibitory compounds discovered in the 200k screen are at least partially selective for TAO2, and are not pan-kinase inhibitors.

Compounds discovered in the 200k screen are inhibitory

Compounds that produced positive T_m shifts, and appeared to have drug-like properties as assessed by Dr. Jef DeBrabander were characterized by radiometric activity assay. Every compound discovered in the 200k screen tested using radiometric assay was shown to have some measure of inhibitory activity (Figures 3.3–3.8.) Furthermore, compounds that appeared more potent on the 200k screen tended to have higher inhibition as assessed by radioassay. Based on this, relative ranking in the 200k appears correlative with potency of the compound. If this is true, we identified > 300 previously unknown TAO2 kinase inhibitors with IC_{50} values better than 100 µM.

Potent inhibitors were discovered

In addition to finding a wide range of compounds that had reasonable affinities ($IC_{50} <$ 100µM), several compounds were found that appeared to tightly bind by orthogonal assay

($IC_{50} < 10$ µM, Figures 3.3, 3.6–3.8.) Unfortunately, not all of the compounds that appeared to be most potent in the screen were available for purchase. If the trends of the 200k assay represent relative inhibitor potency, there are > 150 compounds with known structures that can be expected to have IC_{50} values better than 10 µM. These IC_{50} values are low enough to have possible efficacy both in cells and *in vivo*.

3.5 Discussion and Conclusions

The 200k screen had a high real discovery rate

Every compound identified in the 200k screen and tested using a radiometric inhibition assay demonstrated inhibitory activity. This suggests that the majority of the compounds identified in the 200k screen are, in fact, inhibitors of TAO2 1–320 kinase activity. This supports the idea that the assay has a low false-positive rate, as predicted from the assay mechanism, making subsequent triage of prospective inhibitors easier. While the false-positive rate is low, it was not possible to determine what the false-negative rate was for this assay using our methodology. Nevertheless, the Kinase-Glo assay appears to be a good technique for the identification of kinase inhibitors in a high-throughput format.

Neither Kinase-Glo nor T_m are capable of accurately determining IC_{50}

While Kinase-Glo was able to identify inhibitory compounds quite effectively, it was not as effective at accurately determining compound IC_{50} values. Several compounds tested both radiometrically and with Kinase-Glo showed between 2 and 10 fold differences in calculated IC_{50} between the two techniques. This may be due to inhibition of luciferase by the added compound, or absorption of the luciferase fluorescence by the added compound. In order to avoid additional experiments to distinguish between these two possibilities, radiometric assays were used to generate accurate IC_{50} values.

Similarly, T_m, as determined by DSF, was not predictive of IC_{50}. While the most

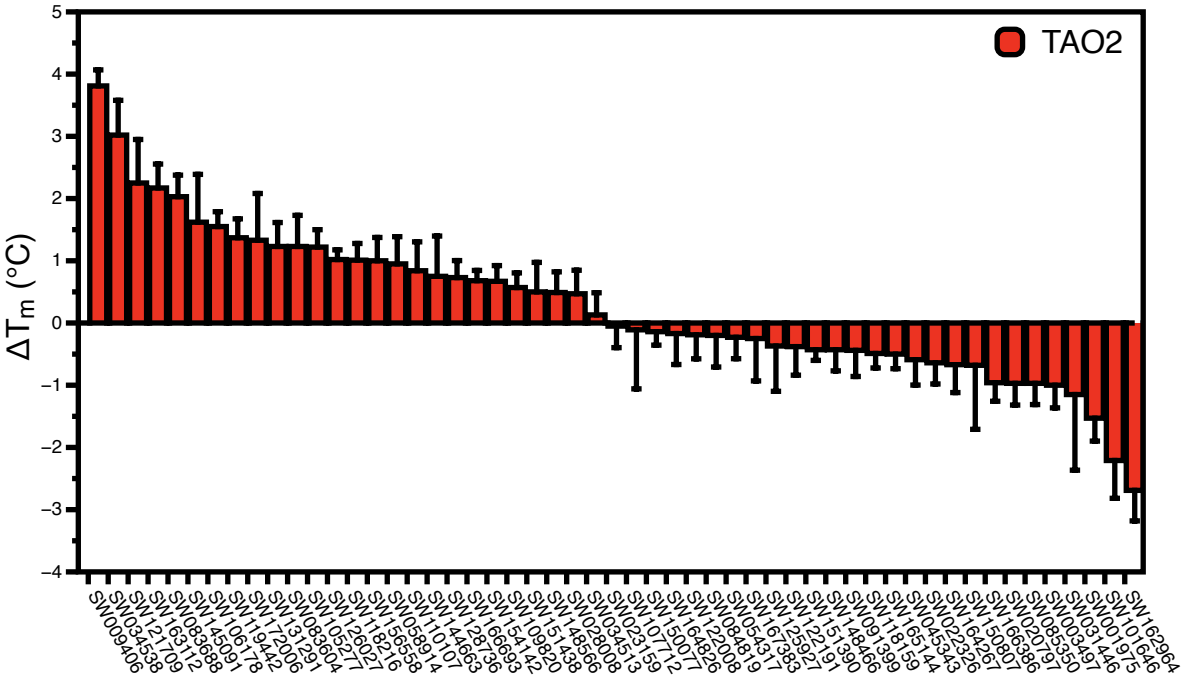

Figure 3.1: **DSF assays of selected TAO2 Inhibitors.** Selected compounds from the 200k screen were assayed using DSF. Higher T_m shifts represent increased stabilization to challenge by increasing temperature. The T_m was calculated as the point of greatest inflection on a graph of RFU vs. temperature (°C).

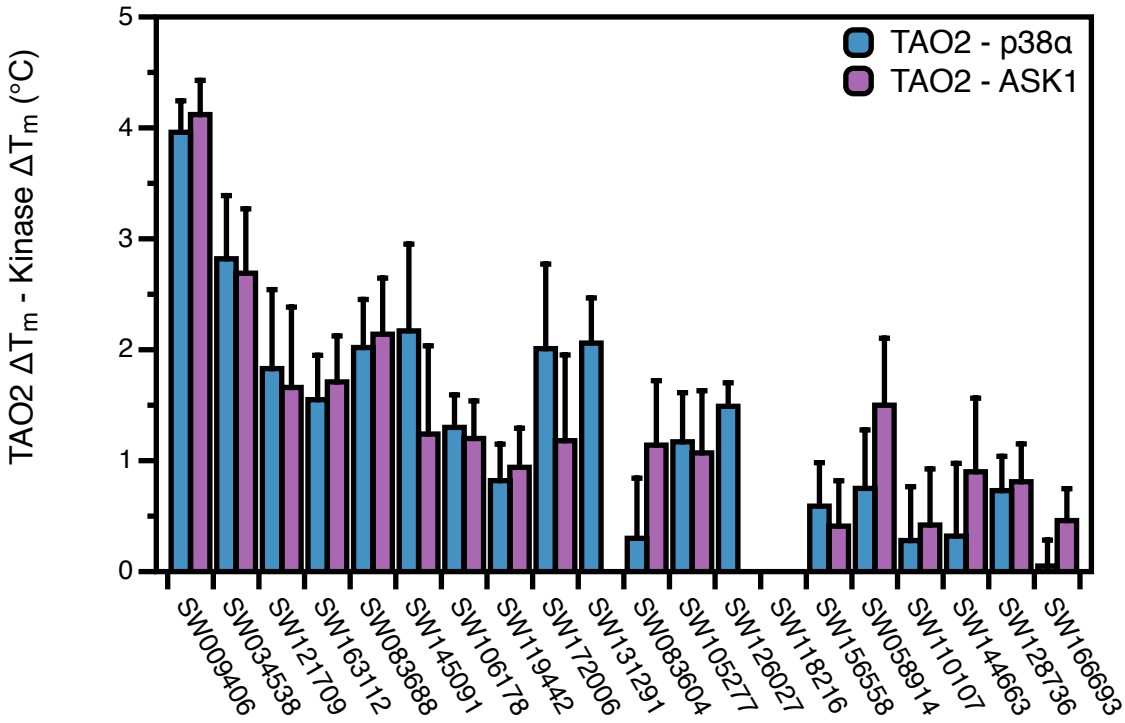

Figure 3.2: **Compound Selectivity as Assessed by DSF.** DSF assays of compounds that generated positive T_m shifts in TAO2 1–320 as determined in Figure 3.1 were examined in the context of other kinases. Their T_m shifts were determined, and subtracted from the T_m shift determined for TAO2. The difference between the two values suggests selective interaction.

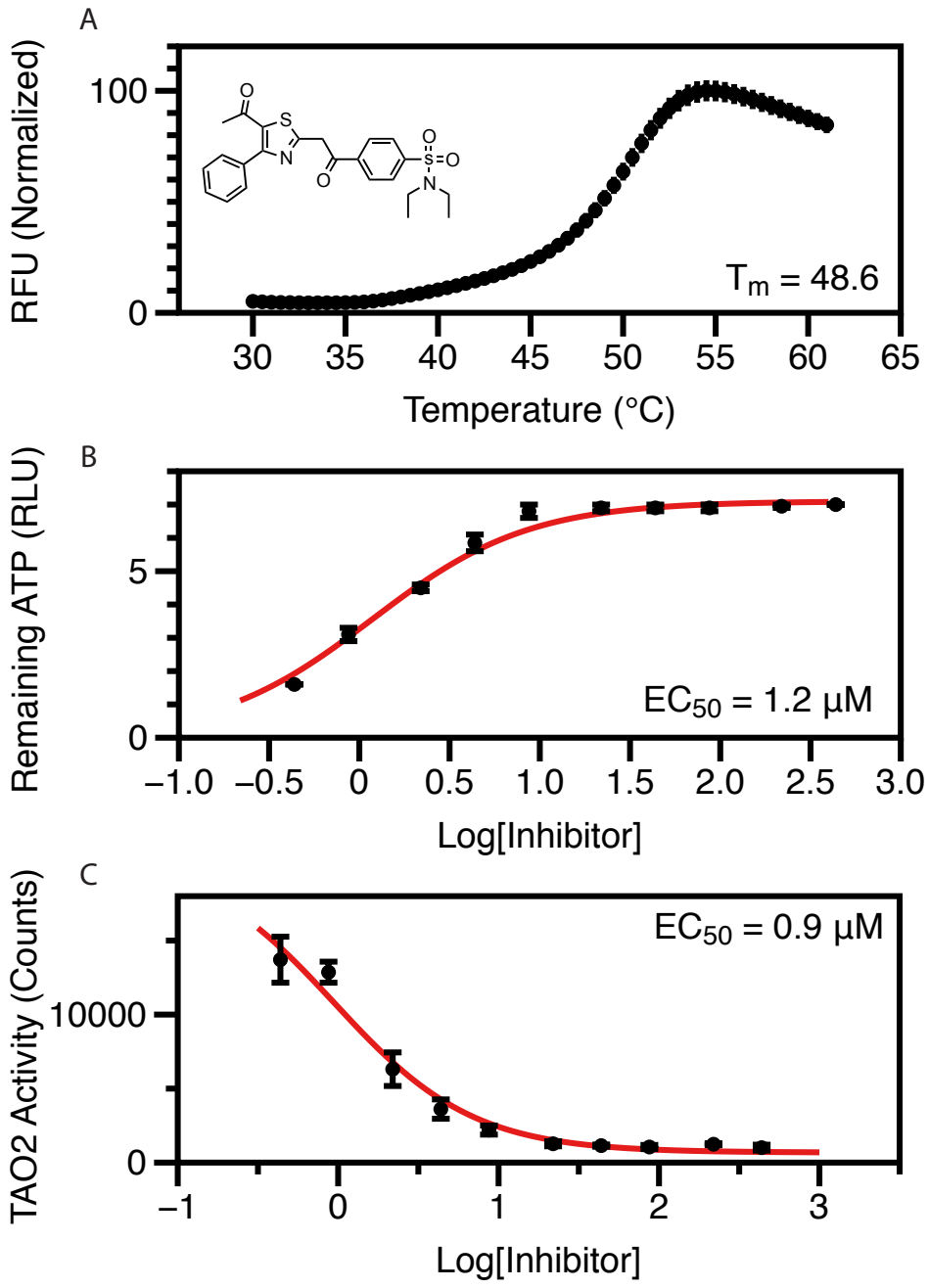

Figure 3.3: **Characterization of SW009406.** Compound SW009406 is characterized by DSF (A), Kinase-Glo (B), and radiography (C). T_m is determined by curve fitting to a sigmoidal dose-reponse and determination of the inflection point. EC_{50} for B and C determined by curve fitting to a sigmoidal inhibition dose-response.

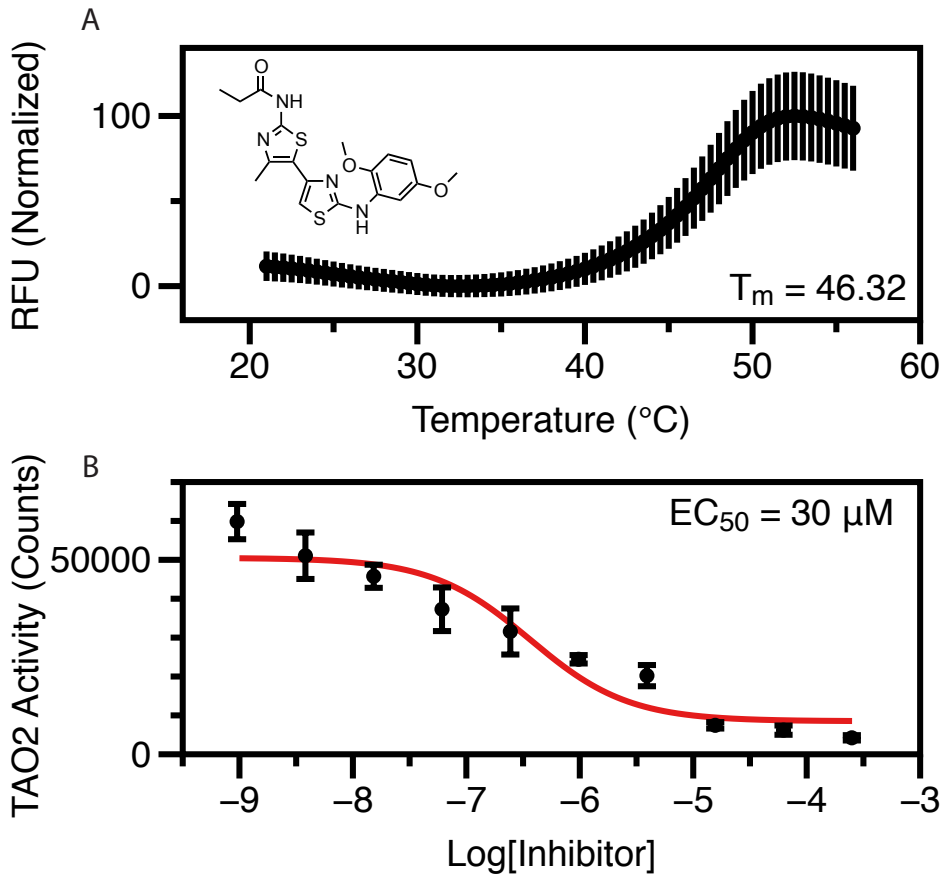

Figure 3.4: **Characterization of SW034538.** Compound SW034538 is characterized by DSF (A) and radiography (B). T_m is determined by curve fitting to a sigmoidal dose-reponse and determination of the inflection point. EC_{50} was determined by curve fitting to a sigmoidal inhibition dose-response.

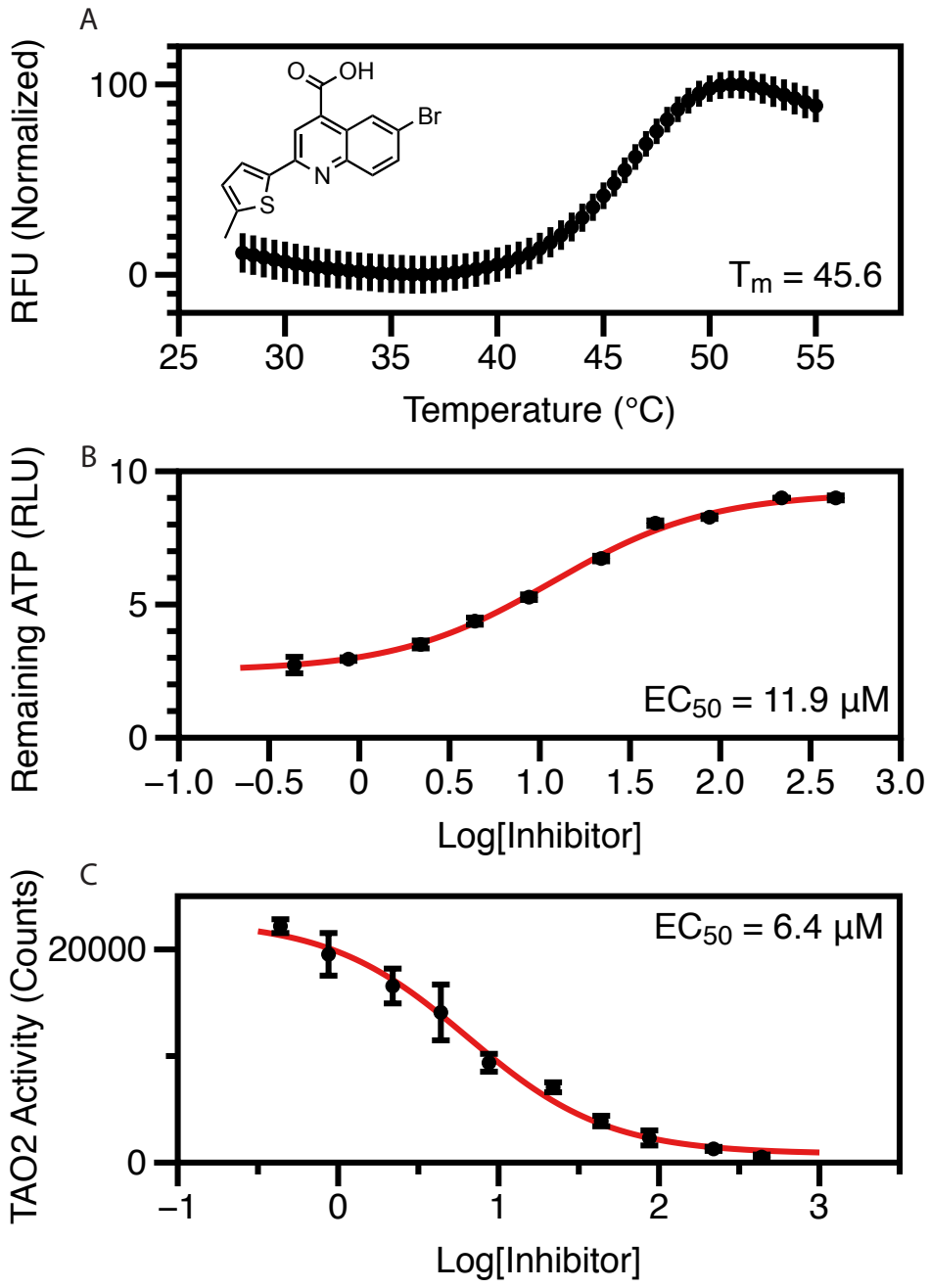

Figure 3.5: **Characterization of SW049966** Compound SW049966 is characterized by DSF (A), Kinase-Glo (B), and radiography (C). T_m is determined by curve fitting to a sigmoidal dose-reponse and determination of the inflection point. EC_{50} for B and C determined by curve fitting to a sigmoidal inhibition dose-response.

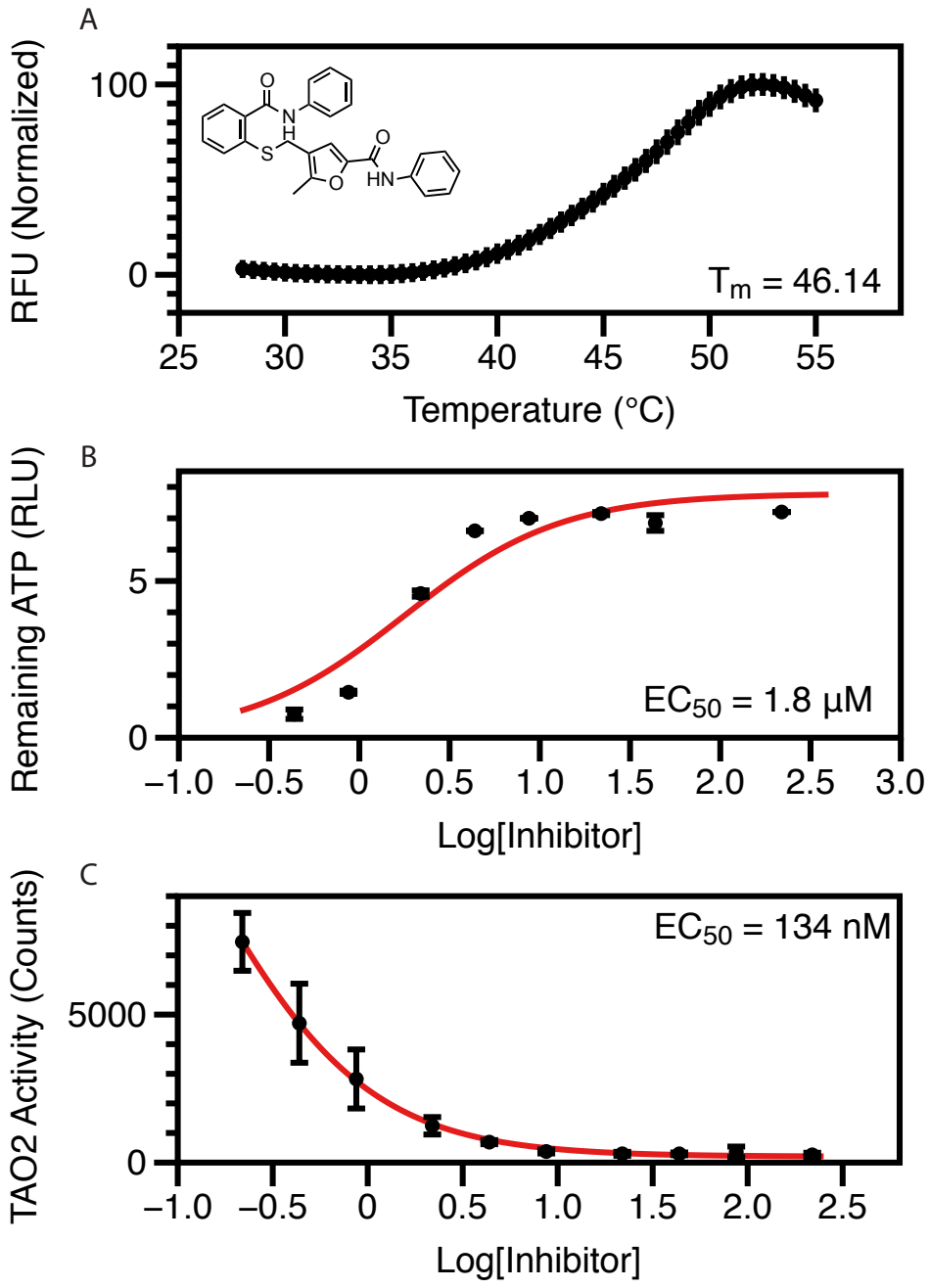

Figure 3.6: **Characterization of SW055060** Compound SW055060 is characterized by DSF (A), Kinase-Glo (B), and radiography (C). T_m is determined by to a sigmoidal dose-reponse and determination of the inflection point. EC_{50} for B and C determined by curve fitting to a sigmoidal inhibition dose-response.

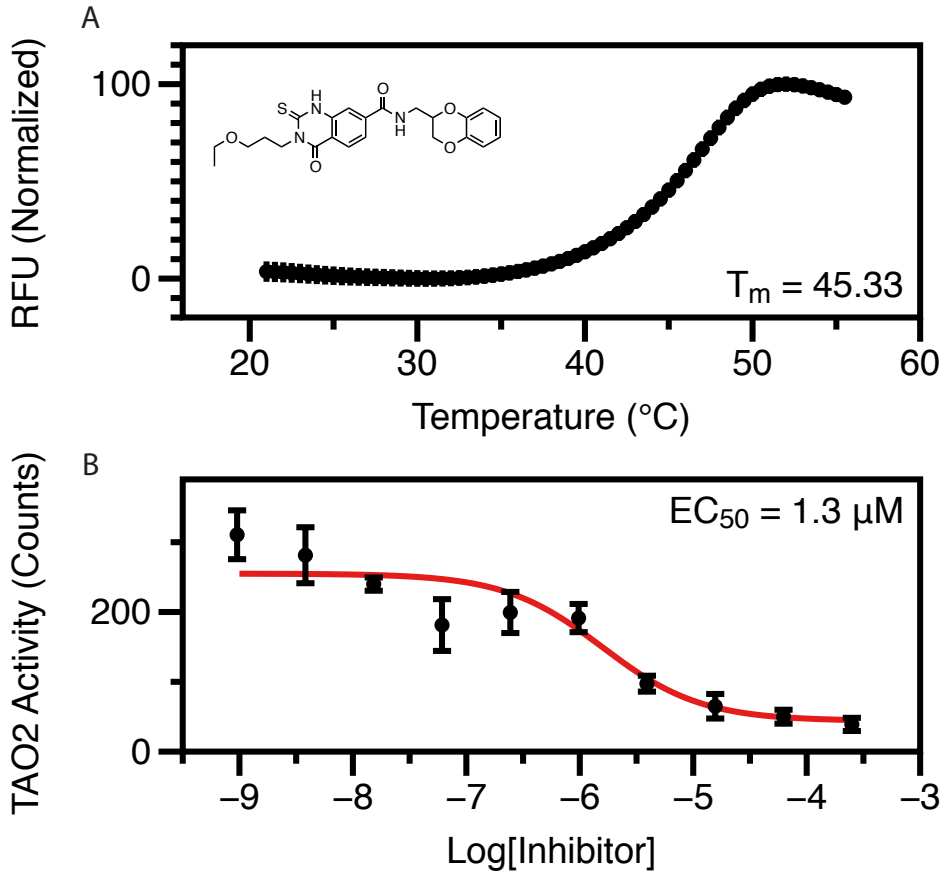

Figure 3.7: **Characterization of SW083688** Compound SW083688 is characterized by DSF (A) and radiography (C). T_m is determined by curve fitting to a sigmoidal dose-reponse and determination of the inflection point. EC_{50} for B determined by curve fitting to a sigmoidal inhibition dose-response.

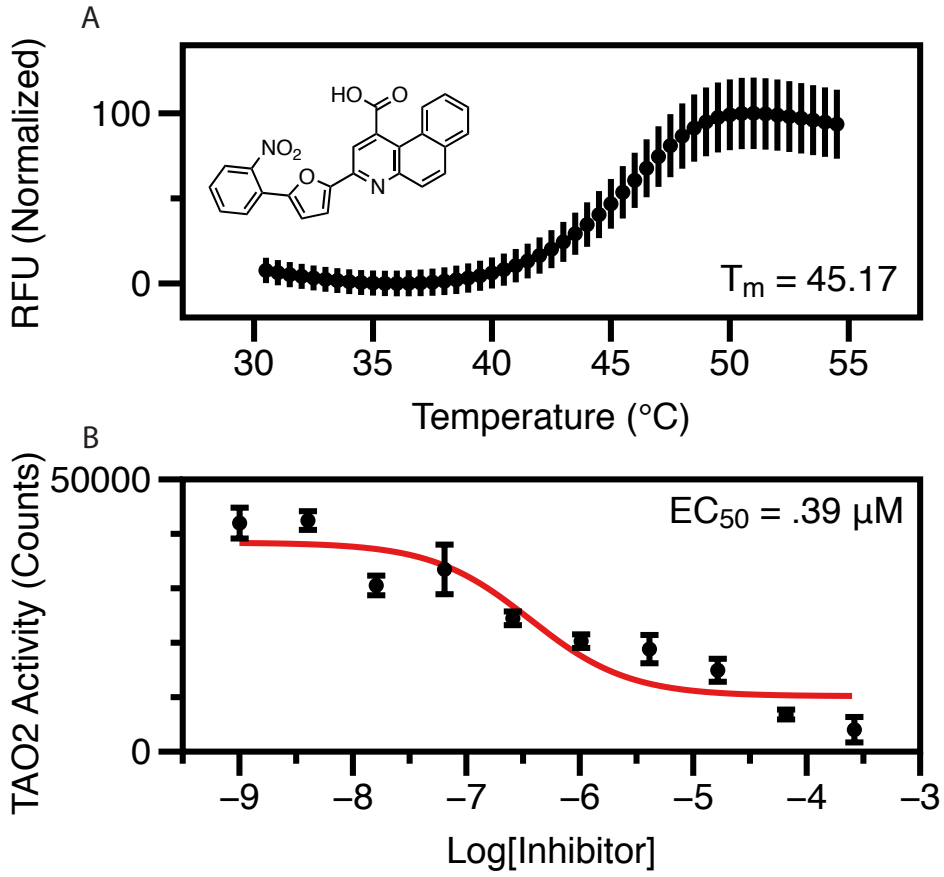

Figure 3.8: **Characterization of SW163112** Compound SW163112 is characterized by DSF (A) and radiography (B). T_m is determined by curve fitting to a sigmoidal dose-reponse and determination of the inflection point. EC_{50} for B determined by curve fitting to a sigmoidal inhibition dose-response.

potent inhibitor had a high T_m value, the other compounds that were both tested by radiometric assay and by DSF had very similar T_m values but widely varying (10 fold) IC_{50} values. This may be due to the different entropic vs. enthalpic contributions that favor binding of the inhibitor to the protein. As temperature increases, the entropic contribution will change, and the enthalpic contribution will not. This gives a different temperature dependence depending on the different binding modalities of the compound in question. While this means that the DSF analysis can inform somewhat on the binding mechanism of the compound, it makes determination of IC_{50} purely on T_m under these conditions impossible.

Many high-affinity inhibitors of TAO2 were found

In addition to finding a large number of TAO2 inhibitors, several of the inhibitor compounds were found to be high-affinity. By radioassay, compound SW055060 was the most potent examined, with a calculated IC_{50} of 134 nM. Because this is calculated in a background of ATP, the actual k_d is substantially lower. These affinities are well within the range of other kinase inhibitors that have entered the clinic, suggesting that some compounds discovered here are potent enough for *in vivo* testing. Several scaffolds appear to 'repeat' within the top discovered inhibitors, suggesting that some SAR may have been performed in the screen itself. This will narrow down subsequent follow-up work to identify the active moiety.

Chapter 4

Structural analysis of inhibitor binding of TAO2

4.1 Introduction

Once a selection of compounds had been identified to be at least partially selective and potent inhibitors of TAO2, it became useful to determine the molecular mechanism by which they bound. This information is useful for several reasons— not only does it inform which parts of the inhibitor are most important for binding, which is useful for subsequent SAR studies, it can also shed light on additional, possibly regulatory, binding sites on TAO2. Examples of these additional binding sites have been found in other MAPK cascade components, suggesting new modes of kinase regulation [27]. Furthermore, these sites tend to vary significantly between kinases, and targeting them could lead to inhibitory compounds more selective than those that compete in the more homogenous ATP binding site.

4.2 Methods and Materials

Robotic Crystallization Condition Screening of TAO2 1–320

It is not currently possible to predict the conditions under which a given protein will crystallize. As such, a wide variety of different solution conditions must be tested in order to produce protein crystals suitable for crystallography. One of the means of doing this is through robotics. This allows for a large number of different conditions to be tested while using a small amount of potentially valuable protein and precipitant solution.

1. TAO2 1-320 protein solution was produced as described in Chapter 2. Final conditions were 1 mg/ml TAO2 1–320, 50 mM Tris pH 8.0, 1 M NaCl, 10% glycerol.

2. 0.2 µl of protein solution was loaded into sitting-drop 90-well plates using a Crystal Phoenix crystallography dispenser (Art Robbins Instruments).

3. 100 µl of well solution was added to the plate wells. The Index, PEGRx (Hampton,) JCSG, ComPAS, Classics (Qiagen), and PACT (Molecular Dimensions) 96-condition screens were used.

4. 0.2 µl of well solution was added to each of the sitting-drop wells.

5. The plates were sealed and incubated at 20 °C.

Condition optimization

Once preliminary crystallization conditions were found *via* robotic screening, the components of that condition were optimized to maximize crystal size and recapitulate the conditions in hanging-drop format. Due to variability in the protein preparation and the exact ratios of protein-solution/precipitate, a two-dimensional optimization was performed. One axis was concentration of the PEG in the precipitant solution, the second axis was the pH. A screen surrounding the hit condition, 0.2 M $MgCl_2$, 0.1 M Bis-Tris pH 6.5, and 25% PEG 3350 was developed.

1. 200 µl of precipitant solution was added to each well of a VDX48 plate with sealant (Hampton). 48 precipitant conditions were tested on a gradient of 15–35% PEG 3350 and pH 5.5–7.5 Bis-Tris.

2. 1 µl protein solution was placed on a siliconized 12 mm circle cover slide (Hampton).

3. 1 µl of precipitant solution was added to the droplet.

4. The cover slides were inverted and placed over the plate wells.

5. The plates were then incubated at 20 °C.

Additive screening

In order to further optimize the crystallization conditions determined in the pH/PEG concentration screen, an additive screen was used. We used the HR2-428 additive screen (Hampton). The additive screen consists of 96 different compound solutions which can be added to the previously determined crystallization condition. This results in an additional 96 different potential crystallization conditions. The previous condition refinement determined that a precipitant solution consisting of 30% PEG 3350, 0.1 M Bis-Tris pH 6.5, and 0.2 M $MgCl_2$ produces the largest TAO2 1–320 crystals.

1. 200 µl of precipitant solution was added to each well of a VDX48 plate with sealant (Hampton).

2. 1 µl protein solution was placed on a siliconized 12 mm circle cover slide (Hampton).

3. 0.8 µl of precipitant solution was added to the droplet.

4. 0.2 µl of solution from the additive screen was added to the droplet.

5. The cover slides were inverted and placed over the plate wells.

6. The plates were then incubated at 20 °C.

Crystal Seeding

Crystal seeding is a technique in which you crush previously formed crystals, then introduce those 'seeds' into a well containing your precipitate and your protein of interest. These smaller seed crystals can then serve as points of nucleation, which allows the crystals

to grow under conditions that might not otherwise be able to form crystals, either due to a precipitate or protein concentration that is too low. Because the crystallization condition is not, by itself, capable of nucleating crystals, the only point of nucleation is the introduced seed, which should, in theory, increase the size of the crystals formed by decreasing the number of crystals formed.

I attempted crystal seeding by using a 'Seed Bead' (Hamption), following the manufacturers' instructions. In short, both the bead and crystals are introduced to a to a vial, and then vial is then mixed *via* vortexing. The solution is then diluted into three sets of conditions: 1:10, 1:100, and 1:1000. Three sets of crystallization conditions were tested, with decreasing amounts of the precipitate PEG 3350: 30%, 27%, 24%, and 20%. Hanging-drop crystallization was performed as described above using these different crystallization conditions, with 0.5 µl of the 'seed solution' being added to each drop.

Cryopreservation of TAO2 crystals

The crystals had to be cryopreserved in order to survive being mounted for data collection. Cryopreservation decreases the amount of water in the crystal, allowing for vitrification on temperature reduction, instead of forming potentially disruptive water crystals.This is typically performed by soaking the crystals in precipitant solutions with progressively increasing concentrations of low-weight PEGs.

1. A series of cryoprotection solutions were generated using the precipitant conditions (30% PEG 3350, 0.1 M Bis-Tris pH 6.5, and 0.2 M $MgCl_2$). The conditions started with an addition of 5% PEG 200 with an equivalent volume of water displaced. A set of 7 cryopreservation conditions were generated, with PEG 200 concentration increasing to 35%, and the PEG 3350 concentration decreasing to 22%.

2. Crystals were soaked in each of the 7 conditions, in order of increasing PEG 200 concentration. Crystals were soaked for 10 minutes per condition.

3. Crystals were allowed to soak in the final condition for 20 minutes for final dehydration.

4. Crystals were flash frozen in liquid nitrogen after the final condition.

Inhibitor soaking of TAO2 crystals

The goal of the crystallography project was to determine the mechanism of inhibitor binding with TAO2 1–320. As such, soaking inhibitors of interest into the crystal was a high priority. Crystals were treated as above, with inhibitors added to a final concentration of 25 µM in the final cryopreservation condition. The crystals were soaked in this final condition for a total of 30 minutes before flash-freezing in liquid nitrogen.

Data collection and processing

Data were collected at UT Southwestern Medical Center and at the Advanced Photon Source at Argonne National Laboratories. The UTSW data were collected at 100 °K on an RAXIS IV image plate using a Cu Kα rotating anode with a wavelength of 1.54 Å. Frames were collected with an 0.5° oscillation and an exposure time of 10 minutes. The data taken at the APS were collected at 100 °K on beamline 19-IDD at a wavelength of 0.979 Å and a 0.5° oscillation. Exposure times were 10 seconds.

4.3 Results

Crystal Optimization

TAO2 1–320 crystallized easily after screening, yielding a condition of 0.2 M $MgCl_2$, 0.1 M Bis-Tris pH 6.5, and 25% PEG 3350. The crystals had a length of 150–200 µm, which was more than sufficient for freezing and structure determination. The additive screen showed that several additives improved the size and consistency of crystal formation (Figures

4.1A –E). Surprisingly, the addition of 2 M NaCl improved the crystals the most, increasing the size to 250 µm (Figure 4.1B). This led to an increase in the NaCl concentration in the isolation buffer from 500 mM to 1 M. The mixing of the precipitant and protein solution was also found to be important (Figures 4.1A and B). Poor mixing yielded a spray of small crystals (A), while more thorough mixing yielded larger, single crystals (B). Attempts to generate larger crystals through seeding did not yield good results, either resulting in no crystals or large sprays of very small crystals.

Data Collection

After crystallization conditions were optimized, the crystals were tested for diffraction. Initial diffraction was only observed to 3.5 Å resolution (Figures 4.2A and B). Believing that the high mosacity and low resolution may be from poor cryoprotection conditions, the cryoprotection gradient was increased from 3 to 7 conditions, and the duration of crystal soaking was improved from 5 to 15 minutes (Table 4.1). Crystals cryopreserved under these modified conditions exhibited improved diffraction and decreased mosacity (Figure 4.2B). These improved conditions were used in tandem with crystal soaking to attempt to determine the mechanism of compound inhibition of TAO2 1–320. Unfortunately, crystals with compound SW034538 soaked in diffracted poorly at the APS, yielding only 3.0 Å data.

4.4 Conclusions

Unfortunately, attempts to crystallize TAO2 to determine the binding modality of different inhibitors were largely unsuccessful. While crystals of TAO2 1–320 were obtained, the crystals did not provide the resolution required to observe the inhibitor binding. While TAO2 1–320 had been previously crystallized by this lab at good resolution, we are currently using a different construct than the one used previously— this change may be responsible for these difficulties. Attempting to soak in the compound did not appear to make the

Table 4.1: TAO2 1–320 Cryopreservation Conditions

Step	Cryopreservation Solution Components					
	PEG 3350	Bis-Tris pH 6.0	Bis-Tris pH 7.0	$MgCl_2$	NaCl	PEG 200
1	30%	50 mM	50 mM	200 mM	50 mM	5%
2	28%	50 mM	50 mM	200 mM	50 mM	10%
3	27%	50 mM	50 mM	200 mM	50 mM	15%
4	26%	50 mM	50 mM	200 mM	50 mM	20%
5	25%	50 mM	50 mM	200 mM	50 mM	25%
6	24%	50 mM	50 mM	200 mM	50 mM	30%
7	22%	50 mM	50 mM	200 mM	50 mM	35%

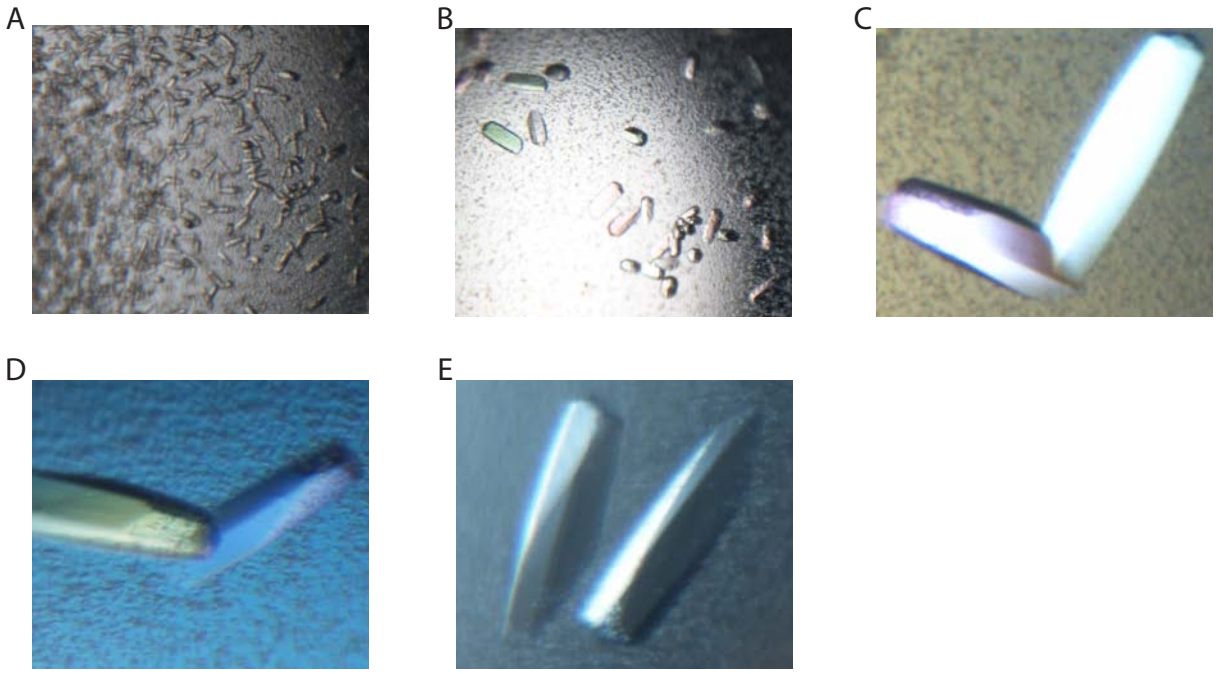

Figure 4.1: **Crystals of TAO2 1–320.** Crystals of TAO2 1–320 were formed as described above. Poorly mixed (A) and well mixed (B) protein/precipitant solutions produced different results. 0.1 M Yttrium(III) Chloride hexahydrate (C), 12% w/v myo-inositol (D), and 30% w/v D-(+)-Trehalose dihydrate (E) each produced large crystals (200 µm)when added to the solution.

diffraction worse.

Future efforts will concentrate on co-crystallization of TAO2 1–320 and the inhibitors. The major disadvantage of this approach is that each compound tested will require a separate screen and different crystallization conditions, which dramatically increases the amount of protein required to produce diffracting crystals for each inhibitor. However, it has the significant advantage that inhibitor binding stabilizes the protein, which can improve the resolution of the produced crystals. Furthermore, no additional 'soak' step is required after the crystals are produced, which can degrade resolution even further. I hope that these efforts will swiftly yield results, and that they will help us determine the mechanism of TAO2–inhibitor binding.

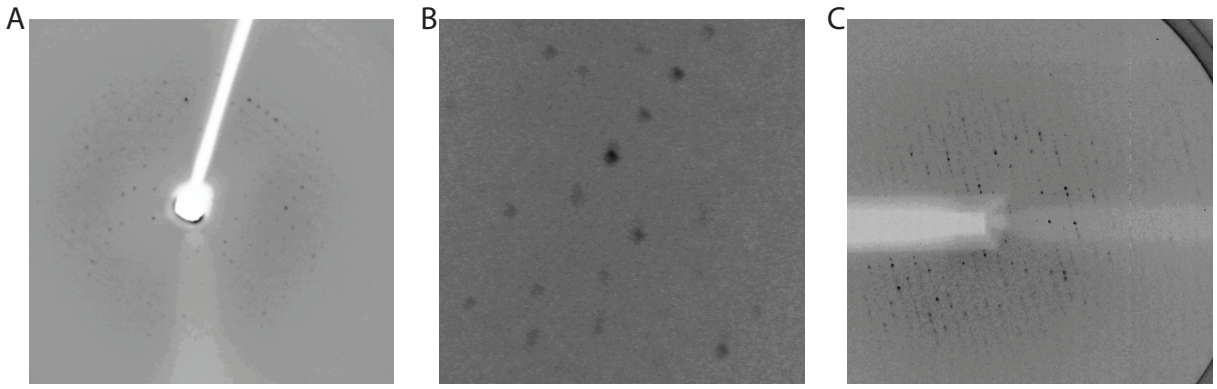

Figure 4.2: **Diffraction of TAO2 1–320 crystals.** Images of TAO2 1–320 diffraction were obtained at UTSW and the APS. Initial crystallization and cryoprotection conditions yielded crystals that only exhibited 3.5 Å diffraction (A and B). Mosascity appeared to be high. Crystals cryopreserved under improved conditions were then soaked with SW034538 and diffracted at the APS (C).

Chapter 5

Characterization of WNK1 chloride sensitivity

5.1 Introduction

Chloride Regulation

One of the kinases that is examined in my thesis is WNK1, which is associated with chloride regulation. As such, I am including a brief literature review of chloride regulation from [28] in order to provide some background. Chloride ion is an important electrolyte involved in blood pressure maintenance, neuronal excitability and nociception, transcellular electrolyte transport, cell volume control, and airway fluid balance [29, 30]. Chloride is uniquely and precisely regulated in diverse cell types; it is maintained at modest (30 to 60 mM) concentrations in most cells, and dips very low (10 mM) in actively transporting epithelia and neurons [31, 32]. Misregulation of chloride is associated with diseases, such as hypertension and epilepsy. Chloride concentration can change radically as a function of osmotic stress [33], and low chloride induces cell cycle arrest [34]. The main transmembrane proteins that set chloride concentrations are members of the solute carrier electroneutral cation-Cl^- cotransporters (SLC12A family, also known as CCCs). Other molecules that influence cellular chloride concentration include members of the SLC26 gene family of exchangers, and chloride channels, such as the cystic fibrosis transmembrane conductance regulator (CFTR) and the γ-aminobutyric acid-gated chloride channel (GABAA) [35–37]. However, the molecules that directly sense and respond to changes in intracellular chloride concentrations are largely unknown.

How chloride binds to proteins in any context is poorly understood. Known chloride-binding sites tend to fall into two structural categories. One category is typified by the ClC

family of chloride channels, which bind chloride through backbone amide and hydrophobic interactions [38]. A similar binding site is observed in the atrial natriuretic peptide (ANP) receptor, a guanyl cyclase involved in volume regulation [39]. Angiotensin-converting enzyme (ACE) is an example of a second structural class of chloride-binding sites [40]. The chloride-binding site in ACE has both hydrophobic and positively charged amino acids. Other proteins that have this binding mode include the serotonin transporter (SERT) and α-amylase [41, 42].

The regulation of transport and other processes through chloride has been demonstrated in various cellular assays, but often, the structural and biochemical mechanisms are poorly defined. Although the chloride-mediated regulation of a few soluble proteins has been defined at both a biochemical and structural level, for example, α-amylase and hemoglobin [41, 43], how changes in chloride concentration regulate other proteins including those in cellular membranes is unknown. For example, chloride regulates the voltage-gated potassium channel KCNB1, increasing the K^+ current as a function of chloride in patch-clamp studies [44]. The chloride-dependent Na^+/H^+ exchanger (Cl-NHE) is activated by chloride, as determined by intracellular pH measurements on exchanger-transfected cells [45]. Both of these processes occur through unknown mechanisms.

Chloride concentrations are set primarily by the action of the specific members of the CCC family, in particular, the transmembrane cotransporters NKCC1 (sodium-potassium-chloride cotransporter 1) and KCC1 (potassium-chloride cotransporter 1) [29, 46]. The cotransporters are passive, acting according to the electrochemical gradient: NKCC1 mediates influx of ions, and KCC1 mediates efflux. The activities of these transporters are regulated. Low intracellular chloride concentrations activate NKCC1 in secreting epithelia [47]. Each of the cation-chloride cotransporters is also regulated by phosphorylation. NKCCs, as well as sodium-chloride cotransporters (NCCs), are activated by phosphorylation [48, 49]. KCCs are inhibited by phosphorylation [50]. As a natural consequence of these combined obser-

vations, it was hypothesized that there should be a chloride-sensitive kinase [47, 48, 51]. This putative kinase might act both as a primary sensor of chloride and as a transducer of this information to the cotransporters. NKCCs and KCCs also regulate cell volume, which has led to the further hypothesis that there should also be a chloride- and volume-sensitive protein kinase [52, 53].

With no lysine kinase 1

Kinases of the WNK [with no lysine (K)] family are serine/threonine protein kinases noted for the unique placement of the catalytic lysine residues [54, 55]. WNK1 was first identified by the Cobb lab in an effort to clone proteins that had high homology to known members of the MEK family of kinases[54]. There are four WNK kinases in humans: WNK1, WNK2, WNK3, and WNK4, and they each differ in sequence and tissue expression patterns [56]. WNK1 is 2126 amino acids long, of which the kinase domain only consists of 265 residues near the N-terminus. The function of the additional length is poorly characterized. The following literature review is adapted from [28].

WNK1 regulates CCCs

Shortly after these kinases were first cloned, mutations in WNK1 or WNK4 genes were found to underlie pseudohypoaldosteronism II, a familial disease characterized by hypertension, hyperkalemia, and hyperchloremia [57]. This disorder is often treated with thiazide diuretics, which are inhibitors of NCCs. Pseudohypoaldosteronism II is symptomatically the inverse of Gitelmans syndrome, which is due to loss of the SLC12A3 gene encoding an NCC [58]. This connection suggested that WNKs are involved in the pathway of SLC12A cotransporter phosphorylation. The linkage was established in studies of NKCC1 (SLC12A2). First, the kinases OSR (oxidative stress responsive kinase) and SPAK (sterile-20 proline-alaninerich kinase) were shown to interact with and phosphorylate the cotransporters NKCC1 and KCCs

[59, 60]. Subsequent studies showed that WNK1 interacts with and phosphorylates OSR and its close homolog SPAK [61–65]. Apparently, there is a two-tiered kinase cascade; WNK phosphorylates and activates OSR and SPAK, which phosphorylate and regulate CCCs.

WNK1 regulates other ion transporters

WNK isoforms exhibit pleiotropic involvement in ion transport regulation. WNK1 and WNK4 inhibit the epithelial sodium channel (ENaC), which is a major mediator of aldosterone-induced salt reabsorption [66, 67], by promoting ubiquitin-mediated degradation of the channel [68]. The regulation of ENaC appears to be mediated by SGK1 (aldosterone-regulated serum and glucocorticoid-induced kinase), which is activated by WNK1 [69]. WNK1 and WNK4 also inhibit the renal outer medullary potassium channel (ROMK), a channel involved in salt reabsorption [70, 71]. In contrast to the ENaC regulation, WNK-mediated inhibition of ROMK is due to clathrin-mediated endocytosis. Both effects on ENaC and ROMK appear to require regions outside the kinase domain of WNK, and the involvement of kinase activity is unknown. WNK1 and WNK4 also affect paracellular chloride flux [72] and maintenance of vascular tone [73].

WNKs modulate chloride concentration

WNK isoforms are activated in response to reduction in intracellular chloride concentrations [65, 74]. Activation of NKCC2 by reduced intracellular chloride is blocked by WNK mutants that affect WNK-OSR docking interactions [74]. Further, overexpression of WNK3 in HEK (human embryonic kidney) 293 cells increases intracellular chloride concentrations. WNKs have been proposed to be chloride-sensitive kinases on the basis of these observations [74–78]. Here, we show that the kinase domain of WNK1 directly binds a chloride ion, and we locate the chloride-binding site in the previously determined crystal structure of the inactive WNK1 kinase domain [55]. Chloride binding inhibited the autophosphorylation of

WNK1, thereby inhibiting kinase activity. Furthermore, we confirmed the residues involved in chloride binding through identification of chloride-insensitive mutants. Our results suggest that WNKs function as direct chloride sensors.

5.2 Approach

Dr. Thomas Moon laid the foundation for most of the biochemical assays described below. While he pursued the crystallization of a WNK1 construct with its autoinhibitory domain intact, he performed stability assays to find optimal crystallization conditions. These assays revealed that WNK1 was stabilized by increasing chloride concentration. His future experiments eventually determined that the WNK1 kinase domain (WNK1-KDm) was also stabilized by chloride, as well as inhibited. It was this combination of results that led to the belief that WNK1 may be capable of sensing chloride directly and then communicating this information down the pathway to ion cotransporters.

It was at this point that I began efforts to evaluate the mechanism of chloride inhibition of WNK1. When control kinases all demonstrated the same inhibition of activity in response to increasing chloride concentration, further experiments determined that autophosphorylation and subsequent autoactivation was uniquely inhibited. This result provided a possible mechanism by which WNK1 would not only be regulated by changing intracellular chloride concentrations, but also by intracellular phosphatases. The proposed shifting equilibrium that arises as a result of the balance between autophosphorylation and dephosphorylation comes from this observation. Here I present the work I performed for this project, some additional experiments performed by others critical to the understanding of our conclusions (demarcated by attribution), and the results and conclusions derived from the study.

Though WNK1-KDm had been demonstrated to bind chloride ion crystallographically by Dr. Thomas Moon, the mechanism by which that binding translated into some

regulatory effect was not understood. I explored two potential mechanisms: direct inhibition by chloride ion, and inhibition of autophosphorylation. The first assay is the simpler of the two— if the kinase is inhibited directly by chloride, that inhibition will show up in a enzymatic assay against substrate. The second assay requires WNK1-KDm both be the enzyme and the substrate for the reaction— this means that the maximum strength of the output signal in the assay is proportional to the WNK1-KDm concentration. This, therefore, requires substantially more WNK1-KDm enzyme than a typical enzymatic assay would. Furthermore, it also requires that WNK1-KDm be dephopshorylated before introduction to the reaction conditions, as WNK1-KDm is phosphorylated when expressed in E. *coli*. This makes assays for auto-inhibition both more difficult and less amenable to several different techniques that could be used to measure activity. Because we are measuring inhibition due to chloride concentration, careful buffer construction was also important. Sources of chloride were minimized wherever possible.

Bromide soaking assays performed by Dr. Thomas Moon revealed a putative chloride binding region. Chloride was modeled into this density on the previously published 3FPQ structure ([55] by Dr. Radha Akella, which revealed the chloride binding mechanism. This allowed for identification of mutants that might abrogate chloride binding, and therefore change sensitivity to chloride. As such, once a mechanism of chloride regulation had been determined from the biochemical assays, I planned on testing these mutants to see if they modified sensitivity to chloride. If they changed chloride sensitivity, that would suggest that the proposed mechanism of action was correctly identified, and prove strong evidence that we understood how chloride regulated WNK1-KDm activity.

5.3 Materials and Methods

Expression and Purification of p38α, MEK6, and ASK1

Each of these proteins was purified and expressed as in previous literature: p38α purification and expression is detailed in [79], MEK6 in [80], and ASK1-KDm in [81].

Expression and Purification of WNK1-KDm and WNK1-KDm mutants

WNK1 expression and purification is detailed in [55]. Mutants were provided by Haixia He of the Goldsmith lab, and created using a Stratagene QuikChange site-directed mutagenesis kit. The original expression and purification was modified to account for chloride concentration in the buffer.

Production of cell-free extract

1. Frozen cell pellets were thawed at RT in a water bath. During thaw, 1 ml protease inhibitor cocktail (Sigma) was added to a final concentration of 1x as per manufacturer recommendation.

2. 100 ml Nickel buffer A (50 mM Tris pH 8.0, 300 mM NaCl, 10 mM imidazole) was added to the cell pellet for every 100 ml of cell pellet solution.

3. 5 µl Benzonase nuclease (Novagen) was added to the cell pellet solution for every 100 ml cell pellet solution, and allowed to react for 30 minutes.

4. Cells were broken mechanically using a french press at 13,000 - 16,000 psi and 4 °C. Cells were broken over 4 passages.

5. The resultant solution was centrifuged at 40,000 rpm in a Beckman Ti-45 rotor at 4 °C for one hour.

6. The supernatant was decanted and passed through a Nalgene Rapid-Flow 2 µm filter.

Immobilized metal-affinity chromatography

1. The filtered extract was loaded onto a column containing 8 ml of Fast-chelating sepherose (Amersham Pharmacia) charged with 0.1 mM $NiSO_4$ and equilibrated with nickel buffer A.

2. The column was washed with 10 column volumes of Ni buffer A, and then eluted with an increase to 250 mM imidazole over a gradient of 10% to 70%.

3. The fractions corresponding to peaks appearing during the imidazole gradient were pooled and run on SDS-PAGE in order to determine presence of WNK1.

4. Pooled fractions were buffer-exchanged into 50 mM HEPES 7.4, 50 mM NaCl through membrane dialysis. During the process, 1 mg tobacco edge virus protease was added to remove the His tag.

5. The protein solution was passed through 2 ml Ni-NTA agarose (Qigen), and the flowthrough was collected. The plug was washed with 3 ml 50 mM HEPES 7.4 and 50 mM NaCl and the flowthrough was collected.

6. The protein solution was assayed with Biorad protein assay to determine protein concentration, and the solution concentrated in an Amicon Ultra-15 3k to 4 mg/ml.

7. The protein solution was then flash-frozen in liquid N_2 for storage.

WNK1-KDm dephosphorylation

The dephosphorylation of WNK1-KDm is described. This reaction appeared very sensitive to $MnCl_2$ concentration, and the lowest possible concentration that gives good reactivity is desired. A significant amount of precipitate can form, and in that case centrifugation to generate a pellet of precipitated protein followed by decantation to remove soluble

protein can recover a usable sample. As always, maintaining a low chloride concentration during these experiments was seen as important in light of future experiments.

1. 1.5 ml WNK1 S*S* was added to 2.9 ml of 15.6 mM $MnCl_2$, 156 mM Tris pH 8.0.
2. The solution was incubated at 30 °C for 5 minutes.
3. 112 µl 4mg/ml His 6 PP1Cγ was then addd to the solution, and the solution was incubated at 30 °C for one hour.
4. The solution was then passed through 2 ml Ni-NTA agarose that was equilibrated to 50 mM Tris pH 8.0, 50 mM NaCl. Flowthrough was collected. The plug was washed with 3 ml 50 mM Tris 8.0 and 50 mM NaCl and the flowthrough was collected.
5. The protein solution was assayed with Biorad protein assay to determine protein concentration, and the solution concentrated in an Amicon Ultra-15 3k to 4 mg/ml.
6. The protein solution was then flash-frozen in liquid N_2 for storage.

Radiometric assays of kinase activity

This assay measures incorporation of the terminally-labeled phosphate of γ^{32}P ATP onto the generic kinase substrate Myelin Basic Protein (MBP). After the kinase is allowed to react for the allotted time, the reaction is stopped by blotting it onto filter paper and plunging it into a trifluoroacetic acid solution, which precipitates the substrate onto the paper. Because soaking the filter paper removes the unreacted ATP, the only source of radioactive signal on the filter paper comes from the incorporated phosphate. This can then be read via scintillation counting.

1. A reaction solution containing 1.5 µM kinase, 15 µM MBP, 30 mM HEPES pH 8.0, 5 mM $MgCl_2$, varying NaCl concentration, and 1 mM DTT was prepared.

2. An ATP solution of 1:20 0.1 µCi/ml ^{32}P γ-labeled ATP:2 mM ATP was made.

3. 13 µl ATP solution was added to 87 µl reaction solution to begin the reaction, and it was allowed to react for 60 minutes at RT.

4. Reactions were stopped by blotting onto filter paper, then submerging the paper in 10% trifluoroacetic acid.

5. Paper was washed 4 times in TFA, then put into scintillation vials.

6. 5 ml Complete Counting Cocktail 3a70B (Research Products International Corp.) was added, and the vials were counted on a Beckman scintillation counter for 10 minutes.

Radiometric assays of kinase auto-phosphorylation

These assays are very similar to those performed above, but concentration of WNK1-KDm had to increase in order to produce sufficient signal-to-noise. This is due to the fact that WNK1-KDm is its own substrate in these reactions. The increased WNK1-KDm concentration also resulted in a somewhat higher minimum chloride concentration, as it was impossible to completely remove chloride from the WNK1-KDm storage buffer.

1. A reaction solution containing 7.5 µM unphosphorylated kinase, 30 mM HEPES pH 8.0, 5 mM $MgCl_2$, varying NaCl concentration, and 1 mM DTT was prepared.

2. An ATP solution of 1:20 0.1 µCi/ml ^{32}P γ-labeled ATP:2 mM ATP was made.

3. 13 µlATP solution was added to 87 µl reaction solution to begin the reaction, and it was allowed to react for 20 minutes at RT.

4. Reactions were stopped by blotting onto filter paper, then submerging the paper in 10% trifluoroacetic acid.

5. Paper was washed 4 times in TFA, then put into scintillation vials.

6. 5 ml Complete Counting Cocktail 3a70B (Research Products International Corp.) was added, and the vials were counted on a Beckman scintillation counter for 10 minutes.

Differential Scanning Fluorimetry assays of kinases

Differential Scanning Fluorimetry measures the stability of proteins in response to thermal challenge. A lipophilic dye is added to the solution— in this case Sypro Orange (Life Technologies). When the protein solution is heated, the protein starts to denature and expose internal hydrophobic regions, allowing Sypro Orange to bind. The bound dye is no-longer quenched by water, and thus allows the amount of bound dye to be measured by fluorescence. As such, fluorescence is proportional to the amount of denatured protein, allowing one to track protein denaturation in response to temperature. Higher protein stability results in greater resistance to thermal denaturation, and binding of small molecules increases protein stability. This technique therefore allows for measurement of direct binding of small molecules to proteins in a medium-throughput fashion.

1. A solution of 5 µM WNK1, 5 mM $MgCl_2$, 30 mM HEPES pH 8.0, varying NaCl concentration, and 2.5x Sypro Orange (Life Technologies) was made.

2. 25 µl of the reaction solution was added to the wells of a Biorad Multiplate 96 well clear PCR plate. The plate was covered with a Biorad Microseal 'B' seal.

3. Plates were read in a Biorad CFX96 Real-Time PCR system. The temperature was increased from 4 °C to 80 °C, with fluorescence measurements being taken every 0.5 °C in the 6-FAM Fluorescein channel.

4. The fluorescence response to heat curve was fit to a binding isotherm in order to determine the inflection point, which was taken as the melt temperature (T_m).

Bromide anomalous diffraction

Bromide anomalous data were provided by Dr. Thomas Moon of the Goldsmith lab, and these data were processed by Dr. Radha Akella of the Goldsmith lab. In brief, crystals were grown using the previously reported crystallization conditions, with sodium chloride replaced by sodium bromide [55]. These crystals were diffracted at the APS (Advanced Photon Source) beam line 19-ID at the bromine anomalous edge. The integration and scaling were performed with the HKL-2000 software suite [82]. A 2.8 Å resolution structure was solved using molecular replacement with MOLREP [83]. The previously determined structure from *Min et al.* (PDB: 3FPQ) provided a search model. Model building was performed in COOT [84]. Details can be found in Piala *et al.* 2014 [28].

5.4 Results and Discussion

WNK1 is stabilized by chloride ion

WNK1 is known regulate CCCs, which in turn regulate salt balance in response to changing salt concentrations. Therefore, it seemed possible that WNK1 may interact with different salts directly *in vitro*. We examined the stability of two forms of the WNK1 kinase domain in response to salt challenge: the inactive form of the kinase domain (WNK1-KDm/SA, in which activation loop phosphorylation site Ser382 was mutated to alanine) [55, 85], and the active kinase domain (WNK1-KDm/S*, where * denotes phosphorylation on Ser382, on the activation loop). We estimated stability from the temperature of protein melting (T_m) as indicated by binding of the dye SYPRO Orange (Figure 5.1) [86]. Both the active and inactive proteins exhibited an 10 °C increase in T_m with increasing NaCl concentration (Figure 5.2). These results indicated that the kinase domain of WNK1 may interact directly with either the sodium or the chloride ion, or both, and that the interaction was independent of Ser382.

To determine which ion WNK1-KDm bound, we measured the change in T_m as a

function of different concentrations of cation-chloride salts (LiCl, NaCl, and KCl) (Figure 5.3A) and sodium-anion salts (NaCl, NaBr, and NaI) (Figure 5.3B). NaCl and NaBr exposure stabilized WNK1-KDm, whereas NaI was destabilizing. LiCl and KCl had similar effects to that of NaCl on the stability of WNK1.

In order to determine whether or not this property was unique to WNK1, or was a more general protein phenomenon, we also tested three other kinases that did not appear to be involved with salt signaling: full-length mitogen- and extracellular kinase-regulated kinase kinase 6 (MEK6), p38α, and the catalytic domain of apoptosis signal-regulating kinase 1 (ASK1-KDm). No increase in stability in response to increased NaCl concentration was identified(Figures 5.4A–C). Indeed, several kinases were destabilized in response to increasing salt concentration— all salts tested other than NaCl destabilized MEK6, p38α, and ASK1-KDm to varying degrees, with ASK1-KDm being destabilized from NaCl concentration as well.

Both Cl^- and Br^- stabilized WNK1-KDm (Figure 5.3B). Iodide was destabilizing. All tested cation-chloride salts stabilized WNK1-KDm, suggesting that the chloride ion was the most important for binding, and may be the cause of the observed stabilization.

Kinase activity is inhibited by chloride

If WNK1 is capable of sensing and responding to chloride, then we would expect chloride binding to affect WNK1 kinase activity. We measured the activity of WNK1 toward the model substrate myelin basic protein (MBP) as a function of NaCl concentration and found that WNK1-KDm/S* activity decreased as a function of NaCl, with an apparent IC_{50} (median inhibitory concentration) of 40 mM (Figure 5.5A). A similar phenomenon was also observed in two of our control kinases (ASK1-KDm and MEK6), and each of these kinases also demonstrated a similar IC_{50} value (30 mM for both (Figure 5.5B)). WNK1-KDm/S* activity toward the kinase domain of the physiological WNK1 substrate OSR (OSR 1295)

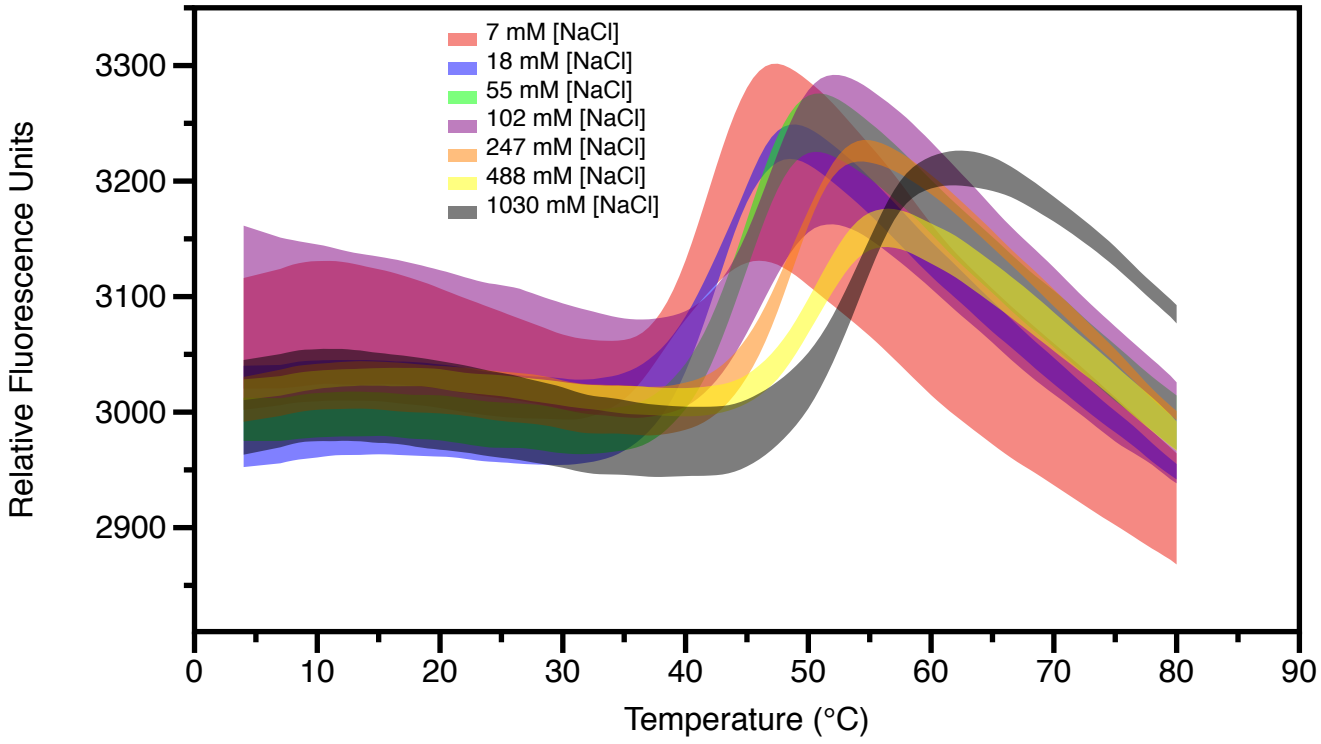

Figure 5.1: **Raw trace of WNK1-KDm/S* DSF using SYPRO Orange.** Each curve represents three independent experiments, with the width of the curve representing one standard error above and below the mean.

was also inhibited by increasing concentrations of NaCl, but the IC_{50} (530 mM) was greater than for activity toward MBP (Figure 5.6). Because both WNK1 and kinases that are not associated with chloride sensing exhibited this behavior, we did not believe this was the mechanism used for chloride-sensitive responses in the WNK1 to CCC pathway.

WNK1 autophosphorylation is inhibited by chloride

WNK1 is autophosphorylated on the activation loop as purified from *E. coli*. This phosphorylation is required for full activity [87]. Because WNK1 activity was not uniquely inhibited by chloride, we tested whether or not autophosphorylation and subsequent autoactivation is inhibited by chloride. We generated the unphosphorylated and inactive WNK1-KDm/S by dephosphorylating WNK1-KDm/S* with protein phosphatase 1cγ (PP1cγ). NaCl inhibited the autophosphorylation of WNK1-KDm/S, as assessed by autoradiography, with an apparent IC_{50} of 20 mM after 20 minutes (Figure 5.7). Furthermore, the observed IC_{50} is similar to reported intracellular chloride concentrations, which tend to range from 5 to 60 mM depending on the cell type [31, 32]. The control kinases MEK6 nor p38α did not phosphorylate under these conditions (Figure 5.7). The MAP3K ASK1-KDm did autophosphorylate, but NaCl was activating as opposed to inhibitory, and the strength of the activation was relatively small (apparent IC_{50} of 1 M). Chloride appears to have a unique inhibitory effect on the activating autophosphorylation of WNK1-KDm, suggesting that this might be a mechanism by which cellular chloride concentrations could be regulated.

3/10 helix mutations reduce effect of chloride inhibition

If chloride binding inhibited WNK1-KDm autophosphorylation as proposed, mutations in the chloride-binding site may reduce chloride binding and increase autophosphorylation. Work by Thomas Moon and Radha Akella found the chloride binding site of WNK1-KDm/S* through crystallographic studies [28]. WNK1-KDm mutants with muta-

tions (L299F, L371F, or L369F) in the chloride-binding site as observed in the WNK1-KDm/S* structure (Figure 5.8A) were expressed and purified. These mutants were active and phosphorylated when expressed in and purified from E. *coli*. Increasing NaCl concentration had the least stabilizing effect on the mutant L369F (2.6 °C at 500 mM NaCl compared with 6.8 °C for WNK1-KDm/SA) (Figure 5.8B). Using PP1cγ-treated proteins, we assessed the effect of increasing NaCl concentrations on autophosphorylation, and the L369F mutant (in the sequence DLG) was less inhibited by NaCl, with an apparent IC_{50} in the autophosphorylation experiment of 50 mM (Figure 5.9B). Nevertheless, even at concentrations in excess of 1 M, we only observed 50% inhibition. The L371F mutant (in the 3/10 helix) also exhibited an increase in IC_{50}, whereas the L299F mutant (in β4) exhibited only slight changes when compared with WNK1-KDm/SA. None of the mutations substantially affected the ability of increasing concentrations of NaCl to inhibit activity toward MBP (Figure 5.9A). Thus, the effects of these mutations on the inhibition of autophosphorylation and kinase activity toward substrates by chloride-containing salt substantiate the crystallographic data for the chloride-binding site and provide a context for understanding effect of chloride binding on autophosphorylation.

5.5 Conclusions and Future Directions

The WNK1 kinase domain directly binds chloride

It is surprising that the WNK1 kinase domain is capable of binding and being regulated by chloride ion. There are relatively few examples of chloride ions directly binding and regulating proteins in the literature. The ClC family chloride channels, for example, have both been observed to bind chloride and to be regulated by it [38, 88, 89]. Several other systems have also been demonstrated with such functionality, but no kinase has been observed to be regulated in such a fashion [39–41]. Adding WNK1 to the list of proteins that bind chloride may lead to the development of methods to predict chloride-binding sites,

which has otherwise been difficult due to their high heterogeneity.

Also interesting is the fact that the site of chloride binding is located on the kinase domain. Other kinases that are regulated directly by small molecules often have specific binding domains outside the kinase domain. Protein kinase A, for example, has a separate cAMP binding subunit that regulates its function [90]. Calcium calmodulin-dependent kinase is similar, in that it also has a separate inhibitory subunit that binds calcium, which then releases inhibition [91]. WNK1, however, appears to the the first kinase observed to have the regulatory site in the kinase domain. This opens up a new avenue for the discovery of metabolite-sensing kinases that has been previously uninvestigated.

Autophosphorylation as a regulatory mechanism

Why does WNK1 regulate itself by autophosphorylation, as opposed to direct effects on activity? Our original hypothesis for WNK1 regulation was much simpler— that binding of chloride directly inhibited the function of the kinase domain. Autophosphorylation seems to add an additional layer of complexity. What advantages are there to regulation *via* autophosphorylation vs. regulation through direct inhibition?

Work by Goldbeter and Kochland provides a potential explanation [92]. If the kinase activity responded directly to a single chloride binding event, the activity would follow some mode of reversible inhibitor kinetics (Figure 5.10). In each of these systems, the response of the kinase to increasing inhibitor concentration is gradual, and the majority of the dynamic range is at the lowest concentrations. This gradual transition could make it difficult to maintain metabolite homeostasis, especially in the case of rapidly-exchanging species like chloride, which are continuously shuttled into and out of the cell and must be maintained at a specific intracellular concentration.

If activity is determined by a phosphorylation event, however, response to the inhibitor can instead be switch-like. Regulation by phosphorylation requires both an 'activat-

ing' pressure (toward phosphorylation) and an 'inactivating' pressure (toward dephosphorylation). Under such conditions, there are several mechanisms by which switch-like responses can arise, such as ultrasensitivity, sequestration, and feed forward/back loops [11, 92, 93]. This would provide an explanation for why the kinase domain is regulated by autophosphorylation, as opposed to direct binding and subsequent inhibition.

WNK1 may be the intracellular chloride sensor

Concurrent with the biochemical work performed to study this system, crystallographic studies were also completed to determine the mechanism of chloride inhibition. These studies, performed by Thomas Moon and Radha Akella of the Goldsmith lab, identified the chloride binding site in WNK1-KDm at the terminus of a 3/10 helix (Figure 5.8)[28]. This informed the mutational investigation of the proposed binding pocket, confirming the mechanism of WNK-KDm autophosphorylation inhibition.

These results coincide with early studies of the NKCCs that postulated the existence of a chloride sensitive kinase [47, 48, 51]. Further, our studies were conducted within a physiological chloride regime— our results suggested an IC_{50} of around 20 mM, which is between the observed concentrations of chloride in the kidney (50 mM) and neuron (10–15 mM) [31, 32]. That the kinase is known to operate in the pathway that regulates chloride transporter function, that the kinase operates in a concentration milieu similar to those in physiological systems, and that the kinase auto-activates in response to changing chloride concentrations, all suggest that cellular chloride concentrations may be, in part, set by the sensitivity of WNK1 to chloride. This would position WNK1 as the first known cellular chloride stator. If the other WNK isoforms each have different chloride sensitivities, this may be one of the means by which different tissues manage to maintain different intracellular chloride concentrations.

While the data suggest a mechanism by which NKCCs could be activated by WNK1

in the event of low intracellular chloride, it does not explain the observed activation of NKCCs in response to extracellular hypertonicity [52]. It has been proposed that responses to extracellular hypertonicity could be mediated by macromolecular crowding [94]. We observed no direct mechanism by which WNK1 could be responsive to macromolecular crowding, but that does not mean that the full-length protein is not. Alternately, some secondary factor may be able to activate WNK1 in response to such stimuli. These questions require further investigation.

The role of phosphatases is also poorly studied, both in this cascade and others. WNK1-KDm/S* was dephosphorylated by PP1cγ in vitro. The activities of NKCCs and other CCC family members are likely regulated by the balance of kinases and phosphatases targeting these proteins. Because WNK1 can autophosphorylate and can be dephosphorylated suggests that the cellular balance of phosphatase and kinase activities may contribute to WNK1 regulation— the relative concentrations of these factors could then serve as an additional regulatory mechanism to 'tune' intracellular chloride concentration. Thus, we propose that as the chloride concentration decreases, autophosphorylation outstrips dephosphorylation and WNK1 activity increases, thereby stimulating downstream signaling (Figure 5.11). As the chloride concentration increases, dephosphorylation outstrips autophosphorylation, and WNK1 activity is inhibited, decreasing downstream signaling. The cellular phosphatase acting on WNKs is unknown, but both protein phosphatase-1 and 4 have been implicated [95, 96]. The discovery that WNK1 is controlled by autophosphorylation, together with a method to induce constitutive activity of WNK1, may prove useful in elucidating the chloride sensitivity and signaling pathways involving WNK1 and other WNK isoforms.

Future Directions

Mutants with differential chloride sensitivity

The mutants chosen for analysis were very conservative. Each mutation substituted a leucine for a phenylalanine, or a hydrophobic group for a slightly more bulky hydrophobic group. As such, it is unsurprising that the effects of mutation were also mild. Of the mutants tested, only one demonstrated a large shift in chloride sensitivity. Due to the position of the residues within the hydrophobic core of the protein, however, it is difficult to make more significant mutations, such as the introduction of a residue with a positive or negative charge. The most interesting mutation would likely be the introduction of a proline into the core of the 3/10 helix, destabilizing it. According to the model, destabilization of the helix would result in removal of both the chloride binding site and the mechanism of autoinhibition.

Despite the potential difficulties of making such mutants, the project could serve several purposes. Most directly, they would confirm our understanding of how chloride binds and inhibits the protein. These efforts were only briefly touched on in the previous work. Secondly, and more interestingly, they could be used as probes to confirm our understanding of what the WNK1 kinase domain is actually doing in cells. The known roles and activities of the protein are only indirect evidence implicating it in chloride concentration regulation. The ability to cause expression of the mutants in cells, then measure intracellular chloride in response to that expression would confirm that role.

Characterization of *in vivo* WNK1 activity

Because the studies performed above were all performed *in vitro*, it is critical that an effort is made to study WNK1 function in cells. There are several physical measurements that can be used to determine the effect of WNK1 in cells, based on its predicted role in chloride balance: direct intracellular chloride measurement, cell volume, and RVI/RVD. Each of these can be assayed through the use of fluorescent cellular imaging, and could help

demonstrate physiological WNK1 function.

Intracellular chloride measurement can be accomplished through the use of chloride-sensitive dyes. The most commonly used of these is 6-methoxy-N-ethyl-quinoline (6-MEQ), which absorbs 350nm light and emits at 435 nm. Chloride binds 6-MEQ, quenching fluorescence. While 6-MEQ is membrane impermeable, the reduced species 6-methoxy-N-ethyl-1,2-hydro-quinoline is membrane permeable, and once taken into the cell oxidizes into 6-MEQ. Because of this, a standard curve of fluorescence in response to increasing chloride concentration can be made to determine intracellular chloride concentration. One can then determine the relationship between WNK1 expression and homeostatic intracellular chloride concentration. Furthermore, intracellular chloride concentration is known to change in response to increasing extracellular chloride concentration. The relationship between this balance and WNK1 expression can also be determined.

Cell volume and osmotic challenge are linked [94]. As such, WNK1 expression could have an effect on cell volume and response to osmotic challenge. In much the same way one can use a dye to measure intracellular chloride concentration, you can use a dye to measure cell volume. The relationship between cell volume, WNK1 expression, and osmotic challenge can then be determined. If these studies are performed in a time-resolved fashion, such as in a flow-cell, the effect of WNK1 on RVI/RVD can also be determined. Previous studies have shown that WNK3 appears to have an effect on the rate of volume recovery in response to osmotic challenge— this has not yet been demonstrated for WNK1 [76]. The combination of these follow-up studies would confirm the role of WNK1 as an intracellular chloride sensor involved in chloride and volume homeostasis.

Autophosphorylation in other kinases

Are there any other kinases that are regulated through direct binding in the kinase domain? As noted above, several kinases have been described that have attached regulatory

domains that alter their behavior in response to stimulus, but no kinases other than WNK1 have been demonstrated to have that functionality intrinsic to the kinase domain [90, 91]. Because of the additional accessory domains on these kinases, it is much easier to find them informatically and determine how they are regulated by small molecules. How would one go about finding other kinases like WNK1 which are regulated by factors that bind directly to the kinase domain?

The answer to this question could illuminate previously unplumbed territory. A straightforward approach would be to dephosphorylate and presumably inactivate all kinases in a given sample, separate all proteins in that sample, and then add in radiolabeled ATP to see which are capable of autophosphorylation. One way to do this would be through native gel electrophoresis. Add phosphatases and kinase inhibitors to a sample of cell lysate, run the lysate on a native gel, then soak in ^{32}P γ-labeled ATP while diluting out the kinase inhibitors. The gel could then be exposed to some stimulus, either soaking in of small molecules, osmotic shock, or anything else one would expect a kinase to be sensitive to. If differential banding patterns are observed after stimulus, there is a strong likelihood that the bands are caused by sensitivity to that stress. Because the proteins have been separated by gel electrophoresis, it is less likely that this requires two different proteins— in order to be in proximity, they would have to have similar chromatographic properties. The bands could then be cut out and their identity determined via mass spectrometric methods. While this would not filter out those kinases that have attached regulatory domains, it would still reveal those kinases that are regulated through autoactivation, potentially illuminating a previously unexamined realm of kinase regulation.

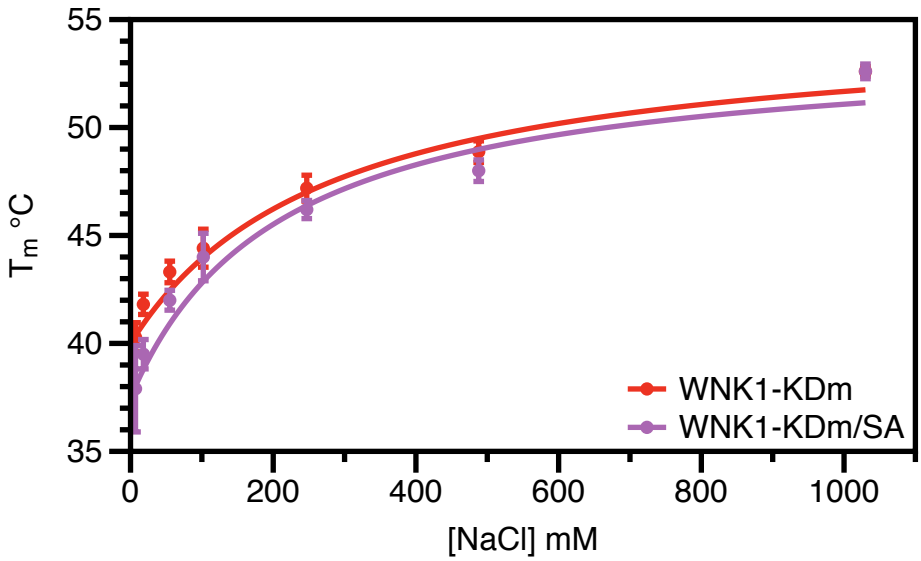

Figure 5.2: **Change in melt temperature (T_m) of WNK constructs as a function of [NaCl].** T_m is taken at the point of greatest δRFU/δt during differential scanning fluorimetry from 0 to 80 °C, where RFU is relative fluorescence units. WNK1 193–482 (WNK1-KDm/S*) and inactive WNK1 193–482 S382A (WNK1-KDm/SA) are plotted.

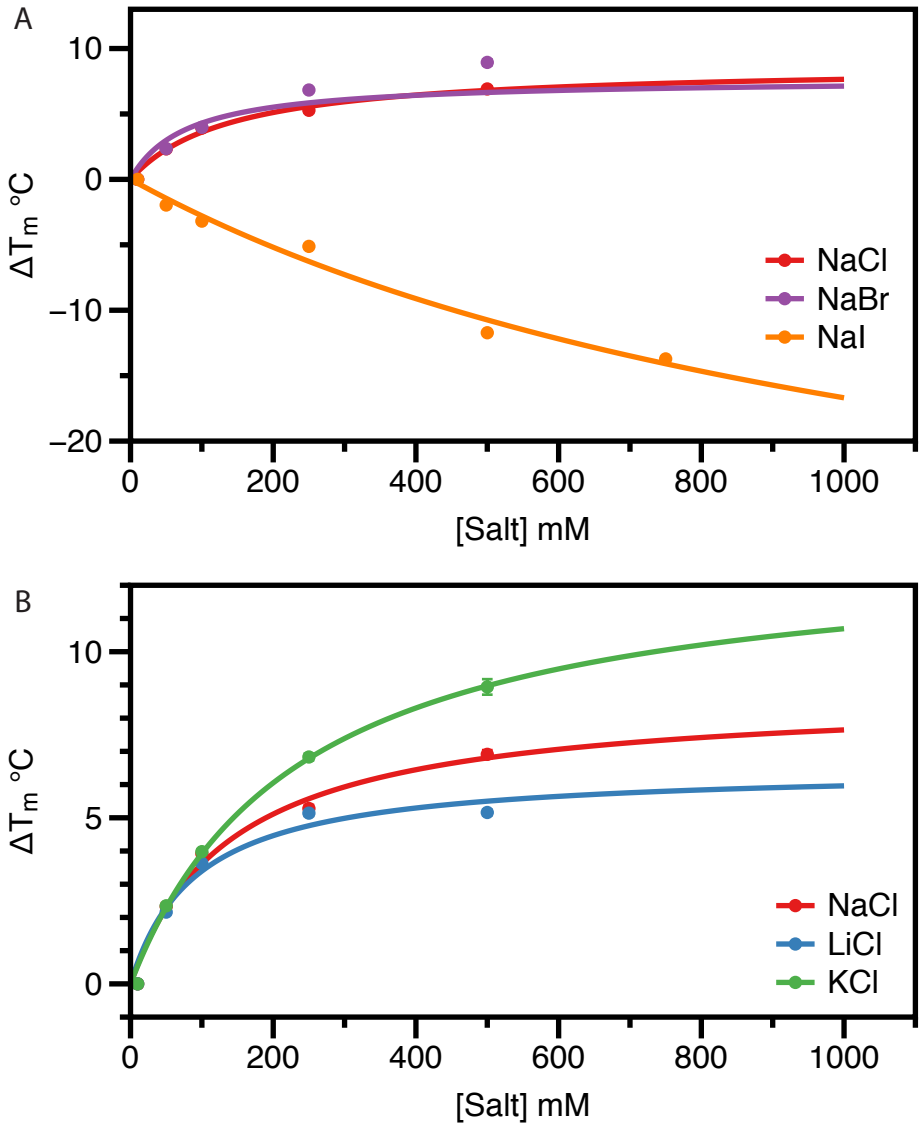

Figure 5.3: **WNK1-KDm response to different cation and anion salts.** Change in melt temperature (T_m) of WNK1-KDm/S* as a function of different cation (A) and anion (B) concentrations. T_m is taken at the point of greatest δRFU/δt during differential scanning fluorimetry from 0 to 80 °C, where RFU is relative fluorescence units. Error bars represent one standard deviation.

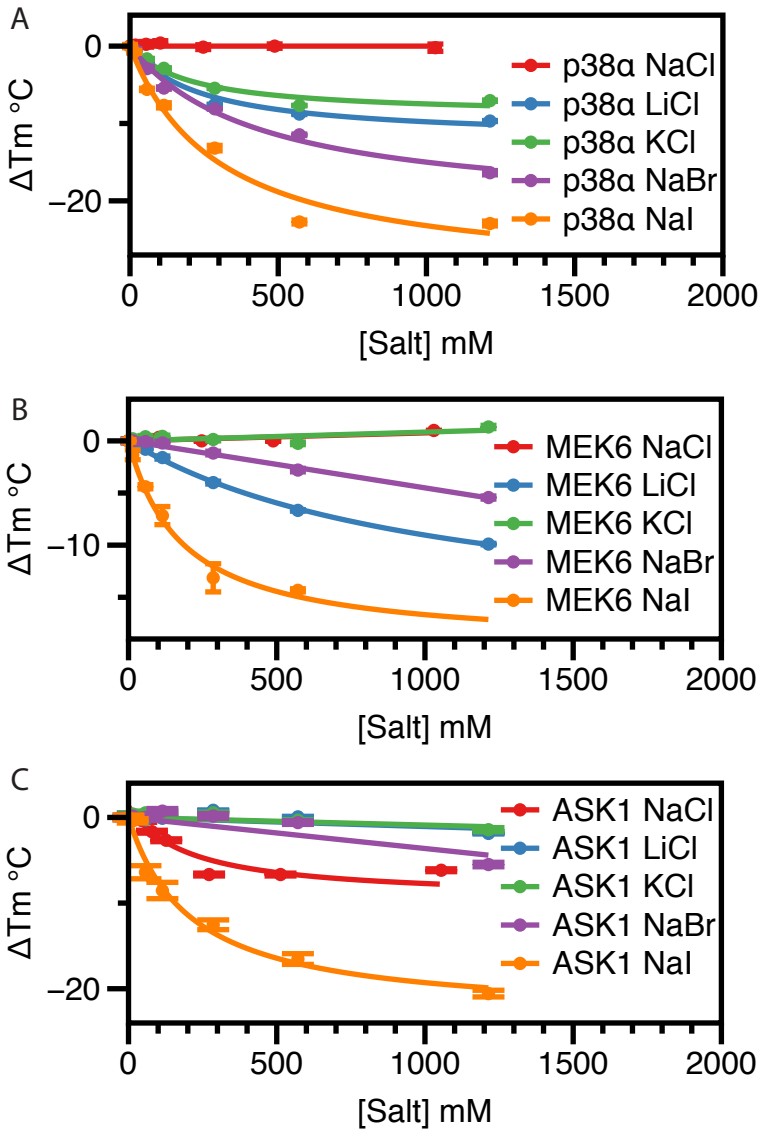

Figure 5.4: **Control kinase stability as a function of salt concentration.** The indicated kinases or kinase catalytic domain were exposed to varying salt concentrations and their T_m was determined. T_m is taken at the point of greatest δRFU/δt during differential scanning fluorimetry from 0 to 80 °C, where RFU is relative fluorescence units. Error bars represent standard error from three independent experiments.

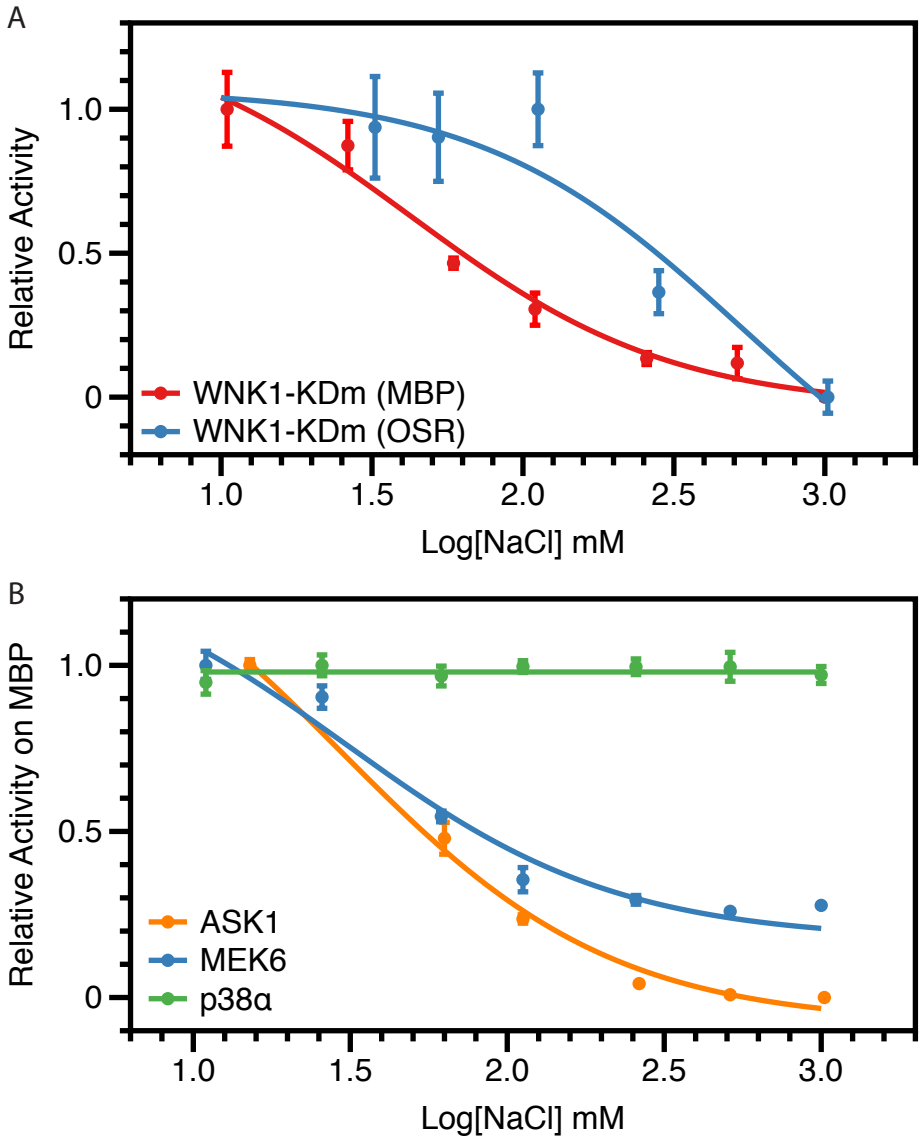

Figure 5.5: **Kinase activity as a function of [NaCl]** (A) Activity of WNK1 as measured by incorporation of ^{32}P onto a model substrate (MBP) as a function of [NaCl]. The highest measured activity was normalized to 1; a control measured in the absence of MBP was taken as 0. (B) Activity of the indicated kinases against MBP as a function of [NaCl]. Activity was analyzed as in (A). All error bars represent standard error from three independent experiments.

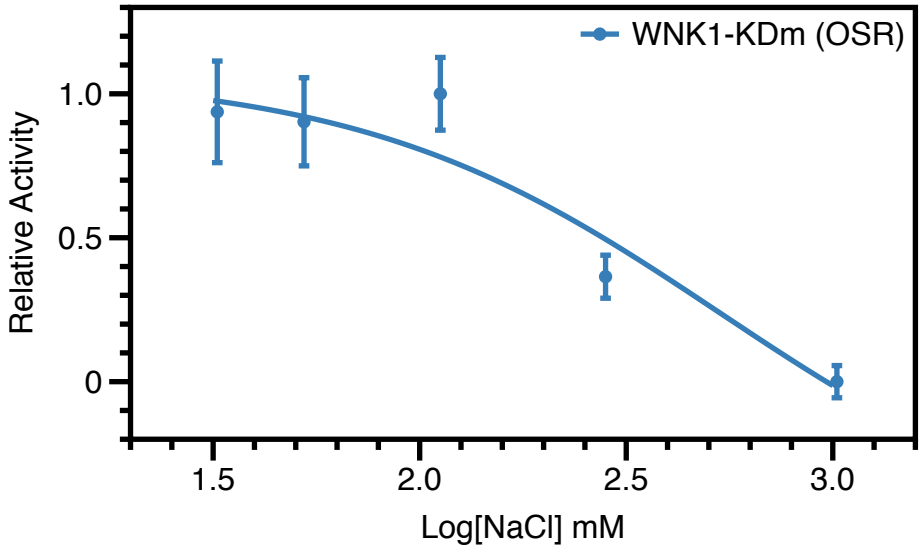

Figure 5.6: **Phosphorylation of OSR1 by WNK1-KDm/S*.** Activity of WNK1 as measured by incorporation of ^{32}P into OSR1 (residues 1-295) as a function of [NaCl]. The highest measured activity was normalized to 1, and a control reaction in the absence of OSR was set as 0. Error bars represent standard error from three independent experiments.

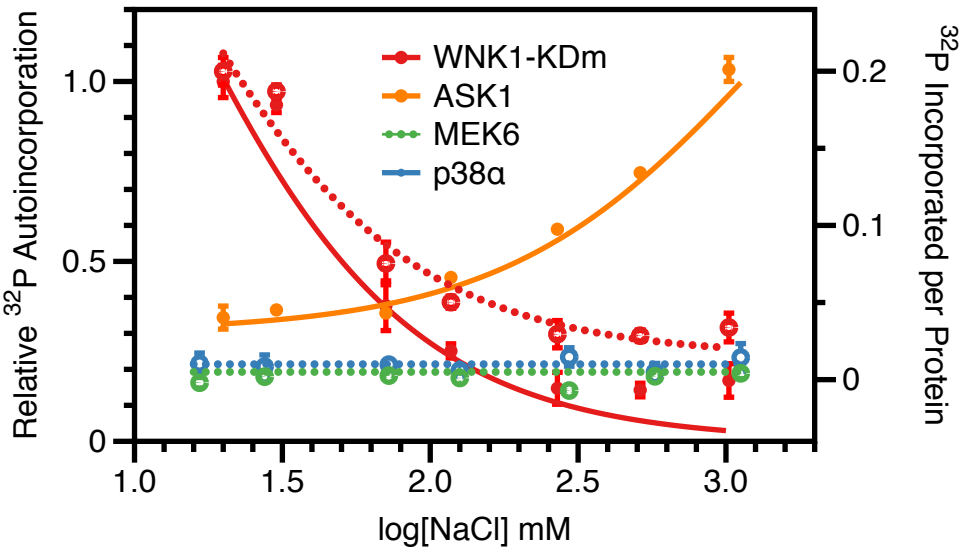

Figure 5.7: **Autophosphorylation of WNK1-KDm and control kinases as a function of [NaCl].** Activity was measured by incorporation of the γ-phosphate of γ-^{32}P-labeled ATP onto the kinase. Solid lines and points indicate data normalized with 1 set to the highest recorded signal and 0 set based on analysis in the absence of kinase. Dotted lines and circles indicate data normalized to the number of phosphate atoms incorporated per protein molecule. In all panels, data are shown as the means and SE from three independent experiments.

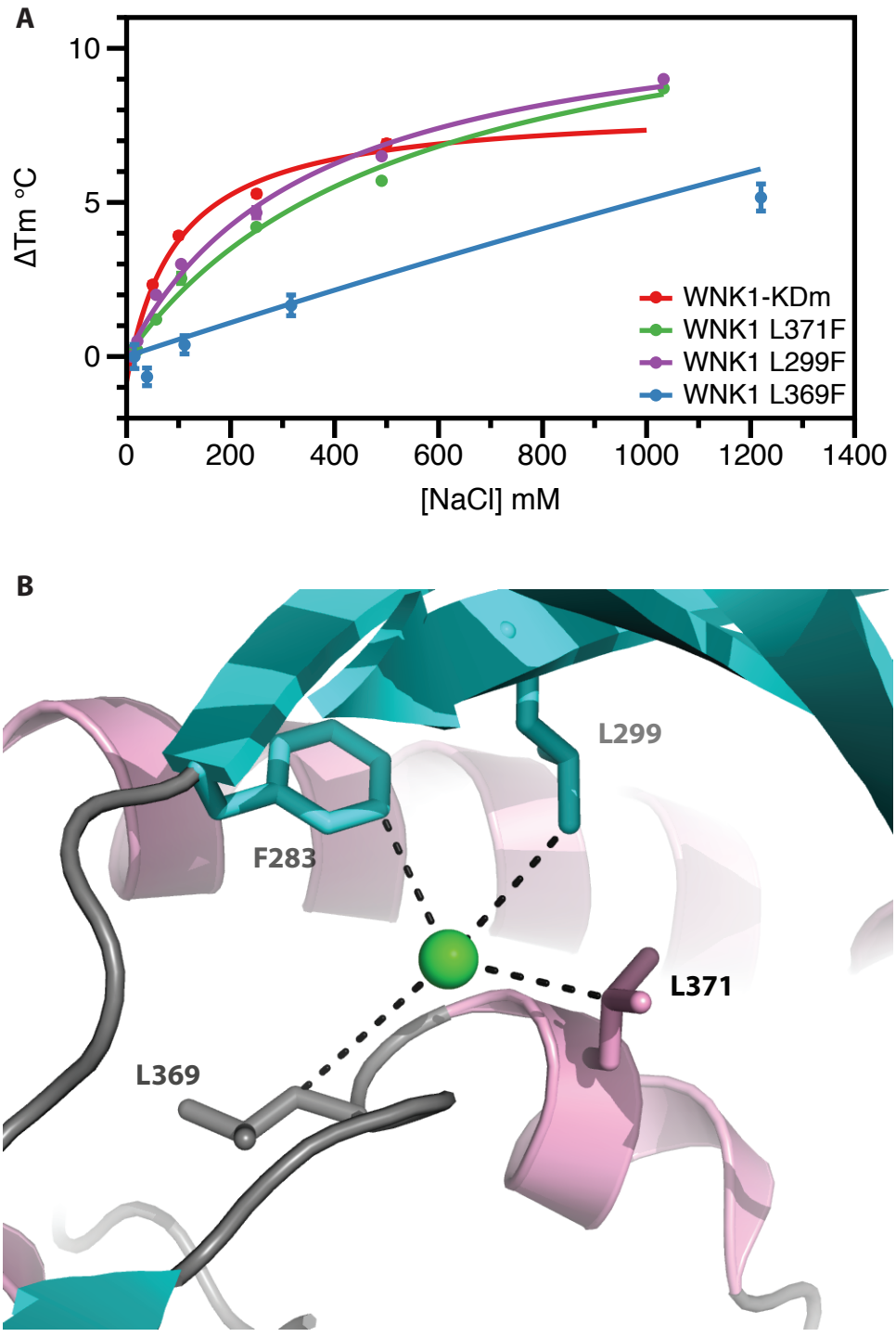

Figure 5.8: **WNK1-KDm mutants.** (A) F283, L299, L369, and L371 form a hydrophobic pocket surrounding the bound chloride. (B) Change in melt temperature (T_m) of WNK1 mutants as a function of [NaCl]. T_m is taken at the point of greatest δRFU/δt during differential scanning fluorimetry from 0 to 80 °C, where RFU is relative fluorescence units. WNK1-KDm (red), WNK1-KDm/L371F (green), WNK1-KDm/L299F (purple), and WNK1-KDm/L369F (blue) are plotted. Data are shown as mean and standard error from three independent experiments.

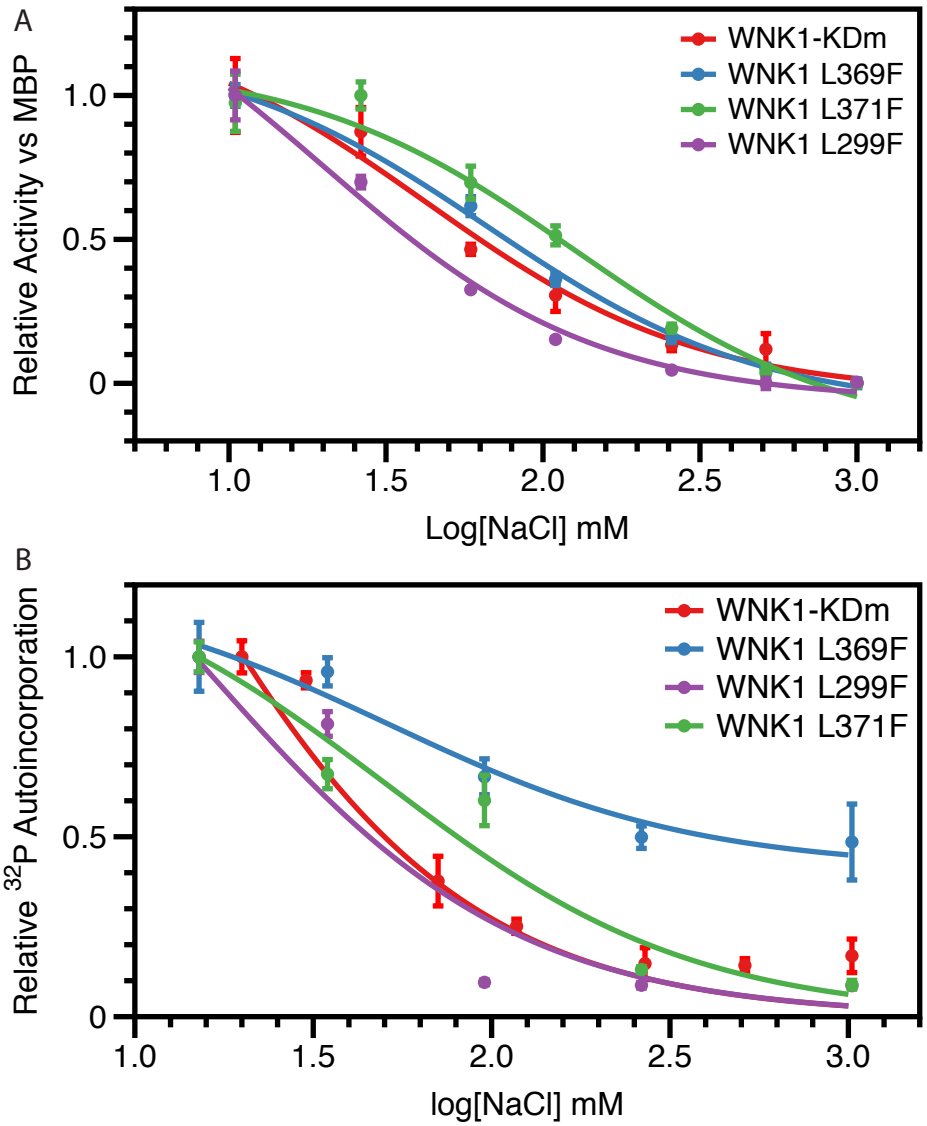

Figure 5.9: **WNK1-KDm mutant activity.** (A) Autophosphorylation of WNK1-KDm mutants in response to varying NaCl concentration as measured by ^{32}P incorporation. Autoincorporation normalized with 1 being the highest signal and a kinase-free background of 0. WNK1-KDm (Red), WNK1-KDm/L371F (Green), WNK1-KDm/L299F (Purple), and WNK1-KDm/L369F (Blue) are plotted. (B) Activity of WNK1 and WNK1 mutants as measured by incorporation of ^{32}P onto the generic kinase substrate myelin basic protein (MBP) as a function of [NaCl]. The highest measured activity was normalized to 1, and an MBP-deprived control was taken as 0. WNK1-KDm (Red), WNK1-KDm/L371F (Green), WNK1-KDm/L299F (Purple), and WNK1-KDm/L369F (Blue) are plotted. Data are shown as mean and standard error from three independent experiments.

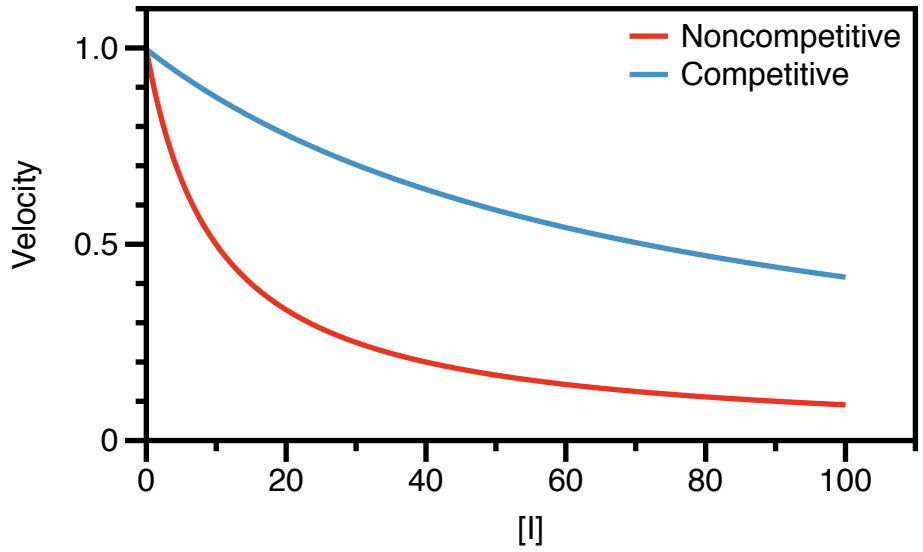

Figure 5.10: **Single-site competitive inhibition is gradual**. A graph of reaction velocity vs. inhibitor concentration is shown for noncompetitive (red line) and competitive (blue line) inhibition of a theoretical kinase. The majority of the dynamic range of inhibition is at the lowest concentrations. In these systems, V_{max} is 1, [S] is 100, K_i for the noncompetitive inhibitor is 10, K_i for the competitive inhibitor is 0.25, and K_m is 0.35.

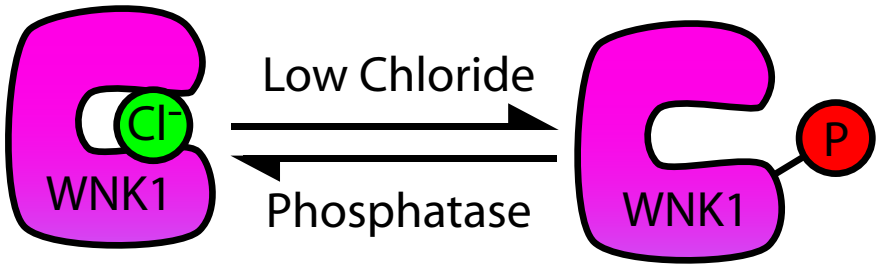

Figure 5.11: **WNK1 serves as an intracellular salt sensor**. WNK1 autoactivation is inhibited by chloride. In low chloride conditions, WNK1 autophosphorylates and becomes active. Phosphatase activity inactivates WNK1, but it can reactivate itself if the chloride concentration remains low.

Chapter 6

Signal transduction in MAPK cascades

6.1 Introduction

Because of the difficulty surrounding isolating each individual component of a kinase cascade, mathematical approaches have been used to guess what the potential role of each component might be. This is reproduced from [97].

Zero Order Effects and Multisite Phosphorylation

Our understanding of the potential of protein modification to induce all-or-nothing responses originates from Goldbeter and Koshland [92]. They used the Michaelis-Menten equation to show that highly sigmoid responses are available from only a single, reversible, protein modification. This phenomenon, Zero-order ultrasensitivity, is possible when both the forward and reverse enzymes, such as kinases and phosphatases, are at or near saturation (thus zero-order, rate proportional to enzyme only) [98]. As the active kinase concentration increases, there is no phosphorylated substrate accumulation until the kinase activity supersedes that of the phosphatase, at which point the substrate phosphorylation increases sharply. The output will be dominated by the enzyme with the highest activity. The importance of long-lived protein-protein interactions is implicit to zero-order ultrasensitivity when the substrate is a protein (since the system must approach saturation). The same authors further showed that addition of multiple cascade tiers enhances the degree of ultrasensitivity, and expands the regime of enzyme and substrate concentrations under which ultrasensitivity is available [98]. Ferrell and colleagues applied these ideas to analysis of the MAP kinase cascade, showing that the same assumptions should lead to a sigmoid response [2]. They

show further that the multiple kinase reactions, two at each tier of the cascade, should be non-processive to have maximal sigmoid responses.

Ordered Phosphorylation is Best for a Signaling Switch

Salazar and Höfer addressed how the order of phosphorylation in multisite phosphorylation reactions affects output [8]. They show analytically that between ordered and random models, ordered reactions generate the greatest sigmoid behavior. In contrast, in the random mechanism, the available kinase substrate drops with kinase/phosphatase activity ratio, and radically increases the available phosphatase substrate, thus limiting the ability to reach the fully phoshorylated form. The authors made the prediction that kinase cascades that include multisite phosphorylation species are likely to operate by a sequential mechanism. In this work, I demonstrate that ordered phosphorylation appears to be a general phenomenon.

How Protein-Protein Interactions Contribute to Switch Behavior

Markevich et al. discussed how protein-protein interactions lead to ultrasensitivity in a multiple phosphorylation reaction of a single protein substrate [11]. Ultrasensitivity can occur when the second reaction is inhibited by the initial substrate. As the reaction progresses, the concentration of the initial substrate is reduced, relieving the inhibition and resulting in positive feedback. If this positive feedback is sufficiently strong, bistability may arise, where two steady substrate phosphorylation states are available for a single set of concentrations of the substrate, kinase, and phosphatase. In addition, competition for a MAP2K within the MAPK module has been proposed as a further source of ultrasensitivity and bistability [99].

6.2 Approach

Why are some reactions in MAPK cascades ordered? Which reactions in the cascade are ordered? Are the double phosphorylation reactions processive or dissociative? How would changes in any of these features modify the downstream signal propagation of the cascade? While many potential features of MAPK cascades have been described on the basis of overall cascade output, fewer have been independently confirmed as either physiological or required for physiological responses. For this reason, it is difficult to determine which features, if any, are required for proper downstream signaling.

Both mathematical and experimental attempts to answer this question have significant associated problems. Mathematical approaches are limited by the amount of experimental data available to constrain their models. Without those constraints, it is impossible to determine which potential mechanism that *can* induce switch-like behavior is actually operative *in vivo*. This can lead to simplifying aspects of the cascade that are important, or adding features that are not experimentally verified. Experimental approaches harbor similar difficulties. The study of signal propagation through cells makes it very difficult to determine what proteins are actually interacting in the system to generate a given output, and purifying each individual component for *in vitro* analysis can potentially remove additional species important to the mechanism.

The combination of mathematical and experimental approaches can, however, provide specific answers to specific questions. It is with this perspective that I began study of MAPK cascade dynamics. I was provided with time-course data of *in vitro* single MAPK modules, i.e. the phosphorylation of a MAPK by a MAP2K, or phosphorylation of a MAP2K by a MAP3K. From these data, I generated kinetic models and parameters. These models and parameters could then be used to infer how the cascade works *in vivo*, and determine whether or not certain observed *in vivo* properties could be recapitulated from this simple system. Furthermore, understanding of the kinetic parameters helps us determine which features of

the cascade are important, and what each feature actually provides to the cascade. Finally, it tells us which features are conserved between different portions of the cascade, and which are not. This suggests that different aspects of the cascade may be more important for proper signal propagation than others. Each of these pieces of information helps us form a framework for understanding how these cascades generate output.

If a simple kinetic model could recapitulate the time-courses generated by *in vitro* kinase reactions, it could be used as a tool to probe the importance of different kinase cascade features. Modifications could be made to the model as a way of finding useful avenues for further experimentation. Here, such a kinetic model is proposed for portions of the p38α MAPK pathway and the MAPK/ERK pathway. Specifically, the the phosphorylation of MEK6 by ASK1, the phosphorylation of p38α by MEK6, and the phosphorylation of MEK1 by MEKK are modeled. In addition, two mutants of MEK1, MEK1/F53L and MEK1/F53S are tested. Both of these mutants are associated with human disease [100, 101].

In each case, kinetic data was generated through the study of *in vitro* kinase reactions performed by Dr. Humphreys. These reactions were then analyzed by mass spectrometry in order to generate through-time measurements of phosphorylation intermediate concentrations. This data was then provided to me, and I performed model building and curve fitting analyses in order to determine the kinetic parameters of the pathway. Different proposed models were compared by Akaike information criterion in order to reduce overparameterization.

In all cases, the reactions are found to be ordered. The phosphorylation events are all dissociative with the exception of the phosphorylation of MEK6 by ASK1 and the phosphorylation of MEK1wt by MEKK, which are processive. In the MAPK/ERK pathway, introduction of a cancer-associated mutant to MEK1 results in a change of phosphorylation order and a switch from processive to distributive. This suggests that the order and rate of phosphorylation may have significance in pathway propagation, and changes in how the

pathway operates may have relevance in cancer. The importance of each of these features, as well as the overall kinetic model, within the wider context of MAPK cascade signal propagation, is then discussed.

6.3 Materials and methods

LC-MS identification of phosphopeptides and time-course analysis of kinase activity

Time courses of kinase activity were provided by Dr. Humphreys of the Goldsmith lab. In short, kinase reactions were performed *in vitro* and digested enzymatically into smaller peptides. Peptides were then run on liquid chromatography and analyzed by mass spectrometry. This analysis was performed to determine the amount of phospho-peptides produced by the reaction at different times, allowing for a reaction time course to be plotted. The data for the phosphorylation of MEK6 by ASK1 and for the phosphorylation of p38αby MEK6 is shown in figure 6.1.

Cascade model building

Kinetic models for the phosphorylation reactions were defined in DynaFit [102, 103]. The DynaFit software uses the Levenberg-Marquardt algorithm to perform nonlinear least squares regression of progress curve data. Global minimization was achieved by a differential evolution of trial parameter sets [103]. Trial parameter values were taken from those obtained for cellular assays of the ERK2 cascade [104]. The program outputs standard error for each variable and a correlation matrix for the model parameters. All likely kinetic steps were included in the initial models, including separate binding steps leading to different chemical outcomes. Two example starting models are shown in Figure 6.2.

Backward dissociation reactions were typically eliminated because they were too slow to affect the model, leading to an irreversible mechanism. Other steps appeared to be too

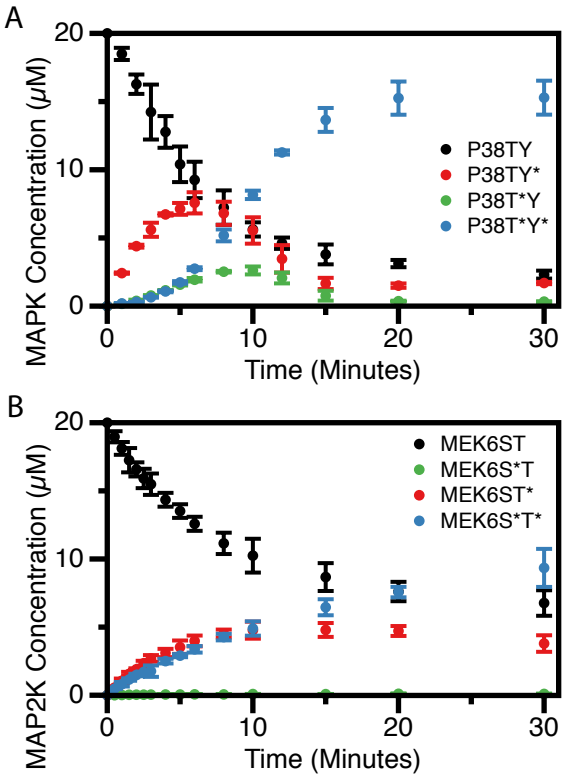

Figure 6.1: **Time course of p38 MAPK cascade components.** Time courses of several tiers of the p38 cascade were provided by Dr. Humphreys of the Goldsmith lab. These data show phosphorylation of p38α by MEK6 (A) and MEK6 by ASK1 (B). Traces represent total iron current selected ion response curves for each proteolytically derived activation loop phosphopeptide, normalized to the initial substrate concentration. Experiments were performed in triplicate with error bars representing one standard deviation. Unphosphorylated (black), monophosphorylated (red and green), and doubly-phosphorylated activation loop peptides were tracked over 30 minutes.

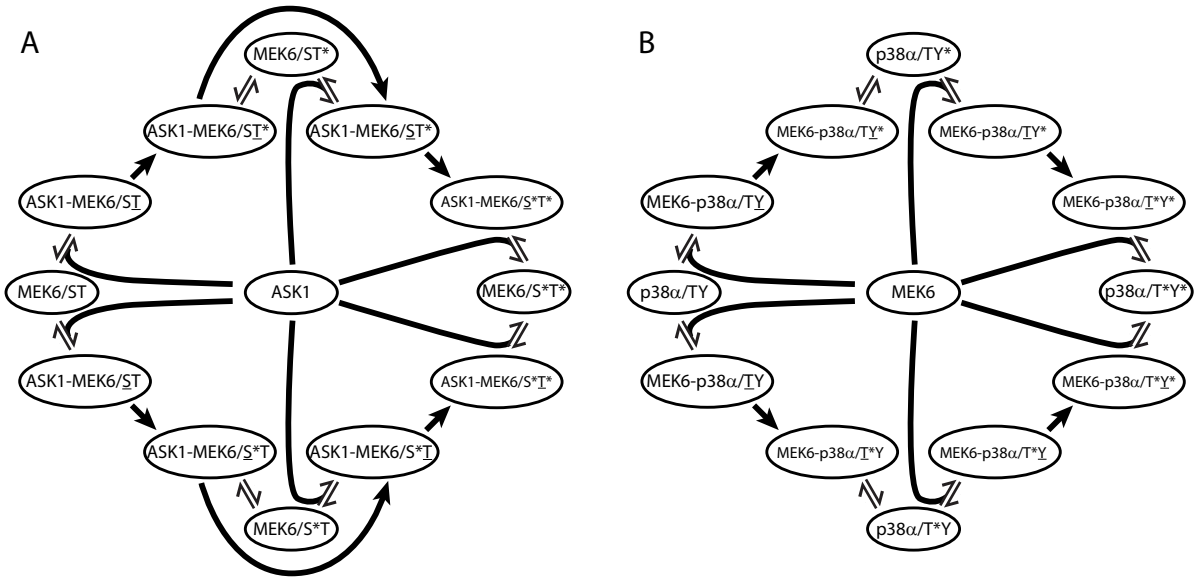

Figure 6.2: **Initial kinetic models for MEK6 and p38α phosphorylation.** (A) ASK1 phosphorylation of MEK6 and (B) MEK6 phosphorylation of p38α are depicted as kinetic models. Each step of the cascade was represented by a series of reversible and irreversible steps. Initial reversible protein complexes leading to a catalytically competent interaction are followed by an irreversible phosphorylation step, then reversible dissociation and rebinding of the monophosphorylated substrate. The model assumes that each binding event positions a single residue in the active site. The residue positioned in the active site is underlined. The second phosphorylation step is similarly modeled leading to a final, doubly phosphorylated product. A processive step was required in the model of ASK1 phosphorylation of MEK6 in order to fit the data. A similar model was used for MEK1 phosphorylation by MEKK.

quick relative to the others to be constrained, and as such they were eliminated. Due to correlation between variables, the forward rate of complex formation was fixed at each level (based on values from the literature), thus improving the fit and the calculated standard error. Equations used are listed in supplemental. Fitting the minority phosphopeptides of the phosphorylation of p38α required normalizing the weight of each intermediate species to 1.

In order to determine whether or not the reaction was processive or distributive, two models were tested for each time-course dataset. One of the models would include a processive kinetic term, one of the models would not. The two models would then be fit to the data, and the fits would be compared. Because it is impossible for the model with the processive term to fit worse than the model without the processive term, the Akaike information criterion was used to compare the two models.

6.4 Results

Kinetic models based on elementary rate constants can describe MAPK cascades

A simple model based on elemental rate constants is capable of recapitulating curves generated from time-courses of *in vitro* kinase reactions. Both the fits for the refined processive and distributive models for ASK1→MEK6 are shown in figure 6.3, and for MEKK + MEK1 in figure 6.4. A processive model for the phosphorylation of p38α by MEK6 and for each of the MEK1 mutants was created, but the processive term was always minimized to zero. As such, only the distributive fit to the model is shown (Figure 6.5, 6.6). The models for each for these fits are similarly shown in figures 6.7–6.11. When the AIC was used to distinguish between processive and distributive models, it is shown in the graph. Processive terms show significantly lower AIC in two of the three models tested, suggesting that a processive term is required for proper fitting. Once models were constructed and fit to the data, parameters were determined for each kinetic step: the parameters for the reactions in

the p38α cascade are shown in table 6.1 and 6.2, the parameters for the phosphorylation of MEK1 by MEKK are shown in table 6.3.

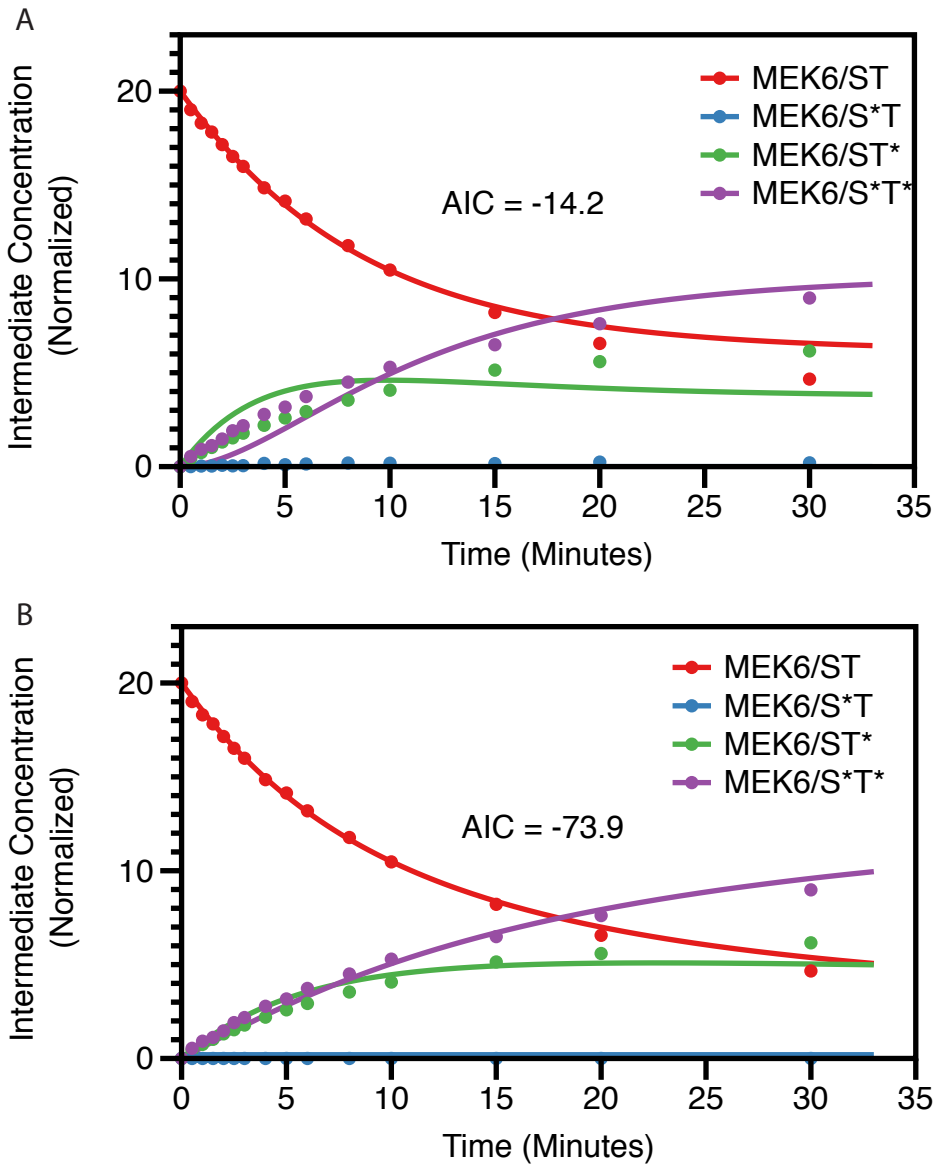

Figure 6.3: **Fit of the ASK1 phosphorylation of MEK6.** Both the distributive (A) and processive (B) models for ASK1 phosphorylation of MEK6 were evaluated using the DynaFit software[102][103]. Calculated progress curve derived from the model and predicted kinetic constants (lines) is shown superimposed on the experimental data (points).

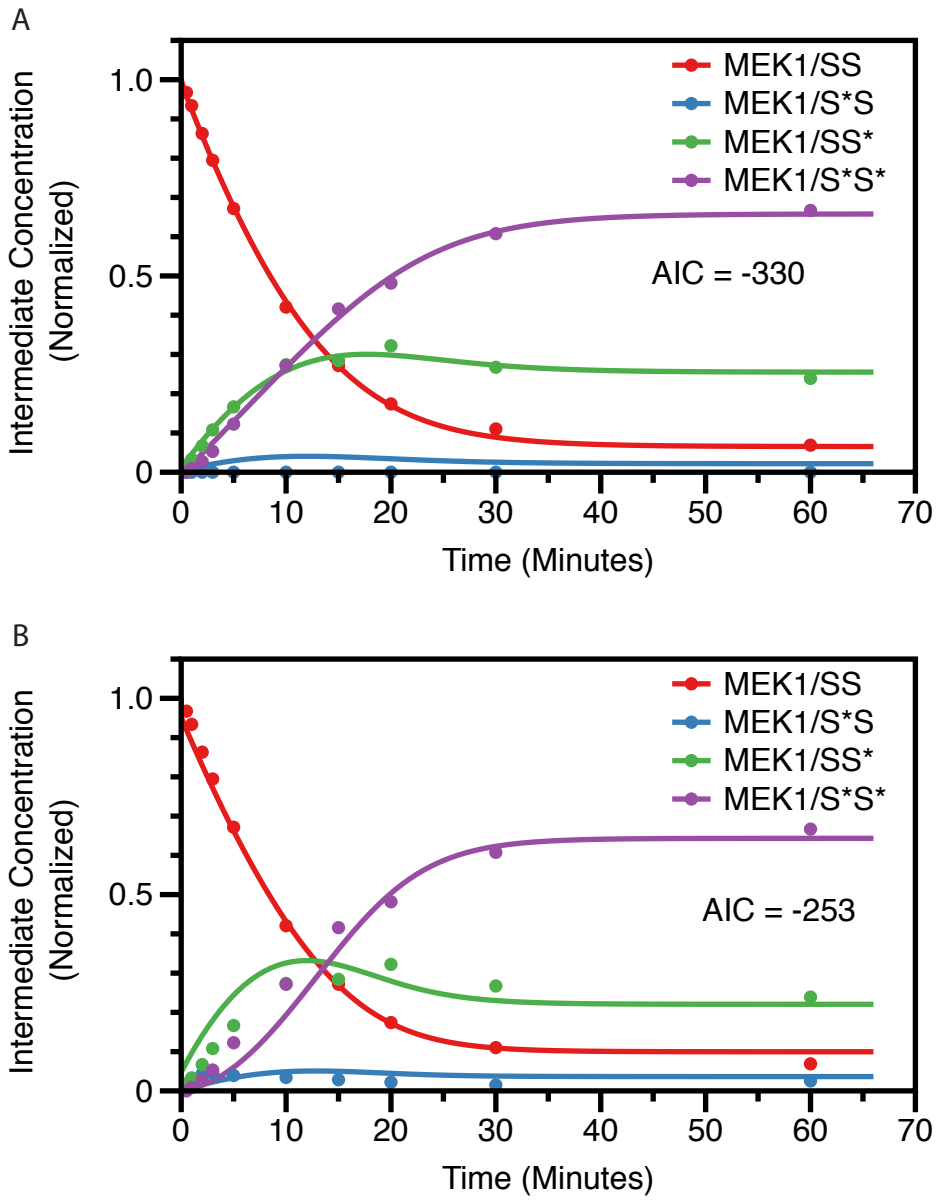

Figure 6.4: **MEK1 phosphorylation curve fitting with distributive and processive models.** The distributive (A) and processive (B) kinetic phosphorylation models of MEK1wt were evaluated using the DynaFit software[102][103]. Calculated progress curves derived from the models (lines) are shown superimposed on the experimental data (points). The AIC is shown for the fit of both models.

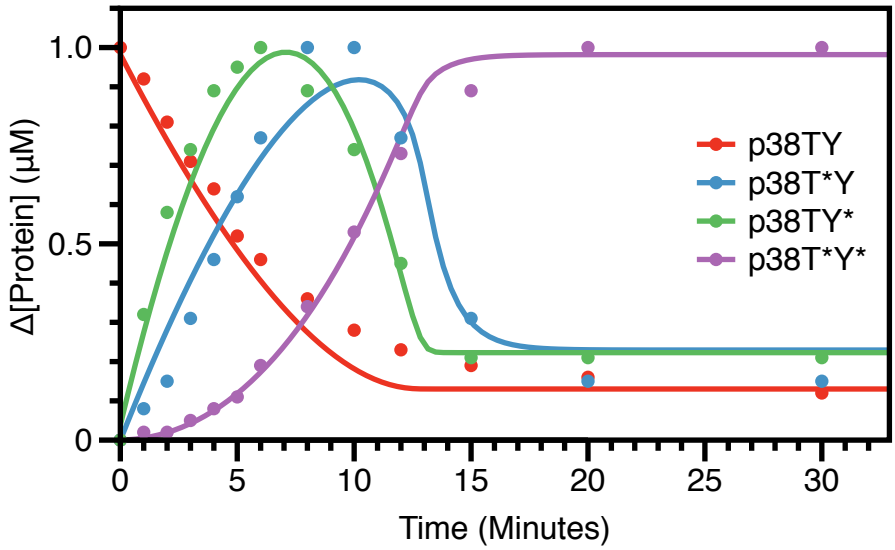

Figure 6.5: **Fit of the MEK6 phosphorylation of p38α.** A distributive model for MEK6 phosphorylation of p38α was evaluated using the DynaFit software[102][103]. Data was normalized to 1 in order to fit low-abundance species. Calculated progress curve derived from the model and predicted kinetic constants for MEK6 phosphorylation of p38α (lines) is shown superimposed on the experimental data (points).

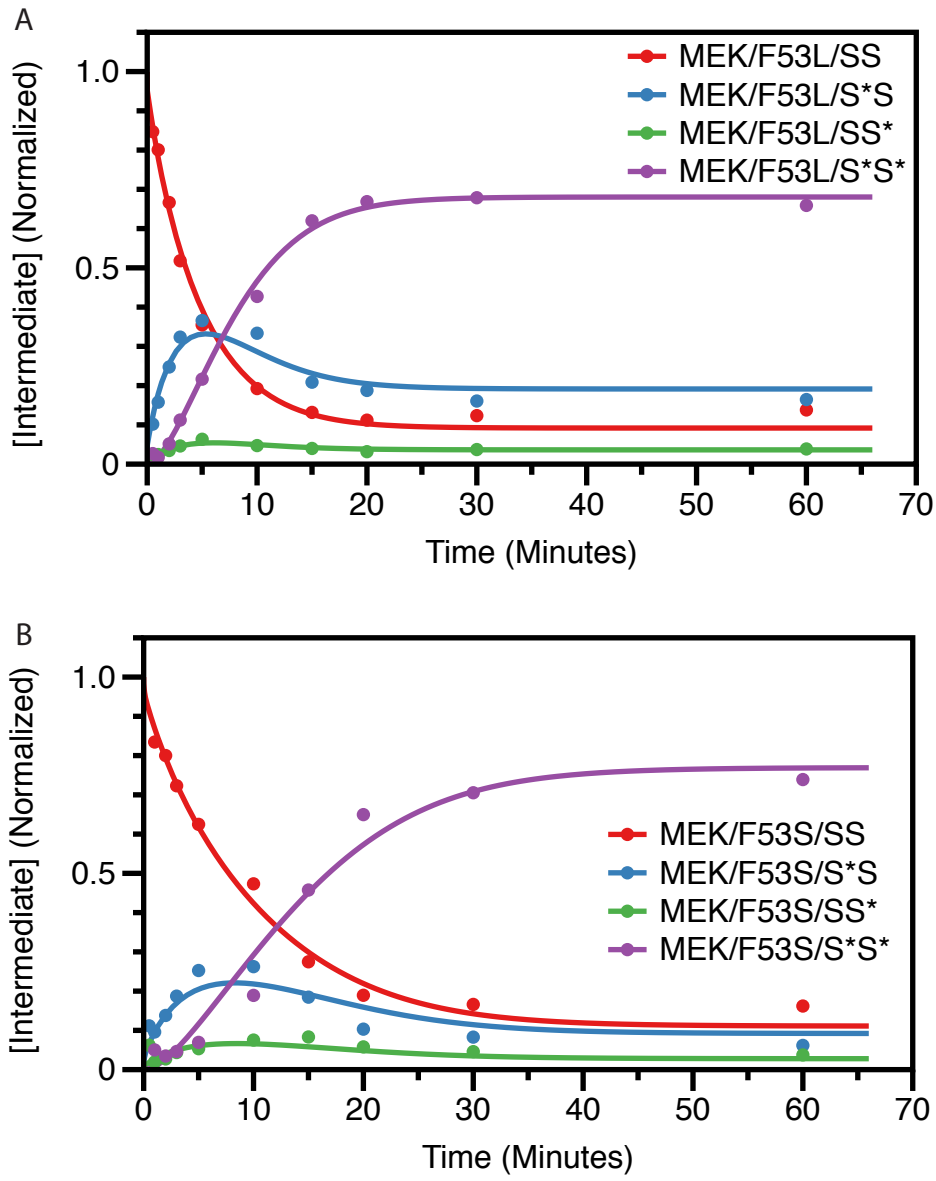

Figure 6.6: **Timecourse of mutant MEK1 phosphorylation.** The kinetic phosphorylation models of MEK1/F53S (A) and MEK1/F53L (B) by MEKK1 were evaluated using the DynaFit software[102][103]. Calculated progress curves derived from the models (lines) are shown superimposed on the experimental data (points).

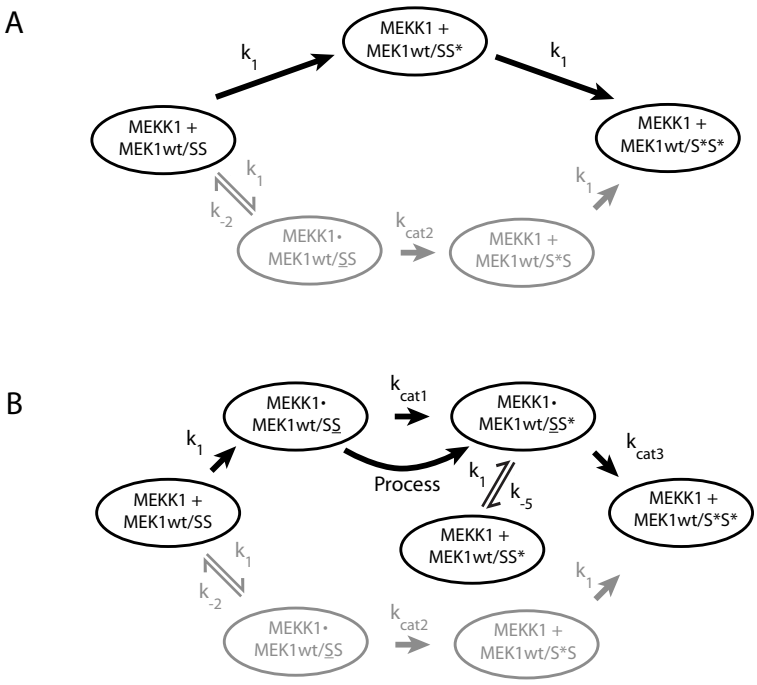

Figure 6.7: **The processive and distributive MEK1 phosphorylation models.** The two models for MEK1wt phosphorylation are presented: distributive (A) and processive (B). In the processive model, the substrate can be phosphorylated twice before it disassociates. In the distributive model, the substrate always completely disassociates between phosphorylation events. The lightly shaded pathway is unfavored. The underlined residue is the residue positioned in the active site for phosphorylation. Each model represented here is the simplest model that fits the data, as assessed by the AIC.

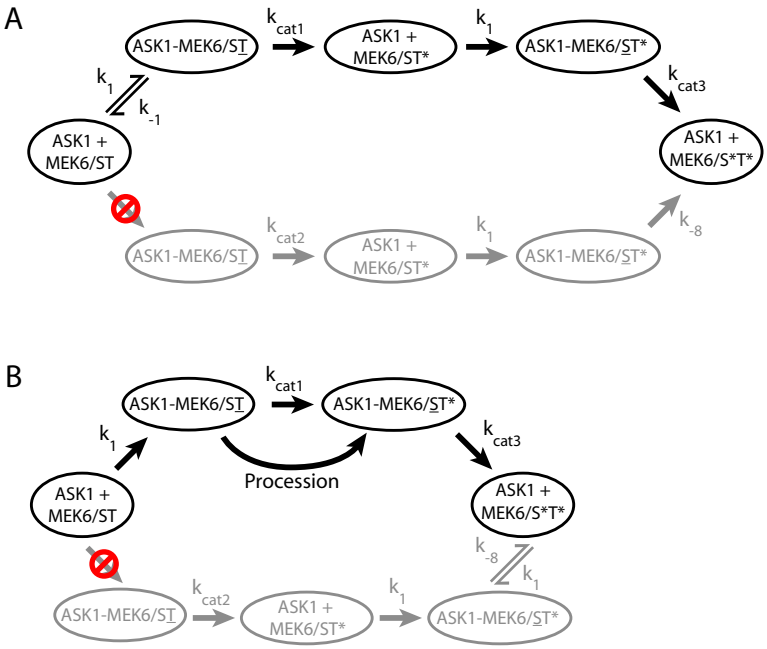

Figure 6.8: **The processive and distributive MEK6 phosphorylation models.** The two models for MEK6 phosphorylation are presented: distributive (A) and processive (B). In the processive model, the substrate can be phosphorylated twice before it disassociates. The 'procession' to the next residue is fast. In the distributive model, the substrate always completely disassociates between phosphorylation events. The lightly shaded pathway is unfavored. The underlined residue is the residue positioned in the active site for phosphorylation. Each model represented here is the simplest model that fits the data, as assessed by the AIC.

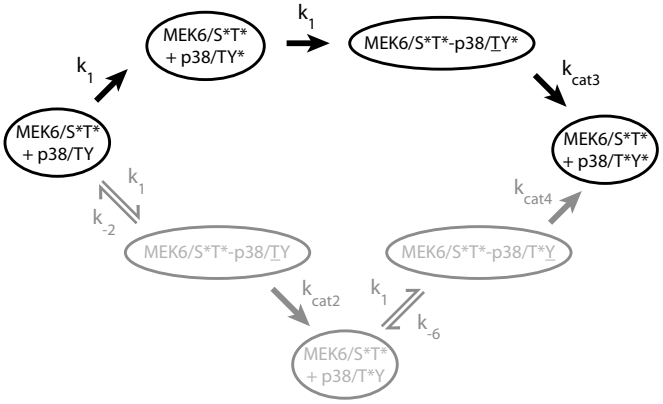

Figure 6.9: **The distributive model of p38α.** The distributive model of p38α is shown. Attempts to generate a processive term resulted in models similar to the distributive model, with the processive term minimized. The lightly shaded pathway is unfavored. The underlined residue is the residue positioned in the active site for phosphorylation. The model represented here is the simplest model that fits the data, as assessed by the AIC.

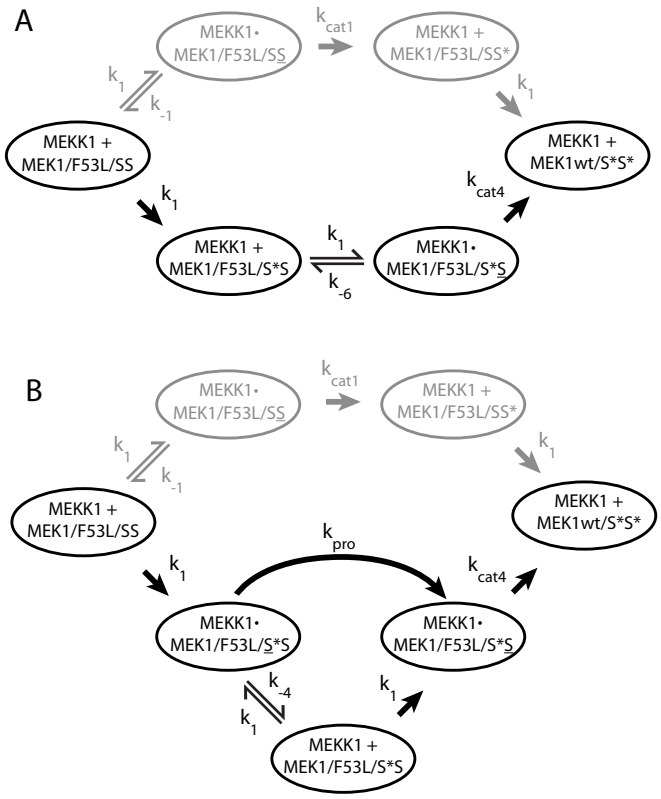

Figure 6.10: **A model of the processive and distributive models in MEK1/F53L** Two models for the phosphorylation of MEK1/F53L are shown: distributive (A) and processive (B). Both models are shown after the number of parameters have been minimized. The only difference between the two models is the addition of a processive term in B.

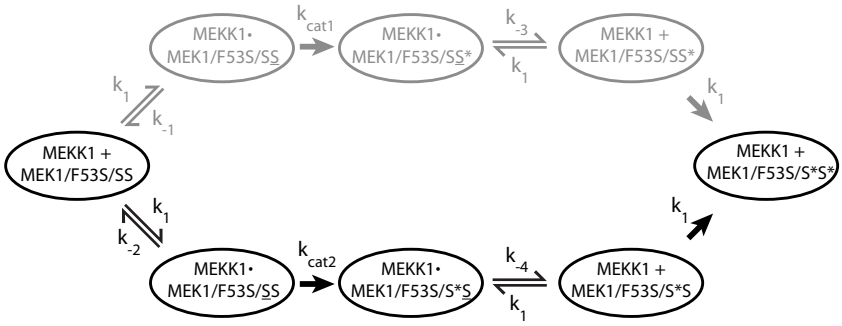

Figure 6.11: **A distributive model of MEK1/F53S phosphorylation** The distributive model for MEK1/F53S phosphorylation used in the final fit is shown. The processive model is not shown as it is identical to the distributive model, with the processive term minimized to zero.

The simulated progress curves based on the derived parameters and models fit the data well. Several broad trends emerged from the data: formation of enzyme:product complexes was often slow compared to catalysis, and complex disassociation rates were often slow in the unfavored pathway. These two phenomenon may be linked. Because the k_{on} rate was fixed, if the chosen value was lower than the actual value, the predicted k_{cat} would have to be significantly higher than the actual value in order to accommodate for the slower k_{on}. This could render the k_{cat} and k_{off} values poorly constrained. Similarly, the fixed k_{on} values restrict the total number of parameters that can distinguish the 'fast' and 'slow' pathways. The slow disassociation rates in the unfavored pathway can help modulate the activity of the favored pathway by 'trapping' enzyme in unproductive complexes for long periods of time. In order to make sure that this is not an artifact of the model architecture, multiple conditions will have to be tested to determine the k_{cat} values at each step of the reaction. At lower substrate concentrations, k_{on} dominates over k_{cat}; in higher concentrations, k_{cat} dominates.

The models for the MAP3K→MAP2K tier and the MAP2K→MAPK tier appear different. A processive term was required to explain the rapid appearance of the doubly-phosphorylated species observed in the MAP3K→MAP2K tier. This means that the MAP3K was able to switch from binding the first activation loop phosphorylation site (MEK6/S$\underline{\text{T}}$*, or MEK1/S$\underline{\text{S}}$*) to binding the second phosphorylation site without disassociation of the enzyme:product complex. The phosphorylation of p38α by MEK6, in comparison, required a strong asymmetry in the K_m between the favored and unfavored intermediate formation in order to offset the peak appearance of the different monophosphorylated intermediates. Whether or not this trend is maintained across other cascades is not yet known.

Table 6.1: Derived parameters of p38α phosphorylation

Parameter	p38α distributive
k_1 [a]	150
k_{-1} [b]	–
k_{cat1} [b]	–
k_{-2} [b]	30±4
k_{cat2} [b]	7±0.7
k_{-3} [b]	–
k_{-4} [b]	–
k_{-5} [b]	–
k_{cat3} [b]	32±6
k_{-6} [b]	$1 \cdot 10^{-6} \pm 7 \cdot 10^{7}$
k_{cat4} [b]	$1.3 \cdot 10^{4} \pm 1 \cdot 10^{7}$
k_{-7} [b]	–
k_{-8} [b]	–
k_{dis} [b]	0.03±0.003

[a] $\mu M^{-1} min^{-1}$
[b] min^{-1}
[c] Values were either too fast or slow to be captured by the model
Steps not accounted for by the model are indicated by —

Table 6.2: Derived parameters of ASK1 phosphorylation of MEK6

Parameter	MEK6 distributive	MEK6 processive
k_1 [a]	150	150
k_{-1} [b]	1800±7000	–
k_{cat1} [b]	128±193	80±186
k_{-2} [b]	–	–
k_{cat2} [b]	–	–
k_{-3} [b]	–	–
k_{-4} [b]	–	–
k_{-5} [b]	$1.9 \cdot 10^5 \pm 6 \cdot 10^7$	1475±82000
k_{cat3} [b]	$3 \cdot 10^5 \pm 1 \cdot 10^7$	930±52000
k_{-6} [b]	–	–
k_{cat4} [b]	–	–
k_{-7} [b]	–	–
k_{-8} [b]	–	41±100
k_{pos1} [b]	–	–
k_{dis} [b]	0.16±0.4	1.5±1.1

[a] $\mu M^{-1} min^{-1}$
[b] min^{-1}
[c] Values were either too fast or slow to be captured by the model
Steps not accounted for by the model are indicated by —

Table 6.3: Derived parameters of MEK1wt and MEK1 mutant phosphorylation

Parameter	MEK1wt distributive	MEK1wt processive	MEK1/F53S distributive	MEK1/F53S processive	MEK1/F53L distributive	MEK1/F53L processive
k_1 [a]	100	100	100	100	100	100
k_{-1} [b]	–	–	28±124	24±332	2.9±0.3	4.4±3.8
k_{cat1} [b]	–	–	3.8±28	3.2±42	0.6±0.1	0.8±0.7
k_{-2} [b]	0.97±0.1	–	1880±84,000	$1688\pm2\cdot10^6$	–	–
k_{cat2} [b]	0.17±0.05	1.9±1.5	1350±606,000	$1200\pm1\cdot10^6$	–	–
k_{-3} [b]	–	2.2±6.6	1.6±7	1.6±9	–	–
k_{-4} [b]	–	0.7±0.9	2.7±7	2.7±8	–	16±41
k_{-5} [b]	–	1.4±2.1	–	–	–	–
k_{cat3} [b]	–	3.7±105	–	–	3.3±0.5	–
k_{-6} [b]	–	–	–	–	–	–
k_{cat4} [b]	–	1.5±2.2	–	–	–	3.3±1.1
k_{-7} [b]	–	–	–	–	–	–
k_{-8} [b]	–	–	–	–	–	–
k_{pos1} [b]	–	3.2±97	–	$1\cdot10^{-7}\pm1\cdot10^{-3}$	–	0.7±1.5
k_{pos2} [b]	–	–	–	–	–	–
k_{dis} [b]	47±2	73±3	36±4	24±7	45±1.2	46±1.4

[a] $\mu M^{-1}min^{-1}$
[b] min^{-1}
[c] Values were either too fast or slow to be captured by the model
Steps not accounted for by the model are indicated by —

Kinetic reaction parameters can be identified

Fitting the model to the data resulted in an estimation of each kinetic parameter in the model. To our delight, the derived parameters shown in tables 6.1 are similar to those found in Fujioka *et al.* for phosphorylation of MEK and ERK in cells [104]. Standard error for parameters was typically in the range of 10–50%. In cases where the error was higher, typically it is because two parameters are directly correlated: so long as the parameters are above a certain threshold, and they maintain the correct ratio, they are unbounded. Restricting these parameters would require a larger dataset taken under more varied enzyme and substrate concentrations. The parameters suggest that the reaction specificity is controlled not only by k_{cat} effects, but also the rate of enzyme:substrate complex formation. Determining the k_{cat} values for each reaction step would dramatically reduce the number of parameters, and allow for the determination of accurate K_m values.

Each phosphorylation event is ordered

The parameters confirm that the majority of the reaction flux progresses through a single intermediate— in the phosphorylation of MEK6, this is MEK6/ST*, in the phosphorylation of p38α, this is p38α/TY*, and in the phosphorylation of MEK1, this is MEK1/SS* (Figure 6.12 and 6.13A). No rate graph is provided for the phosphorylation of MEK6 by ASK1, as almost none of the disfavored intermediate was observed, leading to very small calculated values of MEK6/S*T formation. This is keeping with expectations for the cascade, as ordered reactions result in sharper switch-like behavior [8]. Surprisingly, the order of both mutants MEK1/F53S and MEK1/F53L appears opposite from MEK1wt (Figure 6.13B and C).

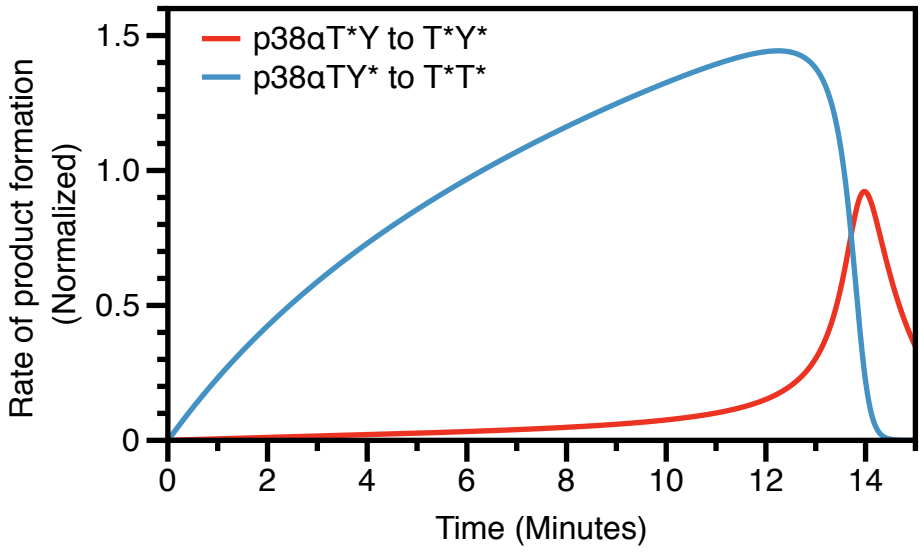

Figure 6.12: **Calculated reaction velocities for the phosphorylation of p38α based on the model.** The relative rate of doubly-phosphorylated product that is produced through the two intermediates p38α/T*Y (red) and p38α/TY* (blue) is plotted. The majority of the flux is observed through the p38α/TY* intermediate, suggesting an order to the reaction.

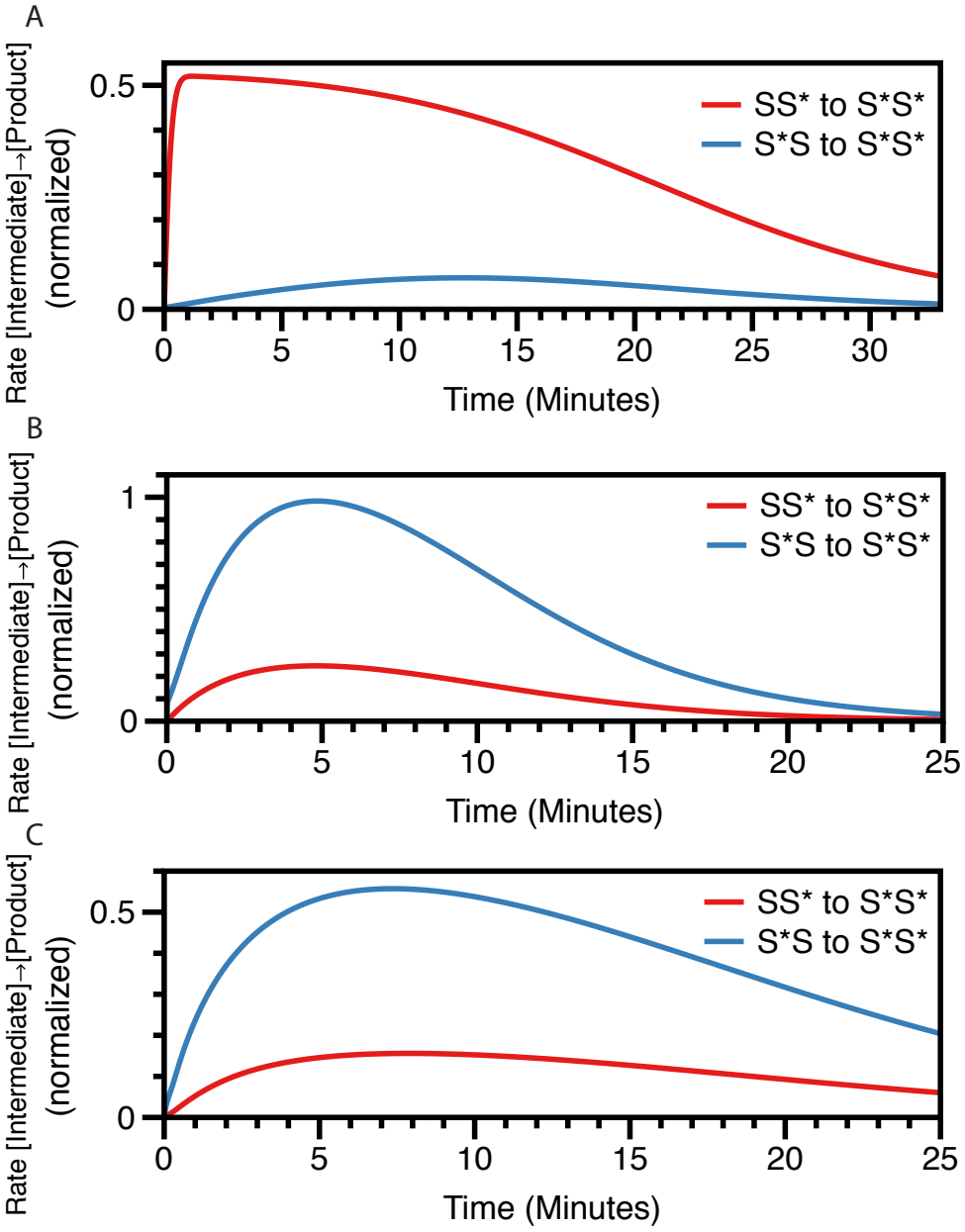

Figure 6.13: **Calculated reaction velocities for the phosphorylation of MEK1 based on the model.** The relative rate of doubly-phosphorylated product that is produced through the two intermediates, MEK1/SS*(red) and MEK1/S*S (blue), is plotted. The phosphorylation of MEK1wt (A), MEK1/F53S (B), and MEK1/F53S (C) are plotted. The majority of the flux for MEK1wt is observed through the MEK1/SS* intermediate, suggesting an order to the reaction. Both of the mutants show an opposite order.

Processivity is neither mandated nor forbidden

Surprisingly, some processivity was observed at the level of MAP2K phosphorylation. In typical models of generic protein kinase cascades, disassociation is required between phosphorylation events. This allows for a 'stepping-stone' effect, where the first phosphorylation primes the kinase for subsequent activation. This stepping-stone phosphorylation is required for the sigmoid appearance of active kinase shown in the time-course of p38α (Figure 6.5, purple line). In the phosphorylation of MEK6 and MEK1, however, the formation of the doubly-phosphorylated species looks much like a single-substrate reaction that follows Michaelis-Menten kinetics. This causes an immediate and more graded formation of the active, doubly-phosphorylated species. Surprisingly, the two disease-associated MEK1 mutants, MEK1/F53S and MEK1/F53L appear to be phosphorylated in a distributive mechanism, as opposed to a processive mechanism. It is not yet known whether or not this change in mechanism is important to their disease-related effects.

6.5 Conclusions

Importance of phosphorylation order

There are three possible outcomes for the experiments performed to determine order of phosphorylation of two residues: phosphorylation of one residue first, phosphorylation of the other residue first, and random order. Each of these three possibilities potentially gives rise to a different response-to-signal downstream output— partially as a result of statistical mechanics, and partially as a result of enzyme mechanism-of-action. That order appears conserved in both of the systems examined is suggestive that it is important.

Mechanistically, if one phosphorylation site is activating, and the other phosphorylation site is not, then an order where the activating phosphorylation site is 'first' is going to have a different output than one where the 'stepping-stone' phosphorylation event is first. In the second circumstance, the through-time sigmoidicity of the output signal will be greater.

This results from the intermediate having no activity, thus delaying the appearance of the active species. This increased sigmoidicity suggests that the p38α/TY* intermediate should be inactive, and direct measurements by other groups agree with this view. In work by YY. Zhang *et al.* [105], monophosphorylated p38α was generated by using either Tyr specific or Ser/Thr specific phosphatases. While p38α/T*Y had 10–20 fold less activity than p38α/T*Y*, p38α/TY* activity was barely detectable. This increase in sigmoidicity assumes that the reaction proceeds using a dissociative mechanism: if the reaction is processive, sigmoidicity is not observed in the production of the final product.

The statistics of an ordered reaction can also increase the sigmoidicity of the output, if the reaction is observed in the context of a phosphatase. Because the system has an enzyme working in the forward (phosphorylation) direction, and an enzyme working in the backward (phosphatase) direction, the sigmoidicity is observed in equilibrium. This is discussed in more detail below.

Importance of reaction processivity

The importance of order in signal propagation is neither as obvious nor as significant as processivity— why, then, is order conserved between tiers while processivity, or a lack thereof, is not? Further, processivity seems to render the two separate phosphorylation events characteristic of MAPK cascade tiers extraneous. Aoki *et al.* [106] measured phosphorylation of ERK, a MAPK, in cells, and also observed processivity, suggesting that this may not be an artifact of conducting the experiment *in vitro*. It is possible that the amount of processivity in the reaction is a way in which the signal-to-response could be modulated. Why the order would be conserved, however, is difficult to explain— order may simply be a consequence of the mechanism by which it attains processivity. The processive mechanism favors immediate production of active kinase product by the upstream kinase. This would not generate the switch-like responses associated with double-phosphorylation events. The active MAP2K

produced in this step could serve as a mechanism for signal amplification or signal conduction. Unfortunately, given the wildly varying cellular MAPK cascade component concentrations reported from different tissues, it is difficult to say whether or not that might be the case [2, 104, 107–111].

6.6 Future Directions

Parameter determination

A number of the kinetic parameters defined by this model analysis offer interesting interpretations of the cascade— for example, the second step of p38α phosphorylation appears to have a low K_m. Low K_m values indicate that the kinase-substrate complex is long-lived, which is by itself sufficient to result in ultrasensitive behaviors under some milieus. While observations like these provide potential insights into why kinase cascades have the kinetic parameters that they do, a number of assumptions had to be made to constrain the model. Because of these assumptions, it is almost certain that the absolute, rather than relative, values for each kinetic parameter were not determined. Determining the actual values for each parameter could shed more light on how these systems work, and help find similarities and differences between each tier of the cascade. This will be especially useful in identifying how, exactly, the different MEK1 mutations were affecting phosphorylation.

Because there are four potential catalytic reactions that result from the mixing of just the kinase and substrate, however, different approaches must be taken to determine the absolute kinetic parameters. In order to minimize the number of species the kinase can interact with, a residue-specific phosphatase can be introduced to the fully-phosphorylated species. This will generate a pure, or relatively pure, monophosphorylated species. Because this intermediate can only be phosphorylated in one position, the reaction is greatly simplified. This simplified system can then be used to determine the different kinetic parameters for the second phosphorylation event. Once these parameters are determined, it could po-

tentially constrain the model enough to properly determine the kinetic parameters at the first stage of the reaction as well.

Mutant analysis

The two mutants MEK1/F53L and MEK1/F53S cause significant qualitative changes to how they are phosphoylated as compared to wild-type. The phosphorylation of MEK1wt by MEKK appears processive and ordered, starting with MEK1/SS*, then proceeding to MEK1/S*S*. Both the mutants appear to progress through the MEK1/S*S intermediate, and both mutants appear to utilize a distributive mechanism. That these two changes appear due to a single mutation suggests that they may be linked.

One possibility that should be investigated is that MEK1wt actually proceeds through the MEK1/S*S intermediate, and not the MEK1/SS* intermediate. This could be the case if the MEK1wt reaction is highly processive, which would make MEK1wt/S*S appear to be a minority species. Unfortunately, this is difficult to test. Mutation of either serine would likely modify the activity of the kinase on MEK1, which would confound the result. Generation of the MEK1/S*S and MEK1/SS* species could provide the answer, as the relative rates of reaction from those species to MEK1/S*S* could then be used to inform the model, and would help distinguish between the two possibilities.

In vitro recapitulation of the entire cascade

In addition to the study of additional MAPK pathways, the addition of phosphatases to the cascade to study steady-state behaviors is critical to our understanding of MAPK cascade dynamics. While the *in vitro* reactions performed with the purified enzyme and substrate can, in theory, give you all kinetic parameters of interest, it is impossible to recapitulate the system behavior with only two species. This is because the *in vivo* system exists in equilibrium, which requires both a forward and reverse reaction. In order to confirm

our understanding of these cascades, a complete tier of the cascade consisting of a kinase, a phosphatase, and a substrate must be reconstituted.

Appendices

Appendix A

Screening Results

This is a comma-deliniated result list of the 200k compound re-screen.

,10 uM Compound concentration,,,,3.3 uM Compound concentration,,,,1 uM Compound concentration,,, SWID,Confirmation Activity 1,Confirmation Activity 2,Mean Activity,Mean Z-Score,Confirmation Activity 1,Confirmation Activity 2,Mean Activity,Mean Z-Score,Confirmation Activity 1,Confirmation Activity 2,Mean Activity,Mean Z-Score

SW200706,95.99,100.28,98.14,13.07,106.94,105.97,106.46,14.18,98.34,90.50,94.42,12.58

SW203569,92.90,98.72,95.81,12.76,102.05,104.44,103.25,13.76,100.13,88.51,94.32,12.57

SW202309,88.21,92.60,90.41,12.04,102.11,102.98,102.55,13.66,100.89,95.40,98.14,13.08

SW200312,84.42,91.28,87.85,11.70,99.43,103.12,101.28,13.49,95.81,84.43,90.12,12.01

SW003832,82.48,101.09,91.79,12.23,102.41,99.01,100.71,13.42,96.18,99.72,97.95,13.05

SW200280,89.36,95.80,92.58,12.33,96.20,103.38,99.79,13.29,72.78,61.48,67.13,8.94

SW200765,87.45,90.27,88.86,11.84,100.43,98.26,99.35,13.24,86.65,83.21,84.93,11.32

SW200266,75.66,84.26,79.96,10.6527597921663+E10,97.26,99.43,98.35,13.10,89.96,89.78,89.87,11.97

SW200279,83.00,84.42,83.71,11.15,95.05,99.31,97.18,12.95,83.66,75.02,79.34,10.57

SW198072,85.81,93.17,89.49,11.92,95.17,99.18,97.18,12.95,63.73,58.24,60.99,8.12

SW203568,84.44,87.84,86.14,11.48,97.13,96.88,97.00,12.92,90.30,89.37,89.83,11.97

SW201128,62.44,55.76,59.10,7.87,95.71,98.08,96.89,12.91,99.02,95.42,97.22,12.95

SW200277,85.37,84.22,84.79,11.30,94.43,99.29,96.86,12.90,76.97,76.23,76.60,10.20

SW200278,80.92,84.19,82.56,11.00,94.84,98.07,96.46,12.85,88.29,83.43,85.86,11.44

SW166159,78.83,90.37,84.60,11.27,95.13,97.69,96.41,12.84,94.84,84.41,89.62,11.94

SW034508,91.47,91.70,91.59,12.20,94.29,98.21,96.25,12.82,99.34,88.67,94.00,12.52

SW202294,82.10,86.87,84.48,11.26,93.79,96.44,95.12,12.67,95.95,87.47,91.71,12.22

SW200263,67.83,84.56,76.19,10.15,90.86,97.36,94.11,12.54,86.17,75.79,80.98,10.79

SW202307,72.56,76.12,74.34,9.90,93.82,94.10,93.96,12.52,86.33,88.35,87.34,11.64

SW202308,78.89,78.29,78.59,10.47,94.18,93.45,93.81,12.50,88.59,85.62,87.10,11.60

SW057184,78.62,88.44,83.53,11.13,94.97,92.35,93.66,12.48,81.51,90.21,85.86,11.44

SW203577,88.91,105.84,100.05,13.33,88.14,90.57,93.61,12.47,79.34,82.19,78.34,10.44

SW035739,80.49,79.92,80.20,10.68,91.50,93.93,92.71,12.35,62.59,64.70,63.64,8.48

SW202425,85.16,87.46,86.31,11.50,91.85,92.78,92.32,12.30,64.83,67.11,65.97,8.79

SW083604,90.39,87.89,89.14,11.88,92.29,92.19,92.24,12.29,70.92,73.70,72.31,9.63

SW200311,63.07,74.36,68.72,9.15,91.22,93.08,92.15,12.28,90.50,84.72,87.61,11.67

SW148459,88.22,105.97,97.10,12.94,92.61,90.33,91.47,12.19,67.00,62.52,64.76,8.63

SW034538,76.58,90.70,83.64,11.14,90.73,91.63,91.18,12.15,80.22,86.27,83.25,11.09

SW202295,69.79,81.28,75.53,10.06,90.24,92.12,91.18,12.15,96.94,88.42,92.68,12.35

SW200245,80.71,92.69,86.70,11.55,89.42,92.05,90.74,12.09,73.82,72.62,73.22,9.75

SW202293,79.73,85.32,82.52,10.99,88.97,91.66,90.31,12.03,66.73,58.78,62.76,8.36

SW202316,86.50,99.74,93.12,12.41,89.74,90.62,90.18,12.01,80.33,82.28,81.31,10.83

SW003833,86.91,88.98,87.94,11.72,90.53,89.72,90.12,12.01,67.90,65.92,66.91,8.91

SW202296,74.59,88.31,81.45,10.85,89.51,90.53,90.02,11.99,90.48,90.49,90.48,12.05

SW200264,73.11,83.81,78.46,10.45,88.05,90.47,89.26,11.89,82.42,77.78,80.10,10.67

SW018385,85.77,105.76,95.77,12.76,89.34,88.47,88.91,11.84,75.93,74.20,75.07,10.00

SW203570,79.28,86.83,83.05,11.07,86.29,90.83,88.56,11.80,80.18,75.85,78.01,10.39

SW203571,80.19,87.38,83.78,11.16,85.96,90.04,88.00,11.72,85.80,72.45,79.13,10.54

SW057425,92.66,89.71,91.19,12.15,88.48,87.46,87.97,11.72,31.91,24.62,28.26,3.77

SW195956,-8.72,-7.40,-8.06,-1.07,89.75,85.28,87.51,11.66,18.45,19.29,18.87,2.51

SW082311,84.20,85.03,84.62,11.27,84.49,90.22,87.35,11.64,83.53,77.34,80.43,10.72

SW200265,76.94,91.02,83.98,11.19,84.25,90.43,87.34,11.64,78.90,79.74,79.32,10.57

SW034452,80.28,80.69,80.48,10.72,86.73,87.92,87.32,11.63,28.53,27.47,28.00,3.73

SW029247,79.23,79.42,79.32,10.57,87.23,85.94,86.58,11.54,81.27,71.34,76.31,10.17

SW200771,88.84,90.05,89.44,11.92,87.52,85.64,86.58,11.53,50.17,48.03,49.10,6.54

SW200707,73.78,84.68,79.23,10.56,82.94,89.70,86.32,11.50,88.11,62.60,75.35,10.04

SW203572,84.80,93.02,88.91,11.85,85.90,86.67,86.28,11.50,60.95,55.30,58.13,7.74

SW003836,72.78,80.08,76.43,10.18,83.19,89.14,86.17,11.48,65.23,56.76,60.99,8.13

SW003142,83.82,86.48,85.15,11.34,86.89,84.83,85.86,11.44,55.62,64.63,60.12,8.01

SW200716,89.15,95.52,92.33,12.30,83.61,87.88,85.74,11.42,49.88,40.39,45.13,6.01

SW200767,80.16,89.51,84.84,11.30,81.98,89.34,85.66,11.41,55.49,40.22,47.86,6.38

SW201127,51.59,51.19,51.39,6.85,81.35,89.11,85.23,11.36,100.44,100.20,100.32,13.37

SW200310,35.83,51.99,43.91,5.85,84.34,85.10,84.72,11.29,74.97,83.91,79.44,10.58

SW109820,80.71,90.26,85.48,11.39,84.71,84.37,84.54,11.26,57.10,53.05,55.08,7.34

SW200768,80.31,85.74,83.03,11.06,80.87,88.15,84.51,11.26,62.26,48.45,55.36,7.37

SW203567,87.00,97.96,92.48,12.32,83.59,84.46,84.02,11.19,56.07,56.43,56.25,7.49

SW159226,75.61,88.41,82.01,10.93,86.66,81.13,83.89,11.18,77.16,76.79,76.98,10.26

SW200281,85.15,93.37,89.26,11.89,78.68,88.87,83.78,11.16,41.63,34.01,37.82,5.04

SW200309,37.55,54.73,46.14,6.15,83.54,82.83,83.18,11.08,82.81,81.81,82.31,10.97

SW200766,80.90,86.65,83.78,11.16,82.46,83.79,83.13,11.07,53.58,42.31,47.95,6.39

SW029232,85.19,86.41,85.80,11.43,82.43,83.11,82.77,11.03,71.41,62.46,66.93,8.92

SW201129,61.99,60.14,61.06,8.14,80.71,84.61,82.66,11.01,61.82,58.66,60.24,8.03

SW200708,78.24,86.36,82.30,10.96,78.53,86.43,82.48,10.99,52.87,36.99,44.93,5.99

SW029249,91.80,95.28,93.54,12.46,82.54,82.14,82.34,10.97,70.36,59.98,65.17,8.68

SW018506,56.96,73.70,65.33,8.70,82.26,82.18,82.22,10.95,63.26,64.69,63.97,8.52

SW170743,83.74,90.22,86.98,11.59,76.39,87.82,82.10,10.94,25.70,21.50,23.60,3.14

SW039634,63.20,78.21,70.71,9.42,81.25,82.65,81.95,10.92,58.69,45.57,52.13,6.95

SW029253,75.91,78.73,77.32,10.30,81.84,81.70,81.77,10.89,65.84,59.91,62.87,8.38

SW034501,70.63,79.35,74.99,9.99,81.43,81.18,81.31,10.83,61.83,65.61,63.72,8.49

SW019351,85.52,86.79,86.15,11.48,78.92,83.31,81.11,10.81,49.89,66.45,58.17,7.75

SW145091,78.35,80.26,79.31,10.57,80.58,81.52,81.05,10.80,58.24,54.98,56.61,7.54

SW034509,75.88,75.16,75.52,10.06,81.20,80.86,81.03,10.80,74.33,69.38,71.86,9.57

SW034524,77.39,83.24,80.32,10.70,81.26,80.18,80.72,10.75,77.29,69.90,73.59,9.80

SW004813,83.08,101.15,92.12,12.27,81.16,79.79,80.47,10.72,23.97,13.85,18.91,2.52

SW200769,81.79,100.08,90.94,12.12,77.01,83.85,80.43,10.72,56.45,53.06,54.76,7.30

SW083688,99.77,91.04,95.41,12.71,83.71,76.58,80.15,10.68,82.31,81.79,82.05,10.93

SW202310,71.05,74.89,72.97,9.72,78.47,80.85,79.66,10.61,50.85,43.19,47.02,6.26

SW083332,88.65,83.14,85.89,11.44,77.87,79.55,78.71,10.49,31.98,35.47,33.73,4.49

SW091392,89.91,79.30,84.60,11.27,86.80,70.60,78.70,10.48,61.27,61.62,61.45,8.19

SW029246,66.14,81.63,73.88,9.84,78.38,78.63,78.51,10.46,59.84,57.08,58.46,7.79

SW029233,70.10,87.08,78.59,10.47,78.95,77.81,78.38,10.44,54.19,51.15,52.67,7.02

SW003835,73.57,69.00,71.28,9.50,77.25,79.00,78.12,10.41,72.48,68.41,70.44,9.38

SW164739,82.58,79.06,80.82,10.77,73.96,82.10,78.03,10.40,43.78,34.83,39.30,5.24

SW127245,73.46,80.71,77.09,10.27,78.58,76.10,77.34,10.30,44.98,47.10,46.04,6.13

SW029250,91.99,90.36,91.18,12.15,79.02,74.69,76.86,10.24,64.32,64.05,64.19,8.55

SW159239,79.05,92.00,85.52,11.39,79.58,74.06,76.82,10.23,58.88,41.57,50.22,6.69

SW029231,79.71,78.62,79.17,10.55,76.63,76.83,76.73,10.22,59.85,47.15,53.50,7.13

SW202348,78.42,79.99,79.21,10.55,76.38,76.58,76.48,10.19,39.89,34.72,37.31,4.97

SW131291,75.66,72.92,74.29,9.90,79.20,73.49,76.35,10.17,42.89,42.11,42.50,5.66

SW122012,76.69,95.46,86.07,11.47,78.21,74.14,76.17,10.15,17.86,21.95,19.90,2.65

SW003834,74.50,69.53,72.02,9.59,74.27,77.55,75.91,10.11,70.35,70.77,70.56,9.40

SW108895,84.68,95.72,90.20,12.02,87.62,63.79,75.70,10.09,25.75,14.43,20.09,2.68

SW164615,87.80,89.48,88.64,11.81,74.80,75.78,75.29,10.03,44.61,37.13,40.87,5.44

SW029248,64.25,81.02,72.64,9.68,73.48,76.87,75.18,10.02,69.54,44.84,57.19,7.62

SW150141,79.79,100.55,90.17,12.01,65.44,84.88,75.16,10.01,26.40,20.11,23.26,3.10

SW055356,77.95,78.99,78.47,10.45,66.29,83.44,74.87,9.97,28.12,16.54,22.33,2.97

SW061892,82.14,90.69,86.42,11.51,74.12,75.12,74.62,9.94,74.67,59.51,67.09,8.94

SW133032,85.56,86.00,85.78,11.43,72.66,74.75,73.71,9.82,52.35,50.52,51.43,6.85

SW085836,67.53,83.43,75.48,10.06,70.65,76.56,73.61,9.81,74.69,42.01,42.01,5.60

SW034513,80.37,81.50,80.93,10.78,72.20,74.97,73.59,9.80,53.34,43.70,48.52,6.46

SW151422,63.04,80.93,71.99,9.59,73.06,73.75,73.40,9.78,46.07,39.51,42.79,5.70

SW164826,86.56,87.82,87.19,11.62,66.61,80.07,73.34,9.77,41.78,45.70,43.74,5.83

SW036988,78.35,77.72,78.04,10.40,69.39,77.29,73.34,9.77,47.21,42.85,45.03,6.00

SW163112,64.05,62.73,63.39,8.45,74.26,72.12,73.19,9.75,57.25,48.66,52.96,7.06

SW002434,68.72,64.91,66.82,8.90,69.88,75.40,72.64,9.68,47.13,44.66,45.90,6.11

SW062885,62.99,69.80,66.40,8.85,71.15,73.75,72.45,9.65,66.45,63.50,64.97,8.66

SW019247,79.53,75.53,77.53,10.33,72.44,72.32,72.38,9.64,50.43,43.29,46.86,6.24

SW082497,82.47,78.77,80.62,10.74,70.99,73.24,72.12,9.61,32.29,34.87,33.58,4.47

SW164318,81.87,80.53,81.20,10.82,70.22,73.68,71.95,9.59,34.71,31.63,33.17,4.42

SW057452,85.84,89.17,87.51,11.66,70.90,71.70,71.30,9.50,53.94,42.50,48.22,6.42

SW200282,67.38,77.60,72.49,9.66,65.73,76.43,71.08,9.47,29.56,7.71,18.64,2.48

SW022326,62.91,76.29,69.60,9.27,72.28,69.79,71.03,9.46,47.84,41.77,44.81,5.97

SW061887,56.98,57.87,57.43,7.65,70.36,71.21,70.79,9.43,62.42,57.11,59.77,7.96

SW200904,77.88,83.75,80.82,10.77,67.60,73.85,70.73,9.42,41.10,19.45,30.27,4.03

SW036272,65.25,80.20,72.72,9.69,70.67,70.43,70.55,9.40,47.54,42.29,44.91,5.98

SW172006,66.36,81.58,73.97,9.85,67.80,73.28,70.54,9.40,38.05,29.43,33.74,4.49

SW200749,77.22,87.71,82.47,10.99,68.49,71.92,70.21,9.35,38.82,31.66,35.24,4.69

SW039634,66.77,62.73,64.75,8.63,69.27,71.10,70.18,9.35,41.49,38.47,39.98,5.33

SW058913,82.96,94.08,88.52,11.79,70.54,69.70,70.12,9.34,43.98,41.10,42.54,5.67

SW203564,74.06,78.57,76.31,10.17,69.20,70.82,70.01,9.33,32.03,27.17,29.60,3.94

SW003497,78.67,91.86,85.26,11.36,68.97,70.79,69.88,9.31,13.52,17.53,15.52,2.07

SW200226,75.08,86.91,81.00,10.79,66.30,73.44,69.87,9.31,18.64,18.19,18.41,2.45

SW002426,66.80,58.82,62.81,8.37,69.69,69.86,69.78,9.30,54.74,40.42,47.58,6.34

SW166693,85.51,67.85,76.68,10.22,66.92,71.71,69.31,9.23,42.23,34.15,38.19,5.09

SW106178,76.45,82.82,79.64,10.61,74.77,63.81,69.29,9.23,34.42,31.45,32.94,4.39

SW163259,64.29,70.98,67.63,9.01,70.11,68.18,69.14,9.21,50.51,29.14,39.82,5.31

SW057210,70.74,80.64,75.69,10.08,70.27,68.00,69.14,9.21,42.42,35.72,39.07,5.20

SW057083,82.65,74.76,78.71,10.49,67.35,70.81,69.08,9.20,40.15,31.60,35.87,4.78

SW085350,75.35,64.85,70.10,9.34,68.30,69.85,69.08,9.20,40.66,55.66,48.16,6.42

SW167383,72.04,70.43,71.24,9.49,66.93,71.20,69.07,9.20,39.70,28.91,34.30,4.57

SW058374,87.15,89.01,88.08,11.73,66.70,71.06,68.88,9.18,22.29,20.57,21.43,2.86

SW097668,72.69,67.62,70.16,9.35,66.84,70.44,68.64,9.15,42.39,44.47,43.43,5.79

SW069414,74.79,77.95,76.37,10.17,66.55,70.07,68.31,9.10,40.86,33.43,37.14,4.95

SW199692,82.33,89.08,85.71,11.42,68.68,67.56,68.12,9.08,31.93,33.36,32.65,4.35

SW091399,75.43,71.33,73.38,9.78,72.12,63.62,67.87,9.04,32.33,39.24,35.79,4.77

SW148566,60.42,82.21,71.32,9.50,65.10,69.94,67.52,9.00,45.97,23.30,34.64,4.61

SW123551,48.63,56.31,52.47,6.99,66.76,67.90,67.33,8.97,38.79,47.16,42.97,5.73

SW200316,67.50,73.40,70.45,9.39,64.48,70.11,67.30,8.97,13.06,-1.72,5.67,0.75

SW200775,80.48,83.26,81.87,10.91,65.36,69.17,67.26,8.96,32.07,25.29,28.68,3.82

SW003813,66.13,60.60,63.36,8.44,64.68,69.69,67.18,8.95,52.02,47.61,49.82,6.64

SW200772,78.17,81.94,80.06,10.67,65.86,68.20,67.03,8.93,30.45,28.62,29.54,3.93

SW199694,62.43,82.77,72.60,9.67,63.98,69.94,66.96,8.92,16.49,23.36,19.93,2.65

SW125581,62.93,72.27,67.60,9.01,69.56,64.14,66.85,8.91,40.52,39.10,39.81,5.30

SW018504,63.09,51.55,57.32,7.64,65.27,68.29,66.78,8.90,56.37,45.04,50.70,6.75

SW056382,81.16,90.55,85.85,11.44,66.88,66.68,66.78,8.90,23.21,20.81,22.01,2.93

SW198073,78.47,80.73,79.60,10.60,63.67,69.25,66.46,8.85,36.07,23.23,29.65,3.95

SW127133,63.13,71.89,67.51,8.99,68.48,63.94,66.21,8.82,30.66,31.10,30.88,4.11

SW165871,70.52,62.91,66.72,8.89,64.23,67.88,66.06,8.80,30.77,21.85,26.31,3.51

SW166114,61.95,59.24,60.60,8.07,63.55,68.44,66.00,8.79,34.25,23.35,28.80,3.84

SW202328,72.51,66.78,69.64,9.28,64.56,67.40,65.98,8.79,27.15,22.87,25.01,3.33

SW073632,63.00,75.28,69.14,9.21,65.48,66.26,65.87,8.78,10.66,6.81,8.73,1.16

SW122720,46.21,59.68,52.94,7.05,65.62,66.03,65.83,8.77,50.12,41.99,46.05,6.14

SW024805,59.49,59.12,59.30,7.90,65.09,66.48,65.78,8.76,37.76,31.02,34.39,4.58

SW034519,67.36,73.07,70.21,9.35,64.75,65.99,65.37,8.71,40.44,40.00,40.22,5.36

SW035768,70.24,63.71,66.98,8.92,63.17,67.23,65.20,8.69,30.11,32.71,31.41,4.18

SW028654,80.60,82.26,81.43,10.85,61.05,68.96,65.00,8.66,19.76,14.19,16.98,2.26

SW105277,65.73,74.05,69.89,9.31,65.79,63.48,64.64,8.61,36.19,38.52,37.35,4.98

SW052570,71.04,68.66,69.85,9.31,62.53,66.56,64.54,8.60,40.29,30.78,35.54,4.73

SW060997,48.71,53.67,51.19,6.82,63.44,65.01,64.23,8.56,41.25,35.76,38.50,5.13

SW144663,61.70,65.31,63.51,8.46,64.00,63.68,63.84,8.50,40.56,35.47,38.02,5.06

SW002429,69.01,82.45,75.73,10.09,59.01,68.32,63.66,8.48,53.37,46.16,49.77,6.63

SW203566,73.09,79.72,76.41,10.18,61.75,65.34,63.55,8.47,17.47,11.69,14.58,1.94

SW200351,73.20,80.14,76.67,10.21,59.87,66.66,63.26,8.43,26.32,17.80,22.06,2.94

SW133255,79.67,85.03,82.35,10.97,63.20,62.75,62.98,8.39,40.98,41.35,41.16,5.48

SW002424,46.39,37.70,42.05,5.60,59.78,65.60,62.69,8.35,35.12,34.88,35.00,4.66

SW200770,73.89,75.38,74.63,9.94,59.74,65.46,62.60,8.34,14.43,22.15,18.29,2.44

SW203565,74.35,78.28,76.31,10.17,60.18,64.93,62.56,8.33,30.54,25.77,28.16,3.75

SW139834,68.52,73.90,71.21,9.49,59.88,65.15,62.51,8.33,35.16,30.21,32.68,4.35

SW122720,58.22,63.17,60.69,8.09,63.34,60.96,62.15,8.28,46.14,38.15,42.14,5.61

SW021474,67.64,74.93,71.29,9.50,61.72,62.54,62.13,8.28,25.57,31.96,28.76,3.83

SW013060,71.97,69.47,70.72,9.42,61.24,62.20,61.72,8.22,39.07,34.14,36.60,4.88

SW128526,53.40,55.09,54.25,7.23,65.75,57.67,61.71,8.22,33.23,28.63,30.93,4.12

SW061888,56.05,60.79,58.42,7.78,60.44,62.78,61.61,8.21,47.97,37.09,42.53,5.67

SW045543,59.80,54.18,56.99,7.59,62.02,60.82,61.42,8.18,26.27,13.58,19.92,2.65

SW148639,70.97,94.23,82.60,11.00,53.44,69.12,61.28,8.16,29.28,20.01,24.65,3.28

SW036305,53.37,49.98,51.68,6.88,59.93,62.49,61.21,8.16,27.53,41.32,34.43,4.59

SW201136,61.72,71.57,66.65,8.88,57.87,64.50,61.19,8.15,62.97,51.91,57.44,7.65

SW110433,70.28,73.65,71.96,9.59,64.43,57.85,61.14,8.15,37.32,32.53,34.92,4.65

SW058914,70.97,86.60,78.78,10.50,60.56,61.70,61.13,8.14,14.19,22.48,18.34,2.44

SW200394,77.03,88.39,82.71,11.02,57.11,64.57,60.84,8.11,31.85,18.84,25.35,3.38

SW031446,77.87,74.54,76.20,10.15,60.18,61.28,60.73,8.09,24.33,21.37,22.85,3.04

SW058630,52.62,52.99,52.81,7.04,59.42,61.94,60.68,8.08,18.28,19.21,18.75,2.50

SW164799,76.31,66.07,71.19,9.48,66.86,54.48,60.67,8.08,31.00,32.58,31.79,4.24

SW119290,63.26,66.70,64.98,8.66,61.91,59.30,60.60,8.07,29.80,31.59,30.70,4.09

SW201125,41.27,39.75,40.51,5.40,55.07,65.83,60.45,8.05,44.56,44.70,44.63,5.95

SW023159,54.21,50.42,52.31,6.97,57.14,63.45,60.29,8.03,42.07,32.17,37.12,4.95

SW101978,69.85,70.29,70.07,9.33,61.59,58.72,60.16,8.01,25.24,33.46,29.35,3.91

SW121709,50.72,58.77,54.74,7.29,60.81,58.67,59.74,7.96,28.60,31.59,30.10,4.01

SW153762,55.73,67.01,61.37,8.18,59.04,60.26,59.65,7.95,27.82,25.70,26.76,3.57

SW021865,74.47,64.86,69.67,9.28,57.95,61.24,59.59,7.94,32.34,24.94,28.64,3.82

SW100021,57.57,70.77,64.17,8.55,59.84,59.15,59.50,7.93,38.13,19.25,28.69,3.82

SW119619,52.98,63.17,58.08,7.74,62.74,56.25,59.49,7.93,36.38,35.19,35.79,4.77

SW102538,65.78,63.18,64.48,8.59,61.21,57.71,59.46,7.92,26.22,28.42,27.32,3.64

SW196031,68.05,82.89,75.47,10.05,57.57,61.34,59.46,7.92,17.82,19.02,18.42,2.45

SW054317,60.13,69.30,64.72,8.62,61.46,57.33,59.40,7.91,29.99,29.01,29.50,3.93

SW195842,50.32,62.12,56.22,7.49,58.49,60.17,59.33,7.90,50.20,36.32,43.26,5.76

SW133363,64.06,65.38,64.72,8.62,56.17,62.36,59.26,7.90,38.76,33.01,35.89,4.78

SW083192,61.76,58.47,60.12,8.01,59.32,58.72,59.02,7.86,39.13,39.34,39.24,5.23

SW166430,47.72,46.02,46.87,6.24,56.95,61.08,59.02,7.86,36.71,21.76,29.24,3.90

SW087449,50.50,49.25,49.88,6.64,60.53,57.13,58.83,7.84,26.99,29.56,28.28,3.77

SW085855,64.79,58.91,61.85,8.24,63.44,53.96,58.70,7.82,26.42,28.43,27.42,3.65

SW018348,51.77,47.56,49.66,6.62,57.08,60.32,58.70,7.82,38.31,40.61,39.46,5.26

SW061025,47.59,50.34,48.97,6.52,56.81,60.01,58.41,7.78,34.31,28.44,31.38,4.18

SW034493,60.75,67.29,64.02,8.53,56.63,60.09,58.36,7.78,25.09,27.16,26.13,3.48

SW029252,74.48,67.39,70.94,9.45,55.71,60.97,58.34,7.77,31.17,33.69,32.43,4.32

SW052370,57.82,67.70,62.76,8.36,59.02,57.47,58.24,7.76,0.42,5.15,2.78,0.37

SW171349,61.60,64.07,62.84,8.37,55.91,60.38,58.15,7.75,33.16,20.06,26.61,3.55

SW060489,59.18,66.71,62.94,8.39,60.06,56.16,58.11,7.74,31.21,29.33,30.27,4.03

SW198075,68.31,75.06,71.68,9.55,53.91,62.22,58.07,7.74,14.70,4.96,9.83,1.31

SW013026,49.45,62.92,56.18,7.48,57.89,58.01,57.95,7.72,26.28,19.50,22.89,3.05

SW119442,51.21,54.97,53.09,7.07,58.93,56.95,57.94,7.72,27.05,22.77,24.91,3.32

SW153104,60.01,71.67,65.84,8.77,56.61,59.22,57.91,7.72,29.12,34.49,31.81,4.24

SW003830,57.72,48.48,53.10,7.07,57.64,57.97,57.81,7.70,36.09,37.33,36.71,4.89

SW167418,61.55,59.43,60.49,8.06,55.36,60.17,57.77,7.70,41.05,25.13,33.09,4.41

SW084819,52.35,46.23,49.29,6.57,58.43,56.90,57.66,7.68,27.04,29.79,28.41,3.79

SW198076,55.83,76.17,66.00,8.79,53.33,61.70,57.52,7.66,26.20,2.03,14.11,1.88

SW201130,68.63,66.29,67.46,8.99,57.37,57.34,57.35,7.64,42.64,35.86,39.25,5.23

SW004060,42.34,49.41,45.87,6.11,58.19,55.90,57.05,7.60,39.75,33.42,36.58,4.87

SW053772,67.15,66.80,66.97,8.92,54.49,59.52,57.01,7.59,36.94,30.34,33.64,4.48

SW102415,67.32,75.09,71.20,9.49,57.02,56.62,56.82,7.57,-9.80,1.16,-4.32,-0.58

SW118216,47.19,54.30,50.74,6.76,58.15,55.29,56.72,7.56,24.33,25.65,24.99,3.33

SW034531,69.74,79.14,74.44,9.92,56.56,56.73,56.65,7.55,32.67,27.34,30.01,4.00

SW113260,62.12,76.98,69.55,9.27,59.11,53.97,56.54,7.53,28.32,30.94,29.63,3.95

SW147881,44.75,60.51,52.63,7.01,55.71,56.68,56.20,7.49,36.98,34.17,35.57,4.74

SW057349,66.52,78.27,72.39,9.64,57.29,54.99,56.14,7.48,32.19,22.43,27.31,3.64

SW151438,67.37,90.52,78.94,10.52,52.81,59.44,56.12,7.48,24.37,21.80,23.09,3.08

SW174938,60.22,65.86,63.04,8.40,54.47,57.18,55.82,7.44,39.35,19.78,29.57,3.94

SW196367,86.27,97.64,91.96,12.25,52.60,58.83,55.72,7.42,37.17,32.20,34.69,4.62

SW164657,69.51,65.57,67.54,9.00,48.27,63.02,55.64,7.41,29.13,22.51,25.82,3.44

SW094040,59.99,43.52,51.76,6.90,57.72,53.41,55.56,7.40,22.76,25.40,24.08,3.21

SW034488,38.58,30.72,34.65,4.62,55.31,55.65,55.48,7.39,30.85,35.96,33.41,4.45

SW162136,47.85,48.54,48.20,6.42,54.77,56.12,55.44,7.39,25.58,23.65,24.61,3.28

SW082320,50.55,48.02,49.29,6.57,56.02,54.65,55.34,7.37,44.83,43.12,43.97,5.86

SW113209,62.22,72.53,67.38,8.98,60.01,50.04,55.02,7.33,28.01,28.06,28.04,3.74

SW199152,102.67,91.67,97.17,12.95,49.07,60.94,55.00,7.33,27.59,13.71,20.65,2.75

SW118674,41.27,55.10,48.18,6.42,61.26,48.74,55.00,7.33,37.60,32.58,35.09,4.67

SW034456,57.61,53.74,55.67,7.42,55.03,54.82,54.92,7.32,27.96,22.39,25.17,3.35

SW003814,48.17,48.98,48.57,6.47,51.35,57.82,54.58,7.27,43.67,41.06,42.36,5.64

SW129490,64.35,60.30,62.32,8.30,62.37,46.62,54.49,7.26,12.26,17.63,14.94,1.99

SW154840,56.17,68.10,62.13,8.28,52.18,56.22,54.20,7.22,24.20,27.63,25.91,3.45

SW201368,83.56,86.90,85.23,11.36,50.30,57.73,54.01,7.20,32.12,13.43,22.77,3.03

SW196001,61.52,72.47,67.00,8.93,50.65,57.30,53.98,7.19,25.75,33.60,29.68,3.95

SW009407,40.94,41.70,41.32,5.51,55.13,52.82,53.98,7.19,35.72,36.34,36.03,4.80

SW166784,79.53,51.71,65.62,8.74,52.61,55.31,53.96,7.19,34.05,22.23,28.14,3.75

SW136195,63.40,66.24,64.82,8.64,49.47,58.24,53.85,7.17,25.70,28.96,27.33,3.64

SW200262,65.38,70.42,67.90,9.05,46.61,60.00,53.31,7.10,3.07,-9.26,-3.10,-0.41

SW058914,61.84,62.52,62.18,8.28,52.01,54.49,53.25,7.09,25.88,26.21,26.04,3.47

SW118042,55.47,58.11,56.79,7.57,55.00,51.32,53.16,7.08,25.67,37.05,31.36,4.18

SW201362,91.61,95.01,93.31,12.43,50.48,55.71,53.09,7.07,25.24,17.79,21.52,2.87

SW196786,37.50,45.44,41.47,5.52,51.27,54.88,53.07,7.07,34.80,22.50,28.65,3.82

SW121306,25.49,41.08,33.29,4.43,51.49,54.61,53.05,7.07,12.44,7.40,9.92,1.32

SW009977,80.06,81.68,80.87,10.77,51.15,54.75,52.95,7.05,0.35,1.42,0.89,0.12

SW153745,56.25,65.82,61.03,8.13,50.96,54.75,52.85,7.04,15.82,21.67,18.75,2.50

SW013025,59.26,56.98,58.12,7.74,53.56,52.12,52.84,7.04,34.30,26.05,30.18,4.02

SW200246,77.03,82.69,79.86,10.64,49.01,56.54,52.78,7.03,13.70,12.49,13.10,1.74

SW200244,56.81,58.63,57.72,7.69,48.38,57.08,52.73,7.03,23.96,10.62,17.29,2.30

SW153669,48.56,63.31,55.93,7.45,52.66,52.76,52.71,7.02,28.03,27.69,27.86,3.71

SW201083,88.68,90.79,89.73,11.96,54.05,51.22,52.63,7.01,99.07,94.64,96.86,12.90

SW103517,59.82,60.37,60.09,8.01,56.58,48.62,52.60,7.01,30.39,30.22,30.30,4.04

SW126035,48.02,64.12,56.07,7.47,55.20,49.88,52.54,7.00,27.07,25.87,26.47,3.53

SW155218,49.31,65.76,57.54,7.67,51.39,53.61,52.50,6.99,23.42,20.38,21.90,2.92

SW057251,72.80,71.78,72.29,9.63,51.41,53.34,52.38,6.98,17.51,11.58,14.55,1.94

SW083358,52.09,51.72,51.91,6.92,51.50,53.16,52.33,6.97,31.30,29.99,30.64,4.08

SW201126,10.76,9.32,10.04,1.34,49.94,54.42,52.18,6.95,66.15,44.74,55.45,7.39

SW163200,50.49,52.84,51.67,6.88,50.96,53.24,52.10,6.94,11.08,11.42,11.25,1.50

SW114043,62.88,74.18,68.53,9.13,61.92,42.09,52.01,6.93,-13.79,-15.85,-14.82,-1.97

SW029006,53.94,55.61,54.77,7.30,51.67,52.30,51.98,6.93,15.32,12.29,13.80,1.84

SW101646,63.79,71.12,67.46,8.99,54.66,49.13,51.89,6.91,19.23,20.83,20.03,2.67

SW122191,43.31,60.43,51.87,6.91,52.96,50.32,51.64,6.88,3.16,5.02,4.09,0.55

SW136636,46.51,46.13,46.32,6.17,52.45,50.74,51.59,6.87,45.01,37.32,41.16,5.48

SW083699,45.44,47.10,46.27,6.16,52.03,50.96,51.49,6.86,29.99,27.62,28.81,3.84

SW036339,49.41,49.39,49.40,6.58,50.91,51.96,51.43,6.85,43.34,35.60,39.47,5.26

SW162670,51.63,57.11,54.37,7.24,51.02,51.77,51.39,6.85,32.87,22.08,27.47,3.66

SW150807,78.34,95.82,87.08,11.60,41.53,61.13,51.33,6.84,2.45,13.15,7.80,1.04

SW087406,76.28,75.38,75.83,10.10,56.85,45.74,51.29,6.83,10.39,5.11,7.75,1.03

SW024715,60.65,57.10,58.88,7.84,49.92,52.34,51.13,6.81,26.37,22.23,24.30,3.24

SW164579,52.82,48.49,50.65,6.75,48.70,53.53,51.12,6.81,36.82,25.90,31.36,4.18

SW110107,82.36,94.51,88.43,11.78,58.94,43.15,51.04,6.80,18.99,17.56,18.27,2.43

SW121777,49.45,60.25,54.85,7.31,52.78,49.30,51.04,6.80,24.07,25.60,24.83,3.31

SW002427,58.01,57.50,57.75,7.69,51.34,50.73,51.04,6.80,34.97,25.09,30.03,4.00

SW165872,53.80,46.47,50.13,6.68,50.24,51.77,51.01,6.80,31.73,16.92,24.32,3.24

SW021473,73.95,72.84,73.40,9.78,50.38,51.64,51.01,6.80,33.85,28.82,31.34,4.17

SW122068,46.96,60.04,53.50,7.13,52.06,49.83,50.94,6.79,28.10,26.19,27.15,3.62

SW029251,32.71,41.74,37.22,4.96,51.45,50.40,50.92,6.78,46.03,46.35,46.19,6.15

SW160535,60.29,67.54,63.92,8.52,50.90,50.83,50.87,6.78,28.62,11.50,20.06,2.67

SW190431,56.02,50.08,53.05,7.07,48.06,53.41,50.74,6.76,21.92,13.67,17.80,2.37

SW122571,47.76,61.82,54.79,7.30,54.93,46.55,50.74,6.76,29.94,27.78,28.86,3.84

SW085347,42.85,54.19,48.52,6.46,51.67,49.79,50.73,6.76,43.85,47.47,45.66,6.08

SW067057,56.85,53.40,55.13,7.34,49.95,51.47,50.71,6.76,25.57,24.96,25.26,3.37

SW058629,51.32,50.37,50.85,6.77,51.24,49.84,50.54,6.73,13.97,14.25,14.11,1.88

SW148305,67.99,88.89,78.44,10.45,47.76,52.92,50.34,6.71,17.32,26.12,21.72,2.89

SW085532,43.65,38.35,41.00,5.46,50.60,49.21,49.91,6.65,41.77,40.99,41.38,5.51

SW164332,68.80,64.72,66.76,8.89,42.15,57.59,49.87,6.64,5.53,5.06,5.29,0.71

SW151403,49.31,57.93,53.62,7.14,47.70,51.96,49.83,6.64,24.63,23.28,23.95,3.19

SW155125,51.17,70.32,60.74,8.09,48.22,51.13,49.67,6.62,25.26,11.48,18.37,2.45

SW013779,60.35,76.76,68.55,9.13,49.91,49.36,49.63,6.61,27.71,24.46,26.08,3.47

SW034507,57.14,55.24,56.19,7.49,49.74,49.30,49.52,6.60,22.94,21.91,22.43,2.99

SW003837,29.93,23.88,26.91,3.58,47.92,51.07,49.50,6.59,40.84,34.35,37.60,5.01

SW198074,62.09,67.27,64.68,8.62,47.22,51.69,49.45,6.59,32.17,17.99,25.08,3.34

SW061094,35.21,43.72,39.46,5.26,49.11,49.72,49.41,6.58,28.11,28.08,28.10,3.74

SW035772,57.61,40.33,48.97,6.52,48.89,49.87,49.38,6.58,29.85,22.53,26.19,3.49

SW156558,35.04,45.75,40.39,5.38,49.98,48.21,49.10,6.54,20.46,16.79,18.63,2.48

SW012690,71.09,71.08,71.08,9.47,49.08,49.10,49.09,6.54,20.70,19.75,20.22,2.69

SW119483,62.37,60.99,61.68,8.22,50.22,47.82,49.02,6.53,15.18,12.50,13.84,1.84

SW122696,53.38,62.70,58.04,7.73,53.94,44.05,48.99,6.53,26.44,25.26,25.85,3.44

SW109137,64.39,61.30,62.84,8.37,49.38,48.47,48.93,6.52,24.44,17.02,20.73,2.76

SW047104,62.85,71.49,67.17,8.95,50.07,47.78,48.92,6.52,12.55,21.56,17.05,2.27

SW027237,82.08,92.05,87.06,11.60,47.69,49.81,48.75,6.49,11.01,19.04,15.03,2.00

SW054876,51.91,52.54,52.23,6.96,46.94,50.49,48.72,6.49,32.58,20.34,26.46,3.53

SW107712,40.46,54.65,47.56,6.34,52.27,44.98,48.62,6.48,29.89,23.52,26.71,3.56

SW111295,67.33,82.91,75.12,10.01,53.29,43.81,48.55,6.47,23.20,17.57,20.39,2.72

SW153737,52.53,60.99,56.76,7.56,49.38,47.15,48.26,6.43,24.21,21.75,22.98,3.06

SW166744,63.99,60.40,62.19,8.29,47.03,49.38,48.20,6.42,14.01,15.92,14.96,1.99

SW164705,42.81,41.09,41.95,5.59,47.64,48.66,48.15,6.42,32.80,24.87,28.83,3.84

SW121797,53.82,55.06,54.44,7.25,48.46,47.84,48.15,6.41,18.37,23.92,21.15,2.82

SW100409,48.58,46.08,47.33,6.31,51.92,44.35,48.13,6.41,28.63,15.63,22.13,2.95

SW013012,31.59,43.77,37.68,5.02,48.51,47.70,48.11,6.41,32.83,28.22,30.52,4.07

SW199693,92.21,107.37,99.79,13.29,50.15,45.97,48.06,6.40,52.77,49.62,51.19,6.82

SW130765,71.13,74.77,72.95,9.72,58.21,37.86,48.03,6.40,-14.62,-19.77,-17.20,-2.29

SW006009,42.24,53.94,48.09,6.41,50.54,44.98,47.76,6.36,27.02,22.77,24.90,3.32

SW085842,42.32,38.32,40.32,5.37,46.53,48.99,47.76,6.36,1.29,-0.74,0.27,0.04

SW029234,64.71,61.81,63.26,8.43,48.54,46.46,47.50,6.33,32.44,21.14,26.79,3.57

SW085854,43.61,40.49,42.05,5.60,45.90,48.96,47.43,6.32,21.33,4.06,12.69,1.69

SW093567,50.66,46.61,48.63,6.48,50.76,43.57,47.16,6.28,21.80,11.17,16.48,2.20

SW107259,45.84,51.38,48.61,6.48,49.69,44.35,47.02,6.26,33.84,29.16,31.50,4.20

SW101035,47.17,52.16,49.67,6.62,48.45,45.40,46.93,6.25,25.00,24.62,24.81,3.31

SW005307,77.64,93.16,85.40,11.38,51.23,42.28,46.75,6.23,21.75,15.27,18.51,2.47

SW020797,14.99,5.55,10.27,1.37,45.95,47.47,46.71,6.22,27.27,28.67,27.97,3.73

SW167534,52.22,57.86,55.04,7.33,43.41,49.50,46.45,6.19,29.84,12.73,21.28,2.84

SW050001,59.73,66.74,63.24,8.42,45.32,47.49,46.40,6.18,27.60,27.68,27.64,3.68

SW110113,51.03,60.45,55.74,7.43,45.75,46.85,46.30,6.17,22.35,-2.72,9.82,1.31

SW076080,46.44,47.43,46.93,6.25,43.77,48.46,46.12,6.14,30.87,25.43,28.15,3.75

SW039803,52.39,55.58,53.99,7.19,47.83,44.37,46.10,6.14,17.24,23.28,20.26,2.70

SW126388,41.81,57.53,49.67,6.62,44.30,47.35,45.83,6.11,30.24,28.49,29.36,3.91

SW083801,47.11,38.11,42.61,5.68,46.85,44.64,45.75,6.09,18.22,24.74,21.48,2.86

SW044209,54.52,59.54,57.03,7.60,45.73,45.59,45.66,6.08,31.71,30.77,31.24,4.16

SW201363,89.49,90.84,90.17,12.01,45.23,45.79,45.51,6.06,22.10,15.59,18.84,2.51

SW112682,41.44,46.20,43.82,5.84,47.03,43.98,45.50,6.06,27.32,23.18,25.25,3.36

SW028008,51.08,59.58,55.33,7.37,45.38,45.46,45.42,6.05,20.87,22.06,21.47,2.86

SW120529,45.69,56.50,51.09,6.81,46.11,44.66,45.38,6.05,-2.81,2.25,-0.28,-0.04

SW036379,43.83,39.47,41.65,5.55,45.10,45.47,45.28,6.03,31.00,27.20,29.10,3.88

SW196786,38.68,46.09,42.39,5.65,45.00,45.51,45.25,6.03,26.61,23.88,25.24,3.36

SW034523,42.20,53.73,47.97,6.39,46.54,43.92,45.23,6.03,24.49,26.02,25.26,3.36

SW007299,60.72,69.41,65.06,8.67,43.46,47.01,45.23,6.03,15.20,18.91,17.06,2.27

SW103222,55.13,58.39,56.76,7.56,48.88,41.52,45.20,6.02,27.83,26.11,26.97,3.59

SW150195,37.94,53.74,45.84,6.11,41.07,49.22,45.14,6.01,27.47,25.45,26.46,3.53

SW061079,36.58,38.99,37.78,5.03,46.32,43.89,45.10,6.01,18.53,16.18,17.36,2.31

SW154321,21.83,31.69,26.76,3.56,45.86,44.27,45.06,6.00,38.07,29.49,33.78,4.50

SW127045,41.45,46.38,43.91,5.85,46.55,43.53,45.04,6.00,12.30,17.41,14.86,1.98

SW113911,41.58,48.53,45.05,6.00,46.07,44.01,45.04,6.00,26.14,22.99,24.57,3.27

SW045343,53.56,54.78,54.17,7.22,43.03,46.52,44.78,5.97,28.63,18.93,23.78,3.17

SW125291,48.90,53.37,51.14,6.81,47.66,41.86,44.76,5.96,16.55,21.16,18.86,2.51

SW201550,58.84,52.38,55.61,7.41,44.49,44.92,44.70,5.96,9.30,10.10,9.70,1.29

SW196606,49.72,40.19,44.95,5.99,42.14,47.24,44.69,5.95,20.61,18.72,19.66,2.62

SW082253,63.52,71.01,67.26,8.96,43.32,46.05,44.68,5.95,30.88,24.47,27.68,3.69

SW201364,89.80,99.67,94.74,12.62,44.46,44.79,44.63,5.95,18.81,17.32,18.06,2.41

SW102543,48.12,44.31,46.21,6.16,45.95,43.13,44.54,5.93,14.04,19.77,16.90,2.25

SW102861,44.04,42.35,43.20,5.75,42.70,46.30,44.50,5.93,18.07,21.72,19.90,2.65

SW045334,49.87,51.41,50.64,6.75,43.92,44.97,44.44,5.92,25.82,28.44,27.13,3.61

SW126027,43.21,55.86,49.54,6.60,43.30,45.54,44.42,5.92,19.52,0.02,9.77,1.30

SW169815,58.99,63.31,61.15,8.15,43.08,45.65,44.36,5.91,25.00,-3.35,10.83,1.44

SW023620,45.80,59.83,52.81,7.04,45.01,43.70,44.36,5.91,24.48,21.21,22.84,3.04

SW086914,54.72,50.82,52.77,7.03,42.66,45.91,44.28,5.90,27.02,24.12,25.57,3.41

SW004129,43.51,36.25,39.88,5.31,43.85,44.39,44.12,5.88,40.21,29.24,34.73,4.63

SW117491,26.00,28.21,27.10,3.61,45.75,42.29,44.02,5.86,24.85,26.87,25.86,3.45

SW148203,43.41,53.82,48.61,6.48,41.62,46.30,43.96,5.86,17.61,14.42,16.02,2.13

SW002963,38.96,50.68,44.82,5.97,44.24,43.24,43.74,5.83,21.32,26.47,23.90,3.18

SW035815,55.04,51.21,53.13,7.08,38.45,48.60,43.53,5.80,20.48,21.73,21.10,2.81

SW012533,78.34,80.17,79.25,10.56,41.25,45.72,43.48,5.79,16.41,14.83,15.62,2.08

SW142618,46.08,51.00,48.54,6.47,40.64,46.29,43.47,5.79,22.71,22.62,22.66,3.02

SW047739,44.57,53.23,48.90,6.51,43.64,43.21,43.43,5.79,12.66,18.98,15.82,2.11

SW125660,27.22,39.22,33.22,4.43,44.88,41.94,43.41,5.78,23.65,25.40,24.52,3.27

SW043827,51.18,47.32,49.25,6.56,42.78,43.75,43.26,5.76,29.79,18.88,24.33,3.24

SW014605,7.88,51.01,7.88,1.05,44.00,42.51,43.25,5.76,21.88,23.84,22.86,3.05

SW128169,43.41,51.98,47.70,6.35,45.39,40.83,43.11,5.74,17.54,17.90,17.72,2.36

SW126954,45.85,44.78,45.32,6.04,44.83,40.48,42.66,5.68,14.01,19.05,16.53,2.20

SW041634,35.08,28.90,31.99,4.26,42.25,43.03,42.64,5.68,37.47,29.33,33.40,4.45

SW165333,57.60,51.82,54.71,7.29,35.93,49.26,42.60,5.67,13.23,-10.22,1.51,0.20

SW005165,53.24,62.52,57.88,7.71,45.05,40.07,42.56,5.67,31.80,27.06,29.43,3.92

SW043827,59.03,69.69,64.36,8.57,43.88,41.23,42.55,5.67,30.79,23.67,27.23,3.63

SW036337,32.41,29.83,31.12,4.15,41.68,43.42,42.55,5.67,30.29,29.21,29.75,3.96

SW100984,47.83,58.40,53.12,7.08,45.29,39.65,42.47,5.66,18.01,20.76,19.38,2.58

SW100308,42.50,52.89,47.70,6.35,44.75,40.15,42.45,5.66,17.08,16.53,16.80,2.24

SW202424,69.32,67.80,68.56,9.13,41.37,42.86,42.12,5.61,11.28,11.13,11.20,1.49

SW114030,84.10,85.36,84.73,11.29,76.19,42.11,42.11,5.61,0.49,5.95,3.22,0.43

SW032234,55.21,66.26,60.74,8.09,42.19,41.96,42.07,5.61,24.58,21.68,23.13,3.08

SW112336,46.02,51.51,48.77,6.50,42.96,41.17,42.07,5.60,15.97,17.38,16.67,2.22

SW197137,54.32,50.07,52.19,6.95,40.24,43.83,42.04,5.60,28.16,16.57,22.37,2.98

SW128216,34.87,45.78,40.32,5.37,44.96,39.05,42.01,5.60,24.64,21.96,23.30,3.10

SW196472,55.18,55.91,55.55,7.40,38.40,45.12,41.76,5.56,1.58,5.90,3.74,0.50

SW143730,38.31,43.67,40.99,5.46,39.34,44.17,41.76,5.56,28.27,21.60,24.93,3.32

SW167040,49.68,43.91,46.80,6.23,39.94,43.57,41.75,5.56,16.46,6.17,11.31,1.51

SW109441,35.37,27.58,31.48,4.19,43.81,39.60,41.71,5.56,19.25,21.14,20.19,2.69

SW136009,44.73,44.08,44.40,5.92,39.15,44.25,41.70,5.56,25.43,22.79,24.11,3.21

SW069151,33.84,24.31,29.07,3.87,41.42,41.88,41.65,5.55,25.41,24.75,25.08,3.34

SW126681,43.90,45.27,44.58,5.94,44.32,38.84,41.58,5.54,10.50,14.37,12.44,1.66

SW164267,61.28,49.27,55.28,7.36,38.49,44.64,41.57,5.54,17.79,15.94,16.87,2.25

SW128736,44.62,46.70,45.66,6.08,47.00,36.13,41.56,5.54,12.56,14.05,13.30,1.77

SW159284,33.20,37.96,35.58,4.74,40.28,42.63,41.46,5.52,24.56,17.32,20.94,2.79

SW148858,43.67,55.29,49.48,6.59,40.44,42.41,41.42,5.52,26.74,24.93,25.84,3.44

SW157797,55.28,66.00,60.64,8.08,41.23,41.37,41.30,5.50,23.45,18.42,20.93,2.79

SW154704,51.51,61.23,56.37,7.51,40.48,41.95,41.22,5.49,24.61,20.46,22.53,3.00

SW154142,24.62,33.13,28.87,3.85,42.22,40.14,41.18,5.49,25.25,21.09,23.17,3.09

SW202311,61.35,65.41,63.38,8.44,38.94,43.42,41.18,5.49,18.94,-0.24,9.35,1.25

SW043616,34.09,33.29,33.69,4.49,41.65,40.42,41.03,5.47,17.18,14.75,15.97,2.13

SW165991,62.40,41.18,51.79,6.90,41.13,40.81,40.97,5.46,12.54,11.06,11.80,1.57

SW013066,41.23,34.19,37.71,5.02,39.32,42.60,40.96,5.46,29.11,25.03,27.07,3.61

SW150304,87.47,102.28,94.88,12.64,32.93,48.97,40.95,5.46,16.87,11.29,14.08,1.88

SW013195,48.65,42.79,45.72,6.09,37.85,43.86,40.86,5.44,13.48,19.13,16.30,2.17

SW029230,25.55,33.91,29.73,3.96,41.87,39.69,40.78,5.43,27.53,27.80,27.66,3.69

SW126245,46.51,60.15,53.33,7.11,45.36,36.18,40.77,5.43,19.72,20.06,19.89,2.65

SW097716,41.48,42.01,41.74,5.56,42.05,39.44,40.75,5.43,21.70,21.74,21.72,2.89

SW156973,22.32,31.38,26.85,3.58,42.04,38.95,40.49,5.39,32.96,23.27,28.11,3.75

SW140628,43.09,43.06,43.07,5.74,39.10,41.60,40.35,5.38,28.89,20.74,24.82,3.31

SW145256,40.53,27.29,33.91,4.52,37.75,42.83,40.29,5.37,15.42,23.85,19.63,2.62

SW045355,43.81,48.84,46.32,6.17,39.52,40.72,40.12,5.35,14.47,15.85,15.16,2.02

SW169766,30.74,38.78,34.76,4.63,37.84,42.33,40.09,5.34,30.40,17.01,23.71,3.16

SW107535,39.32,42.79,41.05,5.47,42.86,37.30,40.08,5.34,25.88,21.28,23.58,3.14

SW103228,55.62,58.02,56.82,7.57,45.56,34.50,40.03,5.33,2.14,10.15,6.15,0.82

SW202315,61.81,66.49,64.15,8.55,40.10,39.93,40.02,5.33,20.07,14.51,17.29,2.30

SW122008,58.67,79.15,68.91,9.18,48.43,31.52,39.97,5.33,2.20,-18.39,-8.09,-1.08

SW101036,37.30,46.58,41.94,5.59,43.07,36.66,39.86,5.31,21.45,20.34,20.90,2.78

SW141498,43.94,23.51,33.72,4.49,37.02,42.60,39.81,5.30,19.35,19.09,19.22,2.56

SW100030,52.39,52.33,52.36,6.98,42.09,37.51,39.80,5.30,11.82,11.48,11.65,1.55

SW151390,63.20,83.84,73.52,9.79,35.01,44.42,39.71,5.29,13.40,20.33,16.86,2.25

SW152363,22.62,40.38,31.50,4.20,38.18,41.14,39.66,5.28,21.75,23.37,22.56,3.01

SW083697,47.54,40.36,43.95,5.86,47.63,31.60,39.62,5.28,18.67,24.49,21.58,2.88

SW069934,53.33,51.78,52.56,7.00,39.09,40.10,39.59,5.27,27.28,22.05,24.67,3.29

SW165407,74.68,72.95,73.82,9.83,36.28,42.88,39.58,5.27,1.82,7.07,4.44,0.59

SW013023,49.24,45.53,47.39,6.31,36.55,42.23,39.39,5.25,25.86,21.45,23.65,3.15

SW125734,36.02,47.90,41.96,5.59,44.01,34.74,39.38,5.25,23.19,19.56,21.38,2.85

SW164526,61.38,55.83,58.61,7.81,36.52,42.18,39.35,5.24,19.31,10.66,14.98,2.00

SW168347,28.36,32.13,30.25,4.03,41.01,37.57,39.29,5.23,23.18,11.71,17.44,2.32

SW129977,29.12,25.50,27.31,3.64,43.25,35.11,39.18,5.22,16.92,22.44,19.68,2.62

SW163900,26.39,25.12,25.75,3.43,38.64,39.72,39.18,5.22,21.61,11.19,16.40,2.18

SW001189,48.29,69.93,59.11,7.88,34.84,43.30,39.07,5.21,26.28,17.09,21.68,2.89

SW130731,34.95,34.50,34.72,4.63,42.30,35.74,39.02,5.20,17.22,17.02,17.12,2.28

SW155217,25.77,17.11,21.44,2.86,38.70,39.19,38.95,5.19,22.59,16.97,19.78,2.64

SW082296,43.83,43.96,43.90,5.85,37.34,40.47,38.90,5.18,32.03,30.40,31.21,4.16

SW125004,42.88,51.00,46.94,6.25,43.28,34.46,38.87,5.18,22.03,23.98,23.01,3.07

SW069160,24.37,22.52,23.45,3.12,38.07,39.52,38.80,5.17,27.10,29.81,28.45,3.79

SW167400,42.41,37.88,40.14,5.35,35.29,42.29,38.79,5.17,26.05,12.66,19.36,2.58

SW045179,39.15,33.31,36.23,4.83,36.29,41.20,38.75,5.16,20.56,19.72,20.14,2.68

SW170186,66.99,70.50,68.75,9.16,36.86,40.57,38.71,5.16,26.20,18.04,22.12,2.95

SW109064,55.02,65.84,60.43,8.05,34.90,42.43,38.66,5.15,20.18,23.52,21.85,2.91

SW158952,46.62,54.33,50.48,6.72,39.10,38.10,38.60,5.14,18.33,12.33,15.33,2.04

SW069086,29.78,30.69,30.24,4.03,39.09,38.09,38.59,5.14,18.42,14.10,16.26,2.17

SW000688,23.45,37.07,30.26,4.03,36.35,40.79,38.57,5.14,25.86,3.83,14.85,1.98

SW148542,51.66,67.88,59.77,7.96,36.56,40.51,38.54,5.13,18.82,25.11,21.97,2.93

SW138286,54.80,55.79,55.30,7.37,37.36,39.67,38.51,5.13,15.23,18.23,16.73,2.23

SW104862,33.65,32.48,33.06,4.40,39.14,37.84,38.49,5.13,24.20,21.15,22.67,3.02

SW069570,36.95,41.78,39.37,5.25,38.42,38.53,38.47,5.13,23.35,21.10,22.23,2.96

SW083603,41.59,53.92,47.75,6.36,39.19,37.73,38.46,5.12,23.25,16.52,19.88,2.65

SW036340,38.51,37.70,38.11,5.08,38.11,38.74,38.43,5.12,35.90,24.11,30.01,4.00

SW165348,32.51,21.53,27.02,3.60,38.09,38.67,38.38,5.11,23.72,12.36,18.04,2.40

SW099700,26.75,34.26,30.51,4.06,37.54,39.19,38.37,5.11,28.44,27.89,28.16,3.75

SW036355,62.31,57.16,59.74,7.96,37.26,39.46,38.36,5.11,11.27,11.89,11.58,1.54

SW187120,40.97,42.44,41.71,5.56,35.32,41.29,38.30,5.10,6.38,-2.41,1.99,0.26

SW070571,48.64,46.16,47.40,6.32,37.13,39.30,38.22,5.09,26.12,22.20,24.16,3.22

SW034523,27.08,40.52,33.80,4.50,36.61,39.79,38.20,5.09,25.02,22.14,23.58,3.14

SW161391,25.54,28.25,26.90,3.58,38.35,38.04,38.19,5.09,21.15,15.52,18.34,2.44

SW126364,43.56,55.75,49.65,6.62,43.99,32.30,38.14,5.08,15.83,19.93,17.88,2.38

SW200750,57.74,61.25,59.50,7.93,34.36,41.92,38.14,5.08,9.90,12.82,11.36,1.51

SW102861,44.40,34.18,39.29,5.23,37.09,38.75,37.92,5.05,18.80,7.06,12.93,1.72

SW097655,53.51,59.02,56.27,7.50,34.80,40.99,37.90,5.05,12.39,19.52,15.95,2.13

SW018357,34.46,42.21,38.33,5.11,39.05,36.68,37.86,5.04,36.06,31.62,33.84,4.51

SW153305,27.71,37.59,32.65,4.35,37.28,38.30,37.79,5.03,27.67,22.45,25.06,3.34

SW139562,38.62,39.79,39.21,5.22,35.65,39.79,37.72,5.03,22.58,20.49,21.54,2.87

SW128601,41.43,46.23,43.83,5.84,41.21,34.12,37.67,5.02,22.07,15.12,18.59,2.48

SW140304,35.61,29.67,32.64,4.35,35.26,39.68,37.47,4.99,24.29,22.14,23.21,3.09

SW083535,36.04,53.35,44.69,5.95,37.47,37.44,37.45,4.99,26.75,22.38,24.56,3.27

SW000818,60.30,60.19,60.25,8.03,36.29,38.57,37.43,4.99,18.71,15.64,17.17,2.29

SW003831,36.30,30.26,33.28,4.43,34.60,40.21,37.40,4.98,22.18,19.14,20.66,2.75

SW161594,38.60,42.05,40.32,5.37,37.59,37.16,37.37,4.98,16.89,12.35,14.62,1.95

SW054325,34.16,36.40,35.28,4.70,37.10,37.63,37.37,4.98,20.23,16.37,18.30,2.44

SW149933,35.46,51.97,43.71,5.82,34.73,39.81,37.27,4.97,-0.66,-1.62,-1.14,-0.15

SW118345,30.47,36.08,33.27,4.43,38.86,35.65,37.25,4.96,13.02,15.68,14.35,1.91

SW148565,36.69,50.75,43.72,5.82,34.56,39.86,37.21,4.96,1.48,0.88,1.18,0.16

SW028081,57.05,58.01,57.53,7.66,36.83,37.54,37.19,4.95,18.35,15.66,17.01,2.27

SW156432,27.03,32.46,29.74,3.96,37.37,36.91,37.14,4.95,16.35,21.41,18.88,2.52

SW131117,48.20,42.41,45.31,6.04,37.92,36.34,37.13,4.95,4.52,-6.70,-1.09,-0.15

SW086578,51.28,44.24,47.76,6.36,34.27,39.93,37.10,4.94,17.08,17.30,17.19,2.29

SW109642,26.52,27.83,27.18,3.62,38.25,35.81,37.03,4.93,15.45,18.04,16.74,2.23

SW165453,59.88,48.24,54.06,7.20,33.48,40.40,36.94,4.92,26.98,10.23,18.60,2.48

SW118673,29.98,40.94,35.46,4.72,38.16,35.44,36.80,4.90,21.15,18.98,20.07,2.67

SW053405,68.13,76.16,72.15,9.61,31.41,42.08,36.75,4.90,18.21,19.15,18.68,2.49

SW148466,66.89,92.26,79.57,10.60,32.74,40.74,36.74,4.89,16.46,15.44,15.95,2.13

SW134839,50.26,51.25,50.76,6.76,31.53,41.69,36.61,4.88,16.59,0.38,8.48,1.13

SW101601,35.62,37.30,36.46,4.86,39.20,33.83,36.52,4.86,18.93,17.94,18.44,2.46

SW004845,72.80,67.39,70.10,9.34,35.14,37.80,36.47,4.86,26.38,24.22,25.30,3.37

SW045498,29.88,25.92,27.90,3.72,30.91,41.93,36.42,4.85,17.25,14.87,16.06,2.14

SW118652,26.28,36.63,31.45,4.19,39.72,33.09,36.41,4.85,24.15,21.74,22.95,3.06

SW108027,35.28,41.11,38.19,5.09,38.22,34.53,36.38,4.85,19.80,16.97,18.38,2.45

SW082321,22.59,34.28,28.43,3.79,36.91,35.79,36.35,4.84,17.07,13.41,15.24,2.03

SW027550,33.35,47.16,40.26,5.36,36.21,36.42,36.32,4.84,16.17,17.51,16.84,2.24

SW027263,51.90,45.68,48.79,6.50,35.70,36.74,36.22,4.83,12.94,15.15,14.04,1.87

SW090447,51.53,56.32,53.92,7.18,38.10,34.26,36.18,4.82,17.47,20.69,19.08,2.54

SW165144,60.11,48.07,54.09,7.21,33.35,38.95,36.15,4.82,22.53,13.83,18.18,2.42

SW079357,38.24,40.39,39.32,5.24,30.79,41.51,36.15,4.82,28.51,20.08,24.30,3.24

SW201369,75.17,78.21,76.69,10.22,36.89,35.33,36.11,4.81,30.27,15.98,23.13,3.08

SW037575,48.23,58.71,53.47,7.12,33.73,38.44,36.09,4.81,3.09,1.63,2.36,0.32

SW012599,37.66,38.95,38.31,5.10,34.64,37.27,35.96,4.79,22.54,18.64,20.59,2.74

SW164386,47.49,41.55,44.52,5.93,41.98,29.92,35.95,4.79,26.10,22.11,24.11,3.21

SW113318,47.47,46.48,46.97,6.26,36.38,35.51,35.95,4.79,0.74,7.51,4.13,0.55

SW004357,39.95,37.97,38.96,5.19,34.00,37.81,35.91,4.78,28.76,23.51,26.13,3.48

SW013858,43.27,34.64,38.95,5.19,30.21,41.59,35.90,4.78,16.73,20.55,18.64,2.48

SW119367,30.04,46.58,38.31,5.10,37.91,33.81,35.86,4.78,15.05,13.83,14.44,1.92

SW036338,31.44,29.09,30.27,4.03,34.74,36.86,35.80,4.77,32.48,22.92,27.70,3.69

SW193725,15.32,16.87,16.10,2.14,33.87,37.51,35.69,4.75,30.34,15.51,22.92,3.05

SW082253,52.93,55.95,54.44,7.25,36.46,34.82,35.64,4.75,11.31,12.19,11.75,1.57

SW201653,47.30,43.55,45.43,6.05,34.93,36.32,35.62,4.75,25.85,16.08,20.97,2.79

SW201365,72.06,70.17,71.12,9.47,34.06,37.12,35.59,4.74,0.19,0.88,0.54,0.07

SW151414,51.96,75.57,63.76,8.49,31.31,39.84,35.57,4.74,11.09,14.01,12.55,1.67

SW125927,62.82,89.62,76.22,10.15,41.81,29.28,35.55,4.74,15.55,14.33,14.94,1.99

SW163161,53.64,60.41,57.02,7.60,34.68,36.33,35.51,4.73,15.70,9.02,12.36,1.65

SW148620,17.01,13.30,15.15,2.02,34.16,36.78,35.47,4.73,20.75,21.51,21.13,2.82

SW057708,45.25,51.00,48.13,6.41,33.92,36.87,35.40,4.72,21.97,14.29,18.13,2.42

SW064901,46.26,47.69,46.97,6.26,35.15,35.57,35.36,4.71,22.91,22.43,22.67,3.02

SW164221,79.21,58.32,68.76,9.16,33.10,37.46,35.28,4.70,10.81,11.48,11.15,1.49

SW086583,44.78,37.86,41.32,5.50,33.87,36.46,35.16,4.68,24.11,18.81,21.46,2.86

SW129302,39.52,32.26,35.89,4.78,39.43,30.62,35.02,4.67,-0.94,7.97,3.52,0.47

SW173226,55.46,55.33,55.40,7.38,32.65,37.23,34.94,4.65,23.68,20.04,21.86,2.91

SW001975,59.13,65.94,62.53,8.33,32.37,37.49,34.93,4.65,18.45,13.43,15.94,2.12

SW087412,40.21,39.10,39.65,5.28,32.83,36.82,34.82,4.64,22.00,15.22,18.61,2.48

SW166217,21.24,-3.27,8.99,1.20,32.13,37.39,34.76,4.63,28.02,13.47,20.74,2.76

SW007804,46.50,46.70,46.60,6.21,32.92,36.58,34.75,4.63,13.34,8.53,10.94,1.46

SW169716,45.94,53.12,49.53,6.60,34.51,34.73,34.62,4.61,32.89,16.19,24.54,3.27

SW163670,28.15,25.77,26.96,3.59,35.31,33.90,34.60,4.61,24.24,13.90,19.07,2.54

SW156969,29.00,40.86,34.93,4.65,34.38,34.75,34.57,4.61,28.64,21.28,24.96,3.33

SW128889,39.81,46.28,43.04,5.73,38.67,30.34,34.51,4.60,29.43,15.09,22.26,2.97

SW155839,29.74,41.51,35.63,4.75,37.26,31.66,34.46,4.59,16.80,14.79,15.80,2.10

SW163952,29.01,30.10,29.56,3.94,34.41,34.41,34.41,4.58,26.98,20.93,23.96,3.19

SW030187,31.16,36.66,33.91,4.52,33.74,34.95,34.34,4.58,18.20,15.59,16.90,2.25

SW082304,39.08,44.09,41.59,5.54,34.12,34.57,34.34,4.58,18.94,11.48,15.21,2.03

SW033595,48.51,68.87,58.69,7.82,35.75,32.87,34.31,4.57,21.37,19.27,20.32,2.71

SW119843,36.85,38.34,37.59,5.01,35.45,33.17,34.31,4.57,11.15,13.70,12.42,1.66

SW195856,27.54,35.07,31.31,4.17,33.55,35.06,34.31,4.57,24.31,20.14,22.23,2.96

SW066782,40.81,59.92,50.36,6.71,31.89,36.70,34.29,4.57,28.36,-6.06,-6.06,-0.81

SW010489,33.03,29.07,31.05,4.14,32.09,36.46,34.27,4.57,9.36,10.63,10.00,1.33

SW027544,40.22,38.91,39.56,5.27,31.89,36.62,34.26,4.56,17.07,15.38,16.22,2.16

SW088959,35.52,34.00,34.76,4.63,32.01,36.45,34.23,4.56,20.42,16.19,18.30,2.44

SW202385,51.49,46.16,48.83,6.51,34.39,34.03,34.21,4.56,13.80,12.11,12.96,1.73

SW162964,49.70,58.65,54.17,7.22,32.35,36.05,34.20,4.56,8.36,5.47,6.92,0.92

SW053401,51.78,51.52,51.65,6.88,33.42,34.96,34.19,4.56,20.65,12.89,16.77,2.23

SW144054,25.13,51.24,38.19,5.09,33.73,34.66,34.19,4.56,32.07,22.46,27.26,3.63

SW185542,15.01,16.65,15.83,2.11,33.15,35.20,34.18,4.55,28.83,14.35,21.59,2.88

SW083574,35.08,31.22,33.15,4.42,30.50,37.75,34.13,4.55,-3.49,4.93,0.72,0.10

SW173152,60.03,54.43,57.23,7.63,31.63,36.41,34.02,4.53,22.26,19.26,20.76,2.77

SW011962,30.17,25.22,27.70,3.69,32.80,35.22,34.01,4.53,22.25,18.80,20.53,2.73

SW087408,38.08,28.81,33.44,4.46,36.45,31.40,33.93,4.52,14.52,16.57,15.55,2.07

SW003498,61.72,84.96,73.34,9.77,34.58,33.22,33.90,4.52,12.88,12.34,12.61,1.68

SW125227,39.15,43.96,41.56,5.54,40.70,26.91,33.80,4.50,21.43,15.30,18.37,2.45

SW166377,36.42,32.54,34.48,4.59,30.50,36.95,33.73,4.49,25.46,10.93,18.19,2.42

SW018970,27.91,23.10,25.50,3.40,29.91,37.29,33.60,4.48,20.80,19.72,20.26,2.70

SW033785,41.97,36.41,39.19,5.22,34.44,32.75,33.60,4.48,17.31,15.82,16.56,2.21

SW150077,58.32,84.10,71.21,9.49,28.82,38.33,33.57,4.47,23.00,19.57,21.28,2.84

SW129064,38.10,45.65,41.87,5.58,39.49,27.60,33.55,4.47,26.24,15.02,20.63,2.75

SW017709,40.01,59.06,49.53,6.60,32.24,34.79,33.52,4.47,20.60,-7.13,6.74,0.90

SW158402,28.62,40.61,34.62,4.61,33.12,33.85,33.49,4.46,21.64,19.68,20.66,2.75

SW028425,41.61,44.50,43.05,5.74,32.57,34.31,33.44,4.45,18.87,15.01,16.94,2.26

SW192772,12.90,14.93,13.92,1.85,32.19,34.66,33.43,4.45,31.14,15.05,23.09,3.08

SW166187,23.39,15.90,19.65,2.62,32.12,34.57,33.35,4.44,19.66,8.58,14.12,1.88

SW110388,20.07,30.72,25.40,3.38,37.38,29.29,33.33,4.44,28.82,18.57,23.70,3.16

SW170041,34.17,34.55,34.36,4.58,29.94,36.63,33.28,4.43,6.12,-3.71,1.21,0.16

SW030049,51.31,42.47,46.89,6.25,31.49,34.91,33.20,4.42,16.30,12.20,14.25,1.90

SW128878,38.97,34.57,36.77,4.90,35.26,30.96,33.11,4.41,12.40,12.62,12.51,1.67

SW109064,53.62,63.96,58.79,7.83,38.35,27.80,33.08,4.41,25.44,17.61,21.53,2.87

SW132488,41.44,40.04,42.18,5.62,35.83,39.67,33.05,4.40,21.62,23.64,23.31,3.11

SW118159,20.04,34.51,27.28,3.63,34.74,31.36,33.05,4.40,22.01,17.84,19.92,2.65

SW118214,30.82,38.02,34.42,4.59,36.53,29.45,32.99,4.39,14.63,15.62,15.13,2.02

SW159610,23.99,35.41,29.70,3.96,32.65,33.21,32.93,4.39,24.65,17.40,21.02,2.80

SW201807,37.03,38.42,37.72,5.03,29.80,36.03,32.92,4.39,20.09,5.95,13.02,1.74

SW004356,35.02,29.86,32.44,4.32,32.50,33.23,32.87,4.38,34.43,22.65,28.54,3.80

SW085522,49.30,44.72,47.01,6.26,23.61,41.98,32.80,4.37,-2.16,13.47,5.66,0.75

SW103220,22.56,25.70,24.13,3.21,30.53,35.04,32.79,4.37,15.61,18.95,17.28,2.30

SW053403,57.82,72.91,65.36,8.71,30.94,34.59,32.77,4.37,7.60,11.37,9.48,1.26

SW001878,16.35,30.16,23.26,3.10,34.41,30.91,32.66,4.35,30.23,24.01,27.12,3.61

SW003033,25.42,25.93,25.68,3.42,31.16,34.06,32.61,4.34,10.64,16.85,13.74,1.83

SW021483,30.90,36.24,33.57,4.47,30.24,34.88,32.56,4.34,12.05,17.00,14.53,1.94

SW087415,43.59,39.04,41.31,5.50,31.74,33.37,32.55,4.34,22.60,14.49,18.55,2.47

SW148540,50.07,68.18,59.13,7.88,29.79,35.28,32.53,4.33,6.25,15.97,11.11,1.48

SW011776,24.89,19.99,22.44,2.99,28.74,35.94,32.34,4.31,17.15,17.99,17.57,2.34

SW027546,43.70,37.38,40.54,5.40,30.63,34.03,32.33,4.31,10.33,10.78,10.56,1.41

SW163329,36.47,27.73,32.10,4.28,33.07,31.58,32.32,4.31,18.20,5.09,11.64,1.55

SW144903,41.98,43.11,42.55,5.67,31.47,33.17,32.32,4.31,21.80,28.12,24.96,3.33

SW154784,53.74,66.25,59.99,7.99,29.95,34.57,32.26,4.30,11.28,11.16,11.22,1.50

SW054011,63.94,71.20,67.57,9.00,30.51,33.96,32.24,4.29,21.59,15.92,18.75,2.50

SW154526,18.73,30.36,24.54,3.27,45.55,18.89,32.22,4.29,14.07,14.39,14.23,1.90

SW171463,15.92,3.50,9.71,1.29,31.13,33.29,32.21,4.29,28.76,14.87,21.82,2.91

SW142316,27.64,30.84,29.24,3.90,29.90,34.51,32.21,4.29,20.59,16.86,18.72,2.49

SW196433,53.20,55.94,54.57,7.27,29.67,34.64,32.16,4.28,13.91,13.28,13.60,1.81

SW125089,39.60,41.32,40.46,5.39,34.28,29.99,32.14,4.28,12.16,15.95,14.05,1.87

SW180041,19.26,16.08,17.67,2.35,30.32,33.95,32.14,4.28,17.85,15.07,16.46,2.19

SW030735,45.13,38.60,41.86,5.58,28.10,35.87,31.98,4.26,18.80,19.62,19.21,2.56

SW192403,28.38,24.27,26.33,3.51,30.72,33.20,31.96,4.26,27.55,11.62,19.58,2.61

SW122313,16.97,30.16,23.56,3.14,33.25,30.62,31.93,4.25,21.95,20.04,20.99,2.80

SW195865,28.80,50.54,39.67,5.28,29.67,34.09,31.88,4.25,28.96,20.70,24.83,3.31

SW117723,45.38,45.13,45.26,6.03,32.74,31.00,31.87,4.25,6.92,10.70,8.81,1.17

SW129217,36.03,50.65,43.34,5.77,35.57,27.91,31.74,4.23,23.33,14.38,18.85,2.51

SW008212,38.25,32.12,35.18,4.69,28.85,34.62,31.73,4.23,14.41,17.71,16.06,2.14

SW133118,47.51,42.92,45.22,6.02,37.84,25.51,31.68,4.22,28.72,24.67,26.70,3.56

SW058824,31.06,23.89,27.48,3.66,31.55,31.73,31.64,4.22,19.59,18.26,18.92,2.52

SW199277,24.48,23.21,23.84,3.18,28.85,34.41,31.63,4.21,25.17,13.68,19.43,2.59

SW142413,64.83,79.80,72.32,9.63,28.30,34.87,31.59,4.21,20.07,21.86,20.96,2.79

SW168897,28.78,34.38,31.58,4.21,29.77,33.34,31.56,4.20,22.48,10.26,16.37,2.18

SW034496,43.23,39.48,41.36,5.51,31.21,31.79,31.50,4.20,8.09,12.07,10.08,1.34

SW110394,25.62,36.78,31.20,4.16,33.50,29.30,31.40,4.18,15.52,13.15,14.34,1.91

SW163254,39.57,53.24,46.40,6.18,28.71,34.00,31.35,4.18,13.81,8.64,11.23,1.50

SW000724,24.23,14.27,19.25,2.56,32.07,30.52,31.30,4.17,27.18,27.65,27.42,3.65

SW085557,41.38,38.44,39.91,5.32,31.95,30.62,31.28,4.17,17.16,20.02,18.59,2.48

SW067947,12.00,10.40,11.20,1.49,30.62,31.90,31.26,4.16,15.77,12.17,13.97,1.86

SW178268,13.60,10.39,11.99,1.60,29.94,32.43,31.19,4.15,25.60,10.44,18.02,2.40

SW165291,92.68,73.58,83.13,11.08,28.99,33.20,31.10,4.14,26.82,17.10,21.96,2.93

SW085349,44.54,33.25,38.90,5.18,29.39,32.80,31.10,4.14,19.52,25.66,22.59,3.01

SW116249,20.46,28.66,24.56,3.27,34.13,27.93,31.03,4.13,22.51,15.92,19.22,2.56

SW164077,43.87,39.60,41.74,5.56,30.13,31.93,31.03,4.13,19.02,18.64,18.83,2.51

SW142579,24.93,23.96,24.45,3.26,30.83,31.14,30.99,4.13,23.54,21.22,22.38,2.98

SW070883,38.56,43.76,41.16,5.48,31.11,30.85,30.98,4.13,18.29,13.14,15.71,2.09

SW166386,25.88,29.60,27.74,3.70,29.93,31.93,30.93,4.12,25.99,8.55,17.27,2.30

SW105695,42.23,46.83,44.53,5.93,34.23,27.47,30.85,4.11,15.26,16.38,15.82,2.11

SW023747,72.75,93.13,82.94,11.05,30.05,31.57,30.81,4.10,10.74,6.86,8.80,1.17

SW067092,28.75,34.29,31.52,4.20,32.04,29.52,30.78,4.10,12.25,12.02,12.14,1.62

SW152880,42.19,63.62,52.90,7.05,29.39,32.05,30.72,4.09,6.62,9.68,8.15,1.09

SW084534,23.26,12.79,18.02,2.40,31.67,29.68,30.67,4.09,17.72,16.04,16.88,2.25

SW123456,31.11,36.71,33.91,4.52,34.53,26.70,30.62,4.08,6.53,11.27,8.90,1.19

SW176887,16.48,15.59,16.03,2.14,30.52,30.69,30.60,4.08,19.72,17.32,18.52,2.47

SW195859,33.88,40.91,37.40,4.98,28.86,32.31,30.59,4.08,24.57,19.33,21.95,2.92

SW023809,47.23,74.43,60.83,8.10,29.94,31.23,30.59,4.07,13.26,10.97,12.12,1.61

SW171207,12.97,12.00,12.48,1.66,28.43,32.62,30.52,4.07,25.46,13.52,19.49,2.60

SW156082,42.51,47.18,44.85,5.97,30.51,30.53,30.52,4.07,12.15,11.73,11.94,1.59

SW128827,23.94,22.52,23.23,3.09,32.95,28.08,30.52,4.07,8.31,8.59,8.45,1.13

SW012705,35.35,34.67,35.01,4.66,30.41,30.60,30.51,4.06,17.31,11.88,14.60,1.94

SW109475,18.16,28.13,23.14,3.08,29.08,31.92,30.50,4.06,10.47,15.42,12.94,1.72

SW128536,30.50,39.42,34.96,4.66,33.25,27.15,30.20,4.02,13.43,10.37,11.90,1.59

SW192437,18.38,14.92,16.65,2.22,28.37,32.02,30.20,4.02,26.46,11.44,18.95,2.53

SW154253,26.39,34.67,30.53,4.07,29.82,30.55,30.18,4.02,19.74,16.40,18.07,2.41

SW000548,26.58,21.59,24.08,3.21,30.07,30.16,30.12,4.01,27.84,27.88,27.86,3.71

SW083576,40.09,36.78,38.43,5.12,28.33,31.89,30.11,4.01,11.71,-3.02,4.34,0.58

SW054887,31.80,45.32,38.56,5.14,28.93,30.95,29.94,3.99,18.55,21.25,19.90,2.65

SW011094,41.15,37.03,39.09,5.21,27.73,32.09,29.91,3.98,10.98,16.20,13.59,1.81

SW027525,38.86,34.21,36.53,4.87,28.31,31.50,29.91,3.98,8.68,14.36,11.52,1.53

SW201309,57.04,63.85,60.44,8.05,28.79,30.97,29.88,3.98,24.37,10.67,17.52,2.33

SW023025,20.32,14.08,17.20,2.29,28.77,30.97,29.87,3.98,20.59,24.16,22.37,2.98

SW028794,40.01,35.90,37.95,5.06,32.82,26.80,29.81,3.97,21.05,11.60,16.32,2.17

SW196147,26.78,37.27,32.03,4.27,28.53,31.01,29.77,3.97,15.58,21.67,18.63,2.48

SW166043,2.41,-1.10,0.66,0.09,30.00,29.44,29.72,3.96,16.97,13.40,15.18,2.02

SW008933,31.04,49.85,40.45,5.39,28.16,31.19,29.67,3.95,12.87,20.63,16.75,2.23

SW091119,41.50,20.38,30.94,4.12,32.12,27.19,29.66,3.95,8.38,8.51,8.45,1.13

SW163994,58.27,54.93,56.60,7.54,30.32,28.94,29.63,3.95,24.61,20.21,22.41,2.99

SW166825,37.17,29.41,33.29,4.43,26.94,32.28,29.61,3.95,17.08,12.42,14.75,1.96

SW153480,5.75,16.18,10.96,1.46,27.01,31.99,29.50,3.93,31.36,29.20,30.28,4.03

SW135154,27.89,25.04,26.47,3.53,33.88,25.05,29.46,3.93,9.21,11.81,10.51,1.40

SW110376,15.62,26.46,21.04,2.80,31.04,27.84,29.44,3.92,20.23,15.24,17.74,2.36

SW106578,46.03,45.88,45.96,6.12,32.31,26.54,29.43,3.92,5.24,8.76,7.00,0.93

SW057692,26.27,39.90,33.09,4.41,29.49,29.32,29.40,3.92,15.37,11.66,13.52,1.80

SW081840,42.59,49.53,46.06,6.14,28.40,30.34,29.37,3.91,10.73,6.08,8.40,1.12

SW116295,35.42,47.18,41.30,5.50,33.37,25.32,29.35,3.91,16.86,12.56,14.71,1.96

SW164200,33.30,29.53,31.41,4.18,28.04,30.64,29.34,3.91,23.84,16.89,20.36,2.71

SW172978,30.29,30.65,30.47,4.06,26.49,32.17,29.33,3.91,10.09,13.00,11.55,1.54

SW021723,23.75,20.38,22.07,2.94,29.12,29.51,29.32,3.91,17.02,14.40,15.71,2.09

SW190422,19.58,22.13,20.85,2.78,29.90,28.59,29.24,3.90,19.37,12.52,15.95,2.12

SW022446,26.82,18.36,22.59,3.01,25.59,32.89,29.24,3.90,17.29,17.59,17.44,2.32

SW148697,13.40,28.24,20.82,2.77,29.81,28.63,29.22,3.89,29.74,23.56,26.65,3.55

SW103107,24.63,27.01,25.82,3.44,30.25,28.18,29.21,3.89,15.26,18.64,16.95,2.26

SW000722,22.88,4.03,13.46,1.79,28.50,29.87,29.18,3.89,29.78,26.97,28.37,3.78

SW013492,18.35,20.83,19.59,2.61,29.63,28.69,29.16,3.88,13.59,22.14,17.86,2.38

SW085429,27.82,23.01,25.41,3.39,30.93,27.24,29.09,3.88,9.02,11.29,10.16,1.35

SW051294,30.43,36.31,33.37,4.45,32.59,25.52,29.06,3.87,25.57,23.70,24.63,3.28

SW142794,10.26,11.61,10.93,1.46,28.38,29.72,29.05,3.87,29.13,24.52,26.82,3.57

SW163740,61.10,54.16,57.63,7.68,28.30,29.77,29.04,3.87,19.80,18.10,18.95,2.52

SW000497,24.37,21.44,22.90,3.05,30.89,27.14,29.01,3.87,33.65,29.59,31.62,4.21

SW021426,25.27,20.01,22.64,3.02,31.04,26.94,28.99,3.86,8.87,10.38,9.63,1.28

SW121293,35.28,50.49,42.88,5.71,34.40,23.54,28.97,3.86,20.33,13.90,17.11,2.28

SW165448,34.15,18.28,26.21,3.49,25.11,32.83,28.97,3.86,19.26,7.70,13.48,1.80

SW094025,48.51,49.64,49.08,6.54,26.94,30.94,28.94,3.86,12.98,5.58,9.28,1.24

SW084448,29.29,30.99,30.14,4.02,30.60,27.25,28.93,3.85,14.50,21.34,17.92,2.39

SW001408,53.27,62.66,57.97,7.72,30.31,27.41,28.86,3.85,16.03,3.38,9.70,1.29

SW150810,68.71,86.37,77.54,10.33,28.11,29.59,28.85,3.84,15.05,22.38,18.72,2.49

SW158941,29.33,37.64,33.48,4.46,29.53,28.09,28.81,3.84,15.21,15.40,15.30,2.04

SW154523,-5.18,7.12,0.97,0.13,40.41,17.19,28.80,3.84,14.16,13.24,13.70,1.83

SW053404,36.79,50.64,43.71,5.82,27.88,29.59,28.74,3.83,8.84,13.02,10.93,1.46

SW170388,15.74,18.82,17.28,2.30,27.57,29.81,28.69,3.82,27.43,8.83,18.13,2.42

SW010972,33.12,27.28,30.20,4.02,25.38,31.96,28.67,3.82,17.51,19.44,18.47,2.46

SW058177,36.58,48.72,42.65,5.68,28.23,29.00,28.61,3.81,16.73,12.10,14.42,1.92

SW110111,64.51,77.08,70.80,9.43,32.16,24.98,28.57,3.81,-13.92,-12.72,-13.32,-1.77

SW118169,29.48,41.81,35.65,4.75,32.42,24.70,28.56,3.80,-5.80,-4.69,-5.25,-0.70

SW000488,22.37,16.91,19.64,2.62,26.26,30.76,28.51,3.80,20.53,22.32,21.43,2.85

SW108263,49.97,64.48,57.22,7.62,29.49,27.52,28.50,3.80,1.48,-19.83,-9.18,-1.22

SW191707,9.83,5.74,7.78,1.04,27.35,29.51,28.43,3.79,23.52,10.06,16.79,2.24

SW000023,15.51,9.40,12.46,1.66,27.10,29.56,28.33,3.77,17.19,19.92,18.55,2.47

SW026936,37.80,27.80,32.80,4.37,26.86,29.70,28.28,3.77,10.94,11.07,11.00,1.47

SW174760,39.83,45.71,42.77,5.70,25.18,31.35,28.27,3.77,21.55,11.45,16.50,2.20

SW085352,12.36,23.01,17.68,2.36,28.11,28.41,28.26,3.76,26.44,22.15,24.30,3.24

SW139561,36.96,36.91,36.93,4.92,23.88,32.63,28.26,3.76,13.42,-4.50,4.46,0.59

SW166891,31.76,13.81,22.79,3.04,26.57,29.92,28.25,3.76,15.37,11.63,13.50,1.80

SW164600,14.91,16.19,15.55,2.07,27.84,28.64,28.24,3.76,25.66,18.85,22.26,2.97

SW165031,26.35,19.91,23.13,3.08,28.09,28.39,28.24,3.76,12.34,3.94,8.14,1.08

SW079345,35.51,31.20,33.36,4.44,25.65,30.82,28.23,3.76,15.86,9.61,12.74,1.70

SW000832,28.91,22.43,25.67,3.42,24.30,32.07,28.18,3.75,19.49,23.69,21.59,2.88

SW070698,26.71,28.59,27.65,3.68,28.66,27.69,28.18,3.75,12.57,13.02,12.79,1.70

SW074105,35.64,35.38,35.51,4.73,28.61,27.74,28.17,3.75,6.90,7.30,7.10,0.95

SW087407,55.18,60.48,57.83,7.70,26.25,30.00,28.13,3.75,9.45,5.83,7.64,1.02

SW163513,39.15,41.13,40.14,5.35,29.84,26.41,28.13,3.75,24.39,17.14,20.77,2.77

SW151028,40.60,51.31,45.96,6.12,23.34,32.88,28.11,3.75,-5.95,8.74,1.40,0.19

SW022034,27.45,42.61,35.03,4.67,27.73,28.44,28.08,3.74,11.09,11.53,11.31,1.51

SW053850,28.80,32.43,30.62,4.08,27.09,28.98,28.03,3.73,23.64,16.50,20.07,2.67

SW094734,17.21,18.16,17.68,2.36,26.76,29.28,28.02,3.73,17.59,20.67,19.13,2.55

SW000720,23.25,9.59,16.42,2.19,26.68,29.27,27.97,3.73,27.00,24.20,25.60,3.41

SW192424,19.48,17.73,18.61,2.48,28.12,27.71,27.92,3.72,26.88,13.94,20.41,2.72

SW131319,39.73,48.06,43.90,5.85,32.20,23.57,27.88,3.71,17.78,8.05,12.92,1.72

SW186990,8.33,13.60,10.96,1.46,27.14,28.62,27.88,3.71,22.17,10.79,16.48,2.20

SW154525,33.98,53.50,43.74,5.83,27.02,28.73,27.87,3.71,19.89,18.65,19.27,2.57

SW142980,10.18,15.60,12.89,1.72,27.86,27.88,27.87,3.71,22.93,24.08,23.50,3.13

SW083775,19.95,9.00,14.48,1.93,28.17,27.48,27.82,3.71,19.36,12.34,15.85,2.11

SW083362,23.13,20.84,21.99,2.93,27.09,28.49,27.79,3.70,18.41,20.14,19.28,2.57

SW098954,12.66,13.71,13.18,1.76,28.49,27.09,27.79,3.70,21.55,14.07,17.81,2.37

SW138877,30.77,31.97,31.37,4.18,27.42,28.11,27.76,3.70,24.39,20.55,22.47,2.99

SW159782,22.13,24.49,23.31,3.11,27.71,27.80,27.76,3.70,18.06,10.79,14.42,1.92

SW082315,20.44,21.19,20.81,2.77,21.96,33.52,27.74,3.70,16.74,19.07,17.90,2.39

SW025047,19.80,17.49,18.65,2.48,21.61,33.84,27.72,3.69,20.47,13.44,16.96,2.26

SW189732,12.69,16.39,14.54,1.94,27.40,28.00,27.70,3.69,29.90,15.77,22.84,3.04

SW153892,42.94,56.94,49.94,6.65,26.55,28.81,27.68,3.69,30.65,26.16,28.41,3.78

SW192648,13.67,15.64,14.66,1.95,30.07,25.25,27.66,3.68,19.90,15.45,17.68,2.36

SW170393,12.18,14.18,13.18,1.76,28.29,26.99,27.64,3.68,31.39,14.02,22.71,3.03

SW006877,38.78,33.45,36.12,4.81,27.33,27.93,27.63,3.68,19.13,9.58,14.35,1.91

SW149329,39.53,50.61,45.07,6.00,26.86,28.28,27.57,3.67,1.45,15.02,8.23,1.10

SW112066,42.56,53.93,48.25,6.43,31.94,23.18,27.56,3.67,10.16,15.00,12.58,1.68

SW170142,13.02,15.03,14.02,1.87,26.97,28.12,27.54,3.67,28.40,11.12,19.76,2.63

SW084376,27.36,25.64,26.50,3.53,28.45,26.62,27.54,3.67,13.91,18.85,16.38,2.18

SW158691,29.83,46.56,38.19,5.09,26.80,28.09,27.45,3.66,25.44,22.32,23.88,3.18

SW128880,20.12,24.60,22.36,2.98,30.13,24.73,27.43,3.65,8.82,12.58,10.70,1.43

SW191166,14.04,12.14,13.09,1.74,25.73,29.00,27.37,3.65,15.68,11.36,13.52,1.80

SW046126,46.72,38.83,42.77,5.70,25.76,28.91,27.34,3.64,8.79,5.08,6.93,0.92

SW094732,18.76,15.76,17.26,2.30,25.12,29.45,27.28,3.64,20.77,21.07,20.92,2.79

SW119346,86.43,100.74,93.58,12.47,66.33,27.23,27.23,3.63,-10.22,-5.84,-8.03,-1.07

SW163645,4.44,5.53,4.99,0.66,27.14,27.31,27.23,3.63,20.33,15.95,18.14,2.42

SW053515,37.43,57.63,47.53,6.33,26.89,27.50,27.19,3.62,8.30,7.35,7.82,1.04

SW176757,11.85,10.92,11.39,1.52,26.07,28.30,27.19,3.62,18.28,7.80,13.04,1.74

SW084386,36.99,41.67,39.33,5.24,26.83,27.44,27.14,3.62,19.90,20.56,20.23,2.70

SW132696,72.39,75.15,24.87,3.31,69.65,74.77,27.09,3.61,43.97,36.66,31.01,4.13

SW052274,37.88,49.68,43.78,5.83,26.90,27.22,27.06,3.61,15.41,8.82,12.12,1.61

SW120375,13.21,27.58,20.40,2.72,27.87,26.15,27.01,3.60,9.37,10.98,10.18,1.36

SW035799,29.07,22.54,25.81,3.44,24.56,29.45,27.00,3.60,10.26,10.00,10.13,1.35

SW063921,29.72,18.17,23.94,3.19,24.68,29.29,26.98,3.59,11.88,8.81,10.34,1.38

SW084373,24.32,20.52,22.42,2.99,27.84,26.05,26.94,3.59,17.55,17.11,17.33,2.31

SW165372,33.35,30.10,31.72,4.23,26.33,27.51,26.92,3.59,21.01,15.73,18.37,2.45

SW176508,9.42,14.04,11.73,1.56,26.90,26.91,26.91,3.58,24.59,9.64,17.11,2.28

SW122825,30.91,48.99,39.95,5.32,29.12,24.70,26.91,3.58,16.35,18.72,17.53,2.34

SW055091,9.92,9.89,9.90,1.32,26.84,26.97,26.91,3.58,22.54,23.20,22.87,3.05

SW052558,42.34,32.78,37.56,5.00,25.87,27.85,26.86,3.58,16.41,14.15,15.28,2.04

SW044570,33.85,31.59,32.72,4.36,25.10,28.45,26.77,3.57,25.25,12.63,18.94,2.52

SW192421,8.62,11.96,10.29,1.37,25.31,28.15,26.73,3.56,21.87,7.53,14.70,1.96

SW117497,34.84,50.95,42.89,5.71,29.43,24.02,26.72,3.56,17.96,14.59,16.28,2.17

SW036353,16.47,15.85,16.16,2.15,25.77,27.65,26.71,3.56,11.15,16.53,13.84,1.84

SW129299,28.17,23.05,25.61,3.41,31.46,21.94,26.70,3.56,11.29,6.43,8.86,1.18

SW166618,16.14,11.76,13.95,1.86,24.33,29.07,26.70,3.56,5.50,-4.72,0.39,0.05

SW183644,13.74,10.85,12.30,1.64,26.36,26.99,26.68,3.55,12.23,14.92,13.57,1.81

SW109741,4.96,18.45,11.70,1.56,26.53,26.81,26.67,3.55,21.23,18.81,20.02,2.67

SW147365,5.48,1.32,3.40,0.45,26.48,26.76,26.62,3.55,23.14,22.32,22.73,3.03

SW152529,45.60,52.16,48.88,6.51,26.79,26.44,26.61,3.55,20.47,18.43,19.45,2.59

SW018839,29.87,24.11,26.99,3.60,25.02,28.18,26.60,3.54,27.26,23.12,25.19,3.36

SW163013,43.20,56.04,49.62,6.61,27.05,26.05,26.55,3.54,16.09,11.33,13.71,1.83

SW145848,22.77,35.98,29.37,3.91,25.00,28.04,26.52,3.53,22.51,21.49,22.00,2.93

SW000543,18.39,11.17,14.78,1.97,26.06,26.98,26.52,3.53,23.37,25.11,24.24,3.23

SW083317,47.53,43.04,45.28,6.03,31.26,21.73,26.50,3.53,4.33,3.24,3.78,0.50

SW118765,18.07,32.61,25.34,3.38,30.53,22.36,26.45,3.52,20.43,14.47,17.45,2.32

SW109372,50.02,52.23,51.12,6.81,28.18,24.68,26.43,3.52,-1.60,8.24,3.32,0.44

SW194307,12.80,8.80,10.80,1.44,27.14,25.64,26.39,3.52,14.78,12.94,13.86,1.85

SW115856,11.57,22.18,16.87,2.25,26.15,26.62,26.39,3.52,14.73,10.50,12.62,1.68

SW089669,21.96,21.82,21.89,2.92,27.92,24.85,26.38,3.51,16.67,19.48,18.07,2.41

SW003081,15.98,12.70,14.34,1.91,25.20,27.55,26.37,3.51,27.90,18.55,23.23,3.09

SW023147,16.93,13.47,15.20,2.02,24.37,28.34,26.35,3.51,16.19,13.27,14.73,1.96

SW156180,31.92,39.86,35.89,4.78,25.32,27.29,26.31,3.50,2.40,8.97,5.68,0.76

SW124269,18.25,21.66,19.96,2.66,28.74,23.87,26.30,3.50,13.60,9.86,11.73,1.56

SW106279,18.47,28.02,23.25,3.10,28.55,24.05,26.30,3.50,-8.48,-9.59,-9.04,-1.20

SW069087,19.82,7.11,13.47,1.79,24.65,27.94,26.30,3.50,7.72,11.34,9.53,1.27

SW101905,85.27,82.20,83.74,11.16,59.97,26.28,26.28,3.50,3.91,6.13,5.02,0.67

SW108834,62.87,72.88,67.87,9.04,30.15,22.40,26.27,3.50,18.09,13.79,15.94,2.12

SW169990,22.77,24.10,23.43,3.12,26.83,25.71,26.27,3.50,27.10,16.33,21.72,2.89

SW149480,45.45,63.31,54.38,7.24,24.51,27.99,26.25,3.50,12.71,12.12,12.41,1.65

SW203409,48.20,50.35,49.27,6.56,28.02,24.46,26.24,3.50,9.01,5.77,7.39,0.99

SW191787,9.97,2.26,6.12,0.81,25.51,26.93,26.22,3.49,14.12,11.21,12.67,1.69

SW140507,23.50,29.20,26.35,3.51,27.80,24.63,26.22,3.49,20.45,21.11,20.78,2.77

SW191175,10.63,0.48,5.56,0.74,25.59,26.83,26.21,3.49,22.14,7.76,14.95,1.99

SW000081,37.40,31.52,34.46,4.59,22.67,29.74,26.21,3.49,15.16,16.79,15.98,2.13

SW137588,22.53,19.77,21.15,2.82,27.82,24.58,26.20,3.49,24.61,20.51,22.56,3.01

SW014635,19.22,16.62,17.92,2.39,24.78,27.56,26.17,3.49,24.14,14.64,19.39,2.58

SW176321,12.97,17.28,15.13,2.02,26.56,25.77,26.17,3.49,25.09,18.62,21.86,2.91

SW000712,20.37,9.30,14.84,1.98,23.59,28.69,26.14,3.48,23.80,21.65,22.72,3.03

SW095142,25.36,39.03,32.20,4.29,29.12,23.08,26.10,3.48,24.43,16.63,20.53,2.74

SW174344,14.29,16.14,15.22,2.03,24.16,27.97,26.07,3.47,17.46,9.78,13.62,1.81

SW197864,4.38,8.56,6.47,0.86,24.08,28.01,26.04,3.47,18.91,6.78,12.84,1.71

SW139580,13.13,14.95,14.04,1.87,25.57,26.48,26.03,3.47,22.88,21.64,22.26,2.97

SW187931,14.89,12.08,13.48,1.80,24.89,27.15,26.02,3.47,17.55,16.03,16.79,2.24

SW084349,22.00,23.05,22.52,3.00,25.03,26.90,25.97,3.46,13.27,18.98,16.12,2.15

SW121405,34.14,55.30,44.72,5.96,24.69,27.12,25.91,3.45,0.06,6.98,3.52,0.47

SW011186,29.69,22.19,25.94,3.46,24.57,27.24,25.90,3.45,13.92,13.00,13.46,1.79

SW170812,11.05,10.52,10.78,1.44,26.00,25.80,25.90,3.45,17.07,13.69,15.38,2.05

SW009095,41.05,61.87,51.46,6.86,25.36,26.40,25.88,3.45,8.40,12.37,10.38,1.38

SW147189,5.34,12.14,8.74,1.16,25.23,26.51,25.87,3.45,25.87,23.24,24.56,3.27

SW163523,43.49,33.50,38.50,5.13,24.37,27.32,25.85,3.44,18.12,16.81,17.47,2.33

SW036989,37.17,35.76,36.47,4.86,22.39,29.31,25.85,3.44,17.01,11.57,14.29,1.90

SW000740,20.66,12.52,16.59,2.21,22.94,28.74,25.84,3.44,22.95,21.81,22.38,2.98

SW154452,15.19,31.42,23.31,3.11,26.74,24.91,25.82,3.44,21.95,19.74,20.84,2.78

SW169016,25.78,24.28,25.03,3.33,23.65,27.98,25.81,3.44,20.71,7.65,14.18,1.89

SW129029,21.56,27.38,24.47,3.26,27.27,24.32,25.79,3.44,19.28,12.95,16.11,2.15

SW167607,17.14,19.27,18.21,2.43,25.14,26.39,25.76,3.43,22.31,22.12,22.22,2.96

SW163479,7.07,-1.64,2.71,0.36,27.96,23.52,25.74,3.43,14.68,16.22,15.45,2.06

SW148916,25.19,49.67,37.43,4.99,24.76,26.70,25.73,3.43,16.52,17.17,16.84,2.24

SW122104,15.60,34.27,24.94,3.32,26.31,25.08,25.69,3.42,12.82,12.47,12.65,1.68

SW000751,17.43,9.24,13.33,1.78,24.09,27.19,25.64,3.42,23.38,22.35,22.86,3.05

SW192441,19.26,21.39,20.33,2.71,27.21,24.07,25.64,3.42,23.40,18.61,21.01,2.80

SW084291,32.85,29.13,30.99,4.13,28.63,22.59,25.61,3.41,12.83,9.98,11.40,1.52

SW164013,32.20,28.89,30.55,4.07,23.42,27.77,25.60,3.41,13.09,14.79,13.94,1.86

SW038554,21.37,36.36,28.87,3.85,26.25,24.94,25.59,3.41,14.12,8.53,11.32,1.51

SW118554,20.26,36.20,28.23,3.76,27.89,23.20,25.55,3.40,19.62,18.77,19.20,2.56

SW178038,12.80,8.69,10.75,1.43,24.28,26.77,25.52,3.40,12.89,3.18,8.04,1.07

SW144437,19.91,17.12,18.51,2.47,27.10,23.92,25.51,3.40,26.62,21.60,24.11,3.21

SW198110,17.17,9.18,13.17,1.75,25.35,25.65,25.50,3.40,15.39,8.14,11.77,1.57

SW013112,15.15,10.33,12.74,1.70,24.48,26.49,25.49,3.40,15.07,9.64,12.36,1.65

SW155222,24.75,40.79,32.77,4.37,25.72,25.23,25.48,3.39,18.75,16.39,17.57,2.34

SW100653,58.06,74.50,66.28,8.83,34.28,16.65,25.46,3.39,5.70,8.01,6.86,0.91

SW013903,15.81,14.68,15.24,2.03,24.65,26.20,25.43,3.39,21.93,14.60,18.27,2.43

SW120425,3.51,14.10,8.81,1.17,25.40,25.44,25.42,3.39,14.68,18.57,16.63,2.21

SW192440,13.31,15.15,14.23,1.90,26.08,24.69,25.39,3.38,21.59,16.77,19.18,2.56

SW102284,25.28,26.22,25.75,3.43,28.05,22.63,25.34,3.38,8.99,11.40,10.20,1.36

SW148861,24.66,32.79,28.72,3.83,24.16,26.50,25.33,3.37,23.92,17.90,20.91,2.79

SW166698,34.25,26.51,30.38,4.05,23.31,27.34,25.33,3.37,18.86,13.18,16.02,2.13

SW158307,20.85,27.97,24.41,3.25,24.57,26.04,25.31,3.37,12.60,12.18,12.39,1.65

SW183509,17.47,9.83,13.65,1.82,25.99,24.62,25.30,3.37,26.55,21.58,24.06,3.21

SW097990,8.71,11.43,10.07,1.34,24.97,25.48,25.23,3.36,14.75,14.87,14.81,1.97

SW082262,41.51,46.90,44.21,5.89,22.11,28.33,25.22,3.36,4.91,8.84,6.88,0.92

SW123746,11.66,27.52,19.59,2.61,25.75,24.69,25.22,3.36,17.13,13.66,15.40,2.05

SW141035,29.37,24.80,27.09,3.61,23.45,26.90,25.18,3.35,10.43,14.99,12.71,1.69

SW000744,18.93,8.15,13.54,1.80,25.23,25.12,25.17,3.35,19.56,21.87,20.71,2.76

SW134470,16.27,15.56,15.91,2.12,22.85,27.48,25.16,3.35,22.18,19.79,20.98,2.80

SW105000,7.97,0.03,4.00,0.53,23.96,26.27,25.12,3.35,17.48,16.62,17.05,2.27

SW192408,18.39,16.58,17.48,2.33,23.83,26.37,25.10,3.34,19.65,7.34,13.49,1.80

SW143436,11.82,9.31,10.56,1.41,25.07,24.98,25.02,3.33,21.95,20.56,21.26,2.83

SW196154,10.66,16.72,13.69,1.82,24.83,25.22,25.02,3.33,16.23,17.16,16.69,2.22

SW203559,6.24,3.43,4.83,0.64,26.18,23.82,25.00,3.33,20.75,15.11,17.93,2.39

SW000469,20.76,8.91,14.84,1.98,21.88,28.05,24.96,3.33,18.57,20.86,19.71,2.63

SW037788,10.92,9.37,10.14,1.35,23.96,25.91,24.94,3.32,17.45,22.78,20.11,2.68

SW070706,28.91,35.11,32.01,4.26,25.16,24.65,24.90,3.32,10.64,6.26,8.45,1.13

SW192406,34.48,31.60,33.04,4.40,23.27,26.43,24.85,3.31,17.07,1.79,9.43,1.26

SW184448,9.36,11.07,10.21,1.36,25.28,24.41,24.84,3.31,22.98,8.51,15.75,2.10

SW015797,17.02,36.14,26.58,3.54,26.26,23.25,24.76,3.30,23.14,22.25,22.69,3.02

SW105241,9.16,12.41,10.78,1.44,23.87,25.63,24.75,3.30,17.99,18.22,18.10,2.41

SW000711,20.03,7.93,13.98,1.86,22.14,27.35,24.75,3.30,19.31,19.96,19.63,2.62

SW139324,10.71,11.10,10.91,1.45,25.96,23.43,24.70,3.29,24.88,20.65,22.76,3.03

SW171921,21.94,25.56,23.75,3.16,24.57,24.71,24.64,3.28,26.87,11.54,19.21,2.56

SW044846,13.92,22.33,18.13,2.41,23.52,25.67,24.59,3.28,20.51,-6.37,7.07,0.94

SW191106,5.07,6.21,5.64,0.75,24.00,25.17,24.59,3.28,16.41,8.17,12.29,1.64

SW167584,5.37,10.22,7.79,1.04,24.24,24.92,24.58,3.28,26.51,10.36,18.44,2.46

SW023297,51.48,73.51,62.49,8.33,25.72,23.44,24.58,3.27,10.36,9.75,10.06,1.34

SW036356,37.04,28.71,32.88,4.38,20.86,28.25,24.55,3.27,4.86,8.80,6.83,0.91

SW137782,18.32,16.65,17.49,2.33,26.20,22.88,24.54,3.27,19.42,20.47,19.94,2.66

SW105917,8.09,12.00,10.05,1.34,24.78,24.27,24.52,3.27,17.67,16.73,17.20,2.29

SW105311,25.56,32.22,28.89,3.85,23.03,25.93,24.48,3.26,13.27,-9.02,2.12,0.28

SW043133,34.27,59.21,46.74,6.23,24.95,23.99,24.47,3.26,3.13,7.03,5.08,0.68

SW084702,32.00,33.91,32.96,4.39,22.70,26.23,24.46,3.26,16.27,10.62,13.44,1.79

SW171794,26.74,27.65,27.20,3.62,22.71,26.19,24.45,3.26,21.79,4.35,13.07,1.74

SW148065,37.16,61.99,49.57,6.60,23.78,24.94,24.36,3.25,13.19,13.09,13.14,1.75

SW000732,19.83,9.62,14.72,1.96,21.49,27.17,24.33,3.24,20.29,20.97,20.63,2.75

SW148676,19.04,37.64,28.34,3.78,23.75,24.87,24.31,3.24,21.39,17.87,19.63,2.62

SW032190,18.09,13.10,15.60,2.08,22.61,25.97,24.29,3.24,4.03,10.72,7.37,0.98

SW164644,9.60,-5.98,1.81,0.24,23.47,25.09,24.28,3.23,16.35,12.88,14.62,1.95

SW155163,21.53,39.33,30.43,4.05,24.83,23.68,24.26,3.23,15.70,12.83,14.27,1.90

SW046161,7.78,10.43,9.10,1.21,24.47,24.03,24.25,3.23,15.52,21.48,18.50,2.46

SW164154,34.33,24.74,29.54,3.94,25.00,23.44,24.22,3.23,22.03,16.18,19.11,2.55

SW034482,35.53,44.20,39.87,5.31,22.63,25.79,24.21,3.23,-0.53,5.41,2.44,0.32

SW160112,19.23,29.32,24.28,3.23,24.30,24.00,24.15,3.22,13.10,8.11,10.60,1.41

SW084139,17.31,11.57,14.44,1.92,24.27,24.01,24.14,3.22,14.67,8.57,11.62,1.55

SW129522,10.20,25.58,17.89,2.38,24.13,24.13,24.13,3.21,20.09,19.30,19.69,2.62

SW143461,18.64,26.59,22.61,3.01,21.31,26.92,24.12,3.21,-3.90,2.13,-0.88,-0.12

SW023275,38.04,36.39,37.21,4.96,20.23,27.96,24.10,3.21,19.70,16.11,17.90,2.39

SW123604,9.18,21.05,15.12,2.01,23.39,24.76,24.07,3.21,16.57,12.02,14.29,1.90

SW079368,34.65,28.89,31.77,4.23,21.78,26.34,24.06,3.21,16.60,11.55,14.07,1.87

SW148209,33.28,42.83,38.06,5.07,21.96,26.15,24.06,3.20,15.44,12.91,14.18,1.89

SW073590,34.22,29.55,31.88,4.25,21.76,26.21,23.98,3.20,14.11,10.05,12.08,1.61

SW132122,22.89,29.27,26.08,3.47,27.53,20.41,23.97,3.19,10.05,4.56,7.31,0.97

SW107859,6.65,10.80,8.72,1.16,23.13,24.72,23.92,3.19,25.30,16.35,20.82,2.77

SW126071,22.69,36.12,29.40,3.92,24.40,23.44,23.92,3.19,14.81,15.75,15.28,2.04

SW103214,18.47,21.67,20.07,2.67,23.70,24.11,23.91,3.18,7.49,13.91,10.70,1.43

SW107726,18.53,8.22,13.37,1.78,22.70,25.03,23.87,3.18,18.99,19.13,19.06,2.54

SW199391,24.64,12.44,18.54,2.47,22.13,25.56,23.85,3.18,19.41,7.09,13.25,1.77

SW169923,44.13,58.70,51.42,6.85,22.44,25.25,23.84,3.18,20.88,18.41,19.64,2.62

SW110820,30.99,30.07,30.53,4.07,24.03,23.51,23.77,3.17,4.81,6.93,5.87,0.78

SW000491,22.83,10.28,16.55,2.21,23.75,23.78,23.76,3.17,24.08,23.49,23.79,3.17

SW061067,12.44,14.45,13.44,1.79,20.99,26.53,23.76,3.17,10.65,-11.81,-0.58,-0.08

SW168093,53.66,28.58,41.12,5.48,26.19,21.29,23.74,3.16,19.10,16.20,17.65,2.35

SW162624,27.64,30.35,28.99,3.86,24.33,23.15,23.74,3.16,12.12,7.71,9.92,1.32

SW147117,5.16,10.54,7.85,1.05,23.22,24.22,23.72,3.16,15.76,21.58,18.67,2.49

SW145531,10.28,20.50,15.39,2.05,22.12,25.27,23.70,3.16,25.49,21.97,23.73,3.16

SW164118,33.03,25.63,29.33,3.91,22.81,24.48,23.65,3.15,16.71,11.80,14.26,1.90

SW034475,30.71,26.76,28.73,3.83,22.79,24.50,23.64,3.15,5.47,5.97,5.72,0.76

SW104164,29.77,26.91,28.34,3.78,24.99,22.19,23.59,3.14,-6.42,-10.07,-8.24,-1.10

SW103603,4.72,9.31,7.01,0.93,22.05,25.08,23.56,3.14,18.12,14.66,16.39,2.18

SW106546,9.75,23.85,16.80,2.24,24.02,23.10,23.56,3.14,4.38,-12.82,-4.22,-0.56

SW114044,53.19,67.78,60.48,8.06,28.20,18.90,23.55,3.14,1.73,-18.53,-8.40,-1.12

SW042004,22.55,19.73,21.14,2.82,21.61,25.47,23.54,3.14,18.68,11.34,15.01,2.00

SW155690,-16.36,-8.19,-12.28,-1.64,28.77,18.30,23.53,3.14,21.73,20.83,21.28,2.84

SW157111,17.81,33.55,25.68,3.42,23.59,23.31,23.45,3.12,15.12,12.10,13.61,1.81

SW010768,34.98,30.68,32.83,4.37,18.97,27.90,23.43,3.12,18.80,20.49,19.65,2.62

SW085353,10.68,24.99,17.84,2.38,22.15,24.66,23.41,3.12,7.66,6.58,7.12,0.95

SW139711,8.32,12.56,10.44,1.39,22.15,24.65,23.40,3.12,2.06,3.81,2.93,0.39

SW125572,5.56,15.91,10.73,1.43,23.25,23.55,23.40,3.12,8.00,11.18,9.59,1.28

SW192431,2.88,2.74,2.81,0.37,22.58,24.14,23.36,3.11,16.15,4.54,10.35,1.38

SW148208,16.31,31.01,23.66,3.15,22.83,23.83,23.33,3.11,18.63,14.55,16.59,2.21

SW112151,28.23,29.96,29.10,3.88,26.37,20.27,23.32,3.11,10.47,11.93,11.20,1.49

SW043053,25.17,36.71,30.94,4.12,22.30,24.18,23.24,3.10,17.97,19.63,18.80,2.50

SW000785,19.27,8.95,14.11,1.88,20.88,25.58,23.23,3.09,15.14,18.15,16.64,2.22

SW059806,21.88,40.94,31.41,4.18,21.21,25.25,23.23,3.09,10.14,14.01,12.08,1.61

SW161496,7.29,8.27,7.78,1.04,23.76,22.64,23.20,3.09,18.85,12.55,15.70,2.09

SW059346,29.21,29.13,29.17,3.89,20.32,25.92,23.12,3.08,15.16,15.38,15.27,2.03

SW128876,26.28,22.77,24.53,3.27,25.53,20.71,23.12,3.08,-1.94,2.22,0.14,0.02

SW125808,23.11,36.70,29.91,3.98,23.70,22.51,23.11,3.08,-7.88,-10.48,-9.18,-1.22

SW106407,4.77,11.29,8.03,1.07,22.11,23.96,23.03,3.07,15.56,17.43,16.50,2.20

SW084482,20.80,24.80,22.80,3.04,20.85,25.22,23.03,3.07,4.98,13.94,9.46,1.26

SW106299,10.96,9.08,10.02,1.34,24.22,21.74,22.98,3.06,14.46,13.24,13.85,1.85

SW000742,11.96,6.31,9.14,1.22,18.99,26.90,22.94,3.06,20.98,18.54,19.76,2.63

SW000688,24.24,39.42,31.83,4.24,19.32,26.56,22.94,3.06,24.11,16.41,20.26,2.70

SW040618,17.64,19.52,18.58,2.48,22.20,23.68,22.94,3.06,23.23,19.26,21.25,2.83

SW136987,18.46,16.25,17.35,2.31,23.57,22.30,22.93,3.06,18.23,19.74,18.98,2.53

SW085348,17.96,9.81,13.88,1.85,23.35,22.46,22.90,3.05,14.72,10.57,12.64,1.68

SW053402,11.85,14.90,13.38,1.78,23.97,21.73,22.85,3.04,14.14,13.03,13.58,1.81

SW122932,15.44,29.27,22.36,2.98,23.38,22.23,22.80,3.04,-0.97,0.11,-0.43,-0.06

SW051934,37.27,60.24,48.76,6.50,23.61,21.94,22.78,3.03,12.79,20.46,16.62,2.21

SW193264,6.90,11.50,9.20,1.23,22.99,22.44,22.72,3.03,18.83,2.96,10.89,1.45

SW100664,35.88,42.05,38.96,5.19,29.14,16.28,22.71,3.03,8.34,8.82,8.58,1.14

SW167795,16.86,26.59,21.72,2.89,22.08,23.31,22.70,3.02,-0.84,8.79,3.97,0.53

SW128312,9.38,18.28,13.83,1.84,22.97,22.36,22.66,3.02,7.57,6.57,7.07,0.94

SW001554,17.31,10.96,14.13,1.88,19.88,25.27,22.58,3.01,20.43,13.53,16.98,2.26

SW047326,26.39,39.74,33.06,4.41,23.92,21.23,22.58,3.01,14.42,11.26,12.84,1.71

SW105759,9.24,6.49,7.87,1.05,25.38,19.75,22.57,3.01,14.85,15.09,14.97,1.99

SW199253,51.43,37.58,44.51,5.93,17.76,27.24,22.50,3.00,10.43,3.73,7.08,0.94

SW147085,14.87,0.78,7.82,1.04,23.65,21.30,22.47,2.99,18.63,21.49,20.06,2.67

SW159806,13.54,24.75,19.14,2.55,23.44,21.50,22.47,2.99,23.75,13.54,18.65,2.48

SW147541,0.61,0.82,0.71,0.10,22.74,22.20,22.47,2.99,22.96,16.75,19.85,2.65

SW171047,2.56,2.35,2.46,0.33,22.63,22.22,22.43,2.99,17.15,6.27,11.71,1.56

SW040840,30.02,35.62,32.82,4.37,16.46,28.39,22.42,2.99,18.60,-8.32,5.14,0.69

SW082319,14.09,23.23,18.66,2.49,17.06,27.78,22.42,2.99,21.22,14.66,17.94,2.39

SW016450,-1.29,7.37,3.04,0.41,23.06,21.75,22.41,2.99,20.19,17.23,18.71,2.49

SW163368,22.63,22.94,22.79,3.04,21.32,23.47,22.40,2.98,15.62,13.14,14.38,1.92

SW164913,17.05,22.76,19.90,2.65,23.33,21.43,22.38,2.98,21.42,17.03,19.22,2.56

SW161243,41.49,42.32,41.91,5.58,22.96,21.76,22.36,2.98,14.30,7.20,10.75,1.43

SW128844,25.85,38.52,32.19,4.29,22.91,21.77,22.34,2.98,8.25,6.84,7.54,1.01

SW097574,26.53,24.25,25.39,3.38,24.33,20.31,22.32,2.97,6.87,-18.36,-5.74,-0.77

SW128770,11.56,15.64,13.60,1.81,22.26,22.34,22.30,2.97,-7.68,-11.08,-9.38,-1.25

SW192418,3.50,14.42,8.96,1.19,20.99,23.60,22.30,2.97,14.35,1.01,7.68,1.02

SW195816,1.19,11.88,6.53,0.87,22.08,22.49,22.29,2.97,19.18,15.37,17.28,2.30

SW036326,15.01,11.23,13.12,1.75,19.67,24.85,22.26,2.97,22.07,19.72,20.89,2.78

SW153975,33.03,38.23,35.63,4.75,26.47,18.05,22.26,2.97,0.61,12.45,6.53,0.87

SW134566,23.03,22.50,22.76,3.03,21.02,23.47,22.25,2.96,-4.35,-0.64,-2.50,-0.33

SW085354,21.96,7.24,14.60,1.95,19.61,24.88,22.25,2.96,11.19,15.92,13.56,1.81

SW172212,30.27,32.51,31.39,4.18,22.35,22.12,22.24,2.96,22.93,15.93,19.43,2.59

SW105677,15.08,15.67,15.37,2.05,23.25,21.20,22.22,2.96,21.08,16.03,18.55,2.47

SW000741,16.90,7.09,12.00,1.60,19.70,24.69,22.20,2.96,18.25,17.44,17.85,2.38

SW195955,29.16,45.58,37.37,4.98,21.89,22.50,22.19,2.96,17.01,16.10,16.55,2.21

SW161263,19.01,25.74,22.37,2.98,21.61,22.73,22.17,2.95,8.89,5.16,7.02,0.94

SW145992,18.36,21.40,19.88,2.65,21.98,22.35,22.17,2.95,22.79,16.09,19.44,2.59

SW166792,21.66,16.92,19.29,2.57,22.21,22.06,22.13,2.95,6.57,12.10,9.33,1.24

SW132697,7.67,-3.09,11.22,1.49,17.28,19.67,22.13,2.95,11.13,14.00,15.77,2.10

SW196270,1.99,19.12,10.55,1.41,23.23,21.00,22.12,2.95,22.34,19.06,20.70,2.76

SW118599,1.96,14.49,8.22,1.10,22.18,22.04,22.11,2.95,16.90,13.31,15.10,2.01

SW125170,23.10,39.81,31.45,4.19,24.79,19.42,22.10,2.94,14.19,14.57,14.38,1.92

SW000468,21.96,11.00,16.48,2.20,17.84,26.32,22.08,2.94,14.60,19.11,16.86,2.25

SW163408,46.87,50.73,48.80,6.50,17.89,26.27,22.08,2.94,6.65,-15.84,-4.59,-0.61

SW072008,3.01,10.19,6.60,0.88,22.41,21.67,22.04,2.94,17.02,18.96,17.99,2.40

SW004556,42.25,36.51,39.38,5.25,19.58,24.47,22.02,2.93,-9.50,0.60,-4.45,-0.59

SW147542,6.96,12.10,9.53,1.27,22.27,21.77,22.02,2.93,31.27,18.62,24.94,3.32

SW157903,20.89,35.72,28.30,3.77,22.55,21.45,22.00,2.93,1.22,2.31,1.76,0.23

SW063797,-20.35,-42.56,-31.45,-4.19,21.79,22.13,21.96,2.93,22.21,19.52,20.87,2.78

SW163262,5.60,6.56,6.08,0.81,23.74,20.15,21.94,2.92,15.02,11.70,13.36,1.78

SW146989,8.66,-18.21,-4.77,-0.64,22.85,20.92,21.89,2.92,27.12,18.41,22.77,3.03

SW014937,5.54,8.31,6.93,0.92,21.20,22.57,21.88,2.92,10.92,18.32,14.62,1.95

SW128246,24.63,32.97,28.80,3.84,24.20,19.55,21.88,2.91,7.41,6.77,7.09,0.94

SW054773,2.48,8.30,5.39,0.72,23.93,19.79,21.86,2.91,14.92,14.26,14.59,1.94

SW167683,5.63,12.71,9.17,1.22,20.90,22.81,21.85,2.91,18.77,10.04,14.41,1.92

SW006647,25.17,39.72,32.44,4.32,20.71,22.95,21.83,2.91,12.68,21.34,17.01,2.27

SW086524,32.34,22.02,27.18,3.62,20.60,23.02,21.81,2.91,9.63,9.20,9.42,1.25

SW033596,36.74,33.37,35.05,4.67,21.33,22.15,21.74,2.90,0.44,5.80,3.12,0.42

SW147613,15.50,10.60,13.05,1.74,22.73,20.70,21.72,2.89,22.60,19.01,20.81,2.77

SW147277,2.15,10.44,6.30,0.84,21.97,21.38,21.68,2.89,21.47,19.05,20.26,2.70

SW152191,7.45,21.62,14.54,1.94,21.55,21.79,21.67,2.89,19.23,15.51,17.37,2.31

SW192215,2.91,4.00,3.45,0.46,20.08,23.21,21.64,2.88,14.49,2.59,8.54,1.14

SW193356,12.84,15.16,14.00,1.86,22.62,20.66,21.64,2.88,20.29,14.17,17.23,2.30

SW166414,16.26,22.35,19.31,2.57,17.50,25.75,21.63,2.88,15.50,-14.89,-14.89,-1.98

SW017286,14.60,8.14,11.37,1.51,18.71,24.50,21.60,2.88,20.51,18.62,19.57,2.61

SW084290,28.93,36.92,32.92,4.39,19.64,23.55,21.59,2.88,3.63,9.96,6.80,0.91

SW197018,16.98,11.36,14.17,1.89,20.47,22.63,21.55,2.87,12.88,4.80,8.84,1.18

SW044556,7.15,19.61,13.38,1.78,22.32,20.77,21.54,2.87,13.02,13.24,13.13,1.75

SW110621,10.34,16.75,13.54,1.80,21.66,21.37,21.51,2.87,26.02,15.58,20.80,2.77

SW163385,33.66,32.58,33.12,4.41,23.46,19.53,21.50,2.86,15.87,12.23,14.05,1.87

SW187196,14.26,13.11,13.69,1.82,20.93,22.06,21.49,2.86,4.82,6.12,5.47,0.73

SW167520,41.15,55.72,48.44,6.45,19.80,23.09,21.44,2.86,17.96,13.58,15.77,2.10

SW080220,19.97,32.46,26.22,3.49,23.32,19.55,21.44,2.86,25.87,16.71,21.29,2.84

SW147622,8.87,4.89,6.88,0.92,21.53,21.32,21.42,2.85,21.99,17.18,19.58,2.61

SW158707,12.77,26.90,19.84,2.64,21.87,20.92,21.40,2.85,10.88,9.77,10.32,1.38

SW054612,2.97,5.72,4.35,0.58,20.31,22.47,21.39,2.85,21.36,12.37,16.87,2.25

SW013385,57.30,67.22,62.26,8.30,14.59,28.06,21.32,2.84,8.97,7.26,8.12,1.08

SW188788,5.28,0.49,2.88,0.38,20.98,21.60,21.29,2.84,11.83,3.49,7.66,1.02

SW150132,17.34,35.82,26.58,3.54,20.74,21.75,21.24,2.83,9.81,11.94,10.88,1.45

SW105484,9.00,1.84,5.42,0.72,19.80,22.65,21.22,2.83,11.40,15.77,13.59,1.81

SW171458,26.73,27.94,27.33,3.64,24.10,18.33,21.21,2.83,17.17,-1.50,7.83,1.04

SW165555,42.70,34.83,38.76,5.16,22.30,20.07,21.18,2.82,7.52,8.02,7.77,1.04

SW055568,10.06,20.19,15.13,2.02,21.06,21.30,21.18,2.82,23.05,17.10,20.08,2.67

SW140417,14.82,24.82,19.82,2.64,21.43,20.86,21.15,2.82,20.40,13.09,16.75,2.23

SW041849,20.12,26.83,23.48,3.13,19.59,22.70,21.15,2.82,20.40,15.74,18.07,2.41

SW116931,16.47,24.25,20.36,2.71,23.06,19.20,21.13,2.81,22.38,15.24,18.81,2.51

SW153989,8.68,12.14,10.41,1.39,21.93,20.31,21.12,2.81,14.61,18.27,16.44,2.19

SW049729,17.17,24.86,21.02,2.80,20.72,21.49,21.11,2.81,23.96,17.12,20.54,2.74

SW123886,9.07,24.37,16.72,2.23,20.37,21.83,21.10,2.81,3.04,6.20,4.62,0.62

SW192442,15.83,23.05,19.44,2.59,22.48,19.71,21.09,2.81,15.54,14.89,15.22,2.03

SW017273,16.57,7.96,12.27,1.63,18.52,23.64,21.08,2.81,20.84,17.79,19.32,2.57

SW153655,23.10,36.17,29.63,3.95,17.71,24.44,21.07,2.81,-13.47,-10.77,-12.12,-1.61

SW125141,17.25,22.61,19.93,2.66,19.76,22.32,21.04,2.80,8.61,15.03,11.82,1.57

SW120648,3.78,15.28,9.53,1.27,22.60,19.47,21.03,2.80,13.12,13.26,13.19,1.76

SW098043,3.23,7.64,5.43,0.72,19.82,22.25,21.03,2.80,10.39,16.82,13.61,1.81

SW163968,3.83,13.54,8.68,1.16,20.32,21.68,21.00,2.80,16.96,17.07,17.02,2.27

SW039344,12.03,16.68,14.35,1.91,20.49,21.49,20.99,2.80,7.21,14.26,10.74,1.43

SW152613,19.44,29.89,24.67,3.29,21.05,20.84,20.95,2.79,15.85,16.15,16.00,2.13

SW025285,27.45,26.74,27.09,3.61,19.79,22.01,20.90,2.78,10.48,7.02,8.75,1.17

SW152369,6.85,23.47,15.16,2.02,21.15,20.56,20.85,2.78,15.82,15.63,15.73,2.10

SW124355,11.97,28.23,20.10,2.68,20.78,20.91,20.84,2.78,6.35,10.36,8.35,1.11

SW005270,17.61,14.71,16.16,2.15,19.17,22.51,20.84,2.78,15.34,5.76,10.55,1.41

SW126883,30.58,32.96,31.77,4.23,21.89,19.72,20.81,2.77,-3.06,2.85,-0.11,-0.01

SW071269,10.93,19.37,15.15,2.02,24.12,17.45,20.79,2.77,22.40,21.11,21.76,2.90

SW028082,25.70,28.63,27.17,3.62,16.90,24.65,20.78,2.77,14.31,10.07,12.19,1.62

SW005351,13.26,12.88,13.07,1.74,18.03,23.42,20.72,2.76,11.94,6.76,9.35,1.25

SW119552,12.56,30.73,21.65,2.88,20.50,20.95,20.72,2.76,13.34,15.69,14.52,1.93

SW200729,56.19,61.96,59.08,7.87,18.91,22.46,20.68,2.76,16.99,10.31,13.65,1.82

SW145359,17.33,17.93,17.63,2.35,19.22,21.98,20.60,2.74,12.37,14.82,13.60,1.81

SW163897,26.32,28.13,27.23,3.63,16.68,24.48,20.58,2.74,-0.60,-20.45,-10.52,-1.40

SW049964,23.94,37.56,30.75,4.10,18.73,22.42,20.58,2.74,-8.17,-12.53,-10.35,-1.38

SW119848,12.60,25.98,19.29,2.57,21.57,19.58,20.58,2.74,3.25,6.46,4.85,0.65

SW147077,14.07,6.90,10.48,1.40,22.21,18.93,20.57,2.74,22.83,17.71,20.27,2.70

SW183603,14.51,23.12,18.82,2.51,21.69,19.38,20.53,2.74,18.15,17.07,17.61,2.35

SW150750,34.95,44.97,39.96,5.32,21.64,19.42,20.53,2.73,15.04,13.15,14.09,1.88

SW049694,19.42,29.42,24.42,3.25,17.24,23.81,20.53,2.73,21.83,15.66,18.75,2.50

SW084805,14.80,10.69,12.75,1.70,14.90,26.15,20.53,2.73,16.06,21.97,19.01,2.53

SW202384,36.94,33.34,35.14,4.68,20.01,21.00,20.50,2.73,-4.11,-1.13,-2.62,-0.35

SW062650,11.46,9.81,10.63,1.42,24.24,16.63,20.44,2.72,21.01,17.05,19.03,2.54

SW184819,19.06,26.68,22.87,3.05,20.87,19.95,20.41,2.72,15.12,13.55,14.33,1.91

SW118091,10.25,21.45,15.85,2.11,23.12,17.70,20.41,2.72,19.27,15.72,17.49,2.33

SW147750,3.66,7.00,5.33,0.71,20.02,20.78,20.40,2.72,10.39,13.65,12.02,1.60

SW085250,31.05,31.76,31.41,4.18,19.41,21.38,20.39,2.72,12.96,8.10,10.53,1.40

SW105126,14.14,5.73,9.94,1.32,22.73,18.02,20.38,2.71,-4.71,-4.19,-4.45,-0.59

SW170596,41.86,38.47,40.16,5.35,16.46,24.24,20.35,2.71,6.77,5.86,6.31,0.84

SW149664,12.70,22.94,17.82,2.37,20.33,20.35,20.34,2.71,11.01,18.94,14.97,2.00

SW000478,13.68,1.46,7.57,1.01,18.40,22.24,20.32,2.71,9.57,14.20,11.88,1.58

SW091358,12.82,2.61,7.72,1.03,15.99,24.58,20.29,2.70,5.66,5.73,5.69,0.76

SW128963,19.14,26.58,22.86,3.05,24.60,15.95,20.28,2.70,6.91,4.88,5.89,0.79

SW131470,11.45,9.71,10.58,1.41,20.69,19.82,20.25,2.70,20.00,17.48,18.74,2.50

SW083323,-0.29,11.16,5.44,0.72,18.51,21.95,20.23,2.70,-0.23,-4.29,-2.26,-0.30

SW159699,12.97,24.15,18.56,2.47,19.08,21.38,20.23,2.69,9.91,4.12,7.02,0.93

SW036725,13.13,8.07,10.60,1.41,17.18,23.26,20.22,2.69,19.31,16.44,17.88,2.38

SW027476,25.52,40.27,32.90,4.38,18.77,21.63,20.20,2.69,9.26,16.31,12.78,1.70

SW085283,36.87,42.16,39.51,5.26,20.80,19.32,20.06,2.67,13.47,8.51,10.99,1.46

SW084389,7.59,26.90,17.24,2.30,20.02,20.00,20.01,2.67,13.08,12.38,12.73,1.70

SW147157,2.48,2.77,2.63,0.35,20.14,19.75,19.95,2.66,20.73,15.09,17.91,2.39

SW036352,21.90,30.96,26.43,3.52,19.28,20.62,19.95,2.66,20.28,13.28,16.78,2.24

SW000710,14.27,3.88,9.08,1.21,16.69,23.19,19.94,2.66,16.58,18.61,17.60,2.34

SW036121,12.03,9.58,10.80,1.44,18.62,21.18,19.90,2.65,25.09,15.14,20.11,2.68

SW105663,7.18,22.46,14.82,1.97,21.78,18.00,19.89,2.65,9.04,8.32,8.68,1.16

SW018829,13.90,7.11,10.51,1.40,18.70,21.06,19.88,2.65,6.41,9.29,7.85,1.05

SW000729,18.25,8.72,13.48,1.80,16.59,23.16,19.87,2.65,12.11,14.55,13.33,1.78

SW108685,16.61,24.77,20.69,2.76,21.58,18.16,19.87,2.65,18.71,12.21,15.46,2.06

SW084292,20.97,18.51,19.74,2.63,20.31,19.35,19.83,2.64,8.34,2.60,5.47,0.73

SW052555,12.58,12.34,12.46,1.66,18.51,21.14,19.83,2.64,8.70,11.37,10.03,1.34

SW013419,39.57,30.53,35.05,4.67,16.03,23.60,19.81,2.64,16.27,17.16,16.72,2.23

SW089494,2.22,12.20,7.21,0.96,21.17,18.45,19.81,2.64,22.00,15.29,18.64,2.48

SW025192,11.84,8.97,10.40,1.39,19.15,20.43,19.79,2.64,16.67,7.16,11.92,1.59

SW152786,15.88,23.71,19.79,2.64,19.71,19.86,19.79,2.64,9.94,16.33,13.14,1.75

SW066767,23.78,27.43,25.60,3.41,17.59,21.98,19.78,2.64,1.09,1.42,1.25,0.17

SW114624,-0.26,9.06,4.40,0.59,19.13,20.36,19.75,2.63,12.65,11.32,11.99,1.60

SW018086,12.09,19.34,15.72,2.09,20.94,18.54,19.74,2.63,18.70,17.00,17.85,2.38

SW165189,18.59,18.73,18.66,2.49,18.89,20.55,19.72,2.63,17.48,9.04,13.26,1.77

SW173054,24.56,24.43,24.49,3.26,18.22,21.22,19.72,2.63,3.41,5.92,4.66,0.62

SW120871,5.31,16.97,11.14,1.48,22.03,17.36,19.70,2.62,11.65,13.04,12.35,1.64

SW108309,1.80,9.58,5.69,0.76,19.32,20.07,19.69,2.62,16.55,10.70,13.63,1.82

SW051246,38.13,26.88,32.50,4.33,14.28,25.09,19.69,2.62,14.43,17.26,15.85,2.11

SW036102,12.47,11.15,11.81,1.57,17.47,21.86,19.67,2.62,19.99,14.12,17.05,2.27

SW163393,11.77,8.49,10.13,1.35,20.92,18.39,19.65,2.62,11.72,9.76,10.74,1.43

SW159908,24.68,30.99,27.84,3.71,19.98,19.28,19.63,2.62,12.37,2.94,7.65,1.02

SW161456,17.24,20.55,18.90,2.52,18.43,20.82,19.63,2.62,-5.28,-11.01,-8.14,-1.08

SW050290,3.51,10.34,6.93,0.92,19.54,19.61,19.57,2.61,10.65,14.26,12.45,1.66

SW195762,-24.32,-11.88,-18.10,-2.41,20.38,18.70,19.54,2.60,16.48,15.65,16.06,2.14

SW160023,15.49,20.11,17.80,2.37,20.10,18.98,19.54,2.60,14.60,7.54,11.07,1.47

SW167535,45.73,46.70,46.22,6.16,16.79,22.21,19.50,2.60,18.86,3.49,11.18,1.49

SW172784,37.15,39.22,38.19,5.09,18.73,20.24,19.49,2.60,15.46,13.47,14.47,1.93

SW150428,22.30,41.96,32.13,4.28,19.51,19.47,19.49,2.60,17.19,13.50,15.35,2.04

SW147781,12.88,2.79,7.84,1.04,19.96,19.01,19.49,2.60,17.58,19.10,18.34,2.44

SW147141,6.86,5.98,6.42,0.86,15.51,23.43,19.47,2.59,17.73,19.55,18.64,2.48

SW184701,6.90,7.75,7.33,0.98,20.07,18.87,19.47,2.59,14.86,10.84,12.85,1.71

SW181726,9.82,6.60,8.21,1.09,19.82,19.03,19.43,2.59,5.14,7.67,6.41,0.85

SW159904,20.49,31.31,25.90,3.45,19.89,18.95,19.42,2.59,13.13,5.08,9.10,1.21

SW000507,16.76,7.93,12.35,1.64,16.66,22.16,19.41,2.59,11.44,16.56,14.00,1.87

SW105689,30.49,33.76,32.12,4.28,27.84,10.98,19.41,2.59,7.67,2.49,5.08,0.68

SW188942,21.80,10.33,16.06,2.14,20.12,18.65,19.38,2.58,17.26,12.49,14.87,1.98

SW131246,28.37,32.38,30.37,4.05,21.54,17.20,19.37,2.58,21.14,9.55,15.34,2.04

SW057898,16.75,9.41,13.08,1.74,15.40,23.28,19.34,2.58,12.72,14.51,13.61,1.81

SW000032,62.32,67.31,64.81,8.64,18.99,19.66,19.33,2.57,5.37,10.35,7.86,1.05

SW034681,16.09,21.70,18.89,2.52,18.79,19.84,19.31,2.57,-5.27,4.81,-0.23,-0.03

SW010899,42.82,36.74,39.78,5.30,15.19,23.43,19.31,2.57,10.72,15.33,13.02,1.73

SW154007,35.83,48.09,41.96,5.59,18.63,19.99,19.31,2.57,12.93,13.29,13.11,1.75

SW149663,15.46,28.10,21.78,2.90,19.36,19.26,19.31,2.57,11.02,19.08,15.05,2.00

SW019566,14.28,8.74,11.51,1.53,16.60,22.00,19.30,2.57,16.14,17.96,17.05,2.27

SW152924,11.36,15.74,13.55,1.81,18.54,20.03,19.29,2.57,2.67,11.45,7.06,0.94

SW036152,13.20,13.18,13.19,1.76,17.27,21.30,19.28,2.57,10.30,9.59,9.95,1.33

SW083316,14.36,11.01,12.68,1.69,17.62,20.95,19.28,2.57,13.63,8.05,10.84,1.44

SW117270,12.88,16.42,14.65,1.95,19.62,18.94,19.28,2.57,-1.50,4.46,1.48,0.20

SW125186,16.05,22.34,19.19,2.56,21.48,17.08,19.28,2.57,14.54,6.91,10.73,1.43

SW000510,15.98,7.52,11.75,1.57,16.35,22.05,19.20,2.56,15.00,17.51,16.25,2.17

SW162703,6.99,8.36,7.67,1.02,18.93,19.40,19.17,2.55,7.80,6.22,7.01,0.93

SW000482,13.03,1.63,7.33,0.98,15.40,22.88,19.14,2.55,12.80,14.76,13.78,1.84

SW087409,31.38,30.81,31.10,4.14,17.02,21.25,19.13,2.55,16.19,8.74,12.47,1.66

SW124758,2.00,12.54,7.27,0.97,19.25,18.99,19.12,2.55,11.72,12.24,11.98,1.60

SW045681,10.97,18.23,14.60,1.95,20.81,17.43,19.12,2.55,17.19,11.16,14.17,1.89

SW154765,21.82,32.16,26.99,3.60,18.48,19.74,19.11,2.55,4.42,9.43,6.92,0.92

SW130302,14.66,19.71,17.19,2.29,22.75,15.38,19.07,2.54,5.12,2.85,3.98,0.53

SW163799,12.72,4.92,8.82,1.17,19.52,18.58,19.05,2.54,19.56,9.71,14.64,1.95

SW045347,49.56,54.86,52.21,6.96,16.01,22.08,19.05,2.54,21.62,8.74,15.18,2.02

SW148536,15.52,25.80,20.66,2.75,19.92,18.17,19.04,2.54,12.99,11.29,12.14,1.62

SW050113,11.28,32.27,21.78,2.90,18.05,20.03,19.04,2.54,8.00,8.94,8.47,1.13

SW031629,16.67,10.92,13.79,1.84,18.38,19.70,19.04,2.54,-5.29,7.01,0.86,0.11

SW154595,-1.32,11.28,4.98,0.66,20.17,17.90,19.04,2.54,13.66,15.37,14.51,1.93

SW163958,38.07,40.22,39.14,5.21,19.09,18.97,19.03,2.53,13.83,13.21,13.52,1.80

SW041377,22.65,23.91,23.28,3.10,15.38,22.61,19.00,2.53,12.28,16.44,14.36,1.91

SW107076,-0.57,10.04,4.74,0.63,19.08,18.90,18.99,2.53,13.25,9.67,11.46,1.53

SW049720,22.17,31.95,27.06,3.60,18.95,18.94,18.95,2.52,17.33,12.11,14.72,1.96

SW156743,9.73,20.53,15.13,2.02,18.73,19.09,18.91,2.52,14.68,11.12,12.90,1.72

SW105656,17.79,21.14,19.46,2.59,21.25,16.50,18.87,2.51,5.38,4.05,4.71,0.63

SW105652,24.81,30.84,27.83,3.71,20.26,17.47,18.87,2.51,3.46,6.99,5.23,0.70

SW147165,8.58,8.21,8.39,1.12,18.42,19.31,18.86,2.51,19.22,17.07,18.14,2.42

SW099736,30.17,22.65,26.41,3.52,17.49,20.04,18.76,2.50,0.30,9.73,5.01,0.67

SW090315,15.95,37.26,26.61,3.54,19.34,18.17,18.76,2.50,22.69,12.36,17.52,2.33

SW146950,-3.54,-12.52,-8.03,-1.07,18.99,18.51,18.75,2.50,11.76,16.39,14.07,1.88

SW113289,-2.02,6.90,2.44,0.32,18.92,18.51,18.72,2.49,12.05,19.73,15.89,2.12

SW168013,26.13,30.34,28.23,3.76,21.27,16.15,18.71,2.49,3.97,8.96,6.46,0.86

SW081943,17.16,27.45,22.30,2.97,18.40,18.94,18.67,2.49,8.43,5.38,6.91,0.92

SW011569,-2.99,5.72,1.36,0.18,17.49,19.83,18.66,2.49,18.76,17.14,17.95,2.39

SW059989,32.87,35.71,34.29,4.57,16.23,21.07,18.65,2.49,12.89,4.65,8.77,1.17

SW161215,12.98,18.44,15.71,2.09,20.36,16.94,18.65,2.48,14.54,6.59,10.57,1.41

SW128369,6.53,-1.49,2.52,0.34,20.87,16.39,18.63,2.48,6.95,7.53,7.24,0.96

SW084533,18.18,10.58,14.38,1.92,19.71,17.51,18.61,2.48,1.54,1.99,1.76,0.24

SW030036,12.20,22.91,17.55,2.34,19.35,17.72,18.54,2.47,14.48,14.90,14.69,1.96

SW165036,-7.18,-8.80,-7.99,-1.06,18.46,18.61,18.53,2.47,11.49,2.37,6.93,0.92

SW156107,17.98,26.69,22.33,2.98,18.89,18.14,18.51,2.47,6.14,13.30,9.72,1.29

SW053615,13.43,9.27,11.35,1.51,17.21,19.79,18.50,2.47,10.32,15.21,12.76,1.70

SW119588,14.02,14.76,14.39,1.92,19.26,17.65,18.46,2.46,-1.78,3.06,0.64,0.08

SW005112,15.76,28.88,22.32,2.97,24.07,12.69,18.38,2.45,23.24,18.54,20.89,2.78

SW056152,37.48,41.81,39.65,5.28,15.90,20.79,18.35,2.44,21.54,13.14,17.34,2.31

SW087405,36.97,34.90,35.93,4.79,16.04,20.65,18.34,2.44,0.18,5.08,2.63,0.35

SW153963,25.20,36.91,31.05,4.14,17.86,18.73,18.29,2.44,10.66,13.10,11.88,1.58

SW147557,6.92,2.01,4.47,0.60,18.41,18.11,18.26,2.43,13.47,10.43,11.95,1.59

SW013968,33.97,56.98,45.48,6.06,19.44,16.90,18.17,2.42,16.09,13.05,14.57,1.94

SW081633,6.68,9.22,7.95,1.06,22.81,13.50,18.15,2.42,9.87,5.85,7.86,1.05

SW164205,46.29,37.12,41.71,5.56,9.02,27.24,18.13,2.42,9.98,-10.97,-0.49,-0.07

SW155367,7.70,19.28,13.49,1.80,19.18,17.06,18.12,2.41,11.01,8.67,9.84,1.31

SW158936,10.24,15.93,13.08,1.74,19.23,16.96,18.10,2.41,10.41,10.93,10.67,1.42

SW067055,7.30,4.87,6.09,0.81,18.20,17.98,18.09,2.41,6.52,9.36,7.94,1.06

SW163228,36.55,47.93,42.24,5.63,14.57,21.48,18.02,2.40,-11.11,-11.61,-11.36,-1.51

SW052543,16.29,6.48,11.39,1.52,15.29,20.75,18.02,2.40,15.56,17.37,16.47,2.19

SW163376,28.04,23.11,25.58,3.41,23.80,12.18,17.99,2.40,2.81,8.46,5.64,0.75

SW119552,25.71,29.56,27.64,3.68,20.07,15.81,17.94,2.39,8.45,11.32,9.89,1.32

SW010913,47.07,40.55,43.81,5.84,17.21,18.65,17.93,2.39,5.96,6.84,6.40,0.85

SW000708,15.87,2.25,9.06,1.21,15.74,20.12,17.93,2.39,15.58,13.39,14.49,1.93

SW055764,11.77,18.23,15.00,2.00,19.70,16.14,17.92,2.39,15.34,15.99,15.67,2.09

SW192404,16.41,17.39,16.90,2.25,18.65,17.18,17.92,2.39,10.79,10.60,10.70,1.43

SW148675,6.24,10.41,8.33,1.11,18.46,17.36,17.91,2.39,14.96,14.35,14.65,1.95

SW058493,15.93,17.48,16.71,2.23,14.89,20.89,17.89,2.38,8.42,9.58,9.00,1.20

SW200084,-0.01,-0.39,-0.20,-0.03,15.04,20.60,17.82,2.37,11.78,-1.94,4.92,0.66

SW145607,13.72,17.40,15.56,2.07,17.38,18.20,17.79,2.37,11.34,11.13,11.24,1.50

SW195344,7.67,5.99,6.83,0.91,18.09,17.47,17.78,2.37,4.15,5.45,4.80,0.64

SW065109,16.26,35.77,26.02,3.47,16.86,18.64,17.75,2.37,-0.12,-8.87,-4.50,-0.60

SW018033,0.26,6.38,3.32,0.44,18.87,16.41,17.64,2.35,18.59,15.52,17.05,2.27

SW147149,-3.46,1.47,-0.99,-0.13,17.82,17.40,17.61,2.35,12.77,16.09,14.43,1.92

SW103317,24.28,25.13,24.71,3.29,18.36,16.83,17.60,2.34,-0.92,-0.29,-0.61,-0.08

SW157157,28.60,47.85,38.23,5.09,15.91,19.25,17.58,2.34,-8.33,-11.97,-10.15,-1.35

SW119719,4.29,4.59,4.44,0.59,19.17,15.96,17.56,2.34,10.04,6.73,8.38,1.12

SW060112,7.44,25.92,16.68,2.22,16.28,18.81,17.55,2.34,10.46,10.43,10.44,1.39

SW081236,25.49,32.55,29.02,3.87,16.47,18.58,17.53,2.34,16.23,11.47,13.85,1.84

SW073598,34.08,39.58,36.83,4.91,12.55,22.43,17.49,2.33,0.01,-0.27,-0.13,-0.02

SW006176,22.93,16.92,19.92,2.65,15.77,19.17,17.47,2.33,7.55,6.10,6.83,0.91

SW177785,9.85,0.27,5.06,0.67,18.79,16.06,17.42,2.32,8.82,9.13,8.97,1.20

SW000553,18.64,16.06,17.35,2.31,13.57,21.28,17.42,2.32,7.12,12.11,9.61,1.28

SW128223,6.67,0.11,3.39,0.45,19.43,15.39,17.41,2.32,6.48,5.94,6.21,0.83

SW022048,-11.78,-7.17,-9.48,-1.26,18.15,16.65,17.40,2.32,17.16,18.05,17.61,2.35

SW094478,27.09,31.98,29.53,3.93,16.26,18.53,17.40,2.32,8.21,0.19,4.20,0.56

SW064688,25.61,19.28,22.44,2.99,14.80,19.94,17.37,2.31,12.35,13.46,12.90,1.72

SW058681,11.52,13.99,12.75,1.70,18.66,16.06,17.36,2.31,16.53,11.41,13.97,1.86

SW105609,1.71,-16.65,-7.47,-1.00,15.52,19.18,17.35,2.31,4.71,9.50,7.11,0.95

SW069101,13.98,22.57,18.28,2.43,15.88,18.75,17.32,2.31,-3.10,-12.19,-7.64,-1.02

SW015149,7.04,23.42,15.23,2.03,17.43,17.02,17.23,2.30,9.15,11.09,10.12,1.35

SW045159,21.73,19.85,20.79,2.77,14.91,19.54,17.22,2.29,16.80,9.02,12.91,1.72

SW163473,50.77,39.35,45.06,6.00,21.10,13.31,17.20,2.29,18.61,16.56,17.58,2.34

SW080772,7.80,11.69,9.74,1.30,16.60,17.76,17.18,2.29,9.38,9.87,9.63,1.28

SW120757,5.70,2.62,4.16,0.55,16.94,17.41,17.17,2.29,10.97,7.11,9.04,1.20

SW170218,38.44,44.14,41.29,5.50,16.47,17.85,17.16,2.29,-0.53,4.98,2.22,0.30

SW163320,28.28,34.99,31.63,4.21,17.21,17.12,17.16,2.29,4.33,0.25,2.29,0.31

SW178474,8.39,14.15,11.27,1.50,16.57,17.68,17.12,2.28,0.64,4.61,2.62,0.35

SW103242,8.12,2.69,5.41,0.72,17.35,16.84,17.09,2.28,9.93,1.88,5.90,0.79

SW162184,54.27,64.94,59.61,7.94,17.50,16.68,17.09,2.28,9.60,8.28,8.94,1.19

SW071216,1.63,-18.24,-8.30,-1.11,17.30,16.84,17.07,2.27,13.03,14.25,13.64,1.82

SW124300,3.78,20.34,12.06,1.61,15.43,18.52,16.97,2.26,6.89,8.66,7.77,1.04

SW055572,4.41,0.59,2.50,0.33,18.84,15.05,16.94,2.26,19.39,12.95,16.17,2.15

SW131399,14.27,29.03,21.65,2.88,20.20,13.62,16.91,2.25,11.05,6.83,8.94,1.19

SW111248,45.46,52.96,49.21,6.56,17.86,15.76,16.81,2.24,-4.01,-3.76,-3.88,-0.52

SW019364,17.09,9.08,13.08,1.74,15.87,17.75,16.81,2.24,21.23,10.13,15.68,2.09

SW102288,20.15,22.31,21.23,2.83,19.02,14.49,16.76,2.23,-0.43,-21.77,-11.10,-1.48

SW004880,6.89,14.17,10.53,1.40,17.46,16.01,16.73,2.23,17.19,15.48,16.33,2.18

SW061659,21.53,16.90,19.21,2.56,16.32,17.14,16.73,2.23,16.63,9.03,12.83,1.71

SW053479,-2.85,-3.69,-3.27,-0.44,17.03,16.37,16.70,2.23,7.85,9.62,8.73,1.16

SW080964,8.68,11.30,9.99,1.33,19.91,13.36,16.64,2.22,24.20,16.43,20.32,2.71

SW192033,6.77,11.23,9.00,1.20,16.10,17.15,16.62,2.21,-2.31,-6.01,-4.16,-0.55

SW084380,6.46,16.94,11.70,1.56,16.69,16.51,16.60,2.21,12.80,14.54,13.67,1.82

SW105634,3.03,4.76,3.89,0.52,15.56,17.63,16.59,2.21,7.19,8.19,7.69,1.02

SW158940,7.99,18.78,13.38,1.78,17.28,15.89,16.59,2.21,7.12,8.83,7.97,1.06

SW059552,1.42,5.32,3.37,0.45,15.42,17.74,16.58,2.21,10.98,10.37,10.67,1.42

SW014088,8.05,7.78,7.91,1.05,15.20,17.90,16.55,2.20,2.21,9.06,5.64,0.75

SW138511,22.16,23.25,22.70,3.02,16.48,16.56,16.52,2.20,4.59,6.91,5.75,0.77

SW061393,-1.37,-0.39,-0.88,-0.12,15.39,17.54,16.46,2.19,17.65,12.89,15.27,2.03

SW200234,20.81,25.13,22.97,3.06,14.72,18.13,16.43,2.19,5.76,4.29,5.03,0.67

SW000528,12.05,3.24,7.64,1.02,13.92,18.91,16.41,2.19,14.17,12.53,13.35,1.78

SW147757,-5.75,3.26,-1.25,-0.17,16.75,15.91,16.33,2.18,9.79,13.69,11.74,1.56

SW083351,0.14,8.00,4.07,0.54,20.22,12.43,16.32,2.17,21.41,17.86,19.63,2.62

SW045150,3.00,-1.74,0.63,0.08,15.37,17.27,16.32,2.17,5.53,9.30,7.41,0.99

SW018014,-0.90,10.01,4.56,0.61,17.61,14.92,16.27,2.17,12.60,10.15,11.37,1.52

SW192763,6.51,16.96,11.73,1.56,12.72,19.74,16.23,2.16,1.27,1.33,1.30,0.17

SW102412,5.70,0.04,2.87,0.38,15.94,16.46,16.20,2.16,0.10,10.42,5.26,0.70

SW154346,35.81,62.54,49.17,6.55,12.24,20.11,16.17,2.15,4.40,-8.47,-2.04,-0.27

SW123066,21.58,22.55,22.07,2.94,14.57,17.72,16.15,2.15,-8.28,3.18,-2.55,-0.34

SW124779,0.26,12.05,6.16,0.82,17.56,14.66,16.11,2.15,8.27,12.43,10.35,1.38

SW100149,11.34,28.46,19.90,2.65,16.45,15.72,16.09,2.14,6.26,4.98,5.62,0.75

SW009946,19.56,20.49,20.02,2.67,15.48,16.58,16.03,2.14,9.39,2.78,6.08,0.81

SW045114,3.49,13.21,8.35,1.11,14.98,17.05,16.01,2.13,6.67,11.77,9.22,1.23

SW035650,36.72,27.94,32.33,4.31,16.63,15.39,16.01,2.13,7.78,11.82,9.80,1.31

SW001275,7.03,2.38,4.71,0.63,14.52,17.45,15.99,2.13,14.54,9.84,12.19,1.62

SW013420,17.96,29.26,23.61,3.15,17.35,14.59,15.97,2.13,19.80,15.38,17.59,2.34

SW092511,5.66,10.93,8.29,1.10,20.11,11.83,15.97,2.13,26.12,17.28,21.70,2.89

SW163575,21.88,19.13,20.51,2.73,18.84,13.07,15.95,2.13,5.49,2.53,4.01,0.53

SW013421,21.67,43.58,32.63,4.35,16.21,15.66,15.94,2.12,16.05,13.14,14.59,1.94

SW010911,41.64,37.42,39.53,5.27,11.44,19.91,15.67,2.09,9.15,12.88,11.01,1.47

SW120646,-8.41,4.64,-1.88,-0.25,14.67,16.51,15.59,2.08,8.05,7.03,7.54,1.00

SW080255,21.01,37.94,29.48,3.93,14.71,16.40,15.55,2.07,19.95,13.24,16.59,2.21

SW098641,-2.72,-1.29,-2.00,-0.27,15.75,15.31,15.53,2.07,10.02,12.34,11.18,1.49

SW005347,27.41,22.12,24.77,3.30,15.57,15.41,15.49,2.06,1.26,4.01,2.64,0.35

SW084466,20.26,22.16,21.21,2.83,18.85,12.12,15.48,2.06,21.81,13.77,17.79,2.37

SW092738,5.99,12.06,9.03,1.20,15.39,15.48,15.44,2.06,21.76,13.72,17.74,2.36

SW071138,5.88,9.96,7.92,1.06,14.50,16.37,15.43,2.06,13.50,11.16,12.33,1.64

SW023395,27.47,19.95,23.71,3.16,12.68,18.18,15.43,2.06,10.52,7.67,9.10,1.21

SW159770,11.52,17.02,14.27,1.90,16.57,14.25,15.41,2.05,7.33,6.91,7.12,0.95

SW133318,12.03,11.72,11.87,1.58,19.27,11.55,15.41,2.05,-0.89,2.54,0.82,0.11

SW015525,27.73,16.00,21.87,2.91,12.34,18.47,15.41,2.05,11.27,10.00,10.64,1.42

SW081492,14.00,14.99,14.49,1.93,13.74,17.05,15.39,2.05,16.66,11.81,14.24,1.90

SW029476,-3.54,5.25,0.85,0.11,15.54,15.23,15.38,2.05,12.99,9.31,11.15,1.48

SW164005,30.83,14.87,22.85,3.04,16.26,14.49,15.38,2.05,2.78,2.47,2.63,0.35

SW157653,15.16,25.56,20.36,2.71,14.91,15.82,15.37,2.05,2.16,8.34,5.25,0.70

SW051933,42.83,34.45,38.64,5.15,12.01,18.68,15.35,2.04,7.16,7.36,7.26,0.97

SW106392,4.11,-2.77,0.67,0.09,14.17,16.44,15.30,2.04,9.51,10.90,10.20,1.36

SW157744,1.72,12.41,7.07,0.94,16.34,14.25,15.29,2.04,9.71,7.98,8.84,1.18

SW157549,41.53,50.43,45.98,6.13,12.38,18.19,15.29,2.04,-9.07,0.39,-4.34,-0.58

SW082161,-1.68,5.71,2.01,0.27,14.64,15.92,15.28,2.04,12.19,9.93,11.06,1.47

SW084465,34.55,31.58,33.07,4.41,16.17,14.32,15.24,2.03,2.57,2.38,2.47,0.33

SW017057,8.90,-4.87,2.01,0.27,11.03,19.40,15.22,2.03,13.52,12.97,13.25,1.76

SW159586,5.41,13.61,9.51,1.27,14.15,16.11,15.13,2.02,7.26,7.60,7.43,0.99

SW017359,10.82,2.67,6.75,0.90,13.60,16.65,15.13,2.02,13.78,10.83,12.31,1.64

SW052319,15.43,22.83,19.13,2.55,16.16,14.05,15.11,2.01,9.79,8.75,9.27,1.24

SW097921,-5.79,-0.84,-3.31,-0.44,14.47,15.72,15.10,2.01,9.47,9.32,9.39,1.25

SW010124,12.13,38.18,25.15,3.35,14.82,15.36,15.09,2.01,8.96,10.36,9.66,1.29

SW054939,3.31,10.81,7.06,0.94,13.48,16.69,15.08,2.01,8.21,-12.83,-2.31,-0.31

SW127301,10.81,24.11,17.46,2.33,17.03,13.14,15.08,2.01,-15.72,-15.35,-15.53,-2.07

SW147789,-5.78,3.33,-1.22,-0.16,16.04,14.12,15.08,2.01,11.41,11.34,11.37,1.51

SW077361,-0.77,5.76,2.49,0.33,13.33,16.79,15.06,2.01,17.96,15.82,16.89,2.25

SW132622,1.66,3.23,2.45,0.33,17.73,12.32,15.02,2.00,14.94,5.96,10.45,1.39

SW029414,21.56,16.21,18.88,2.52,13.97,16.02,15.00,2.00,7.98,5.95,6.96,0.93

SW024708,10.56,20.34,15.45,2.06,14.91,15.03,14.97,1.99,11.94,8.94,10.44,1.39

SW098200,8.78,7.04,7.91,1.05,13.01,16.89,14.95,1.99,12.14,17.81,14.97,2.00

SW149775,18.00,34.42,26.21,3.49,14.81,15.07,14.94,1.99,9.79,10.82,10.31,1.37

SW068621,10.89,8.88,9.88,1.32,11.86,17.99,14.93,1.99,18.29,11.70,14.99,2.00

SW147974,19.69,28.51,24.10,3.21,15.32,14.47,14.89,1.98,16.34,12.79,14.57,1.94

SW163667,17.86,9.84,13.85,1.85,17.05,12.70,14.87,1.98,6.26,-0.49,2.89,0.38

SW033830,10.57,0.43,5.50,0.73,16.84,12.90,14.87,1.98,-2.37,1.14,-0.61,-0.08

SW099727,33.97,22.56,28.27,3.77,13.72,15.99,14.86,1.98,4.07,5.94,5.00,0.67

SW106379,25.00,22.70,23.85,3.18,13.86,15.83,14.85,1.98,1.89,3.61,2.75,0.37

SW067771,8.72,0.18,4.45,0.59,13.19,16.46,14.83,1.98,2.69,8.58,5.63,0.75

SW161655,28.15,30.51,29.33,3.91,15.63,13.99,14.81,1.97,8.44,5.21,6.82,0.91

SW052080,6.92,0.40,3.66,0.49,11.91,17.52,14.71,1.96,12.61,11.91,12.26,1.63

SW186735,-2.24,2.18,-0.03,0.00,12.88,16.54,14.71,1.96,13.11,-12.23,0.44,0.06

SW023398,21.46,14.58,18.02,2.40,10.20,19.13,14.67,1.95,12.63,10.72,11.68,1.56

SW189825,-3.23,2.52,-0.35,-0.05,13.01,16.18,14.60,1.94,13.85,-14.05,-0.10,-0.01

SW105681,42.29,35.90,39.10,5.21,14.92,14.22,14.57,1.94,-4.51,-9.04,-6.78,-0.90

SW044552,7.88,6.68,7.28,0.97,11.03,18.09,14.56,1.94,15.78,8.50,12.14,1.62

SW154578,-0.60,15.30,7.35,0.98,12.87,16.14,14.50,1.93,-11.97,-9.43,-10.70,-1.43

SW000466,15.19,8.26,11.73,1.56,10.73,18.21,14.47,1.93,11.89,13.44,12.66,1.69

SW045123,35.63,54.82,45.22,6.03,14.30,14.61,14.45,1.93,12.22,10.61,11.41,1.52

SW149372,29.18,43.96,36.57,4.87,13.17,15.59,14.38,1.92,0.08,10.36,5.22,0.70

SW128346,7.80,16.95,12.37,1.65,12.51,16.25,14.38,1.92,-1.81,-17.80,-9.80,-1.31

SW077103,7.42,0.53,3.98,0.53,12.76,15.98,14.37,1.91,11.64,7.74,9.69,1.29

SW038719,19.24,34.92,27.08,3.61,15.60,13.14,14.37,1.91,11.07,5.45,8.26,1.10

SW125181,7.74,21.61,14.68,1.96,17.24,11.49,14.37,1.91,12.82,7.14,9.98,1.33

SW034145,44.89,87.42,44.89,5.98,14.29,14.32,14.31,1.91,13.59,8.92,11.26,1.50

SW059642,13.96,11.68,12.82,1.71,10.32,18.24,14.28,1.90,10.20,7.07,8.64,1.15

SW106037,-2.72,0.68,-1.02,-0.14,12.98,15.58,14.28,1.90,4.33,7.73,6.03,0.80

SW033531,7.19,0.18,3.69,0.49,10.59,17.96,14.28,1.90,15.69,11.16,13.42,1.79

SW058320,7.15,12.55,9.85,1.31,11.21,17.25,14.23,1.90,2.59,4.90,3.74,0.50

SW012175,39.05,38.88,38.96,5.19,10.17,18.29,14.23,1.90,7.59,8.13,7.86,1.05

SW006549,12.99,18.21,15.60,2.08,11.84,16.43,14.13,1.88,0.35,11.86,6.10,0.81

SW059830,10.95,10.31,10.63,1.42,12.27,15.98,14.12,1.88,16.27,7.35,11.81,1.57

SW011958,7.51,-2.93,2.29,0.31,10.51,17.74,14.12,1.88,9.81,9.62,9.72,1.29

SW126677,10.99,16.44,13.71,1.83,13.54,14.58,14.06,1.87,1.31,9.40,5.35,0.71

SW075283,7.85,4.83,6.34,0.84,12.51,15.50,14.00,1.87,12.88,10.64,11.76,1.57

SW010905,44.77,39.63,42.20,5.62,10.27,17.66,13.96,1.86,6.08,8.51,7.29,0.97

SW019003,7.72,6.77,7.24,0.96,11.61,16.30,13.95,1.86,0.61,6.35,3.48,0.46

SW013587,20.53,21.18,20.86,2.78,13.28,14.59,13.93,1.86,18.60,9.59,14.10,1.88

SW157038,5.11,21.59,13.35,1.78,13.87,13.88,13.88,1.85,8.44,10.26,9.35,1.25

SW001273,14.69,12.37,13.53,1.80,8.61,19.11,13.86,1.85,2.19,9.87,6.03,0.80

SW112294,-2.55,0.65,-0.95,-0.13,12.42,15.24,13.83,1.84,5.64,6.45,6.04,0.81

SW147229,5.66,3.95,4.80,0.64,14.76,12.82,13.79,1.84,2.71,9.88,6.30,0.84

SW084435,8.84,20.24,14.54,1.94,14.40,13.18,13.79,1.84,23.07,13.09,18.08,2.41

SW015478,14.76,13.94,14.35,1.91,13.99,13.52,13.75,1.83,10.28,7.56,8.92,1.19

SW165054,12.73,7.38,10.06,1.34,5.85,21.65,13.75,1.83,-4.41,-11.23,-7.82,-1.04

SW163411,17.51,16.46,16.99,2.26,11.79,15.65,13.72,1.83,-9.05,-14.95,-12.00,-1.60

SW156163,12.05,21.30,16.68,2.22,14.72,12.66,13.69,1.82,3.87,6.69,5.28,0.70

SW059851,4.86,14.61,9.73,1.30,13.04,14.25,13.64,1.82,3.33,0.83,2.08,0.28

SW145148,5.42,-0.18,2.62,0.35,13.78,13.47,13.63,1.82,3.73,7.33,5.53,0.74

SW027243,49.95,51.29,50.62,6.74,12.39,14.83,13.61,1.81,-4.48,1.90,-1.29,-0.17

SW163747,27.14,12.77,19.95,2.66,15.57,11.65,13.61,1.81,4.53,4.66,4.60,0.61

SW150173,7.84,13.99,10.91,1.45,14.86,12.32,13.59,1.81,12.77,12.77,12.77,1.70

SW192405,32.36,17.76,25.06,3.34,10.85,16.28,13.57,1.81,-3.70,-12.29,-8.00,-1.07

SW084467,16.80,34.80,25.80,3.44,14.44,12.67,13.55,1.81,16.27,13.62,14.95,1.99

SW021377,43.20,35.32,39.26,5.23,10.00,16.98,13.49,1.80,3.00,6.76,4.88,0.65

SW091104,11.86,12.26,12.06,1.61,12.02,14.96,13.49,1.80,14.75,7.85,11.30,1.50

SW000532,11.22,1.52,6.37,0.85,7.98,18.94,13.46,1.79,14.07,16.55,15.31,2.04

SW034637,6.62,1.42,4.02,0.54,10.94,15.93,13.43,1.79,14.39,7.92,11.16,1.49

SW106136,11.78,18.19,14.99,2.00,14.75,11.96,13.35,1.78,-14.04,-13.27,-13.66,-1.82

SW039384,5.48,-2.76,1.36,0.18,12.19,14.46,13.32,1.77,9.44,7.69,8.57,1.14

SW024945,6.97,13.23,10.10,1.35,12.38,14.25,13.32,1.77,12.91,13.12,13.02,1.73

SW163533,5.33,2.93,4.13,0.55,12.16,14.41,13.29,1.77,-5.42,-3.93,-4.67,-0.62

SW059553,25.37,25.99,25.68,3.42,11.14,15.27,13.21,1.76,6.42,5.90,6.16,0.82

SW153149,-7.32,1.38,-2.97,-0.40,14.02,12.39,13.21,1.76,7.49,10.27,8.88,1.18

SW186578,5.53,10.30,7.92,1.05,15.96,10.44,13.20,1.76,-0.04,3.43,1.70,0.23

SW017569,13.15,9.92,11.53,1.54,10.80,15.59,13.19,1.76,-2.25,4.47,1.11,0.15

SW000726,9.55,-1.10,4.22,0.56,12.67,13.56,13.11,1.75,7.38,18.05,12.72,1.69

SW024643,20.53,18.20,19.36,2.58,12.11,14.07,13.09,1.74,5.47,2.71,4.09,0.55

SW059207,3.10,9.47,6.28,0.84,12.53,13.42,12.98,1.73,2.68,2.90,2.79,0.37

SW121828,-1.24,6.27,2.52,0.34,9.27,16.65,12.96,1.73,6.86,14.48,10.67,1.42

SW146925,8.60,10.84,9.72,1.29,15.59,10.30,12.94,1.72,6.18,11.43,8.80,1.17

SW160765,12.53,16.18,14.35,1.91,13.63,12.20,12.92,1.72,4.30,3.87,4.08,0.54

SW164251,7.28,7.00,7.14,0.95,14.44,11.36,12.90,1.72,0.73,1.08,0.90,0.12

SW128857,11.75,30.96,21.36,2.85,12.42,13.37,12.90,1.72,1.34,2.75,2.04,0.27

SW158299,-4.40,-3.00,-3.70,-0.49,12.65,13.14,12.89,1.72,4.76,10.15,7.45,0.99

SW053843,5.52,0.84,3.18,0.42,10.61,15.09,12.85,1.71,14.18,9.11,11.65,1.55

SW161458,7.91,11.75,9.83,1.31,11.76,13.90,12.83,1.71,0.77,-12.30,-5.77,-0.77

SW025030,3.73,4.24,3.99,0.53,10.84,14.75,12.79,1.70,-0.15,5.95,2.90,0.39

SW144458,12.45,10.25,11.35,1.51,16.47,9.05,12.76,1.70,4.54,8.94,6.74,0.90

SW060548,8.56,7.18,7.87,1.05,10.76,14.70,12.73,1.70,15.26,8.92,12.09,1.61

SW117537,17.34,20.68,19.01,2.53,9.12,16.32,12.72,1.69,-3.33,5.16,0.91,0.12

SW053636,1.93,0.85,1.39,0.18,10.19,14.99,12.59,1.68,12.72,24.62,18.67,2.49

SW152770,-1.61,6.62,2.50,0.33,13.44,11.72,12.58,1.68,11.30,12.62,11.96,1.59

SW135208,-2.93,-5.64,-4.29,-0.57,15.36,9.76,12.56,1.67,1.35,2.42,1.88,0.25

SW002142,1.41,8.60,5.00,0.67,13.52,11.55,12.53,1.67,15.94,11.45,13.69,1.82

SW081018,8.96,24.54,16.75,2.23,13.12,11.90,12.51,1.67,17.49,16.72,17.10,2.28

SW123578,-8.04,-0.91,-4.48,-0.60,11.67,13.23,12.45,1.66,2.20,4.70,3.45,0.46

SW030050,21.41,24.39,22.90,3.05,11.87,12.99,12.43,1.66,9.10,5.01,7.05,0.94

SW202035,13.25,9.23,11.24,1.50,14.66,10.11,12.39,1.65,5.67,2.61,4.14,0.55

SW061820,-2.20,-2.28,-2.24,-0.30,12.08,12.66,12.37,1.65,11.61,5.32,8.47,1.13

SW082034,8.09,0.59,4.34,0.58,8.67,15.94,12.30,1.64,5.69,10.34,8.01,1.07

SW013422,22.27,31.11,26.69,3.56,7.67,16.90,12.29,1.64,-0.48,11.85,5.68,0.76

SW132256,6.11,8.56,7.34,0.98,15.68,8.87,12.28,1.64,7.23,2.68,4.95,0.66

SW105846,9.71,-1.42,4.14,0.55,10.22,14.22,12.22,1.63,0.67,2.82,1.74,0.23

SW129312,-1.86,9.66,3.90,0.52,14.56,9.87,12.22,1.63,16.10,6.79,11.45,1.52

SW045957,17.95,31.79,24.87,3.31,13.85,10.58,12.22,1.63,13.13,8.80,10.97,1.46

SW041938,-2.37,4.24,0.93,0.12,9.11,15.29,12.20,1.63,6.07,10.25,8.16,1.09

SW036520,4.64,15.35,10.00,1.33,10.19,14.22,12.20,1.63,7.16,6.73,6.95,0.93

SW096170,6.82,5.67,6.24,0.83,9.74,14.51,12.13,1.62,-1.06,10.42,4.68,0.62

SW067511,5.82,-1.84,1.99,0.27,9.41,14.83,12.12,1.61,11.59,9.62,10.60,1.41

SW061161,6.70,16.38,11.54,1.54,11.44,12.69,12.06,1.61,6.04,0.56,3.30,0.44

SW084444,9.64,18.74,14.19,1.89,11.58,12.48,12.03,1.60,19.82,11.29,15.56,2.07

SW164010,17.43,0.44,8.93,1.19,11.31,12.75,12.03,1.60,11.08,8.79,9.94,1.32

SW163119,0.78,3.13,1.96,0.26,12.47,11.44,11.95,1.59,5.99,3.95,4.97,0.66

SW091217,13.38,18.54,15.96,2.13,10.39,13.40,11.89,1.58,11.61,6.78,9.19,1.22

SW077587,3.47,-0.83,1.32,0.18,8.55,15.20,11.88,1.58,10.47,7.15,8.81,1.17

SW194103,-2.16,2.06,-0.05,-0.01,12.66,11.05,11.85,1.58,2.59,-10.97,-4.19,-0.56

SW065671,4.99,5.61,5.30,0.71,11.28,12.41,11.85,1.58,6.84,3.20,5.02,0.67

SW065119,1.69,2.92,2.30,0.31,11.97,11.68,11.83,1.58,9.88,6.93,8.40,1.12

SW096240,9.59,20.00,14.80,1.97,10.29,13.33,11.81,1.57,16.71,13.95,15.33,2.04

SW053270,3.31,1.43,2.37,0.32,9.60,13.96,11.78,1.57,-0.02,1.70,0.84,0.11

SW102639,9.04,10.41,9.72,1.30,8.61,14.84,11.73,1.56,-3.76,1.84,-0.96,-0.13

SW132107,18.90,14.07,16.48,2.20,14.83,8.58,11.71,1.56,2.62,6.51,4.57,0.61

SW072942,4.34,6.27,5.30,0.71,11.75,11.63,11.69,1.56,11.51,8.02,9.76,1.30

SW161239,0.56,-3.74,-1.59,-0.21,13.27,9.98,11.62,1.55,10.23,5.36,7.80,1.04

SW013000,-3.16,6.13,1.49,0.20,8.83,14.30,11.57,1.54,15.13,-13.47,0.83,0.11

SW074341,4.51,0.79,2.65,0.35,9.29,13.80,11.55,1.54,8.82,7.64,8.23,1.10

SW159376,14.34,19.97,17.16,2.29,11.40,11.67,11.54,1.54,-1.13,3.07,0.97,0.13

SW081544,-0.23,0.19,-0.02,0.00,12.03,10.99,11.51,1.53,12.09,13.29,12.69,1.69

SW147581,3.57,4.71,4.14,0.55,11.24,11.68,11.46,1.53,1.13,6.25,3.69,0.49

SW130318,-1.11,-3.48,-2.29,-0.31,13.00,9.85,11.42,1.52,0.92,-1.43,-0.26,-0.03

SW195761,-32.65,-21.06,-26.85,-3.58,9.98,12.72,11.35,1.51,7.78,-7.86,-0.04,-0.01

SW051365,-7.19,-2.35,-4.77,-0.64,11.28,11.41,11.35,1.51,5.42,6.70,6.06,0.81

SW016986,9.72,31.16,20.44,2.72,11.26,11.37,11.32,1.51,-7.45,-8.64,-8.05,-1.07

SW083442,20.19,20.08,20.13,2.68,9.00,13.63,11.31,1.51,8.44,3.73,6.08,0.81

SW045362,-5.88,3.87,-1.01,-0.13,11.74,10.81,11.28,1.50,10.08,6.05,8.07,1.07

SW131424,28.46,33.52,30.99,4.13,13.62,8.92,11.27,1.50,6.39,8.42,7.40,0.99

SW121488,28.71,34.77,31.74,4.23,8.36,14.18,11.27,1.50,-6.99,4.03,-1.48,-0.20

SW199151,-3.19,-3.11,-3.15,-0.42,9.44,13.00,11.22,1.49,0.09,-13.76,-6.84,-0.91

SW064689,18.47,8.69,13.58,1.81,8.76,13.52,11.14,1.48,8.27,6.02,7.14,0.95

SW171329,20.62,28.00,24.31,3.24,9.88,12.29,11.08,1.48,9.48,-16.10,-3.31,-0.44

SW028653,10.25,8.36,9.30,1.24,10.72,11.44,11.08,1.48,8.78,4.54,6.66,0.89

SW047872,-4.41,-5.84,-5.13,-0.68,11.07,11.08,11.08,1.48,0.90,7.40,4.15,0.55

SW034502,-6.69,0.15,-3.27,-0.44,10.76,11.38,11.07,1.47,2.37,5.29,3.83,0.51

SW072074,-0.37,1.51,0.57,0.08,10.26,11.75,11.00,1.47,6.46,1.91,4.19,0.56

SW054919,30.26,55.11,42.68,5.69,8.71,13.24,10.97,1.46,-8.56,-7.31,-7.93,-1.06

SW197131,0.09,0.39,0.24,0.03,7.82,14.07,10.94,1.46,11.58,-15.14,-1.78,-0.24

SW046144,2.70,5.14,3.92,0.52,11.77,10.01,10.89,1.45,11.09,5.98,8.53,1.14

SW006982,11.46,3.65,7.56,1.01,6.67,15.06,10.86,1.45,5.03,9.43,7.23,0.96

SW058308,42.92,40.34,41.63,5.55,7.69,13.99,10.84,1.44,6.70,7.51,7.11,0.95

SW163265,-2.40,-1.32,-1.86,-0.25,13.53,8.03,10.78,1.44,12.13,6.61,9.37,1.25

SW006520,2.15,-3.68,-0.76,-0.10,10.10,11.46,10.78,1.44,14.76,7.59,11.18,1.49

SW065046,-1.49,-1.31,-1.40,-0.19,10.84,10.70,10.77,1.43,7.06,1.97,4.51,0.60

SW159303,21.12,29.26,25.19,3.36,10.38,11.04,10.71,1.43,-4.63,-0.72,-2.68,-0.36

SW055299,26.87,53.27,40.07,5.34,10.15,11.18,10.66,1.42,-9.74,-14.82,-12.28,-1.64

SW000177,21.91,8.20,15.06,2.01,9.20,12.10,10.65,1.42,3.00,3.89,3.45,0.46

SW118091,-1.84,16.16,7.16,0.95,11.31,9.92,10.62,1.41,6.25,8.35,7.30,0.97

SW118929,12.33,15.04,13.68,1.82,13.09,8.12,10.61,1.41,-3.40,-16.89,-10.14,-1.35

SW024999,8.26,10.43,9.34,1.24,8.91,12.31,10.61,1.41,-3.83,8.97,2.57,0.34

SW109380,9.67,8.35,9.01,1.20,7.70,13.32,10.51,1.40,-0.12,2.65,1.26,0.17

SW163152,4.75,6.53,5.64,0.75,12.72,8.27,10.50,1.40,11.26,5.47,8.36,1.11

SW153768,11.30,31.75,21.52,2.87,10.18,10.33,10.25,1.37,5.08,7.17,6.12,0.82

SW039524,-6.49,-3.25,-4.87,-0.65,8.54,11.83,10.18,1.36,-2.82,2.82,0.00,0.00

SW192447,-1.68,-3.48,-2.58,-0.34,8.60,11.76,10.18,1.36,7.59,-18.40,-5.40,-0.72

SW167401,28.90,28.55,28.73,3.83,8.64,11.60,10.12,1.35,-2.15,-13.30,-7.73,-1.03

SW073074,5.51,8.76,7.13,0.95,8.67,11.52,10.10,1.35,8.09,4.39,6.24,0.83

SW000504,13.07,3.69,8.38,1.12,10.38,9.79,10.08,1.34,8.64,11.34,9.99,1.33

SW155941,5.46,16.55,11.00,1.47,7.68,12.44,10.06,1.34,-6.62,5.08,-0.77,-0.10

SW095290,0.08,2.88,1.48,0.20,7.92,12.20,10.06,1.34,-11.74,-8.52,-10.13,-1.35

SW145806,14.58,20.40,17.49,2.33,7.70,12.37,10.03,1.34,-7.40,-4.33,-5.86,-0.78

SW063647,11.99,3.40,7.69,1.02,6.43,13.58,10.00,1.33,3.24,6.10,4.67,0.62

SW004253,16.76,44.37,30.56,4.07,8.16,11.67,9.91,1.32,15.33,-15.03,-15.03,-2.00

SW167247,24.07,26.15,25.11,3.35,7.15,12.63,9.89,1.32,8.67,-19.50,-5.41,-0.72

SW128875,7.72,2.83,5.27,0.70,9.40,10.33,9.86,1.31,-7.73,-4.53,-6.13,-0.82

SW015179,6.70,6.38,6.54,0.87,9.22,10.47,9.85,1.31,11.77,6.71,9.24,1.23

SW030010,14.71,11.29,13.00,1.73,7.47,12.18,9.83,1.31,-9.83,-1.53,-5.68,-0.76

SW150408,11.02,25.47,18.24,2.43,11.29,8.25,9.77,1.30,19.56,18.24,18.90,2.52

SW081976,29.41,28.61,29.01,3.86,6.78,12.75,9.77,1.30,-1.60,3.67,1.03,0.14

SW177447,-6.55,-5.86,-6.20,-0.83,7.92,11.58,9.75,1.30,-5.43,-18.12,-11.78,-1.57

SW147461,6.39,7.14,6.77,0.90,13.16,6.04,9.60,1.28,-0.32,10.97,5.33,0.71

SW102287,10.82,15.45,13.13,1.75,12.88,6.32,9.60,1.28,0.32,1.58,0.95,0.13

SW126216,9.52,20.22,14.87,1.98,6.37,12.65,9.51,1.27,-17.34,-9.91,-13.62,-1.82

SW002193,10.54,9.45,10.00,1.33,3.54,15.41,9.47,1.26,0.32,12.79,6.55,0.87

SW194089,-8.45,-5.85,-7.15,-0.95,7.60,11.33,9.47,1.26,12.12,-20.84,-20.84,-2.78

SW125384,12.41,18.75,15.58,2.08,8.01,10.84,9.43,1.26,-4.67,-4.66,-4.66,-0.62

SW129294,12.42,15.84,14.13,1.88,11.61,7.24,9.42,1.26,-11.82,-9.76,-10.79,-1.44

SW058182,4.48,-3.93,0.28,0.04,6.35,12.45,9.40,1.25,5.74,5.82,5.78,0.77

SW129426,-4.54,-9.71,-7.13,-0.95,11.69,7.07,9.38,1.25,-3.18,-0.06,-1.62,-0.22

SW124199,-3.62,7.10,1.74,0.23,7.84,10.87,9.35,1.25,-22.22,-18.46,-20.34,-2.71

SW131031,10.90,17.92,14.41,1.92,10.13,8.40,9.27,1.23,-4.40,-18.40,-11.40,-1.52

SW163021,-1.56,2.22,0.33,0.04,11.50,6.97,9.24,1.23,6.10,3.37,4.74,0.63

SW030200,7.77,10.64,9.21,1.23,7.84,10.60,9.22,1.23,1.10,4.99,3.04,0.41

SW039505,6.67,7.52,7.10,0.95,7.28,11.10,9.19,1.22,-5.21,3.89,-0.66,-0.09

SW014427,29.60,36.01,32.80,4.37,7.59,10.56,9.07,1.21,10.86,6.60,8.73,1.16

SW199666,19.28,19.86,19.57,2.61,8.36,9.77,9.06,1.21,-0.87,-3.04,-1.96,-0.26

SW131784,-2.28,9.71,3.71,0.49,10.38,7.67,9.03,1.20,5.50,1.77,3.64,0.48

SW081021,7.10,10.34,8.72,1.16,5.45,12.58,9.01,1.20,0.63,8.23,4.43,0.59

SW120425,-8.02,4.96,-1.53,-0.20,6.99,10.92,8.96,1.19,-0.41,-17.43,-8.92,-1.19

SW051212,1.88,16.53,9.21,1.23,9.21,8.38,8.80,1.17,4.56,1.41,2.98,0.40

SW049036,-9.37,3.65,-2.86,-0.38,8.70,8.76,8.73,1.16,0.58,-2.86,-1.14,-0.15

SW128093,-0.46,-7.04,-3.75,-0.50,11.63,5.80,8.72,1.16,-5.89,-9.54,-7.72,-1.03

SW127927,-1.39,-8.57,-4.98,-0.66,10.73,6.70,8.72,1.16,-3.92,-0.50,-2.21,-0.29

SW118241,1.40,17.34,9.37,1.25,7.27,9.98,8.63,1.15,5.91,-14.86,-4.47,-0.60

SW163172,1.09,6.97,4.03,0.54,10.68,6.55,8.61,1.15,4.15,1.34,2.74,0.37

SW058492,-3.81,-8.73,-6.27,-0.84,7.27,9.69,8.48,1.13,-5.81,0.79,-2.51,-0.33

SW079060,1.10,-3.63,-1.27,-0.17,6.05,10.55,8.30,1.11,10.46,2.40,6.43,0.86

SW003082,3.21,1.29,2.25,0.30,7.03,9.55,8.29,1.10,7.11,4.56,5.84,0.78

SW038463,1.21,9.99,5.60,0.75,7.52,8.93,8.23,1.10,6.97,2.65,4.81,0.64

SW077026,3.45,-4.86,-0.71,-0.09,5.23,11.12,8.18,1.09,-1.89,4.62,1.36,0.18

SW026349,3.05,2.17,2.61,0.35,7.84,8.33,8.08,1.08,8.69,3.62,6.16,0.82

SW048671,-16.55,-15.15,-15.85,-2.11,7.65,8.29,7.97,1.06,-2.46,5.11,1.32,0.18

SW154729,7.77,32.15,19.96,2.66,6.53,9.14,7.84,1.04,-10.65,0.53,-5.06,-0.67

SW074696,-7.71,-16.88,-12.30,-1.64,6.76,8.70,7.73,1.03,-0.30,-1.05,-0.67,-0.09

SW159877,4.67,12.89,8.78,1.17,6.61,8.79,7.70,1.03,-10.45,-14.15,-12.30,-1.64

SW154847,9.06,17.68,13.37,1.78,6.66,8.64,7.65,1.02,-8.21,-0.68,-4.44,-0.59

SW057302,9.77,1.74,5.76,0.77,3.88,11.35,7.61,1.01,-0.43,4.26,1.92,0.26

SW143474,-5.87,-1.33,-3.60,-0.48,4.95,10.13,7.54,1.00,8.49,-9.01,-0.26,-0.03

SW082526,0.95,-3.91,-1.48,-0.20,4.67,10.32,7.50,1.00,4.28,4.18,4.23,0.56

SW125111,18.65,24.52,21.58,2.88,2.70,12.27,7.48,1.00,-8.30,-4.70,-6.50,-0.87

SW077017,6.17,-3.59,1.29,0.17,5.12,9.83,7.48,1.00,-1.23,1.27,0.02,0.00

SW051978,16.46,35.59,26.03,3.47,4.02,10.87,7.44,0.99,10.12,8.16,9.14,1.22

SW077276,-6.24,-8.65,-7.44,-0.99,3.30,11.39,7.35,0.98,0.08,2.30,1.19,0.16

SW003734,6.67,5.06,5.87,0.78,7.27,7.38,7.33,0.98,7.80,2.38,5.09,0.68

SW038718,9.92,23.43,16.68,2.22,6.76,7.88,7.32,0.98,6.60,2.36,4.48,0.60

SW128590,-4.04,-10.80,-7.42,-0.99,9.44,5.07,7.25,0.97,-6.71,-3.91,-5.31,-0.71

SW051857,-1.33,6.26,2.47,0.33,7.18,7.33,7.25,0.97,5.75,3.59,4.67,0.62

SW083577,-5.59,4.34,-0.62,-0.08,4.02,10.38,7.20,0.96,13.84,-15.44,-0.80,-0.11

SW082647,1.09,2.23,1.66,0.22,7.16,7.09,7.12,0.95,5.26,2.52,3.89,0.52

SW199924,14.67,12.10,13.39,1.78,5.48,8.76,7.12,0.95,-5.49,-5.95,-5.72,-0.76

SW163375,2.01,6.69,4.35,0.58,8.23,5.97,7.10,0.95,0.89,0.82,0.86,0.11

SW147453,-11.57,-17.35,-14.46,-1.93,5.50,8.69,7.10,0.95,-7.02,-3.81,-5.41,-0.72

SW157801,1.04,14.96,8.00,1.07,7.92,6.16,7.04,0.94,1.31,6.19,3.75,0.50

SW081241,-3.62,-3.86,-3.74,-0.50,6.51,7.56,7.03,0.94,-0.16,-3.44,-1.80,-0.24

SW152900,20.17,40.36,30.27,4.03,3.72,10.17,6.94,0.93,-7.82,7.56,-0.13,-0.02

SW066496,2.57,-1.70,0.43,0.06,5.77,8.11,6.94,0.92,-4.60,-1.14,-2.87,-0.38

SW163625,-4.24,-6.91,-5.57,-0.74,7.97,5.74,6.85,0.91,3.44,-0.42,1.51,0.20

SW082087,2.06,-4.52,-1.23,-0.16,6.17,7.53,6.85,0.91,7.66,5.96,6.81,0.91

SW021788,15.65,7.38,11.52,1.53,0.90,12.63,6.77,0.90,-0.12,3.80,1.84,0.25

SW195718,-14.14,-0.91,-7.53,-1.00,6.31,6.88,6.60,0.88,-11.05,-4.41,-7.73,-1.03

SW062641,33.06,26.51,29.79,3.97,5.02,8.13,6.58,0.88,-2.94,2.18,-0.38,-0.05

SW155719,-4.03,1.68,-1.18,-0.16,77.67,6.57,6.57,0.88,2.13,5.92,4.02,0.54

SW013582,-1.22,18.11,8.45,1.13,3.97,9.12,6.55,0.87,-1.66,-12.50,-7.08,-0.94

SW061157,0.05,15.17,7.61,1.01,4.04,8.90,6.47,0.86,-12.53,-11.79,-12.16,-1.62

SW082984,0.49,5.54,3.02,0.40,5.54,7.35,6.45,0.86,2.37,-0.09,1.14,0.15

SW157630,27.25,41.68,34.46,4.59,5.27,7.59,6.43,0.86,-9.66,-2.83,-6.25,-0.83

SW020271,-2.95,-10.18,-6.57,-0.88,4.16,8.45,6.30,0.84,0.69,0.78,0.74,0.10

SW158782,-7.79,0.57,-3.61,-0.48,4.98,7.44,6.21,0.83,-12.48,-12.60,-12.54,-1.67

SW122646,13.22,20.60,16.91,2.25,4.55,7.87,6.21,0.83,-11.14,1.07,-5.03,-0.67

SW163704,-8.88,-7.60,-8.24,-1.10,7.63,4.68,6.15,0.82,2.24,-0.15,1.05,0.14

SW128532,-4.62,-12.40,-8.51,-1.13,8.78,3.46,6.12,0.82,-13.40,-6.12,-9.76,-1.30

SW006659,7.01,0.19,3.60,0.48,4.45,7.58,6.02,0.80,3.97,1.32,2.64,0.35

SW159883,-8.43,2.29,-3.07,-0.41,4.89,7.13,6.01,0.80,2.88,-13.79,-5.45,-0.73

SW054804,-1.32,4.88,1.78,0.24,3.26,8.63,5.94,0.79,12.31,-14.86,-1.28,-0.17

SW163194,-9.04,-12.43,-10.74,-1.43,6.75,5.09,5.92,0.79,-1.04,-2.31,-1.68,-0.22

SW164246,-52.09,-39.64,-45.86,-6.11,6.87,4.97,5.92,0.79,11.37,4.64,8.01,1.07

SW147245,-11.22,-0.25,-5.73,-0.76,4.69,7.12,5.91,0.79,8.82,-8.58,0.12,0.02

SW079964,-10.28,-15.80,-13.04,-1.74,3.96,7.69,5.83,0.78,-1.57,-2.42,-2.00,-0.27

SW160582,20.93,26.50,23.71,3.16,4.47,6.88,5.68,0.76,-15.42,-11.84,-13.63,-1.82

SW132693,-0.24,6.41,3.08,0.41,6.62,4.46,5.54,0.74,-14.36,-15.38,-14.87,-1.98

SW027023,8.24,15.27,11.75,1.57,6.50,4.08,5.29,0.70,7.00,3.60,5.30,0.71

SW097621,8.37,3.41,5.89,0.78,3.12,7.38,5.25,0.70,-5.20,-4.14,-4.67,-0.62

SW130260,-14.91,-10.69,-12.80,-1.71,6.22,4.10,5.16,0.69,-4.60,-1.42,-3.01,-0.40

SW003611,-14.61,-4.16,-9.39,-1.25,4.96,5.33,5.15,0.69,-1.97,-9.51,-5.74,-0.76

SW160940,-7.97,-3.95,-5.96,-0.79,4.13,6.11,5.12,0.68,-2.56,0.18,-1.19,-0.16

SW148145,7.24,30.69,18.97,2.53,2.82,7.15,4.99,0.66,2.72,-13.12,-5.20,-0.69

SW058292,-6.02,-9.41,-7.72,-1.03,2.96,6.98,4.97,0.66,-6.96,-5.90,-6.43,-0.86

SW003982,6.03,8.84,7.43,0.99,3.89,6.03,4.96,0.66,4.25,1.46,2.85,0.38

SW046887,-5.13,-5.83,-5.48,-0.73,0.22,9.67,4.95,0.66,-10.26,-7.77,-9.02,-1.20

SW164204,-38.58,-24.82,-31.70,-4.22,7.74,2.05,4.90,0.65,-5.57,-8.35,-6.96,-0.93

SW077027,-6.92,-9.75,-8.34,-1.11,1.88,7.62,4.75,0.63,-3.27,0.11,-1.58,-0.21

SW131559,-14.36,-2.59,-8.47,-1.13,4.95,4.52,4.74,0.63,-12.35,-7.81,-10.08,-1.34

SW151820,-3.91,10.00,3.05,0.41,3.11,6.21,4.66,0.62,-14.42,-12.60,-13.51,-1.80

SW163423,-11.17,-9.11,-10.14,-1.35,6.17,2.81,4.49,0.60,-0.92,-2.04,-1.48,-0.20

SW163076,-5.95,-5.80,-5.88,-0.78,4.10,4.67,4.38,0.58,-5.84,-4.66,-5.25,-0.70

SW163454,3.03,2.74,2.88,0.38,4.91,3.55,4.23,0.56,1.92,-2.03,-0.05,-0.01

SW126804,-0.40,-3.22,-1.81,-0.24,6.38,2.03,4.20,0.56,-15.70,-12.64,-14.17,-1.89

SW047611,-1.83,4.48,1.32,0.18,2.43,5.94,4.18,0.56,-8.03,-3.28,-5.66,-0.75

SW145870,-5.14,-8.66,-6.90,-0.92,1.92,6.29,4.10,0.55,7.13,-11.58,-2.23,-0.30

SW096204,-3.63,-11.68,-7.65,-1.02,1.64,6.16,3.90,0.52,-4.38,0.27,-2.06,-0.27

SW133514,-4.43,-5.98,-5.20,-0.69,5.14,2.41,3.78,0.50,-9.39,-7.55,-8.47,-1.13

SW006137,-5.85,-11.98,-8.91,-1.19,2.23,5.15,3.69,0.49,3.90,-1.23,1.34,0.18

SW160672,8.99,24.16,16.58,2.21,4.51,2.52,3.51,0.47,-1.06,-5.04,-3.05,-0.41

SW023396,-0.35,21.92,10.79,1.44,1.19,5.83,3.51,0.47,-12.03,-15.56,-13.80,-1.84

SW077653,-4.82,-10.73,-7.78,-1.04,1.66,5.32,3.49,0.47,4.49,-1.98,1.25,0.17

SW009037,4.99,-0.45,2.27,0.30,2.86,4.02,3.44,0.46,3.72,-1.76,0.98,0.13

SW171240,-23.80,-19.86,-21.83,-2.91,3.55,3.21,3.38,0.45,-6.71,-14.33,-10.52,-1.40

SW102287,-0.71,-0.05,-0.38,-0.05,0.85,5.51,3.18,0.42,-19.30,-15.73,-17.51,-2.33

SW163069,-13.26,-7.53,-10.39,-1.38,3.97,2.05,3.01,0.40,-4.05,-4.84,-4.45,-0.59

SW027238,25.72,30.53,28.12,3.75,1.32,4.62,2.97,0.40,-8.63,-2.67,-5.65,-0.75

SW150218,-13.99,0.59,-6.70,-0.89,1.75,3.99,2.87,0.38,0.80,-12.62,-5.91,-0.79

SW045259,-67.72,-98.99,-98.99,-13.19,2.09,3.23,2.66,0.35,-4.81,-10.83,-7.82,-1.04

SW049033,0.41,10.59,5.50,0.73,-2.14,7.31,2.59,0.34,6.93,-16.53,-4.80,-0.64

SW061168,-5.52,7.43,0.96,0.13,-2.11,6.17,2.03,0.27,8.39,-18.53,-5.07,-0.68

SW015975,1.03,0.67,0.85,0.11,-0.19,3.25,1.53,0.20,-9.60,-3.86,-6.73,-0.90

SW128775,-5.60,2.05,-1.78,-0.24,2.51,0.39,1.45,0.19,-4.59,-23.46,-14.02,-1.87

SW076977,3.71,-1.53,1.09,0.15,-0.90,3.71,1.41,0.19,-13.25,-13.05,-13.15,-1.75

SW069841,-6.86,-4.45,-5.66,-0.75,-0.96,3.69,1.37,0.18,-0.62,-21.22,-10.92,-1.45

SW157192,-8.41,6.60,-0.90,-0.12,1.25,1.12,1.19,0.16,2.35,-13.12,-5.39,-0.72

SW082395,7.76,4.47,6.12,0.81,-4.73,7.08,1.17,0.16,-8.42,-2.55,-5.49,-0.73

SW060321,-15.88,-15.20,-15.54,-2.07,-0.43,2.70,1.13,0.15,-11.93,-19.33,-15.63,-2.08

SW159041,-14.87,-1.75,-8.31,-1.11,-0.04,1.61,0.79,0.10,-1.31,-13.80,-7.56,-1.01

SW003992,2.26,-3.51,-0.62,-0.08,-1.58,2.91,0.67,0.09,-6.80,-10.39,-8.60,-1.15

SW073604,-8.82,-10.80,-9.81,-1.31,-0.73,1.91,0.59,0.08,-8.44,-10.11,-9.28,-1.24

SW022809,-4.21,15.53,5.66,0.75,-1.66,2.79,0.56,0.08,4.99,-21.17,-8.09,-1.08

SW163176,-8.83,-3.42,-6.13,-0.82,0.51,0.28,0.39,0.05,-10.57,-7.85,-9.21,-1.23

SW011754,-19.16,-8.84,-14.00,-1.87,-0.49,1.23,0.37,0.05,-7.60,-11.67,-9.63,-1.28

SW190768,-8.25,-9.58,-8.91,-1.19,2.07,-1.75,0.16,0.02,-14.59,-8.78,-11.68,-1.56

SW147931,-9.46,10.33,0.43,0.06,4.32,-4.28,0.02,0.00,-11.53,-8.73,-10.13,-1.35

SW117716,-14.63,-6.34,-10.48,-1.40,-2.71,2.40,-0.16,-0.02,-21.98,-20.25,-21.12,-2.81

SW074763,-14.14,-7.58,-10.86,-1.45,-3.51,2.95,-0.28,-0.04,11.36,-16.72,-2.68,-0.36

SW126514,-6.32,-5.57,-5.94,-0.79,0.91,-2.55,-0.82,-0.11,-15.74,-19.37,-17.55,-2.34

SW128877,-10.11,-15.04,-12.58,-1.68,-1.47,-0.28,-0.88,-0.12,-17.90,-22.73,-20.31,-2.71

SW124081,-22.70,-9.24,-15.97,-2.13,-6.20,4.21,-1.00,-0.13,-2.19,-20.84,-11.51,-1.53

SW035588,-14.20,2.88,-5.66,-0.75,-2.61,0.48,-1.06,-0.14,-15.56,-20.43,-18.00,-2.40

SW160508,-20.97,-20.12,-20.54,-2.74,-0.69,-1.49,-1.09,-0.15,-9.71,-7.26,-8.48,-1.13

SW163135,-10.67,-5.63,-8.15,-1.09,-0.05,-2.42,-1.24,-0.16,-13.45,-15.16,-14.31,-1.91

SW081967,-3.24,2.18,-0.53,-0.07,-3.98,0.69,-1.64,-0.22,-8.25,-21.16,-14.70,-1.96

SW077252,-1.59,-5.49,-3.54,-0.47,-7.33,3.97,-1.68,-0.22,-19.54,-4.94,-12.24,-1.63

SW050238,-4.49,11.44,3.48,0.46,-3.43,-0.07,-1.75,-0.23,-2.54,-24.43,-13.49,-1.80

SW081969,-0.80,3.20,1.20,0.16,-3.87,0.03,-1.92,-0.26,-5.27,-25.55,-15.41,-2.05

SW129290,-8.56,-5.88,-7.22,-0.96,-1.61,-2.53,-2.07,-0.28,-14.83,-17.08,-15.96,-2.13

SW155115,-18.77,-9.91,-14.34,-1.91,-1.59,-3.17,-2.38,-0.32,-16.15,-14.20,-15.18,-2.02

SW113282,-11.92,-11.14,-11.53,-1.54,-4.29,-6.34,-5.31,-0.71,-13.22,-7.03,-10.12,-1.35

SW153629,-15.03,4.06,-5.48,-0.73,-6.56,-4.91,-5.74,-0.76,-6.22,-14.90,-10.56,-1.41

SW036227,-23.44,-12.35,-17.89,-2.38,-9.90,-4.68,-7.29,-0.97,-0.16,-26.80,-13.48,-1.80

SW163611,-4.78,-1.09,-2.94,-0.39,-9.71,-6.40,-8.06,-1.07,-15.43,-25.35,-20.39,-2.72

SW161990,34.27,24.79,29.53,3.93,-15.66,27.51,-15.66,-2.09,-0.10,1.07,0.49,0.06

Appendix B

Equations used for modeling

Table B.1: MEK1 non-processive model differential equations

$\frac{\delta[\text{MEKK}]}{\delta t}$	- k_1[MEKK][MEK1/SS] + k_{-2}[MEKK·MEK1/$\underline{\text{S}}$S] - k_1[MEKK][MEK1/SS] + k_1[MEKK][MEK1/SS] - k_1[MEKK][MEK1/S*S] + k_1[MEKK][MEK1/S*S] - k_1[MEKK][MEK1/SS*] + k_1[MEKK][MEK1/SS*] - k_{cat2}[MEKK·MEK1/$\underline{\text{S}}$S] - k_{deg}[MEKK]
$\frac{\delta[\text{MEK1/SS}]}{\delta t}$	- k_1[MEKK][MEK1/SS] + k_{-2}[MEKK·MEK1/$\underline{\text{S}}$S] - k_1[MEKK][MEK1/SS]
$\frac{\delta[\text{MEKK·MEK1/}\underline{\text{S}}\text{S}]}{\delta t}$	+ k_1[MEKK][MEK1/SS] - k_{-2}[MEKK·MEK1/$\underline{\text{S}}$S] - k_{cat2}[MEKK·MEK1/$\underline{\text{S}}$S]
$\frac{\delta[\text{MEK1/SS*}]}{\delta t}$	+ k_1[MEKK][MEK1/SS] - k_1[MEKK][MEK1/SS*]
$\frac{\delta[\text{MEK1/S*S}]}{\delta t}$	- k_1[MEKK][MEK1/S*S] + k_{cat2}[MEKK·MEK1/$\underline{\text{S}}$S]
$\frac{\delta[\text{MEK1/S*S*}]}{\delta t}$	+ k_1[MEKK][MEK1/S*S] + k_1[MEKK][MEK1/SS*]
$\frac{\delta[\text{MEKKD}]}{\delta t}$	+ k_{deg}[MEKK]

Table B.2: MEK1wt processive model differential equations

$\frac{\delta[\text{MEKK}]}{\delta t}$	- k_1[MEKK][MEK1/SS] - k_1[MEKK][MEK1/SS] - k_1[MEKK][MEK1/S*S] - k_1[MEKK][MEK1/SS*] + k_{-5}[MEKK·MEK1/$\underline{S}$S*] + k_{-4}[MEKK·MEK1/$\underline{S}$*S] - k_1[MEKK][MEK1/S*S] + k_{-3}[MEKK·MEK1/S$\underline{S}$*] + k_{cat4}[MEKK·MEK1/S*$\underline{S}$] + k_{cat3}[MEKK·MEK1/$\underline{S}$S*] - k_{deg}[MEKK]
$\frac{\delta[\text{MEK1/SS}]}{\delta t}$	- k_1[MEKK][MEK1/SS] - k_1[MEKK][MEK1/SS]
$\frac{\delta[\text{MEKK·MEK1/}\underline{S}\text{S}]}{\delta t}$	+ k_1[MEKK][MEK1/SS] - k_{cat2}[MEKK·MEK1/$\underline{S}$S]
$\frac{\delta[\text{MEKK·MEK1/S}\underline{S}\text{*}]}{\delta t}$	+ k_1[MEKK][MEK1/SS] - k_{-3}[MEKK·MEK1/S$\underline{S}$*]
$\frac{\delta[\text{MEK1/S*S}]}{\delta t}$	- k_1[MEKK][MEK1/S*S] + k_{-4}[MEKK·MEK1/$\underline{S}$*S] - k_1[MEKK][MEK1/S*S]
$\frac{\delta[\text{MEKK·MEK1/S*}\underline{S}]}{\delta t}$	+ k_1[MEKK][MEK1/S*S] + k_{pos1}[MEKK·MEK1/$\underline{S}$*S] - k_{cat4}[MEKK·MEK1/S*$\underline{S}$]
$\frac{\delta[\text{MEK1/SS*}]}{\delta t}$	- k_1[MEKK][MEK1/SS*] + k_{-5}[MEKK·MEK1/$\underline{S}$S*] + k_{-3}[MEKK·MEK1/S$\underline{S}$*]
$\frac{\delta[\text{MEKK·MEK1/}\underline{S}\text{S*}]}{\delta t}$	+ k_1[MEKK][MEK1/SS*] - k_{-5}[MEKK·MEK1/$\underline{S}$S*] - k_{cat3}[MEKK·MEK1/$\underline{S}$S*]
$\frac{\delta[\text{MEKK·MEK1/}\underline{S}\text{*S}]}{\delta t}$	- k_{-4}[MEKK·MEK1/$\underline{S}$*S] + k_1[MEKK][MEK1/S*S] - k_{pos1}[MEKK·MEK1/$\underline{S}$*S] + k_{cat2}[MEKK·MEK1/$\underline{S}$S]
$\frac{\delta[\text{MEK1/S*S*}]}{\delta t}$	+ k_{cat4}[MEKK·MEK1/S*$\underline{S}$] + k_{cat3}[MEKK·MEK1/$\underline{S}$S*]
$\frac{\delta[\text{MEKKD}]}{\delta t}$	+ k_{deg}[MEKK]

Table B.3: MEK1/F53S nonprocessive model differential equations

$\frac{\delta[\text{MEKK}]}{\delta t}$	- k_1[MEKK][MEK1/SS] + k_1[MEKK][MEK1/SS] - k_1[MEKK][MEK1/SS] + k_{-1}[MEKK·MEK1/S$\underline{\text{S}}$] - k_1[MEKK][MEK1/S*S] - k_1[MEKK][MEK1/SS*] + k_1[MEKK][MEK1/SS*] + k_{cat1}[MEKK·MEK1/S$\underline{\text{S}}$] + k_{cat4}[MEKK·MEK1/S*$\underline{\text{S}}$] - k_{deg}[MEKK]
$\frac{\delta[\text{MEK1/SS}]}{\delta t}$	- k_1[MEKK][MEK1/SS] - k_1[MEKK][MEK1/SS] + k_{-1}[MEKK·MEK1/S$\underline{\text{S}}$]
$\frac{\delta[\text{MEK1/S*S}]}{\delta t}$	+ k_1[MEKK][MEK1/SS] - k_1[MEKK][MEK1/S*S]
$\frac{\delta[\text{MEKK·MEK1/S}\underline{\text{S}}]}{\delta t}$	+ k_1[MEKK][MEK1/SS] - k_{-1}[MEKK·MEK1/S$\underline{\text{S}}$] - k_{cat1}[MEKK·MEK1/S$\underline{\text{S}}$]
$\frac{\delta[\text{MEKK·MEK1/S*}\underline{\text{S}}]}{\delta t}$	+ k_1[MEKK][MEK1/S*S] - k_{cat4}[MEKK·MEK1/S*$\underline{\text{S}}$]
$\frac{\delta[\text{MEK1/SS*}]}{\delta t}$	- k_1[MEKK][MEK1/SS*] + k_{cat1}[MEKK·MEK1/S$\underline{\text{S}}$]
$\frac{\delta[\text{MEK1/S*S*}]}{\delta t}$	+ k_1[MEKK][MEK1/SS*] + k_{cat4}[MEKK·MEK1/S*$\underline{\text{S}}$]
$\frac{\delta[\text{MEKKD}]}{\delta t}$	+ k_{deg}[MEKK]

Table B.4: MEK1/F53S processive model differential equations

$\frac{\delta[\text{MEKK}]}{\delta t}$	- k_1[MEKK][MEK1/SS] + k_1[MEKK][MEK1/SS] - k_1[MEKK][MEK1/SS] + k_{-1}[MEKK·MEK1/S$\underline{\text{S}}$] - k_1[MEKK][MEK1/S*S] - k_1[MEKK][MEK1/SS*] + k_1[MEKK][MEK1/SS*] + k_{-4}[MEKK·MEK1/$\underline{\text{S}}$*S] - k_1[MEKK][MEK1/S*S] + k_{cat1}[MEKK·MEK1/S$\underline{\text{S}}$] + k_{cat4}[MEKK·MEK1/S*$\underline{\text{S}}$] - k_{deg}[MEKK]
$\frac{\delta[\text{MEK1/SS}]}{\delta t}$	- k_1[MEKK][MEK1/SS] - k_1[MEKK][MEK1/SS] + k_{-1}[MEKK·MEK1/S$\underline{\text{S}}$]
$\frac{\delta[\text{MEK1/S*S}]}{\delta t}$	+ k_1[MEKK][MEK1/SS] - k_1[MEKK][MEK1/S*S] + k_{-4}[MEKK·MEK1/$\underline{\text{S}}$*S] - k_1[MEKK][MEK1/S*S]
$\frac{\delta[\text{MEKK·MEK1/S}\underline{\text{S}}]}{\delta t}$	+ k_1[MEKK][MEK1/SS] - k_{-1}[MEKK·MEK1/S$\underline{\text{S}}$] - k_{cat1}[MEKK·MEK1/S$\underline{\text{S}}$]
$\frac{\delta[\text{MEKK·MEK1/S*}\underline{\text{S}}]}{\delta t}$	+ k_1[MEKK][MEK1/S*S] + k_{pos1}[MEKK·MEK1/$\underline{\text{S}}$*S] - k_{cat4}[MEKK·MEK1/S*$\underline{\text{S}}$]
$\frac{\delta[\text{MEK1/SS*}]}{\delta t}$	- k_1[MEKK][MEK1/SS*] + k_{cat1}[MEKK·MEK1/S$\underline{\text{S}}$]
$\frac{\delta[\text{MEK1/S*S*}]}{\delta t}$	+ k_1[MEKK][MEK1/SS*] + k_{cat4}[MEKK·MEK1/S*$\underline{\text{S}}$]
$\frac{\delta[\text{MEKK·MEK1/}\underline{\text{S}}\text{*S}]}{\delta t}$	- k_{-4}[MEKK·MEK1/$\underline{\text{S}}$*S] + k_1[MEKK][MEK1/S*S] - k_{pos1}[MEKK·MEK1/$\underline{\text{S}}$*S]
$\frac{\delta[\text{MEKKD}]}{\delta t}$	+ k_{deg}[MEKK]

Table B.5: MEK1/F53L nonprocessive model differential equations

$\frac{\delta[\text{MEKK}]}{\delta t}$	- k_1[MEKK][MEK1/SS] + k_{-1}[MEKK·MEK1/S$\underline{\text{S}}$] - k_1[MEKK][MEK1/S*S] - k_1[MEKK][MEK1/SS*]+ k_1[MEKK][MEK1/SS*] + k_{cat1}[MEKK·MEK1/S$\underline{\text{S}}$] + k_{cat4}[MEKK·MEK1/S*$\underline{\text{S}}$] - k_{deg}[MEKK]
$\frac{\delta[\text{MEK1/SS}]}{\delta t}$	- k_1[MEKK][MEK1/SS] - k_1[MEKK][MEK1/SS] + k_{-1}[MEKK·MEK1/S$\underline{\text{S}}$]
$\frac{\delta[\text{MEK1/S*S}]}{\delta t}$	+ k_1[MEKK][MEK1/SS] - k_1[MEKK][MEK1/S*S]
$\frac{\delta[\text{MEKK·MEK1/S}\underline{\text{S}}]}{\delta t}$	+ k_1[MEKK][MEK1/SS] - k_{-1}[MEKK·MEK1/S$\underline{\text{S}}$] - k_{cat1}[MEKK·MEK1/S$\underline{\text{S}}$]
$\frac{\delta[\text{MEKK·MEK1/S*}\underline{\text{S}}]}{\delta t}$	+ k_1[MEKK][MEK1/S*S] - k_{cat4}[MEKK·MEK1/S*$\underline{\text{S}}$]
$\frac{\delta[\text{MEK1/SS*}]}{\delta t}$	- k_1[MEKK][MEK1/SS*] + k_{cat1}[MEKK·MEK1/S$\underline{\text{S}}$]
$\frac{\delta[\text{MEK1/S*S*}]}{\delta t}$	+ k_1[MEKK][MEK1/SS*] + k_{cat4}[MEKK·MEK1/S*$\underline{\text{S}}$]
$\frac{\delta[\text{MEKKD}]}{\delta t}$	+ k_{deg}[MEKK]

Table B.6: MEK1/F53L processive model differential equations

$\frac{\delta[\text{MEKK}]}{\delta t}$	- k_1[MEKK][MEK1/SS] - k_1[MEKK][MEK1/SS] + k_{-1}[MEKK·MEK1/S$\underline{\text{S}}$] - k_1[MEKK][MEK1/S*S] - k_1[MEKK][MEK1/SS*]+ k_1[MEKK][MEK1/SS*] + k_{-6}[MEKK·MEK1/$\underline{\text{S}}$*S] - k_1[MEKK][MEK1/S*S] + k_{cat1}[MEKK·MEK1/S$\underline{\text{S}}$] + k_{cat4}[MEKK·MEK1/S*$\underline{\text{S}}$] - k_{deg}[MEKK]
$\frac{\delta[\text{MEK1/SS}]}{\delta t}$	- k_1[MEKK][MEK1/SS] - k_1[MEKK][MEK1/SS] + k_{-1}[MEKK·MEK1/S$\underline{\text{S}}$]
$\frac{\delta[\text{MEKK·MEK1/}\underline{\text{S}}\text{*S}]}{\delta t}$	+k_1[MEKK][MEK1/SS] - k_{-6}[MEKK·MEK1/$\underline{\text{S}}$*S] + k_1[MEKK][MEK1/S*S] - k_{pos1}[MEKK·MEK1/$\underline{\text{S}}$*S]
$\frac{\delta[\text{MEKK·MEK1/S}\underline{\text{S}}]}{\delta t}$	+ k_1[MEKK][MEK1/SS] - k_{-1}[MEKK·MEK1/S$\underline{\text{S}}$] - k_{cat1}[MEKK·MEK1/S$\underline{\text{S}}$]
$\frac{\delta[\text{MEK1/S*S}]}{\delta t}$	- k_1[MEKK][MEK1/SS] + k_{-6}[MEKK·MEK1/$\underline{\text{S}}$*S] - k_1[MEKK][MEK1/S*S]
$\frac{\delta[\text{MEKK·MEK1/S*}\underline{\text{S}}]}{\delta t}$	+ k_1[MEKK][MEK1/S*S] + k_{pos1}[MEKK·MEK1/$\underline{\text{S}}$*S] - k_{cat4}[MEKK·MEK1/S*$\underline{\text{S}}$]
$\frac{\delta[\text{MEK1/SS*}]}{\delta t}$	- k_1[MEKK][MEK1/SS*] + k_{cat1}[MEKK·MEK1/S$\underline{\text{S}}$]
$\frac{\delta[\text{MEK1/S*S*}]}{\delta t}$	+ k_1[MEKK][MEK1/SS*] + k_{cat4}[MEKK·MEK1/S*$\underline{\text{S}}$]
$\frac{\delta[\text{MEKKD}]}{\delta t}$	+ k_{deg}[MEKK]

Table B.7: p38α phosphorylation by MEK6 differential equations

$\frac{\delta[\text{MEK6}]}{\delta t}$	$- k_1[\text{MEK6}][\text{p38}\alpha/\text{TY}] + k_1[\text{MEK6}][\text{p38}\alpha/\text{TY}] - k_1[\text{MEK6}][\text{p38}\alpha/\text{TY}] + k_{-2}[\text{MEK6}\cdot\text{p38}\alpha/\underline{\text{T}}\text{Y}] - k_1[\text{MEK6}][\text{p38}\alpha/\text{TY}^*] - k_1[\text{MEK6}][\text{p38}\alpha/\text{T}^*\text{Y}] + k_{-4}[\text{MEK6}\cdot\text{p38}\alpha/\text{T}^*\underline{\text{Y}}] + k_{\text{cat2}}[\text{MEK6}\cdot\text{p38}\alpha/\underline{\text{T}}\text{Y}] + k_{\text{cat3}}[\text{MEK6}\cdot\text{p38}\alpha/\underline{\text{T}}\text{Y}^*] + k_{\text{cat4}}[\text{MEK6}\cdot\text{p38}\alpha/\text{T}^*\underline{\text{Y}}]$
$\frac{\delta[\text{p38}\alpha/\text{TY}]}{\delta t}$	$- k_1[\text{MEK6}][\text{p38}\alpha/\text{TY}] - k_1[\text{MEK6}][\text{p38}\alpha/\text{TY}] + k_{-2}[\text{MEK6}\cdot\text{p38}\alpha/\underline{\text{T}}\text{Y}] - k_{\text{dis}}[\text{p38}\alpha/\text{TY}]$
$\frac{\delta[\text{p38}\alpha/\text{TY}^*]}{\delta t}$	$+ k_1[\text{MEK6}][\text{p38}\alpha/\text{TY}] - k_1[\text{MEK6}][\text{p38}\alpha/\text{TY}^*] - k_{\text{dis}}[\text{p38}\alpha/\text{TY}^*]$
$\frac{\delta[\text{MEK6}\cdot\text{p38}\alpha/\underline{\text{T}}\text{Y}]}{\delta t}$	$+ k_1[\text{MEK6}][\text{p38}\alpha/\text{TY}] - k_{-2}[\text{MEK6}\cdot\text{p38}\alpha/\underline{\text{T}}\text{Y}] - k_{\text{cat2}}[\text{MEK6}\cdot\text{p38}\alpha/\underline{\text{T}}\text{Y}]$
$\frac{\delta[\text{MEK6}\cdot\text{p38}\alpha/\underline{\text{T}}\text{Y}^*]}{\delta t}$	$+ k_1[\text{MEK6}][\text{p38}\alpha/\text{TY}^*] - k_{\text{cat3}}[\text{MEK6}\cdot\text{p38}\alpha/\underline{\text{T}}\text{Y}^*]$
$\frac{\delta[\text{p38}\alpha/\text{T}^*\text{Y}]}{\delta t}$	$- k_1[\text{MEK6}][\text{p38}\alpha/\text{T}^*\text{Y}] + k_{-4}[\text{MEK6}\cdot\text{p38}\alpha/\text{T}^*\underline{\text{Y}}] + k_{\text{cat2}}[\text{MEK6}\cdot\text{p38}\alpha/\underline{\text{T}}\text{Y}] - k_{\text{dis}}[\text{p38}\alpha/\text{T}^*\text{Y}]$
$\frac{\delta[\text{MEK6}\cdot\text{p38}\alpha/\text{T}^*\underline{\text{Y}}]}{\delta t}$	$+ k_1[\text{MEK6}][\text{p38}\alpha/\text{T}^*\text{Y}] - k_{-4}[\text{MEK6}\cdot\text{p38}\alpha/\text{T}^*\underline{\text{Y}}] - k_{\text{cat4}}[\text{MEK6}\cdot\text{p38}\alpha/\text{T}^*\underline{\text{Y}}]$
$\frac{\delta[\text{p38}\alpha/\text{T}^*\text{Y}^*]}{\delta t}$	$+ k_{\text{cat3}}[\text{MEK6}\cdot\text{p38}\alpha/\underline{\text{T}}\text{Y}^*] + k_{\text{cat4}}[\text{MEK6}\cdot\text{p38}\alpha/\text{T}^*\underline{\text{Y}}] - k_{\text{dis}}[\text{p38}\alpha/\text{T}^*\text{Y}^*]$
$\frac{\delta[\text{SUBooG}]}{\delta t}$	$+ k_{\text{dis}}[\text{p38}\alpha/\text{TY}]$
$\frac{\delta[\text{SUBpoG}]}{\delta t}$	$+ k_{\text{dis}}[\text{p38}\alpha/\text{T}^*\text{Y}]$
$\frac{\delta[\text{SUBopG}]}{\delta t}$	$+ k_{\text{dis}}[\text{p38}\alpha/\text{TY}^*]$
$\frac{\delta[\text{SUBppG}]}{\delta t}$	$+ k_{\text{dis}}[\text{p38}\alpha/\text{T}^*\text{Y}^*]$

Table B.8: ASK1 phosphorylation of MEK6 distributive model equations

$\frac{\delta[\text{ASK1}]}{\delta t}$	- k_1[ASK1][MEK6/ST] + k_{-1}[ASK1·MEK6/S$\underline{\text{T}}$] - k_1[ASK1][MEK6/ST*] + k_{-5}[ASK1·MEK6/$\underline{\text{S}}$T*] + k_{cat1}[ASK1·MEK6/S$\underline{\text{T}}$] + k_{cat3}[ASK1·MEK6/$\underline{\text{S}}$T*] - k_{dis}[ASK1]
$\frac{\delta[\text{MEK6/ST}]}{\delta t}$	- k_1[ASK1][MEK6/ST] + k_{-1}[ASK1·MEK6/S$\underline{\text{T}}$]
$\frac{\delta[\text{ASK1·MEK6/S}\underline{\text{T}}]}{\delta t}$	k_1[ASK1][MEK6/ST] - k_{-1}[ASK1·MEK6/S$\underline{\text{T}}$] - k_{cat1}[ASK1·MEK6/S$\underline{\text{T}}$]
$\frac{\delta[\text{MEK6/ST*}]}{\delta t}$	- k_1[ASK1][MEK6/ST*] + k_{-5}[ASK1·MEK6/$\underline{\text{S}}$T*] + k_{cat1}[ASK1·MEK6/S$\underline{\text{T}}$]
$\frac{\delta[\text{ASK1·MEK6/}\underline{\text{S}}\text{T*}]}{\delta t}$	+ k_1[ASK1][MEK6/ST*] - k_{-5}[ASK1·MEK6/$\underline{\text{S}}$T*] - k_{cat3}[ASK1·MEK6/$\underline{\text{S}}$T*]
$\frac{\delta[\text{MEK6/S*T*}]}{\delta t}$	+ k_1[ASK1][MEK6/S*T] + k_{cat3}[ASK1·MEK6/$\underline{\text{S}}$T*]
$\frac{\delta[\text{KIND}]}{\delta t}$	+ k_{dis}[ASK1]

Table B.9: ASK1 phosphorylation of MEK6 processive model equations

$\frac{\delta[\text{ASK1}]}{\delta t}$	- k_1[ASK1][MEK6/ST] - k_1[ASK1][MEK6/ST*] - k_1[ASK1][MEK6/ST*] + k_{-5}[ASK1·MEK6/$\underline{\text{S}}$T*] - k_1[ASK1][MEK6/S*T*]- k_1[ASK1][MEK6/S*T*] + k_{-8}[ASK1·MEK6/S*$\underline{\text{T}}$*] - k20[ASK1]
$\frac{\delta[\text{MEK6/ST}]}{\delta t}$	- k_1[ASK1][MEK6/ST]
$\frac{\delta[\text{ASK1·MEK6/S}\underline{\text{T}}]}{\delta t}$	+ k_1[ASK1][MEK6/ST] - k_{cat1}[ASK1·MEK6/S$\underline{\text{T}}$]
$\frac{\delta[\text{ASK1·MEK6/}\underline{\text{S}}\text{T*}]}{\delta t}$	+ k_{cat1}[ASK1·MEK6/S$\underline{\text{T}}$] + k_1[ASK1][MEK6/ST*] + k_1[ASK1][MEK6/ST*] - k_{-5}[ASK1·MEK6/$\underline{\text{S}}$T*] - k_{cat3}[ASK1·MEK6/$\underline{\text{S}}$T*]
$\frac{\delta[\text{MEK6/ST*}]}{\delta t}$	- k_1[ASK1][MEK6/ST*] - k_1[ASK1][MEK6/ST*] + k_{-5}[ASK1·MEK6/$\underline{\text{S}}$T*]
$\frac{\delta[\text{ASK1·MEK6/}\underline{\text{S}}\text{*T*}]}{\delta t}$	+ k_{cat3}[ASK1·MEK6/$\underline{\text{S}}$T*] + k_1[ASK1][MEK6/S*T*]
$\frac{\delta[\text{MEK6/S*T*}]}{\delta t}$	- k_1[ASK1][MEK6/S*T*] - k_1[ASK1][MEK6/S*T*] + k_{-8}[ASK1·MEK6/S*$\underline{\text{T}}$*]
$\frac{\delta[\text{ASK1·MEK6/S}\underline{\text{T}}\text{*}]}{\delta t}$	+ k_1[ASK1][MEK6/S*T*] - k_{-8}[ASK1·MEK6/S*$\underline{\text{T}}$*]
$\frac{\delta[\text{KIND}]}{\delta t}$	+ k_{dis}[ASK1]

References

[1] Zhu Chen, Tara Beers Gibson, Fred Robinson, Loraine Silvestro, Gray Pearson, Bing-e Xu, Angelique Wright, Colleen Vanderbilt, and Melanie H Cobb. Map kinases. *Chemical reviews*, 101(8):2449–2476, 2001.

[2] Chi-Ying Huang and James E Ferrell. Ultrasensitivity in the mitogen-activated protein kinase cascade. *Proceedings of the National Academy of Sciences*, 93(19):10078–10083, 1996.

[3] Michel Janicot and M Daniel Lane. Activation of glucose uptake by insulin and insulin-like growth factor i in xenopus oocytes. *Proceedings of the National Academy of Sciences*, 86(8):2642–2646, 1989.

[4] WJ Malaisse. Insulin secretion: multifactorial regulation for a single process of release. *Diabetologia*, 9(3):167–173, 1973.

[5] Timothy AJ Haystead, Paul Dent, Jie Wu, Clare MM Haystead, and Thomas W Sturgill. Ordered phosphorylation of p42 mapk by map kinase kinase. *FEBS letters*, 306(1):17–22, 1992.

[6] James E Ferrell and Ramesh R Bhatt. Mechanistic studies of the dual phosphorylation of mitogen-activated protein kinase. *Journal of Biological Chemistry*, 272(30):19008–19016, 1997.

[7] David J Robbins, Erzhen Zhen, Hajime Owaki, Colleen A Vanderbilt, Douglas Ebert, Thomas D Geppert, and Melanie H Cobb. Regulation and properties of extracellular signal-regulated protein kinases 1 and 2 in vitro. *Journal of Biological Chemistry*, 268 (7):5097–5106, 1993.

[8] Carlos Salazar and Thomas Höfer. Versatile regulation of multisite protein phosphorylation by the order of phosphate processing and protein–protein interactions. *FEBS journal*, 274(4):1046–1061, 2007.

[9] Donald K Blumenthal, Koji Takio, Arthur M Edelman, Harry Charbonneau, Koiti Titani, Kenneth A Walsh, and Edwin G Krebs. Identification of the calmodulin-binding domain of skeletal muscle myosin light chain kinase. *Proceedings of the National Academy of Sciences*, 82(10):3187–3191, 1985.

[10] Jonathan Goldberg, Angus C Nairn, and John Kuriyan. Structural basis for the autoinhibition of calcium/calmodulin-dependent protein kinase i. *Cell*, 84(6):875–887, 1996.

[11] Nick I Markevich, Jan B Hoek, and Boris N Kholodenko. Signaling switches and bistability arising from multisite phosphorylation in protein kinase cascades. *The Journal of cell biology*, 164(3):353–359, 2004.

[12] Jeremy Gunawardena. Multisite protein phosphorylation makes a good threshold but can be a poor switch. *Proceedings of the National Academy of Sciences of the United States of America*, 102(41):14617–14622, 2005.

[13] Michele Hutchison, Kevin S Berman, and Melanie H Cobb. Isolation of tao1, a protein kinase that activates meks in stress-activated protein kinase cascades. *Journal of Biological Chemistry*, 273(44):28625–28632, 1998.

[14] Syu-ichi Hirai, Kumi Noda, Tetsuo Moriguchi, Eisuke Nishida, Akio Yamashita, Tetsuya Deyama, Keiko Fukuyama, and Shigeo Ohno. Differential activation of two jnk activators, mkk7 and sek1, by mkn28-derived nonreceptor serine/threonine kinase/mixed lineage kinase 2. *Journal of Biological Chemistry*, 273(13):7406–7412, 1998.

[15] Lee Anne Tibbles, YL Ing, F Kiefer, J Chan, N Iscove, JR Woodgett, and NJ Lassam. Mlk-3 activates the sapk/jnk and p38/rk pathways via sek1 and mkk3/6. *The EMBO journal*, 15(24):7026, 1996.

[16] Zhu Chen, Michele Hutchison, and Melanie H Cobb. Isolation of the protein kinase tao2 and identification of its mitogen-activated protein kinase/extracellular signal-regulated kinase kinase binding domain. *Journal of Biological Chemistry*, 274(40):28803–28807, 1999.

[17] Zhu Chen and Melanie H Cobb. Regulation of stress-responsive mitogen-activated protein (map) kinase pathways by tao2. *Journal of Biological Chemistry*, 276(19): 16070–16075, 2001.

[18] Zhu Chen, Malavika Raman, Linda Chen, Sheu Fen Lee, Alfred G Gilman, and Melanie H Cobb. Tao (thousand-and-one amino acid) protein kinases mediate signaling from carbachol to p38 mitogen-activated protein kinase and ternary complex factors. *Journal of Biological Chemistry*, 278(25):22278–22283, 2003.

[19] Costas Mitsopoulos, Ceniz Zihni, Ritu Garg, Anne J Ridley, and Jonathan DH Morris. The prostate-derived sterile 20-like kinase (psk) regulates microtubule organization and stability. *Journal of Biological Chemistry*, 278(20):18085–18091, 2003.

[20] Ceniz Zihni, Costas Mitsopoulos, Ignatius A Tavares, Buzz Baum, Anne J Ridley, and Jonathan DH Morris. Prostate-derived sterile 20-like kinase 1-α induces apoptosis jnk- and caspase-dependent nuclear localization is a requirement for membrane blebbing. *Journal of Biological Chemistry*, 282(9):6484–6493, 2007.

[21] Ravinesh A Kumar, Christian R Marshall, Judith A Badner, Timothy D Babatz, Zohar Mukamel, Kimberly A Aldinger, Jyotsna Sudi, Camille W Brune, Gerald Goh, Samer

KaraMohamed, et al. Association and mutation analyses of 16p11. 2 autism candidate genes. *PloS one*, 4(2):e4582, 2009.

[22] Froylan Calderon de Anda, Ana Lucia Rosario, Omer Durak, Tracy Tran, Johannes Gräff, Konstantinos Meletis, Damien Rei, Takahiro Soda, Ram Madabhushi, David D Ginty, et al. Autism spectrum disorder susceptibility gene taok2 affects basal dendrite formation in the neocortex. *Nature neuroscience*, 15(7):1022–1031, 2012.

[23] Ignatius A Tavares, Dona Touma, Steven Lynham, Claire Troakes, Megan Schober, Mirsada Causevic, Ritu Garg, Wendy Noble, Richard Killick, Istvan Bodi, et al. Prostate-derived sterile 20-like kinases (psks/taoks) phosphorylate tau protein and are activated in tangle-bearing neurons in alzheimer disease. *Journal of Biological Chemistry*, 288(21):15418–15429, 2013.

[24] Angelique W Whitehurst, Brian O Bodemann, Jessica Cardenas, Deborah Ferguson, Luc Girard, Michael Peyton, John D Minna, Carolyn Michnoff, Weihua Hao, Michael G Roth, et al. Synthetic lethal screen identification of chemosensitizer loci in cancer cells. *Nature*, 446(7137):815–819, 2007.

[25] Tianjun Zhou, Malavika Raman, Yan Gao, Svetlana Earnest, Zhu Chen, Mischa Machius, Melanie H Cobb, and Elizabeth J Goldsmith. Crystal structure of the tao2 kinase domain: activation and specificity of a ste20p map3k. *Structure*, 12(10):1891–1900, 2004.

[26] Tian-Jun ZHOU, Li-Guang SUN, Yan Gao, and Elizabeth J Goldsmith. Crystal structure of the map3k tao2 kinase domain bound by an inhibitor staurosporine. *Acta biochimica et biophysica Sinica*, 38(6):385–392, 2006.

[27] Radha Akella, Thomas M Moon, and Elizabeth J Goldsmith. Unique map kinase

binding sites. *Biochimica et Biophysica Acta (BBA)-Proteins and Proteomics*, 1784 (1):48–55, 2008.

[28] Alexander T Piala, Thomas M Moon, Radha Akella, Haixia He, Melanie H Cobb, and Elizabeth J Goldsmith. Chloride sensing by wnk1 involves inhibition of autophosphorylation. *Science signaling*, 7(324):ra41–ra41, 2014.

[29] John M Russell. Sodium-potassium-chloride cotransport. *Physiological Reviews*, 80(1): 211–276, 2000.

[30] Kristopher T Kahle, Jesse Rinehart, and Richard P Lifton. Phosphoregulation of the na–k–2cl and k–cl cotransporters by the wnk kinases. *Biochimica et Biophysica Acta (BBA)-Molecular Basis of Disease*, 1802(12):1150–1158, 2010.

[31] Max Salomonsson, ERNESTO Gonzalez, Per Westerlund, and AE Persson. Chloride concentration in macula densa and cortical thick ascending limb cells. *Kidney international. Supplement*, 32:S51–4, 1991.

[32] Christophe Pellegrino, Olena Gubkina, Michael Schaefer, Hélène Becq, Anastasia Ludwig, Marat Mukhtarov, Ilona Chudotvorova, Severine Corby, Yuriy Salyha, Sergey Salozhin, et al. Knocking down of the kcc2 in rat hippocampal neurons increases intracellular chloride concentration and compromises neuronal survival. *The Journal of physiology*, 589(10):2475–2496, 2011.

[33] Hiroaki Miyazaki, Atsushi Shiozaki, Naomi Niisato, and Yoshinori Marunaka. Physiological significance of hypotonicity-induced regulatory volume decrease: reduction in intracellular cl- concentration acting as an intracellular signaling. *American Journal of Physiology-Renal Physiology*, 292(5):F1411–F1417, 2007.

[34] Rumi Ohsawa, Hiroaki Miyazaki, Naomi Niisato, Atsushi Shiozaki, Yoshinobu Iwasaki, Eigo Otsuji, and Yoshinori Marunaka. Intracellular chloride regulates cell proliferation

through the activation of stress-activated protein kinases in mkn28 human gastric cancer cells. *Journal of cellular physiology*, 223(3):764–770, 2010.

[35] William B Guggino and Bruce A Stanton. New insights into cystic fibrosis: molecular switches that regulate cftr. *Nature reviews Molecular cell biology*, 7(6):426–436, 2006.

[36] Mary Chebib and Graham AR Johnston. The 'abc'of gaba receptors: a brief review. *Clinical and experimental pharmacology and physiology*, 26(11):937–940, 1999.

[37] Michael R Dorwart, Nikolay Shcheynikov, Dongki Yang, and Shmuel Muallem. The solute carrier 26 family of proteins in epithelial ion transport. *Physiology*, 23(2):104–114, 2008.

[38] Raimund Dutzler, Ernest B Campbell, Martine Cadene, Brian T Chait, and Roderick MacKinnon. X-ray structure of a clc chloride channel at 3.0 å reveals the molecular basis of anion selectivity. *Nature*, 415(6869):287–294, 2002.

[39] Haruo Ogawa, Yue Qiu, John S Philo, Tsutomu Arakawa, Craig M Ogata, and Kunio S Misono. Reversibly bound chloride in the atrial natriuretic peptide receptor hormone-binding domain: Possible allosteric regulation and a conserved structural motif for the chloride-binding site. *Protein Science*, 19(3):544–557, 2010.

[40] Andreas G Tzakos, Athanassios S Galanis, Georgios A Spyroulias, Paul Cordopatis, Evy Manessi-Zoupa, and Ioannis P Gerothanassis. Structure–function discrimination of the n-and c-catalytic domains of human angiotensin-converting enzyme: implications for cl–activation and peptide hydrolysis mechanisms. *Protein engineering*, 16(12):993–1003, 2003.

[41] Ravi Pokhrel, Iain L McConnell, and Gary W Brudvig. Chloride regulation of enzyme turnover: application to the role of chloride in photosystem ii. *Biochemistry*, 50(14): 2725–2734, 2011.

[42] Sotiria Tavoulari, Ahsan N Rizwan, Lucy R Forrest, and Gary Rudnick. Reconstructing a chloride-binding site in a bacterial neurotransmitter transporter homologue. *Journal of Biological Chemistry*, 286(4):2834–2842, 2011.

[43] Max F Perutz, Daniel T-b Shih, and David Williamson. The chloride effect in human haemoglobin: a new kind of allosteric mechanism. *Journal of molecular biology*, 239 (4):555–560, 1994.

[44] Xiantao Li, Alexei Surguchev, Shumin Bian, Dhasakumar Navaratnam, and Joseph Santos-Sacchi. Extracellular chloride regulation of kv2. 1, contributor to the major outward kv current in mammalian outer hair cells. *American Journal of Physiology-Cell Physiology*, 302(1):C296–C306, 2012.

[45] Pitchai Sangan, Vazhaikkurichi M Rajendran, John P Geibel, and Henry J Binder. Cloning and expression of a chloride-dependent na+-h+ exchanger. *Journal of Biological Chemistry*, 277(12):9668–9675, 2002.

[46] Gerardo Gamba. Molecular physiology and pathophysiology of electroneutral cation-chloride cotransporters. *Physiological reviews*, 85(2):423–493, 2005.

[47] CHRISTIAN Lytle and B Forbush. Regulatory phosphorylation of the secretory na-k-cl cotransporter: modulation by cytoplasmic cl. *American Journal of Physiology-Cell Physiology*, 270(2):C437–C448, 1996.

[48] CHRISTIAN Lytle and B Forbush. Na-k-cl cotransport in the shark rectal gland. ii. regulation in isolated tubules. *American Journal of Physiology-Cell Physiology*, 262 (4):C1009–C1017, 1992.

[49] Diana Pacheco-Alvarez, Pedro San Cristóbal, Patricia Meade, Erika Moreno, Norma Vazquez, Eva Muñoz, Abigail Díaz, María Eugenia Juárez, Ignacio Giménez, and Gerardo Gamba. The na+: Cl–cotransporter is activated and phosphorylated at the

amino-terminal domain upon intracellular chloride depletion. *Journal of Biological Chemistry*, 281(39):28755–28763, 2006.

[50] MICHAEL L Jennings and RICHARD K Schulz. Okadaic acid inhibition of kcl cotransport. evidence that protein dephosphorylation is necessary for activation of transport by either cell swelling or n-ethylmaleimide. *The Journal of General Physiology*, 97(4): 799–817, 1991.

[51] Mark Haas and Bliss Forbush III. The na-k-cl cotransporter of secretory epithelia. *Annual Review of Physiology*, 62(1):515–534, 2000.

[52] Christian Lytle and Thomas McManus. Coordinate modulation of na-k-2cl cotransport and k-cl cotransport by cell volume and chloride. *American Journal of Physiology-Cell Physiology*, 283(5):C1422–C1431, 2002.

[53] Mark Haas, Donna McBrayer, and Christian Lytle. [cl-] i-dependent phosphorylation of the na-k-cl cotransport protein of dog tracheal epithelial cells. *Journal of Biological Chemistry*, 270(48):28955–28961, 1995.

[54] Bing-e Xu, Jessie M English, Julie L Wilsbacher, Steve Stippec, Elizabeth J Goldsmith, and Melanie H Cobb. Wnk1, a novel mammalian serine/threonine protein kinase lacking the catalytic lysine in subdomain ii. *Journal of Biological Chemistry*, 275(22): 16795–16801, 2000.

[55] Xiaoshan Min, Byung-Hoon Lee, Melanie H Cobb, and Elizabeth J Goldsmith. Crystal structure of the kinase domain of wnk1, a kinase that causes a hereditary form of hypertension. *Structure*, 12(7):1303–1311, 2004.

[56] Fatima Verissimo and Peter Jordan. Wnk kinases, a novel protein kinase subfamily in multi-cellular organisms. *Oncogene*, 20(39):5562–5569, 2001.

[57] Frederick H Wilson, Sandra Disse-Nicodeme, Keith A Choate, Kazuhiko Ishikawa, Carol Nelson-Williams, Isabelle Desitter, Murat Gunel, David V Milford, Graham W Lipkin, Jean-Michel Achard, et al. Human hypertension caused by mutations in wnk kinases. *Science*, 293(5532):1107–1112, 2001.

[58] Henny H Lemmink, Nine VAM Knoers, Lothar Károlyi, Henk van Dijk, Patrick Niaudet, Corinne Antignac, Lisa M Guay-Woodford, Paul R Goodyer, Jean-Claude Carel, Ad Hermes, et al. Novel mutations in the thiazide-sensitive nacl cotransporter gene in patients with gitelman syndrome with predominant localization to the c-terminal domain. *Kidney international*, 54(3):720–730, 1998.

[59] Kerstin Piechotta, Jianming Lu, and Eric Delpire. Cation chloride cotransporters interact with the stress-related kinases ste20-related proline-alanine-rich kinase (spak) and oxidative stress response 1 (osr1). *Journal of Biological Chemistry*, 277(52):50812–50819, 2002.

[60] Brian FX Dowd and Biff Forbush. Pask (proline-alanine-rich ste20-related kinase), a regulatory kinase of the na-k-cl cotransporter (nkcc1). *Journal of Biological Chemistry*, 278(30):27347–27353, 2003.

[61] Anna Zagórska, Eulalia Pozo-Guisado, Jérôme Boudeau, Alberto C Vitari, Fatema H Rafiqi, Jacob Thastrup, Maria Deak, David G Campbell, Nick A Morrice, Alan R Prescott, et al. Regulation of activity and localization of the wnk1 protein kinase by hyperosmotic stress. *The Journal of cell biology*, 176(1):89–100, 2007.

[62] Anthony N Anselmo, Svetlana Earnest, Wei Chen, Yu-Chi Juang, Sung Chan Kim, Yingming Zhao, and Melanie H Cobb. Wnk1 and osr1 regulate the na+, k+, 2cl- cotransporter in hela cells. *Proceedings of the National Academy of Sciences*, 103(29): 10883–10888, 2006.

[63] Ciaran Richardson, Fatema H Rafiqi, Håkan KR Karlsson, Ntsane Moleleki, Alain Vandewalle, David G Campbell, Nick A Morrice, and Dario R Alessi. Activation of the thiazide-sensitive na+-cl–cotransporter by the wnk-regulated kinases spak and osr1. *Journal of cell science*, 121(5):675–684, 2008.

[64] Alberto# x00a0c Vitari, Maria Deak, Nick# x00a0a Morrice, and Dario# x00a0r Alessi. The wnk1 and wnk4 protein kinases that are mutated in gordon's hypertension syndrome phosphorylate and activate spak and osr1 protein kinases. *Biochem. J*, 391: 17–24, 2005.

[65] Tetsuo Moriguchi, Seiichi Urushiyama, Naoki Hisamoto, Shun-ichiro Iemura, Shinichi Uchida, Tohru Natsume, Kunihiro Matsumoto, and Hiroshi Shibuya. Wnk1 regulates phosphorylation of cation-chloride-coupled cotransporters via the ste20-related kinases, spak and osr1. *Journal of Biological Chemistry*, 280(52):42685–42693, 2005.

[66] Aaron M Ring, Sam X Cheng, Qiang Leng, Kristopher T Kahle, Jesse Rinehart, Maria D Lalioti, Heather M Volkman, Frederick H Wilson, Steven C Hebert, and Richard P Lifton. Wnk4 regulates activity of the epithelial na+ channel in vitro and in vivo. *Proceedings of the National Academy of Sciences*, 104(10):4020–4024, 2007.

[67] Bing-e Xu, Steve Stippec, Ahmed Lazrak, Chou-Long Huang, and Melanie H Cobb. Wnk1 activates sgk1 by a phosphatidylinositol 3-kinase-dependent and non-catalytic mechanism. *Journal of Biological Chemistry*, 280(40):34218–34223, 2005.

[68] Christophe Debonneville, Sandra Y Flores, Elena Kamynina, Pamela J Plant, Caroline Tauxe, Marc A Thomas, Carole Münster, Ahmed Chraïbi, J Howard Pratt, Jean-Daniel Horisberger, et al. Phosphorylation of nedd4-2 by sgk1 regulates epithelial na+ channel cell surface expression. *The EMBO journal*, 20(24):7052–7059, 2001.

[69] Bing-e Xu, Steve Stippec, Po-Yin Chu, Ahmed Lazrak, Xin-Ji Li, Byung-Hoon Lee, Jessie M English, Bernardo Ortega, Chou-Long Huang, and Melanie H Cobb. Wnk1 activates sgk1 to regulate the epithelial sodium channel. *Proceedings of the National Academy of Sciences of the United States of America*, 102(29):10315–10320, 2005.

[70] Hao-Ran Wang, Zhen Liu, and Chou-Long Huang. Domains of wnk1 kinase in the regulation of romk1. *American Journal of Physiology-Renal Physiology*, 295(2):F438–F445, 2008.

[71] Kristopher T Kahle, Frederick H Wilson, Qiang Leng, Maria D Lalioti, Anthony D O'Connell, Ke Dong, Alicia K Rapson, Gordon G MacGregor, Gerhard Giebisch, Steven C Hebert, et al. Wnk4 regulates the balance between renal nacl reabsorption and k+ secretion. *Nature genetics*, 35(4):372–376, 2003.

[72] Akihito Ohta, Sung-Sen Yang, Tatemitsu Rai, Motoko Chiga, Sei Sasaki, and Shinichi Uchida. Overexpression of human wnk1 increases paracellular chloride permeability and phosphorylation of claudin-4 in mdckii cells. *Biochemical and biophysical research communications*, 349(2):804–808, 2006.

[73] Hyun Woo Park, Joo Young Kim, Soo-Kyoung Choi, Young-Ho Lee, Weizhong Zeng, Kyung Hwan Kim, Shmuel Muallem, and Min Goo Lee. Serine-threonine kinase with-no-lysine 4 (wnk4) controls blood pressure via transient receptor potential canonical 3 (trpc3) in the vasculature. *Proceedings of the National Academy of Sciences*, 108(26): 10750–10755, 2011.

[74] José Ponce-Coria, Pedro San-Cristobal, Kristopher T Kahle, Norma Vazquez, Diana Pacheco-Alvarez, Paola de Los Heros, Patricia Juárez, Eva Muñoz, Gabriela Michel, Norma A Bobadilla, et al. Regulation of nkcc2 by a chloride-sensing mechanism involving the wnk3 and spak kinases. *Proceedings of the National Academy of Sciences*, 105(24):8458–8463, 2008.

[75] Kristopher T Kahle, Jesse Rinehart, Paola de Los Heros, Angeliki Louvi, Patricia Meade, Norma Vazquez, Steven C Hebert, Gerardo Gamba, Ignacio Gimenez, and Richard P Lifton. Wnk3 modulates transport of cl-in and out of cells: implications for control of cell volume and neuronal excitability. *Proceedings of the National Academy of Sciences of the United States of America*, 102(46):16783–16788, 2005.

[76] Silvia Cruz-Rangel, Gerardo Gamba, Gerardo Ramos-Mandujano, and Herminia Pasantes-Morales. Influence of wnk3 on intracellular chloride concentration and volume regulation in hek293 cells. *Pflügers Archiv-European Journal of Physiology*, 464 (3):317–330, 2012.

[77] Jesse Rinehart, Norma Vázquez, Kristopher T Kahle, Caleb A Hodson, Aaron M Ring, Erol E Gulcicek, Angeliki Louvi, Norma A Bobadilla, Gerardo Gamba, and Richard P Lifton. Wnk2 kinase is a novel regulator of essential neuronal cation-chloride cotransporters. *Journal of Biological Chemistry*, 286(34):30171–30180, 2011.

[78] Diana Pacheco-Alvarez and Gerardo Gamba. Wnk3 is a putative chloride-sensing kinase. *Cellular Physiology and Biochemistry*, 28(6):1123–1134, 2011.

[79] Marina Bukhtiyarova, Katrina Northrop, Xiaomei Chai, David Casper, Michael Karpusas, and Eric Springman. Improved expression, purification, and crystallization of p38α map kinase. *Protein expression and purification*, 37(1):154–161, 2004.

[80] Xiaoshan Min, Radha Akella, Haixia He, John M Humphreys, Susan E Tsutakawa, Seung-Jae Lee, John A Tainer, Melanie H Cobb, and Elizabeth J Goldsmith. The structure of the map2k mek6 reveals an autoinhibitory dimer. *Structure*, 17(1):96–104, 2009.

[81] Gabor Bunkoczi, Eidarus Salah, Panagis Filippakopoulos, Oleg Fedorov, Susanne Müller, Frank Sobott, Sirlester A Parker, Haifeng Zhang, Wang Min, Benjamin E

Turk, et al. Structural and functional characterization of the human protein kinase ask1. *Structure*, 15(10):1215–1226, 2007.

[82] Zbyszek Otwinowski, Wladek Minor, and Charles Carter W Jr. Processing of x-ray diffraction data collected in oscillation mode. 1997.

[83] Computational Project Collaborative et al. The ccp4 suite: programs for protein crystallography. *Acta crystallographica. Section D, Biological crystallography*, 50(Pt 5):760, 1994.

[84] Paul Emsley, Bernhart Lohkamp, William G Scott, and Kevin Cowtan. Features and development of coot. *Acta Crystallographica Section D: Biological Crystallography*, 66 (4):486–501, 2010.

[85] Lisa Y Lenertz, Byung-Hoon Lee, Xiaoshan Min, Bing-e Xu, Kyle Wedin, Svetlana Earnest, Elizabeth J Goldsmith, and Melanie H Cobb. Properties of wnk1 and implications for other family members. *Journal of Biological Chemistry*, 280(29):26653–26658, 2005.

[86] Michael W Pantoliano, Eugene C Petrella, Joseph D Kwasnoski, Victor S Lobanov, James Myslik, Edward Graf, Ted Carver, Eric Asel, Barry A Springer, Pamela Lane, et al. High-density miniaturized thermal shift assays as a general strategy for drug discovery. *Journal of biomolecular screening*, 6(6):429–440, 2001.

[87] Bing-e Xu, Xiaoshan Min, Steve Stippec, Byung-Hoon Lee, Elizabeth J Goldsmith, and Melanie H Cobb. Regulation of wnk1 by an autoinhibitory domain and autophosphorylation. *Journal of Biological Chemistry*, 277(50):48456–48462, 2002.

[88] Michael Pusch, Uwe Ludewig, Annett Rehfeldt, and Thomas J Jentsch. Gating of the voltage-dependent chloride channel cic-0 by the permeant anion. 1995.

[89] Tsung-Yu Chen and Christopher Miller. Nonequilibrium gating and voltage dependence of the clc-0 cl-channel. *The Journal of General Physiology*, 108(4):237–250, 1996.

[90] Choel Kim, Cecilia Y Cheng, S Adrian Saldanha, and Susan S Taylor. Pka-i holoenzyme structure reveals a mechanism for camp-dependent activation. *Cell*, 130(6): 1032–1043, 2007.

[91] Boštjan Kobe, Jörg Heierhorst, Susanne C Feil, Michael W Parker, Guy M Benian, Klaudiusz R Weiss, and Bruce E Kemp. Giant protein kinases: domain interactions and structural basis of autoregulation. *The EMBO journal*, 15(24):6810, 1996.

[92] Albert Goldbeter and Daniel E Koshland. An amplified sensitivity arising from covalent modification in biological systems. *Proceedings of the National Academy of Sciences*, 78(11):6840–6844, 1981.

[93] Xinfeng Liu, Lee Bardwell, and Qing Nie. A combination of multisite phosphorylation and substrate sequestration produces switchlike responses. *Biophysical journal*, 98(8): 1396–1407, 2010.

[94] JOHN C Parker. In defense of cell volume? *American Journal of Physiology-Cell Physiology*, 265(5):C1191–C1200, 1993.

[95] Rachel B Darman, Andreas Flemmer, and Biff Forbush. Modulation of ion transport by direct targeting of protein phosphatase type 1 to the na-k-cl cotransporter. *Journal of Biological Chemistry*, 276(37):34359–34362, 2001.

[96] Mark Glover, Annie Mercier Zuber, Nikki Figg, and Kevin M O'Shaughnessy. The activity of the thiazide-sensitive na+-cl-cotransporter is regulated by protein phosphatase pp4. *Canadian journal of physiology and pharmacology*, 88(10):986–995, 2010.

[97] Alexander T Piala, John M Humphreys, and Elizabeth J Goldsmith. Map kinase modules: The excursion model and the steps that count. *Biophysical journal*, 107(9): 2006–2015, 2014.

[98] Albeter Goldbeter and DE Koshland. Ultrasensitivity in biochemical systems controlled by covalent modification. interplay between zero-order and multistep effects. *Journal of Biological Chemistry*, 259(23):14441–14447, 1984.

[99] Stefan Legewie, Birgit Schoeberl, Nils Blüthgen, and Hanspeter Herzel. Competing docking interactions can bring about bistability in the mapk cascade. *Biophysical journal*, 93(7):2279–2288, 2007.

[100] Maria E Arcila, Alexander Drilon, Brooke E Sylvester, Christine M Lovly, Laetitia Borsu, Boris Reva, Mark G Kris, David B Solit, and Marc Ladanyi. Map2k1 (mek1) mutations define a distinct subset of lung adenocarcinoma associated with smoking. *Clinical Cancer Research*, pages clincanres–2124, 2014.

[101] Pablo Rodriguez-Viciana, Osamu Tetsu, William E Tidyman, Anne L Estep, Brenda A Conger, Molly Santa Cruz, Frank McCormick, and Katherine A Rauen. Germline mutations in genes within the mapk pathway cause cardio-facio-cutaneous syndrome. *Science*, 311(5765):1287–1290, 2006.

[102] Petr Kuzmič. Program dynafit for the analysis of enzyme kinetic data: application to hiv proteinase. *Analytical biochemistry*, 237(2):260–273, 1996.

[103] Petr Kuzmič. Application of the van slyke–cullen irreversible mechanism in the analysis of enzymatic progress curves. *Analytical biochemistry*, 394(2):287–289, 2009.

[104] Aki Fujioka, Kenta Terai, Reina E Itoh, Kazuhiro Aoki, Takeshi Nakamura, Shinya Kuroda, Eisuke Nishida, and Michiyuki Matsuda. Dynamics of the ras/erk mapk

cascade as monitored by fluorescent probes. *Journal of biological chemistry*, 281(13): 8917–8926, 2006.

[105] Yuan-Yuan Zhang, Zi-Qing Mei, Jia-Wei Wu, and Zhi-Xin Wang. Enzymatic activity and substrate specificity of mitogen-activated protein kinase p38α in different phosphorylation states. *Journal of Biological Chemistry*, 283(39):26591–26601, 2008.

[106] Kazuhiro Aoki, Masashi Yamada, Katsuyuki Kunida, Shuhei Yasuda, and Michiyuki Matsuda. Processive phosphorylation of erk map kinase in mammalian cells. *Proceedings of the National Academy of Sciences*, 108(31):12675–12680, 2011.

[107] Upinder S Bhalla. Signaling in small subcellular volumes. i. stochastic and diffusion effects on individual pathways. *Biophysical journal*, 87(2):733–744, 2004.

[108] Birgit Schoeberl, Claudia Eichler-Jonsson, Ernst Dieter Gilles, and Gertraud Müller. Computational modeling of the dynamics of the map kinase cascade activated by surface and internalized egf receptors. *Nature biotechnology*, 20(4):370–375, 2002.

[109] Satoru Sasagawa, Yu-ichi Ozaki, Kazuhiro Fujita, and Shinya Kuroda. Prediction and validation of the distinct dynamics of transient and sustained erk activation. *Nature cell biology*, 7(4):365–373, 2005.

[110] Frances A Brightman and David A Fell. Differential feedback regulation of the mapk cascade underlies the quantitative differences in egf and ngf signalling in pc12 cells. *FEBS letters*, 482(3):169–174, 2000.

[111] Mariko Hatakeyama, Shuhei Kimura, Takashi Naka, Takuji Kawasaki, Noriko Yumoto, Mio Ichikawa, J Kim, Kazuki Saito, Mihoro Saeki, Mikako Shirouzu, et al. A computational model on the modulation of mitogen-activated protein kinase (mapk) and akt pathways in heregulin-induced erbb signalling. *Biochem. J*, 373:451–463, 2003.

[112] Rana Dajani, Elizabeth Fraser, S Mark Roe, Neville Young, Valerie Good, Trevor C Dale, and Laurence H Pearl. Crystal structure of glycogen synthase kinase 3β: structural basis for phosphate-primed substrate specificity and autoinhibition. *Cell*, 105(6): 721–732, 2001.

[113] Nicole B Trunnell, Andy C Poon, Sun Young Kim, and James E Ferrell. Ultrasensitivity in the regulation of cdc25c by cdk1. *Molecular cell*, 41(3):263–274, 2011.

[114] Ciaran Richardson and Dario R Alessi. The regulation of salt transport and blood pressure by the wnk-spak/osr1 signalling pathway. *Journal of cell science*, 121(20): 3293–3304, 2008.

[115] Kerry Inder, Angus Harding, Sarah J Plowman, Mark R Philips, Robert G Parton, and John F Hancock. Activation of the mapk module from different spatial locations generates distinct system outputs. *Molecular biology of the cell*, 19(11):4776–4784, 2008.

[116] Deborah K Morrison. Ksr: a mapk scaffold of the ras pathway? *Journal of cell science*, 114(9):1609–1612, 2001.

[117] Walter Kolch. Coordinating erk/mapk signalling through scaffolds and inhibitors. *Nature reviews Molecular cell biology*, 6(11):827–837, 2005.

[118] Ashok K Pullikuth and Andrew D Catling. Scaffold mediated regulation of mapk signaling and cytoskeletal dynamics: a perspective. *Cellular signalling*, 19(8):1621–1632, 2007.

[119] Sally J Leevers, Hugh F Paterson, and Christopher J Marshall. Requirement for ras in raf activation is overcome by targeting raf to the plasma membrane. *Nature*, 369 (6479):411–414, 1994.

[120] Gang Lu, Young Jun Kang, Jiahuai Han, Harvey R Herschman, Enrico Stefani, and Yibin Wang. Tab-1 modulates intracellular localization of p38 map kinase and downstream signaling. *Journal of Biological Chemistry*, 281(9):6087–6095, 2006.

[121] Michelle C Mendoza, E Emrah Er, Wenjuan Zhang, Bryan A Ballif, Hunter L Elliott, Gaudenz Danuser, and John Blenis. Erk-mapk drives lamellipodia protrusion by activating the wave2 regulatory complex. *Molecular cell*, 41(6):661–671, 2011.